EFFECTS OF MICROSTRUCTURE AND PORE FLUIDS ON THE ACOUSTIC PROPERTIES OF GRANULAR SEDIMENTARY MATERIALS

A DISSERTATION

SUBMITTED TO THE DEPARTMENT OF GEOPHYSICS

AND THE COMMITTEE ON GRADUATE STUDIES

OF STANFORD UNIVERSITY

IN PARTIAL FULFILLMENT OF THE REQUIREMENTS

FOR THE DEGREE OF

DOCTOR OF PHILOSOPHY

By

William F. Murphy III

June 1982

TABLE OF CONTENTS

Effects of Microstructure and Pore Fluids on the Acoustic Properties of Granular Sedimentary Materials

William F. Murphy III, Ph.D.
Stanford University, 1982

The response to small stress waves is the principle measure used in geophysics to study material bodies in the earth's crust. Sands and sandstones are porous, granular, sedimentary materials. This volume demonstrates how granular microstructure and water saturation determine the compressional and shear wave velocities and attenuation in the frequency range from 10 to 10^6 Hz.

Granular sedimentary materials consist of a disordered packing of elastic quartz grains in tangential contact. Porosities range from 0.01 to 0.50. We have measured velocities and specific attenuation in unconsolidated sands, high porosity sandstones, and low porosity sandstones. Unambiguous results have been established as a function of frequency, water saturation, grain characteristics, relative humidity, and strain amplitude. The results are explained by analysis of the micromechanics at the grain contacts. We propose a model which relates the contact micromechanics to linear viscoelastic frame moduli. The frame moduli represent the continuum stiffness and relaxation of the granular frame. They are strongly dependent on frequency and water saturation.

Several particular problems are solved.

Low frequency compressional and shear wave velocities in water saturated sands are determined by grain contact area. Using a simple compaction model, we can qualitatively predict the velocities as a

function of porosity, grain characteristics, and effective pressure.

In dry sandstones, velocities are high and specific attenuation, Q^{-1}, is small. Q^{-1} is independent of frequency. Velocities and attenuation are independent of strain amplitude, below strains of 10^{-6}, yet are strongly dependent on relative humidity. When dry, grain contacts are nearly elastic with strong adhesion. Molecular water is chemically adsorbed on the grain surfaces and forms an electrical double layer. Acoustic displacements deform the double layer. Hydrogen bonds are broken, and energy is absorbed. Wetting significantly softens the contacts and greatly enhances energy loss.

In partially and fully water saturated materials, Q^{-1} is found to be strongly dependent on frequency and degree of water saturation. The grain contacts are immersed in water. During each cycle, the water is driven to and from the near-contact gaps and their pore neighborhoods by local pressure gradients. Energy loss between 10 and 10^5 Hz is controlled by viscous dissipation. Shear losses, Q_s^{-1}, are maximum and larger than compressional losses, Q_p^{-1}, at full saturation. However, in partially saturated materials, Q_p^{-1} is greater than Q_s^{-1} and rises to a strong peak at water saturations between 0.75 and 0.95. The observed relaxations are centered between 1 and 10 kHz. The distribution of relaxation times is quite narrow, only somewhat broader than for a single relaxation time.

Significant velocity dispersion is required. At frequencies a decade below the center frequency, ~100 Hz, water flow in the contact gaps is diffusive. The frame can fully relax. The observed velocities are well described by the Biot-Gassmann relations which govern the fully relaxed case. Velocities measured above 100 kHz are clearly unrelaxed.

At ultrasonic frequencies, the water does not have sufficient time to flow out of the contact gaps, and the contacts are effectively stiffened.

Other processes, such as frictional grain sliding, scattering, solid-fluid inertial coupling, and thermoelasticity are shown to have limited significance.

Chapter I

INTRODUCTION*

"Geology is rapidly approaching a point where an ultimate problem which has been staring it in the face can no longer be side-stepped, namely, to determine the actual specific physical and chemical behavior of those materials which do actually constitute the earth's crust."

P. Bridgeman, 1936[2]

1. BACKGROUND

Small stress waves are the crux of geophysical research. They are easily generated and detected, and they obey simple laws of physics. Because they propagate with relatively small energy loss and are sensitive to changes in material properties, small stress waves provide the principle source of information we have regarding the earth's interior.

Perhaps the most remarkable aspect of geophysical research is that it has been accomplished, thus far, on the basis of a very crude knowledge of the actual material response to stress waves. Until quite recently, seismologists have been content with the assumptions that rocks respond elastically and that rough measurements of compressional and shear velocities at ultrasonic frequencies would suffice to delimit the response under most conditions. Two developments have occurred which have drastically altered the situation.

First, the behavior of earth materials has stirred the interest of a handful of geophysicists and applied physicists. Originally, the work of Bridgeman (1931[1], 1935[2], 1945[6]), Birch (1938[4], 1960[9]),

---

*References cited in American Institute of Physics format and in historical order.

and Griggs (1936 , 1939) at Harvard in the 1930's lead to several new problems and to the work of Biot (1956[8], 1962[11,12]) on a general theory for porous materials, Brace and Walsh (1965[13-16]) on rock compressibility, and Nur and Simmons (1969[17]) on pore fluids and velocities. Out of these studies, the discipline of rock physics arose in the late 1960's. Rock physics endeavors to understand how microstructure, pore fluids, and environmental conditions determine the behavior of earth materials. Acoustic properties is a principle focus of rock physics.

The second impetus came during the 1970's when applied geophysicists engaged in the oil industry began to recognize the potential power of rock physics. Domenico (1974[18]) proposed that the commonly observed strong reflectors or "bright spots" in sedimentary basins might be due to the presence of natural gas. He reasoned from theory (Gassman, 1951[7]; Biot, 1956[8]; Geertsma and Smit, 1961[10]) and laboratory experiments (published in 1976[19], 1977[20]) that the presence of highly compressible methane gas would significantly increase the compressional reflection coefficient of an unconsolidated sand, particularly when encased in a water saturated shale. Consequently, bright spot technology has resulted in a marked increase of drilling success throughout the world (Ostrander, 1981[21]). Today, with the increasing demand for, and dwindling supply of hydrocarbons, the oil industry is risking production on ever more marginal reservoirs and enhanced recovery techniques. More extensive reservoir evaluations are planned. And better interpretation of interval velocities, borehole sonic logs, and vertical seismic profiles are being sought as measures of rock lithology, porosity, and gas saturation.

2. OBJECTIVES

Rock or sediment from the upper crust is a complicated, porous material. Porous materials are poorly understood in general, yet better understood than rocks. A prevailing strategy in rock physics has been to simplify the complicated features of the rock problem and to pursue those aspects which are common to all porous media. This is an approach carried over from solid-state physics.

Yet arguably, the most outstanding discovery in science in the last 50 years has come in biophysics[22]. Given the structure of deoxyribose nucleic acid, one is lead immediately to an understanding of replication and mutation, and inevitably to genetic engineering[23]. The double helix is not however, a general property of all molecules. It is, in fact, that structure which distinguishes recombinant DNA from all other molecules.

This dissertation originally aimed at explaining what seemed at the time to be two differing aspects of the acoustic properties of rocks: i) how do grain properties affect the shear velocity in sands? and ii) how does partial water saturation affect acoustic energy loss in sandstones? As the work developed however, it became clear that these phenomena were actually two of several important corollary effects derived from the same fundamental behavior. In our experiments, several new phenomena are observed. We find predictable velocities in sands under pressure, strong moisture effects on "dry" rock velocities, frequency dependent Q's, velocity dispersion , and strong energy losses even in very low porosity rocks. In seeking to explain these observations, we have found the concepts of grain contacts and granular frame moduli to be persistently successful. Each suc-

ceeding observation involves either contacts between elastic grains, surface energy reduction at grain contacts, or viscoelastic relaxation due to water flow to and from oscillating near-contact gaps. The work thus reduces to a single research problem:

> How does the response and relaxation under sinusoidal loading of contacts between elastic grains which are immersed in water relate to the frequency dependent, dynamic frame moduli of a partially saturated, granular sedimentary material?

The frame moduli are macroscopic parameters representing the global stiffness of the granular frame.

Although in this volume I focus on the particular class of *granular sedimentary materials* (especially on quartz grains as the solid constituent and water-air mixture as the pore fluid), I think it is the granular nature of rocks - contained in the microphysics of grain contacts and packing - which is characteristic of the behavior of upper crustal materials.

3. PLAN

This volume is a sequence of four self-contained papers[24]. Each formulates and solves a particular aspect of the general research problem. The volume taken as a whole represents a satisfactory disposition of our objectives.

Chapter II investigates the problem of predicting low frequency velocities in marine unconsolidated granular sediments as a function of porosity and depth. Our strategy focuses on understanding how grain contacts, grain packing, and grain characteristics determine the dry frame moduli.

The set of experimental results presented in Chapter III reveals the strong dependence of specific attenuation on water saturation and

frequency in the acoustic frequency range. Important conclusions concerning the micromechanics involved are drawn from the measurements which were made in high porosity Massillon sandstone[25] and Vycor porous glass.

Previous work reports that in low porosity sandstones, undersaturation generates no significant effect on ultrasonic velocities. Chapter IV examines low porosity sandstones. At borehole frequencies, we find that water saturation strongly affects both velocities and specific attenuation. New ultrasonic measurements corroborate previous work, and dispersion is discovered to be important.

In Chapter V, we propose a general theoretical framework for the micromechanics of acoustic wave dissipation in granular sedimentary materials. Analytical development of contact relaxation leads to complex frame moduli which we embed in Biot's[11] general equations for acoustic wave propagation in porous media. Specific predictions result which test well against our experimental data. Other models such as frictional grain sliding, scattering, and thermoelasticity are found to have limited significance. Biot's solid-fluid inertial coupling may be important near 1 MHz.

References

1. P. Bridgeman, The Physics of High Pressure, G. Bell and Sons, Ltd., (1931) 398 p. Also Dover Publ., Inc. (1970).
2. P. Pridgeman, Shearing phenomena at high pressures of possible importance for geology", J. Geol. 44, 653-669 (1936).
3. D.T. Griggs, "Deformation of rocks under high confining pressure", J. Geol. 44, 541-577 (1936).
4. F. Birch and D. Bancroft, "Elasticity and internal friction in a long column of granite", Seism. Soc. Am. Bull. 28, 243-254 (1938).
5. D.T. Griggs, "Creep of rocks", J. Geol. 47, 225-251 (1939).
6. P. Bridgeman, "Polymorphic transitions and geological phenomena", Am. J. Sci. 243a (Daly volume), 90-97, 1945.
7. F. Gassman, "Ueber die elastizitat poroser medien", Vierteljahrs-schrift Naturforsch. Ges. Zuerich, Heft I (1951).
8. M.A. Biot, "Theory of propagation of elastic waves in a fluid-saturated porous solid, I. Low frequency range", J. Acoust. Soc. Am. 28, 186-178 (1956).

   "Theory of propagation of elastic waves in a fluid-saturated porous solid, II. High frequency range", J. Acoust. Soc. Am. 28, 179-191 (1956).
9. F. Birch, "The velocity of compressional waves in rocks to 10 kb, Part I", J. Geophys. Res. 65, 1083-1102 (1960).

   "The velocity of compressional waves in rocks to 10 kb, Part II", J. Geophys. Res. 66, 2199-2224 (1961).
10. J. Geertsma and D.C. Smit, "Some aspects of elastic wave propagation in fluid-saturated porous solids", Geophys. 26, 169-181 (1961).

11. M.A. Biot, "Generalized theory of acoustic propagation in porous dissipative media", J. Acoust. Soc. Am. 54, 1254-1265 (1962).

12. M.A. Biot, "Mechanics of deformation and acoustic propagation in porous media", J. Appl. Phys. 33, 1482-1498 (1962).

13. W.F. Brace, "Some new measurements of linear compressibility of rocks", J. Geophys. Res. 70, 391-398 (1965).

14. J.B. Walsh, "The effects of cracks on the compressibility of rocks", J. Geophys. Res. 70, 381-389 (1965).

15. G. Simmons and W.F. Brace, "Comparison of static and dynamic measurements of compressibility of rocks", J. Geophys. Res. 70, 5649-5656 (1965).

16. J.B. Walsh, W.F. Brace, and A.W. England, "Effect of porosity on the compressibility of glass", J. Am. Ceramic Soc. 48, 605-608 (1965).

17. A. Nur and G. Simmons, "The effect of saturation on velocity in low porosity rocks", Earth Plan. Sci. Lett. 7, 183-193 (1969).

18. S.N. Domenico, "Effect of water saturation on seismic reflectivity of sand reservoirs encased in shale", Geophys. 39, 759-769 (1974).

19. S.N. Domenico, "Effect of brine-gas mixture on velocity in an unconsolidated sand reservoir", Geophys. 41, 882-894 (1976).

20. S.N. Domenico, "Elastic properties of unconsolidated porous sand reservoirs", Geophys. 43, 1339-1368 (1977).

21. W. Ostrander, "Direct hydrocarbon detection", Visiting lecture at Dept. Geophys., Stanford Univ. (1981).

22. J.D. Watson and F.H.C. Crick, "Molecular structure of nucleic acids: A structure for deoxyribose nucleic acid", Nature 171, 737-738 (1953).

23. J.D. Watson, The Double Helix, Atheneum, New York (1968), 143 pp.

24. A comment is necessary regarding the citation formats which are different from chapter to chapter. Parts of each chapter have been or are to be submitted to certain journals, as noted by a footnote on each opening page. Thus, each chapter is formated according to the requirements of that specified journal.

25. I only recently learned (J. Oliver, personal communication) that the correct spelling is "Massillon sandstone", with two 'l's. Chapters III and IV have gone into the publication process with the spelling "Massilon", following the pioneering work of Winkler and Nur in their various publications over the last 3 years. The discrepancy has been preserved in this volume for historical reasons, rather than for expedience.

Chapter II

Grain Contacts, Disordered Microstructure, and Dynamic Frame Moduli in Granular Sediments*

Contents

1. INTRODUCTION

Hamilton's pioneering work in geoacoustics (1970, 1971, 1974a,b, 1976a, 1978, 1979a,b, 1980a) has shown the velocities of marine sediments to be strongly dependent on porosity, granular fabric, and depth.

Particularly sensitive to stress conditions and grain size appears to be the shear velocity, V_s. Predictive estimates, laboratory experiments, and in situ measurements exhibit an order of magnitude scatter. The depth dependence of V_s in water saturated sands and silts has been measured anywhere from a 1/3 to a 1/8 power of pressure. Reliable predictive knowledge of V_s is important because the rigidity has been

*Parts to be submitted to the Journal of Geophysical Research and Journal of the Acoustical Society of America in July, 1982.

shown to contribute significantly to the sediment-water reflection coefficient (Hamilton 1971, 1974, 1978). Its depth gradient, $\frac{\partial V_s}{\partial h}$, is an important factor in the refraction of low frequency sound through the ocean floor (Christensen et al., 1975; Hamilton, 1976, 1978, 1980; Fryer, 1981). Shear velocity also holds interest as a possible measure of the nonlinear response and liquefaction potential of coastal and offshore foundations to earthquakes and storm waves (Bea, 1978; Woods, 1978; Hardin, 1978; Stokoe, 1978; Anderson et al., 1978).

The compressional velocity V_p in marine sediments appears to vary quite simply with porosity. Yet attempts thus far to convert interval velocities to formation porosities on the basis of simple averaging models (eg. the time average equation (Wyllie et al., 1956, 1958)) have been unsatisfactory (Geertsma and Smit, 1961; Telford et al., 1976; Watt et al., 1976). V_p in water saturated sands is dependent on the effective pressure (Domenico, 1977) and the depth gradient, $\frac{\partial V_p}{\partial h}$, has been studied extensively in situ. However, no theory has been proposed which has satisfactorily explained the measurements (Brandt, 1960; White, 1965; Walton, 1975; Stoll, 1980; Digby, 1982).

Gassmann (1951a), Biot (1956), and Brown and Korringa (1975) have shown theoretically that in a macroscopically homogeneous porous media at low acoustic (<500 Hz) and seismic frequencies (figure 1), the dependence of V_p and V_s on microstructure is contained solely within the porosity and the dynamic frame moduli.

Biot's (1956) theory is frequency dependent, attempting to cover the entire range of interest (figure 1). It requires an additional parameter, the so-called structure factor, $\bar{\alpha}$. The structure factor, $\bar{\alpha}$, is a measure of the pore geometry similar to a tortuosity or an

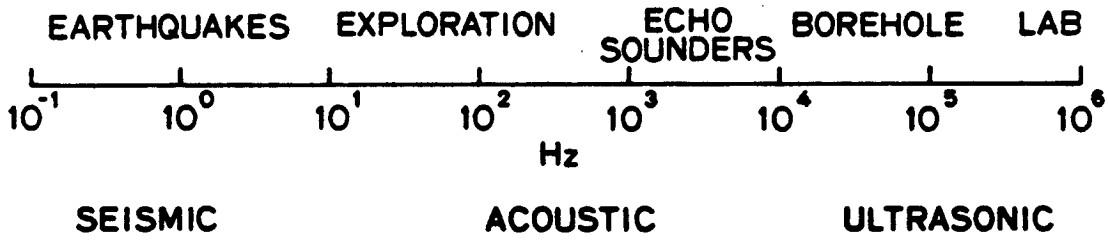

Fig. 1. Spectrum of geoacoustic interest.

index of refraction (Johnson, 1980; Johnson and Sen, 1982). $\bar{\alpha}$ enters Biot's theory in the inertial coupling of the pore fluid to the solid frame and drops out in the low frequency limit, the Biot-Gassmann relations. $\bar{\alpha}$'s significance in the ultrasonic range is under extensive study elsewhere (D.L. Johnson, personal communication).

The porosity, ϕ, is the ratio of the pore volume to the total of the material and is a function of the packing.

The dynamic frame moduli represent the macroscopic or effective stiffness of the granular frame. Neglecting clays and other compositional impurities, we may say that in granular sediments, these stiffnesses result from the tangential contact of elastic quartz grains embedded in a disordered packing. The porosity is related to the frame moduli through the coordination number, i.e. the number of contacts per grain. Understanding how grain contacts and disordered packing determine the dynamic frame moduli is an important step in predicting the acoustic velocities of marine sediments on the one hand, and deciphering the microstructural information contained in measured velocities on the other.

The purpose of this paper is to explain the effects of granular microstructure and effective pressure on low frequency vleocities in water saturated granular materials. Micromechanical models are developed for the dry frame moduli. Unambiguous predictions are stated explicitly for V_p, V_s, and V_p/V_s as a function of grain characteristics, porosity, and effective pressure. The predictions of each step are systematically tested by laboratory measurements of V_p and V_s in glass beads and quartz sands. Signal velocities were measured by an ultrasonic pulse transmission technique (similar to that of Elliott

and Wiley, 1975) at frequencies ~200 kHz. All measurements were obtained in vacuum dry (<10μm) samples. Although signal velocities are generally equivalent to group velocities in dissipative media (Morse and Ingard, 1968), we are aware of no evidence for dispersion in vacuum dry samples of similar composition. Errors in the moduli are expected to be less than 5%. These moduli are in fact frequency-independent, dry frame moduli and as such are expected to apply across seismic, acoustic, and ultrasonic frequency ranges.

We find that the low frequency, dynamic frame moduli in granular sediments are determined by the grain contact area. At low pressures, the increase in contact area is dominated by the increase in actual contacts per grain. A compaction model is proposed based on the transformation of a Gaussian radial distribution function with pressure. In the high pressure limit where coordination number is constant, granular sediments are well described as a disordered, Hertz-Mindlin granular material. When input into the Biot-Gassmann relations, predictions fit a set of compiled in situ data remarkably well.

2. THE PROBLEM

In situ measurements of V_p versus porosity in ocean bottom sediments are shown in figure 2. The data are taken from Hamilton (1971, 1974b) and Smith (1974). V_p declines gradually with increasing porosity. Scatter is generally less than 5% reaching a maximum of 12% at $\phi \approx 0.45$. Figure 3 gives in situ V_s versus porosity. It is important to note that Hamilton's data are actually calculated from V_p assuming a hypothetical bulk frame modulus (1971), yet this methodological fact is omitted from Anderson and Hampton's recent (1980) replot of the

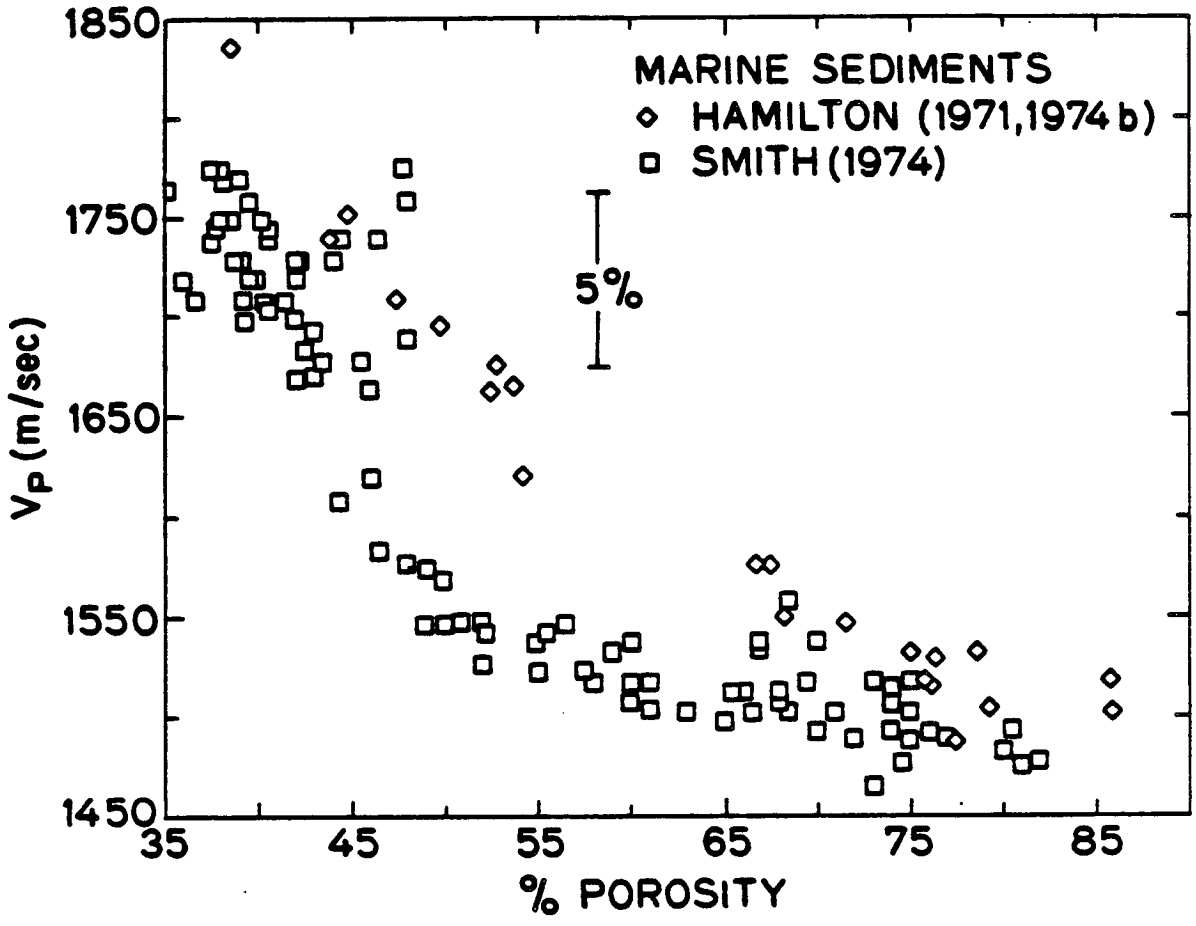

Fig. 2. Compiled measurements of V_p vs. porosity in marine sediments. Hamilton's (1971, 1974b) data is from North Pacific sediments, while Smith's (1974) data is from the North Atlantic sediments.

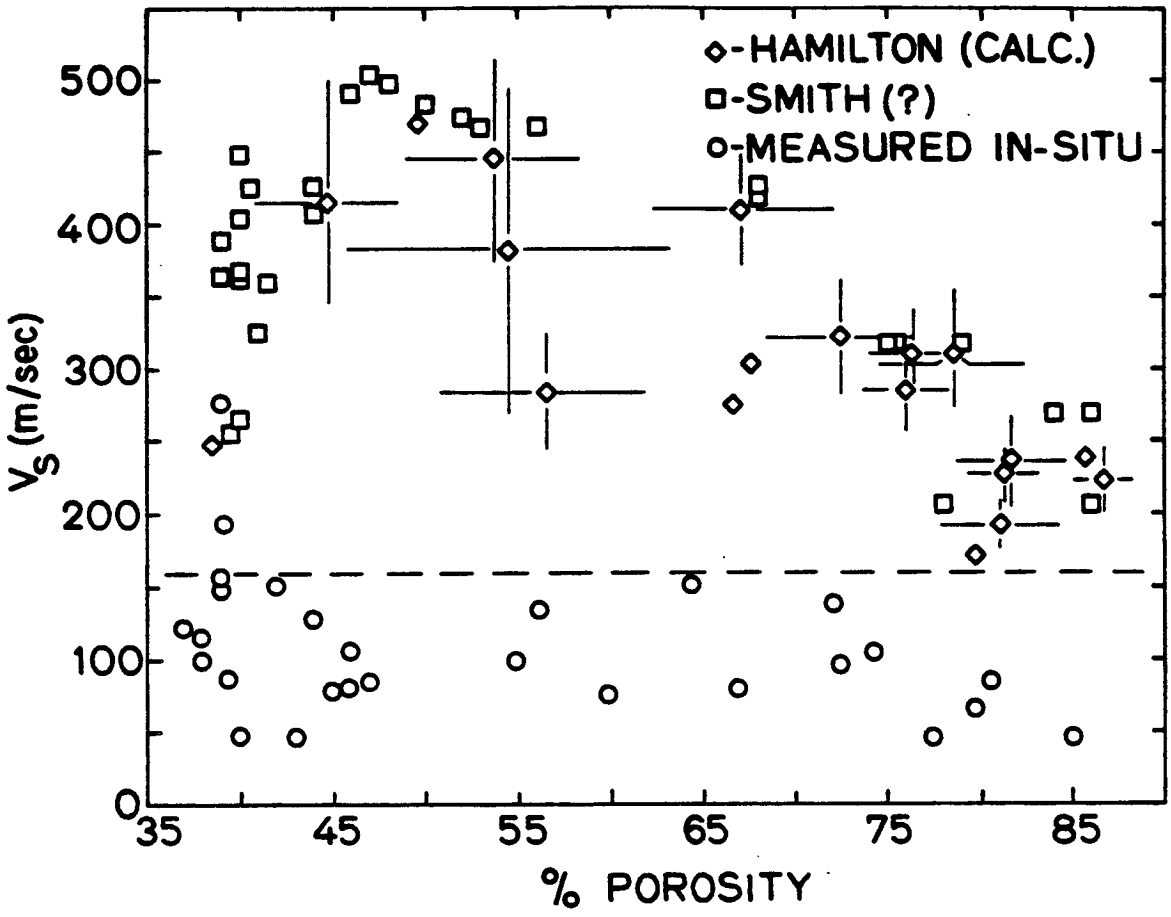

Fig. 3. Compiled data for V_s vs. porosity in in situ sediments. Hamilton's (1971, 1974b) data was calculated from V_p assuming a hypothetical bulk frame modulus. Smith's (1974) techniques were unspecified. Well documented in situ geotechnical measurements (○) are from Anderson et al. (1978), Arango et al. (1978), Kudo and Shima (1970), Hamilton (1976), Barker (1962), Stokoe and Woods (1973), Cunny and Fry (1976), Warrick (1974), and Wilson et al. (1978).

data (their figure 3). Smith's data was first presented in 1974 without description of the measurement technqiues. Smith's data has also been replotted in the same figure 3 of Anderson and Hampton (1980). In figure 3 of this paper the "compiled" in situ measurements are taken from the geotechnical literature for water saturated sediments, in which the measurement technqiues are fully and explicitly documented. Figure 4 gives the measured porosity in marine sediments versus grain size in microns. The grain size scale is based on a negative logarithm to the base 2, which is equivalent to the phi grain size scale used in sedimentology. The roughly linear plot implies that if the data presented in figures 2 and 3 were plotted against grain size (log to the base 2), homologous effects would be observed.

At low frequency, V_p and V_s are governed by the Biot-Gassmann relations in which

$$V_p = \left(\frac{M_r}{\rho_c} \right)^{1/2} \quad , \quad V_s = \left(\frac{N_r}{\rho_c} \right)^{1/2} \tag{1}$$

where M_r is the low frequency or relaxed compressional wave modulus given by

$$M_r = \frac{(K_s - K_{wr})^2}{K_s\left(1-\phi- \frac{K_{wr}}{K_s} + \phi\frac{K_s}{K_f}\right)} + K_{wr} + \frac{4}{3}\mu_{wr} \tag{2}$$

when N_r is the low frequency or relaxed shear wave modulus given by

$$N_r = \mu_{wr} \tag{3}$$

and ρ_c is the composite density given by

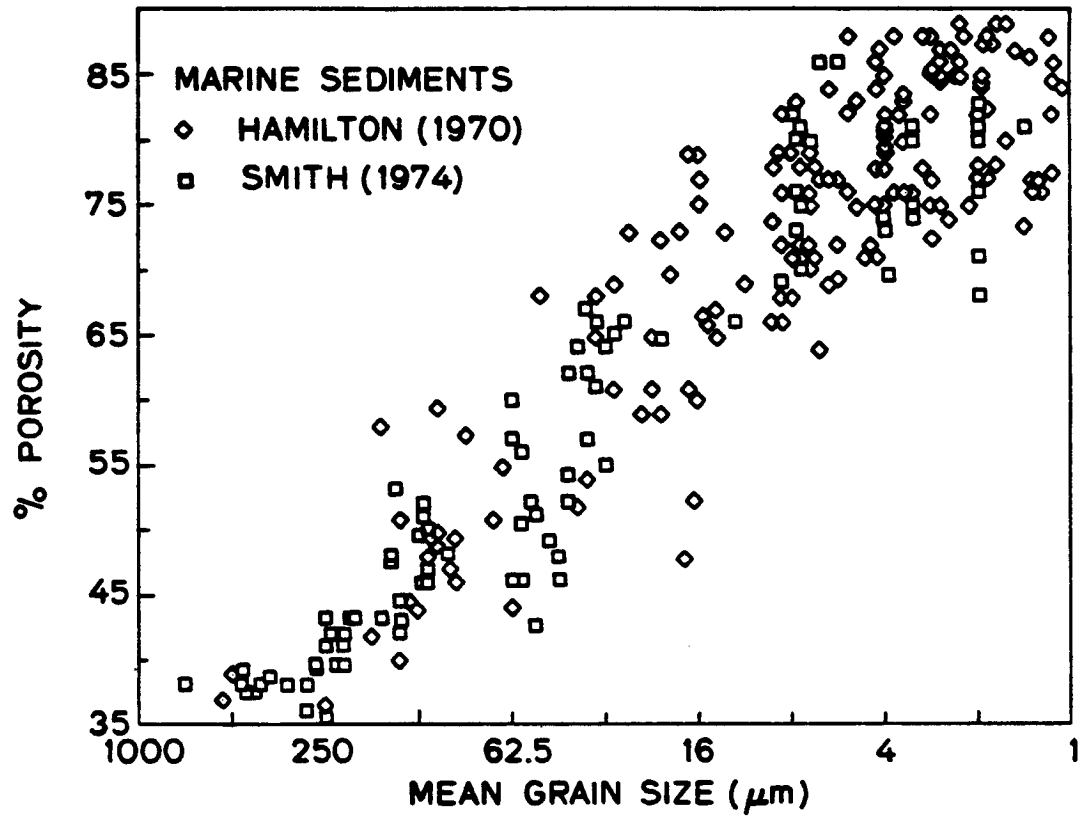

Fig. 4. Porosity vs. grain size in natural sediments.

$$\rho_c = (1 - \phi)\rho_s + \phi S_w \rho_w \quad . \tag{4}$$

K_s is the bulk modulus of the solid grains, ρ_s is the density of the solid grains, ρ_w is the density of the water, and S_w is the water saturation which is equal to 1.0 in a fully saturated material. K_f is the bulk modulus of the pore fluid given by

$$\frac{1}{K_f} = \beta_g(1 - S_w) + \beta_w S_w \tag{5}$$

where β_g is the compressibility of the gas and β_w is the compressibility of the water.

K_{wr} and μ_{wr} are the real parts of the relaxed bulk and shear water-wetted frame moduli, respectively. They replace the more ambiguous "frame moduli of the bulk material" of say, Geertsma and Smit (1961). We have observed (e.g. Hardin and Richart, 1963; Spencer, 1981; Murphy, 1982a) a strong modulus defect in sands and sandstones at low acoustic frequencies with the addition of small amounts of moisture. In general, the bulk and shear frame moduli, $\bar{K}$ and $\bar{G}$, respectively, are complex and strongly frequency dependent on water saturation and frequency as shown in figure 5. These effects of water saturation and frequency are the subject of the related papers (Murphy, 1982a; Murphy, 1982b, Murphy and Nur, 1982a).

In this paper, we focus on i) the dry bulk and shear frame moduli, K_d and μ_d, respectively, which are independent of frequency, and ii) the softening of K_d and μ_d to K_{wr} and μ_{wr}. While it is necessary to predict the low frequency softening in order to test agreement with in situ data, our primary objective is to understand how grain characteristics and granular microstructure determine K_d and μ_d.

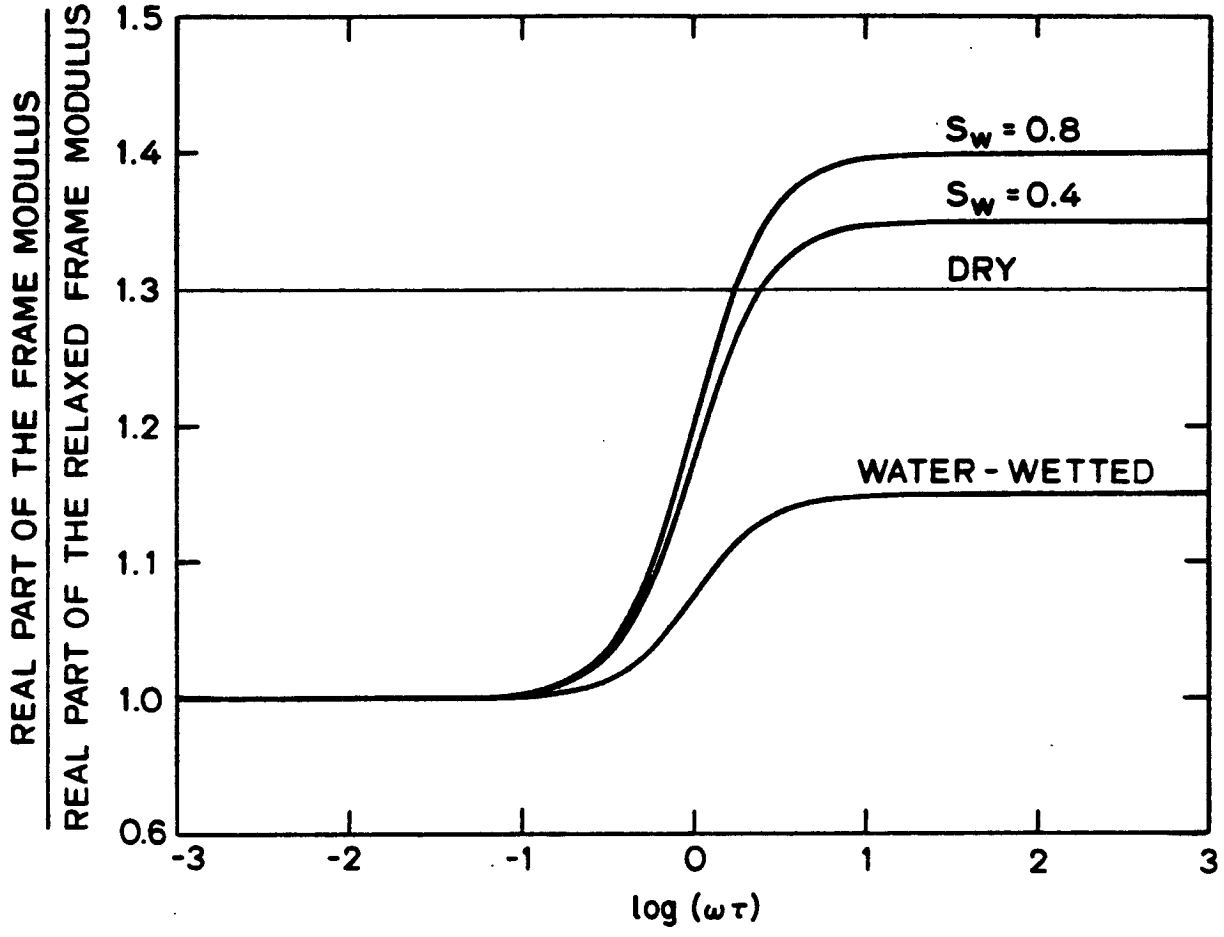

Fig. 5. Theoretical dispersion, as a function of water saturation, of the real part of the frame modulus normalized to the real part of the relaxed frame modulus. In granular sedimentary materials, $\tau \approx 10^{-3} - 10^{-4}$ sec. In this paper, we focus on the dry frame moduli, and the relaxed wetted frame moduli. Dispersion is neglected.

Microstructure may be decomposed into two categories of relations. The relations between two adjacent individual grains in contact or near contact are called contact theory. The relations between an individual grain and the aggregate of grains are called packing theory. Development of these theories leads to unambiguous predictions for the effects of grain size, shape, and size distribution, as well as for the effects of porosity and effective pressure. All of which are directly testable by simple experiment.

Digression

This problem is intimately related to the nature of the seismic properties of the shallow lunar crust which have been studied by Warren and Anderson (1973), Talwani et al. (1973), Gangi (1981), Johnson et al. (1982), and most notably by Tittmann et al. (1972, 1976, 1977, 1978, 1979). The results of this work are applied to lunar problems in a subsequent article (Murphy and Nur, 1982b).

3. HERTZ-MINDLIN THEORY OF SMOOTH ELASTIC SPHERES IN CONTACT

Consider two identical smooth elastic spheres in tangential contact at a point (fig. 6a). The application of a finite force normal to the plane of contact results in a circular area of contact (fig. 6b). We assume that the radius of the contact is small compared to the radii of the spheres. The classical theory of Hertz (Timoshenko and Goodier, 1951) shows the relation between the normal contact force, n, and the radius of the area of contact, a, to be

$$a = \left[\frac{3(1-\nu)nR}{8\mu} \right]^{1/3} \tag{6}$$

where R is the radius of the grains, and ν and μ are, respectively,

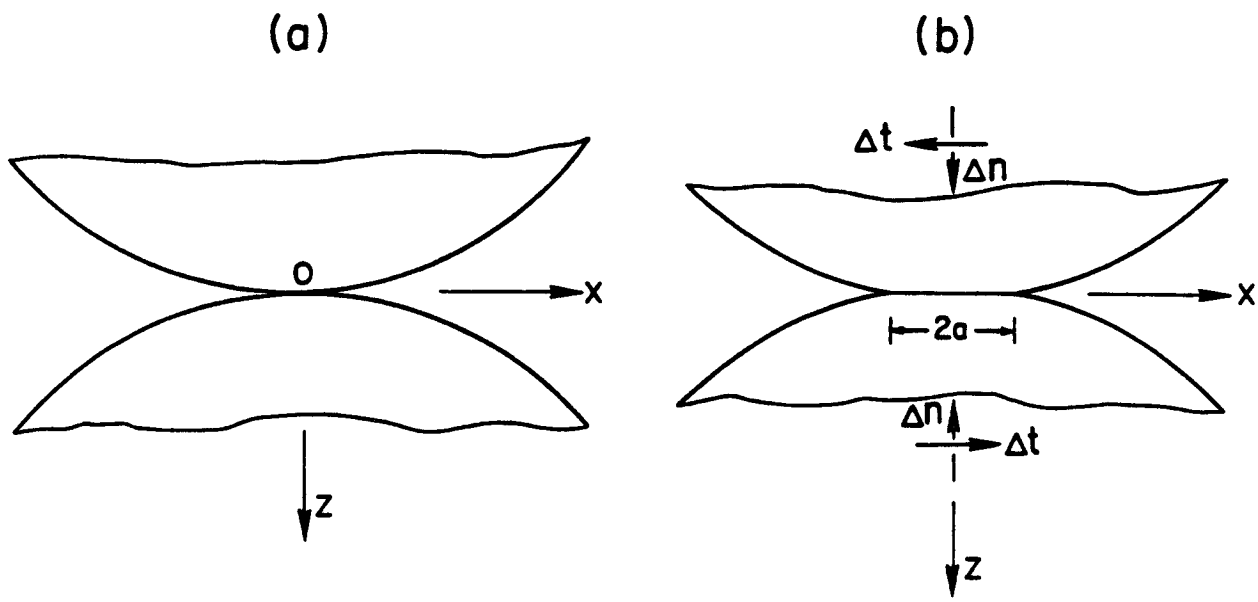

Fig. 6. Elastic spheres in contact.

a) unstressed state,

b) spheres pressed together under normal force, n, applied along the z axis. Circular contact area of radius, a, is formed. Δn and Δt are small (i.e. $\Delta n, \Delta t \ll n$) increments of applied normal and shear stress, respectively, superimposed on n.

the Poisson's ratio and the rigidity (i.e., shear modulus) of the material of the grains. The contact area, A, varies with $n^{2/3}$. The distribution of pressure (fig. 6c) on the contact is

$$\sigma = \frac{3n}{2\pi a^3}(a^2 - r^2)^{1/2} \quad . \tag{7}$$

The relative displacement of the centers of the spheres under the imposition of n, or normal approach is

$$\alpha = 2\left[\frac{3(1-\nu)n}{8\mu R^{1/2}}\right]^{2/3} \quad . \tag{8}$$

From equations (6) and (8), we obtain for the normal compliance, J_n,

$$J_n = \frac{d\alpha}{dn} = \frac{1-\nu}{2\mu a} \quad . \tag{9}$$

Mindlin extended the theory to include an additional component of force, t, tangential to the contact surface where $t < fn$. With the application of t, regardless of how small t may be, slip is expected to occur on the contact surface. An infinite traction would otherwise be required along the circumference of the area of contact. Slip begins at the contact circumference and progresses radially inward. The region on which slip occurs (fig. 6c) is an annulus of outer radius, a, and an inner radius, c, given by

$$c = a\left(1 - \frac{t}{fn}\right)^{1/3} \quad , \tag{10}$$

where f is the coefficient of friction of the material of the grains. The distribution of tangential traction on the contact area (fig. 7) is

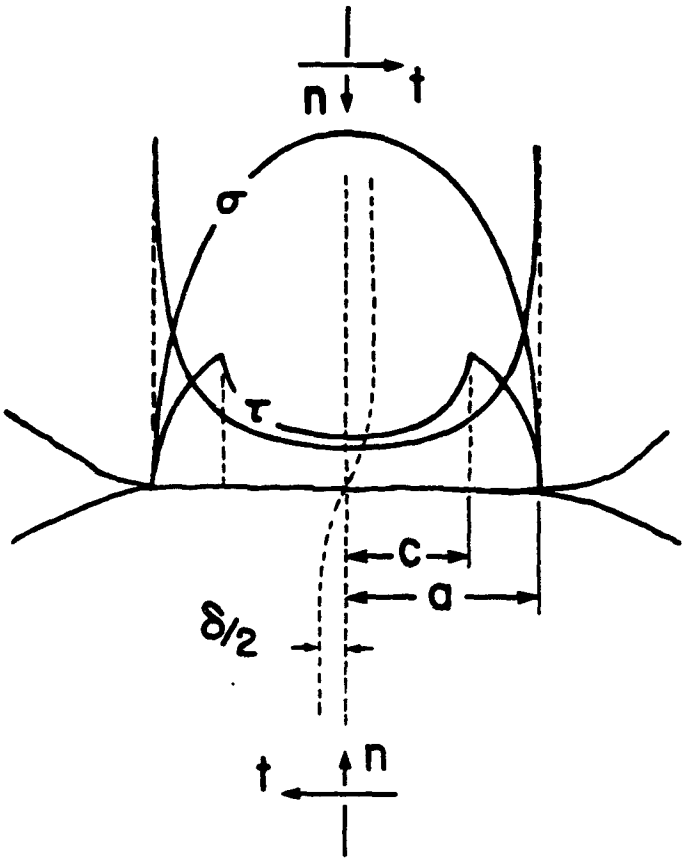

Fig. 6. c) Distribution of normal (σ) and tangential (τ) components of traction on the contact surface.

$$\tau = \begin{cases} \frac{3fn}{2\pi a^3}(a^2-r^2)^{1/2} , & c \leq r \leq a \\ \frac{3fn}{2\pi a^3}[(a^2-r^2)^{1/2} - (c^2-r^2)^{1/2}] , & r \leq a \quad . \end{cases} \tag{11}$$

The relative displacement of the centers of the two spheres is

$$\delta = \frac{3fn(2-\nu)}{8\mu a}\left[1 - \left(1 - \frac{t}{fn}\right)^{2/3}\right] \quad . \tag{12}$$

Thus, the tangential compliance is

$$J_t = \frac{d\delta}{dt} = \frac{2-\nu}{4\mu a}\left(1 - \frac{t}{fn}\right)^{1/3} \quad . \tag{13}$$

Mindlin et al. (1951) studied the oscillation of the tangential force between $\pm t^*$ for small amplitudes of loading, i.e. $t << fn$. They found that a stable hysteresis cycle is obtained after the first quarter cycle and that the frictional energy loss per cycle due to grain slippage is

$$\phi = \frac{(2-\nu)\ t^{*3}}{36\mu afn} \tag{14}$$

The annulus of slip was observed experimentally, and equation 10 was experimentally verified. Johnson (1955) experimentally confirmed the load-displacement relation (equation 10). Energy loss, however, was found to obey equation (14) only for large amplitudes of tangential force. At smaller amplitudes, the energy loss per cycle varied with the square of the amplitude, rather than the cube as predicted by equation (14). Goodman and Brown (1962) elucidated Johnson's findings. And in the discussion following that paper, Johnson revealed that the energy loss dependence on the square of the amplitude had also been observed for oscillating normal force at small amplitudes.

Mindlin and Deresiewicz (1953) further extended the theory to include the addition of a varying force of constant obliquity across a contact surface under the initial normal load, n_0. The tangential compliance in loading in the stable cycle is

$$J_L = \frac{2-\nu}{4\mu a}\,\theta + (1-\theta)\left[1 - (1+\theta)\,\frac{L^*+L}{2(1+\theta L)}\right]^{-1/3} \qquad (15)$$

where $L = t/fn_0$, $L^* = t^*/fn_0$, $\theta = f/\beta$, and $\beta = \frac{dt}{dn} \geq f$. The compliance for unloading, J_U, is given by the same expression except that the signs of θ and L are reversed. For small loading, (small L^*) the frictional loss per cycle is

$$\Phi = \frac{(2-\nu)\,t^{*3}}{36\mu a_0 fn_0}\,(1-\theta^2) \quad , \qquad (16)$$

where a_0 is the contact radius resulting from n_0.

4. PREDICTED VELOCITIES FOR ORDERED PACKINGS

The dynamic frame moduli of ordered packings of identical smooth elastic spheres may be calculated explicitly. The structural properties of ordered packings of spheres have been formulated by Graton and Fraser (1935). Early models (Hara, 1935; Iida, 1938, 1939; Gassmann, 1951b) developed dynamic stress-strain relations based on Hertz' contact theory. These models however consistently predict velocities that are too low when tested against experimental results. Furthermore, we know that the tangential stiffness of a contact is of the same order of magnitude as the normal stiffness. Duffy and Mindlin (1958) and Duffy (1959) have since demonstrated how to derive stress-strain relations based on Hertz-Mindlin micromechanics. Directly followed

their approach, we are able to pose explicit expressions for the compressional wave modulus, M_d, and the shear wave modulus, N_d, for simple cubic, hexagonal, close-packed, and face-centered cubic arrays.

Interest focuses on these packings because the hexagonal close-packed (hcp) and face-centered cubic (fcc) arrays constitute the densest packing of identical spheres with $\phi = 0.2595$, while in the simple cubic (sc) array, $\phi = 0.4764$. Smith, Foote, and Busang (1927) have suggested that a random packing may be modeled as a mixture of clusters of hcp and sc microstates.

Duffy and Mindlin (1958) and Duffy (1959) found the fcc and hcp arrays, respectively, to be statically undetermined. That is, the equilibrium equations were not sufficient to determine the stress-strain relations. For these arrays, the relative displacements among the spheres in the lattice are required to simultaneously satisfy the compatibility equations. The compatibility equations involve the contact compliances, they are nonlinear owing to the nonlinearity between the normal contact force and the normal approach in equations (8) and (9). And because of the inelasticity between the tangential force and tangential displacement in equations (12) and (13), they depend on the entire loading history.

Deresiewicz (1958) found the sc packing to be statically determinate. But although the history of loading does not enter into the calculation of the contact forces, the nonlinearity and inelasticity remain in the compliances at each contact.

Two assumptions greatly simplify the equations. i) If the loading history is isotropic and homothetic, then from symmetry considerations, the initial contact forces are all equal and have no tengential components. From the equilibrium equations and the definition of stress,

the initial contact forces are

$$n_0 = \sqrt{2}\ R^2\sigma_0 \tag{17}$$

where σ_0 is the isotropic stress or hydrostatic pressure. Since the loading history is the same, the initial compliances do not vary from contact to contact. ii) If the applied arbitrary stress increments are small compared to n_0, then the total stress never significantly departs from n_0. The contact radius becomes

$$a = a_0 = \left[\frac{3(1-\nu)n_0 R}{8\mu} \right]^{1/3} \tag{18}$$

The normal compliance is

$$J_n = \frac{1-\nu}{2\mu a_0} \tag{19}$$

By letting $L^* \to 0$ in accordance with the small amplitude assumption, we find that

$$J_t = J_L = J_U = \frac{2-\nu}{4\mu a_0} \quad . \tag{20}$$

Given these assumptions exact solutions are obtained for the case of an initial isotropic, compressive stress, σ_0, followed by an arbitrary, yet small, incremental stress. Clearly, these solutions are appropriate for acoustic wave propagation in a granular material under hydrostatic confining pressure.

The set of explicit, continuum, differential constitutive equations takes the general form $dT = C\ dE$, where T is the stress tensor, E is the strain tensor, and C is the compliance tensor. The equations for the sc packing have the particular form of an isotropic solid. The

independent moduli are two,

$$c_{11} = c_0 \quad ,$$
$$c_{12} = \frac{\nu}{2(2-\nu)} c_0 \quad , \tag{21}$$

where $c_0 = \left[\frac{3\mu^2\sigma_0}{2(1-\nu)^2} \right]^{1/3}$. The equations for the hcp array have a symmetry corresponding to a tetragonal crystal with six independent moduli,

$$c_{11} = \frac{1152 - 1848\nu + 725\nu^2}{24(2-\nu)(12-11\nu)} c_o \quad ,$$
$$c_{12} = \frac{\nu(120 - 109\nu)}{24(2-\nu)(12-11\nu)} c_0 \quad ,$$
$$c_{13} = \frac{\nu}{3(2-\nu)} c_0 \quad ,$$
$$c_{33} = \frac{4(3-2\nu)}{3(2-\nu)} c_0 \quad , \tag{22}$$
$$c_{44} = c_{55} = \frac{6-5\nu}{4(2-\nu)} c_0 \quad ,$$
$$c_{66} = \frac{576 - 948\nu + 417\nu^2}{24(2-\nu)(12-11\nu)} c_0 \quad .$$

The equations for the fcc array correspond to a cubic crystal. The moduli are

$$c_{11} = 2c_{44} = \frac{4-3\nu}{2-\nu} c_0 \quad , \tag{23}$$
$$c_{12} = \frac{\nu}{2(2-\nu)} c_0 \quad .$$

Results are compiled in Tables 1 and 2.

TABLE 1. Relevant characteristics of the three pertinent ordered packings. The symbol '.' denotes a zero component in the stiffness matrix.

	Symbol	Coordination Number	Porosity	Stiffness Matrix
Simple cubic	sc	6	0.47	$\begin{pmatrix} C_{11} & C_{12} & C_{12} & . & . & . \\ . & C_{11} & C_{12} & . & . & . \\ . & . & C_{11} & . & . & . \\ . & . & . & \frac{1}{2}(C_{11}-C_{12}) & . & . \\ . & . & . & . & \frac{1}{2}(C_{11}-C_{12}) & . \\ . & . & . & . & . & \frac{1}{2}(C_{11}-C_{12}) \end{pmatrix}$
Hexagonal Close-packed	hcp	12	0.25	$\begin{pmatrix} C_{11} & C_{12} & C_{13} & . & . & . \\ . & C_{11} & C_{13} & . & . & . \\ . & . & C_{33} & . & . & . \\ . & . & . & C_{44} & . & . \\ . & . & . & . & C_{44} & . \\ . & . & . & . & . & C_{66} \end{pmatrix}$

TABLE 1 (cont.)

	Symbol	Coordination Number	Porosity	Stiffness Matrix
Face-centered Cubic	fcc	12	0.25	$\begin{pmatrix} C_{11} & C_{12} & C_{12} & \cdot & \cdot & \cdot \\ \cdot & C_{11} & C_{12} & \cdot & \cdot & \cdot \\ \cdot & \cdot & C_{11} & \cdot & \cdot & \cdot \\ \cdot & \cdot & \cdot & C_{44} & \cdot & \cdot \\ \cdot & \cdot & \cdot & \cdot & C_{44} & \cdot \\ \cdot & \cdot & \cdot & \cdot & \cdot & C_{44} \end{pmatrix}$

TABLE 2. Predicted wave moduli, where $C_o = \left[\frac{3\mu^2\sigma_0}{2(1-\nu)^2} \right]^{1/3}$.

Array	Direction of Propagation	ρ_c	$M_d = \rho_c V_p^2 = K_d + \frac{4}{3}\mu_d$	$N_d = \rho_c V_s^2 = \mu_d$
sc	isotropic	$0.5236\ \rho_s$	$C_{11} = C_0$	$\frac{1}{2}(C_{11}-C_{12}) = \frac{1-\nu}{2-\nu} C_0$
hcp	[100]	$0.7405\ \rho_s$	$C_{33} = \frac{4(3-2\nu)}{3(2-\nu)} C_0$	$C_{44} = \frac{6-5\nu}{3(2-\nu)} C_0$
fcc	[100]	$0.7405\ \rho_s$	$C_{11} = \frac{4-3\nu}{2-\nu} C_0$	$C_{44} = \frac{4-3\nu}{2(2-\nu)} C_0$

The predictions are unambiguous, and several points are important. Velocities are predicted to be independent of grain size. Velocities depend on the pressure to the 1/6 power. As V_p and V_s for a given packing have the same pressure dependence, V_p/V_s as a function of pressure is a constant. Both V_p and V_s are proportional to the fourth root of the contact area. In fact in general, V_p and V_s are predicted to behave qualitatively the same.

The material has ultimately been modeled as an elastic solid. However, should frictional inelasticity be important, amplitude dependence would be observed in the moduli, velocities, and Q^{-1}, where Q^{-1} is a dimensionless measure of the enrgy loss per cycle divided by 2π times the maximum energy stored per cycle. Analysis of the frictional dissipation mechanism is deferred to Murphy (1982b).

5. GRAIN SIZE EFFECTS

The apparently strong peak in V_s observed for fine sand at $\phi = 0.45$ observed in the Hamilton and Smith data (fig. 3) finds no support in the careful experiments of Hardin and Richart (1963) or Edil and Luh (1978). By varying grain characteristics in their measurements, Hardin and Richart (1963) found V_s to be independent of grain size, weakly dependent on grain shape, significantly dependent on porosity and dependent on confining pressure to the 1/4 power. Pilbeam and Vaisnys (1973) have made the problem interesting by finding a strong grain size effect and power law pressure dependences with exponents ranging from 1/3 to 1/6. The work of Edil and Luh (1978) generally agrees with Hardin and Richart finding no grain size effect and a weak grain shape effect; however, their empirical

relationship for V_s as a function of porosity and confining pressure is more complicated.

In order to test the theoretical predictions, and to determine once and for all whether or not grain size per se affects velocities, we have measured V_p and V_s in disordered packings of vacuum dry, soda-lime glass beads as a function of grain size. The measurements were made under uniaxial pressures P_a from 0.1 to 35 MPa. The vacuum achieved in the pores was ~5μm. Glass beads were chosen as the test material because a change in bead size entails minimal inherent changes in other potentially significant grain characteristics, such as grain shape and grain roughness. The measurements are made in carefully compacted samples. The beads are first delicately spooned into the cylindrical pressure vessel. They are then subjected to two preliminary slow, uniaxial pressure cycles in order to obtain reproducible, stabilized packings. In glass beads, the hysteresis cycles stabilize after the initial cycle. An example of a third cycle is given in figure 7. Recalling that the predictions were derived for an isotropic compressive stress, we have been concerned with the uniaxial nature of our applied stress. In figure 7, we compare our example of a pressure cycle with data for similar samples from Domenico (1977). Domenico's data represents an average at each given confining pressure of the loading and unloading cycles. The agreement is satisfactory for the qualitative objectives of our experimental tests. The quantitative discrepancies shall be considered when appropriate in the discussion of the data.

Hereafter, all experimental pressure data given will have been taken from unloading part of the third pressure cycle.

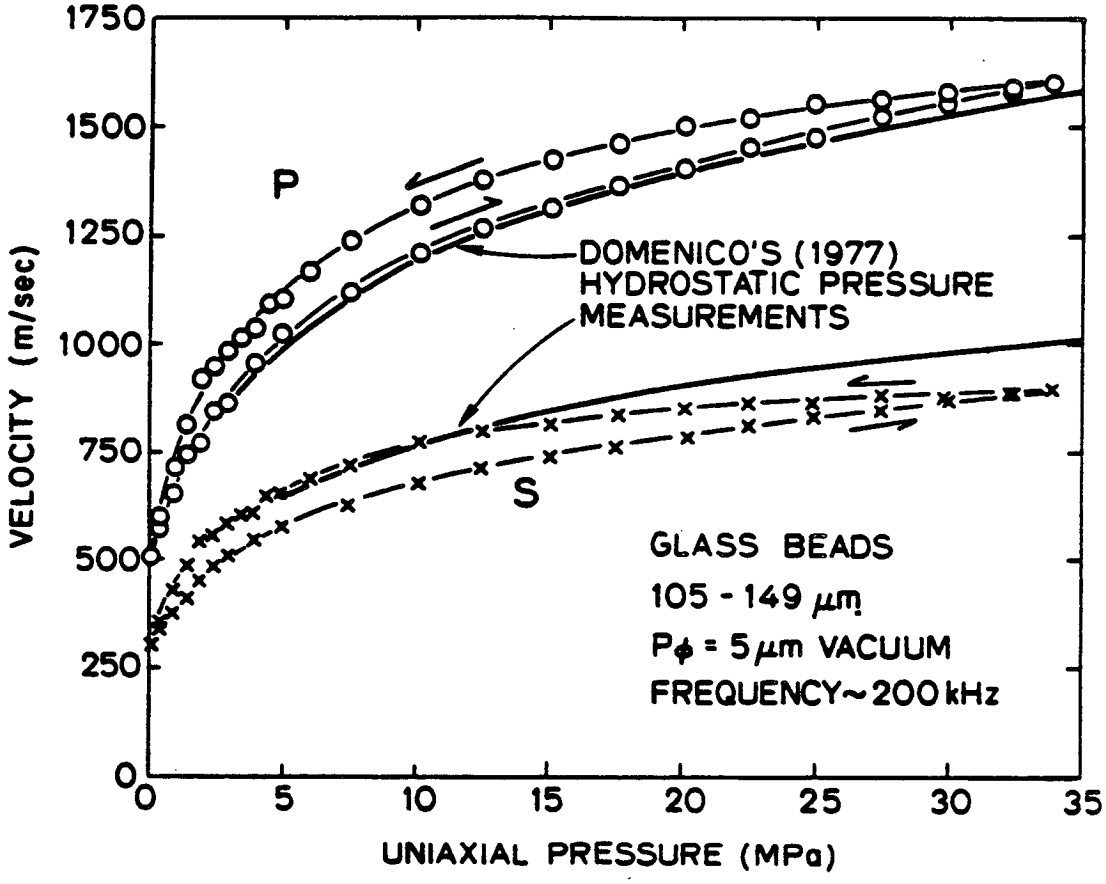

Fig. 7. V_p and V_s vs. uniaxial pressure in vacuum dry glass beads during the third hysteresis cycle. Also plotted is a thicker line which represents a fit to Domenico's (1977) corresponding yet hydrostatic pressure data.

We have tested for strain amplitude dependence in velocities by varying the input voltage which is delivered to the lead zirconate transducers (PZTs). The amplitude was increased at 100 volt intervals from 100 to 1000 volts at P_a = 0.4, 1.0, and 5.0 MPa. No strain amplitude effects were observed. Stoll (1979) has reported the absence of strain amplitude effects in dry and saturated sands below strains of 10^{-6}. Stoll's measurements were made under very low confining pressures. Similar behavior has been observed in sandstones (Winkler et al., 1979; Murphy, 1982a).

Figure 8 gives V_p and V_s against diameter 2R divided by sample length, L, at 4 MPa. We observe that if sample length is greater than 100 grain diameters, then the velocities are independent of grain size. Clearly, when 2R/L = 1, the velocity measured is closer to the speed in a homogeneous block of glass. As 2R/L approaches 0.01, the grain packing approaches that of a uniform, disordered granular continuum. In the intermediate range, $0.01 < 2R/L < 1.0$, we may suppose that macroscopic heterogeneities produce high stressed columns of grains in which contact areas are large and dynamic moduli are high.

The theoretical predictions for the glass bead samples in which ρ_s = 2450 kg/m^3, ν = 0.21, and μ = 29.655 GPa are given in Table 3. In figure 9, we have plotted measured V_p and V_s vs. uniaxial pressure as a function of grain size, along with the theoretical curves. The porosities in the two samples are virtually identical. As the pressure increases from 0.1 to 35 MPa, the porosity in the 149-210 μm sample decreases from 0.392 to 0.372; while porosity in the 74-105 μm samples decreases from 0.387 to 0.370. The two sets of data for the 74-105 μm and 149-174 μm samples represent the largest discrepancy,

TABLE 3

Predicted velocities for soda-lime glass beads, where ρ_s = 2.45×10^3 kg/m^3, $\nu = 0.21$, and $\mu = 29.655$ 6Pa.

	V_p	V_s	V_p/V_s
sc	$1000\ p^{1/6}$	$664.5\ p^{1/6}$	1.505
hcp	$1166\ p^{1/6}$	$808\ p^{1/6}$	1.443
fcc	$1155.4\ p^{1/6}$	$817\ p^{1/6}$	1.414

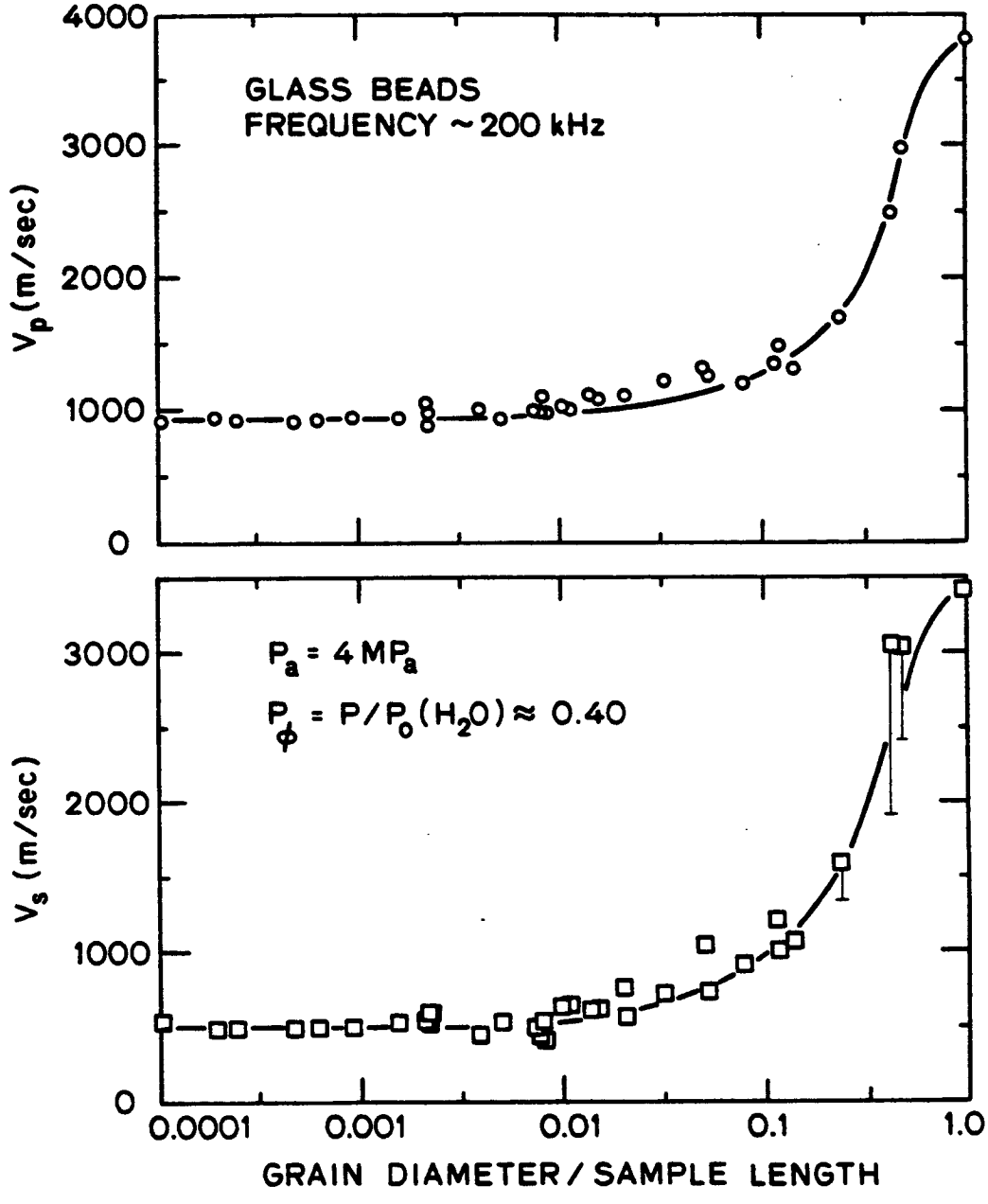

Fig. 8. V_p and V_s vs. grain diameter divided by sample length. Grain diameter divided by sample length is the inverse of the number of grains along the primary wave path.

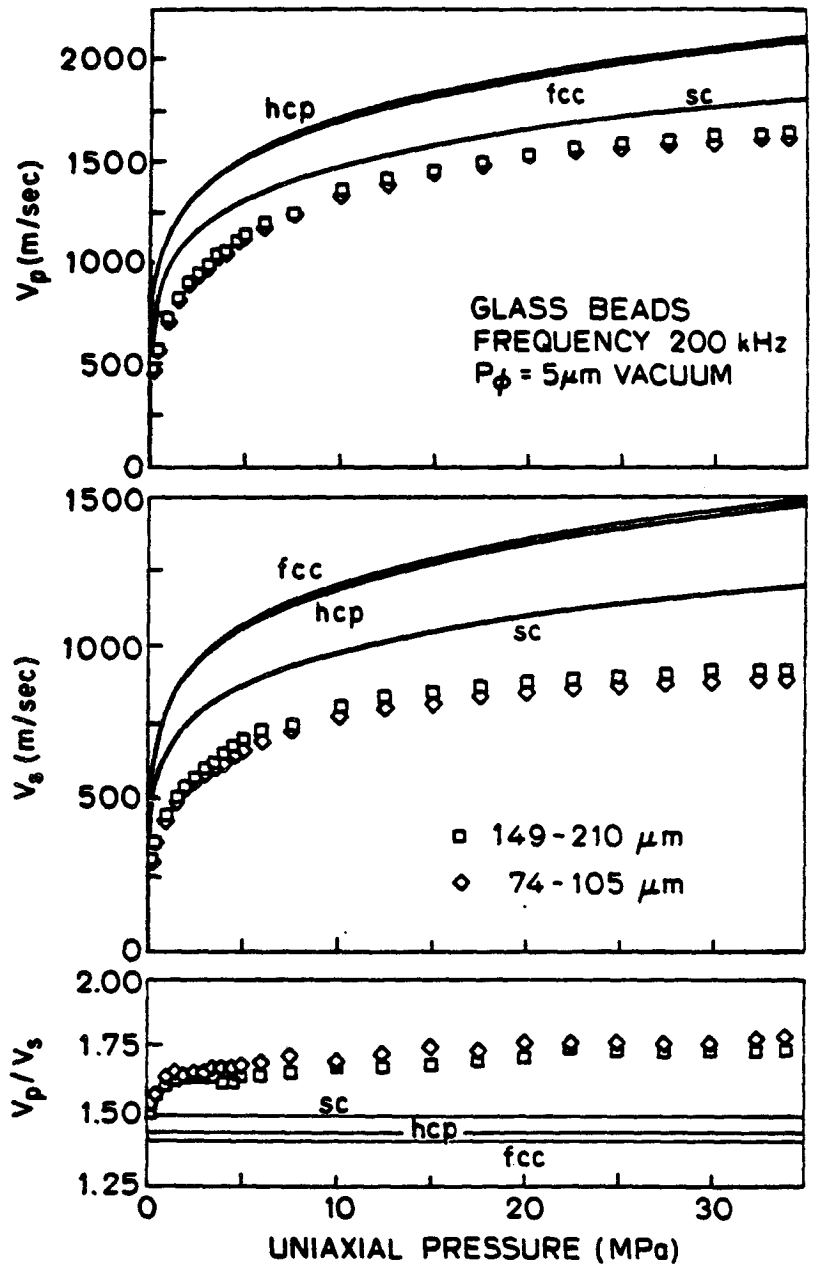

Fig. 9. V_p , V_s , and V_p/V_s vs. uniaxial pressure in vacuum dry samples of different size glass beads. Also plotted are the theoretical predictions from Table 3.

~ 4%, that we have measured in the eight sieve fractions between 62.5 and 250 μm. The larger sieve fractions consistently tend to have higher velocities than the smaller sieve fractions, particularly in shear, but by no more than 4%.

Within experimental tolerance, the model correctly predicts that velocities are indeed independent of grain size. At worst, we find an extremely weak dependence.

However, the velocity dependence on pressure does not conform to a uniform 1/6 power law. In fact, we observe distinct segments of behavior (figure 10). V_p is best fit by 920 $p^{1/6}$ above 10 MPa, but below that pressure it is best described by 750 $p^{1/4}$. While V_s is given by 525 $p^{1/6}$ at high pressures, and by 450 $p^{1/4}$ at low pressures. The transition occurs at lower pressure, 5 MPa, in shear wave velocities. In short, what we are observing is a steeper 1/4 power law dependence at low pressures, rapidly flattening to a Hertz-Mindlin dependence at intermediate pressures.

If the packing in our disordered samples could be modeled as a mixture of clusters of hcp and sc microstates, as suggested by Smith et al. (1927) the measured velocities would fall between the hcp and sc predictions. Clearly, they do not.

Lastly, V_p/V_s was predicted to be independent of pressure. In figure 9, we find a significant dependence on pressure, particularly below 5 MPa.

6. ADHESION AT GRAIN CONTACTS

The model which has been derived for ordered packings of spheres in Hertz-Mindlin contact has achieved limited success. Improvement may be attempted in two ways: i) better understanding of individual

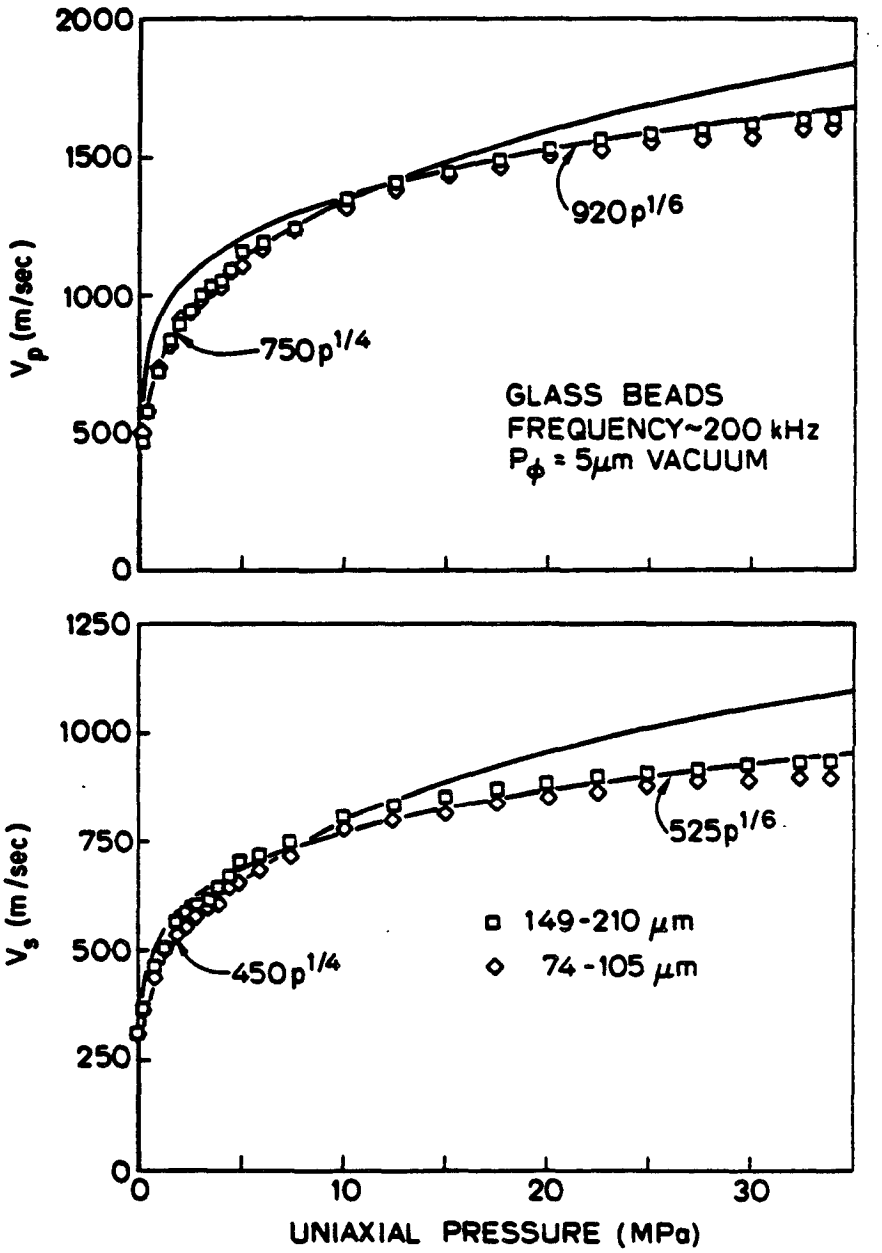

Fig. 10. V_p and V_s data replotted along with best fit power laws.

grain-to-grain contacts and ii) better understanding of disordered packings of grains.

We have thus far treated the grain-to-grain contacts as a purely mechanical interaction responding to a compressive load. A Hertz-Mindlin contact cannot sustain an applied tensile traction. Observations of contacts between spheres and flat plates of low modulus materials have shown that at low applied loads, the Hertz theory (equation 6) predicts contact radii that are consistently too low.

Associated with every surface is a surface energy resulting from the action of surface forces. As two grain surfaces are brought together, there exists an equilibrium separation, z_0, at which the competing van der Waals forces of attraction and repulsion between atoms and molecules in the two grains are balanced. At a distance less than z_0 the surfaces will repel each other. At distances greater than z_0 they will attract. The force per unit area varies as a function of separation by

$$\sigma_a = -Az^{-3} + Bz^{-6} \tag{24}$$

which graphically has the familiar appearance of figure 11.

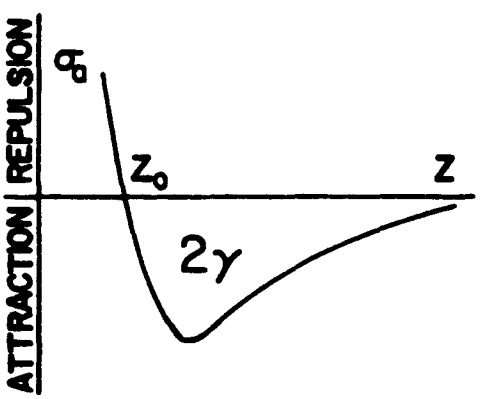

Fig. 11

Repulsion is taken to be positive such that we may speak of heights of energy barriers. Attraction is to be negative, thus we may discuss the depth of energy minima. It is clear that in this construction, a tensile force or force of adhesion must be exerted in order to separate the two grains. The two surfaces each possess a surface energy per unit area, γ, equal in total to the work done in separating the surfaces. γ is given by (Verwey and Overbeek, 1948)

$$2\gamma = \int_{z_0}^{\infty} \sigma_a dz = \frac{A}{6\pi z_0^2} \tag{25}$$

where A is known as the Hamaker constant. The surface energy of silica in a vacuum has been reported to be ~0.280 J/m^2 (Brunauer et al., 1956). The Hamaker constant of quartz is roughly 7×10^{-20} J (Israelachivili and Tabor, 1973). z_0 is then $\tilde{=}$ 1 to 2 Å, and the maximum adhesive fraction is ~10 GPa, which falls off 2 orders of magnitude at a separation of 5 Å. The forces of adhesion are large, but their range of action is quite small.

Johnson et al. (1971) have derived an exact expression for the modified Hertz contact area taking into account the surface energy. It is

$$a^3 = a_0^3 \left[1 + \frac{w}{n} \left\{ (2wn+w^2)^{1/2} \right\}\right] \tag{26}$$

where $w = 3\gamma\pi R$ and a_0 is the Hertz contact radius given by equation (6). Several new predictions are immediate. Surface energy generates a larger contact area at a given normal force, especially at small loads, as shown in figure 12. The dependence on normal force is flattened from $n^{1/3}$ to $n^{1/3} + n^{1/2}$.

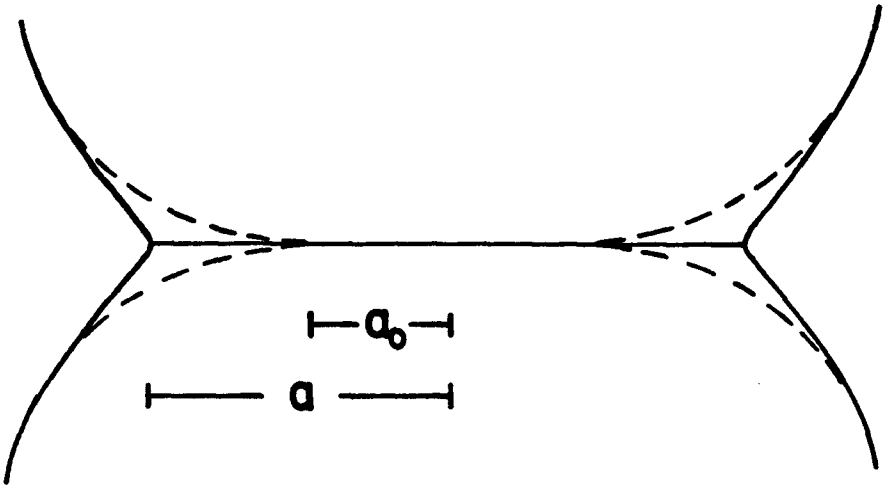

Fig. 12. Increase in the contact radius from A_0 (Hertz) to a (equation 27) due to the force of adhesion.

When $\gamma = 0$, equation (27) reduces to equation (6). At $n = 0$, the contact area remains finite and is given by

$$\hat{a}^3 = \frac{8(1-\nu)\ R}{3} \quad ; \tag{27}$$

and an applied tensile traction equal to

$$n = -\frac{3}{2}\ \gamma\pi R \tag{28}$$

is required to separate the spheres. Johnson et al. (1971) have verified these relations experimentally.

Another important point is that the energy loss per cycle under small amplitudes is no longer dominated by friction but by the surface energy which will resist grain slip at the contact edges. During each cycle as contact edges are deformed, hydrogen bonds between surface hyroxyls and molecular water may be broken and energy absorbed (Spencer, 1981). Velocities and Q^{-1} would then be strain independent.

The surface energy of quartz and silica glass is controlled by moisture. Indeed, the surface energy of silica immersed in water drops to 0.139 J/m^2 from 0.280 J/m (Van Voorhis et al., 1957). It is generally thought that the hydration of a fully hydroxylated silica (silanol) surface strongly increases the molecular repulsion forces (Aronson and Princen, 1978; Israelachivili and Adams, 1978; Pashley, 1980; Pashley and Israelachivili, 1981). Diagramatically, we see in figure 13 that hydration strengthens the short range repulsion forces, dramatically weakens the energy minima, and produces an energy barrier in the electrical double layer (DVLO theory; eg. Sonnatg and Strenge, 1972). Kitchner, 1971) has further postulated that a layer of silica gel forms at the silica surface.

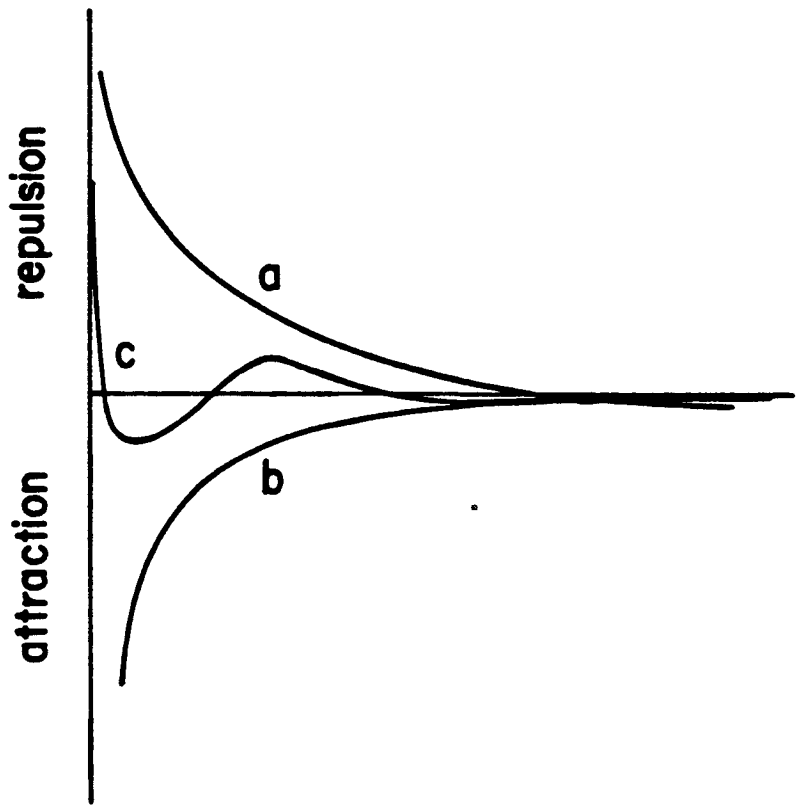

Fig. 13. Sketch of surface forces between wetted grains.

a) repulsion,

b) van der Walls attraction, and

c) resultant of curves a and b.

The reduction in surface energy substantially eliminates the adhesive contribution the the contact compliance. In our uniaxial experiments, we have consistently noted a significant volume expansion in vacuum dry samples when wetted with water. In sands (Hardin and Richart, 1963; Elliott and Wiley, 1975) and sandstones in general, (Pandit and King, 1979; Clark et al., 1980: Spencer, 1981; Murphy, 1982a) a strong defect in the dry frame moduli is observed with a loss of vacuum, or an increase in relative humidity, or bulk wetting. This effect is described in figure 5. Although the effect is relatively weak at 200 kHz, a 15% decline in the V_s of Ottawa sand at 0.1 MPa has been measured in the present experiments with the addition of 0.10 water saturation.

In short, adhesion, though crucial to the dry frame moduli is negligible in the wetted frame moduli. Adhesion cannot help to explain the behavior of V_s in figure 3.

Murphy (1982a) proposed an additional surface mechanism to explain the frame modulus defect. The surface tension of small amounts of water between two quartz grains applies a force of adhesion on the contact given by $n = 2\pi\tilde{\gamma}R$, where $\tilde{\gamma}$ is the surface tension of water. McFarlane and Tabor (1951) have indeed observed such adhesion between a glass sphere and a glass plate as a function of relative humidity. The effect is negligible below a relative humidity of 0.80 and reaches a plateau at 0.85 or 20 monolayers of H_2O. We have observed no such dependence in dynamic moduli, only a monotomic, exponential decrease with increasing relative humidity (Murphy, 1982a; Clark et al., 1980). Although this mechanism is crucial in the construction of sand castles, it appears to be irrelevant to the acoustic properties of granular sediments.

7. GRAIN ROUGHNESS

Grain roughness may or may not be significant in the glass bead samples in which the individual spheres are quite smooth; but it is undoubtedly an important consideration in quartz sand where the relief on the grain surfaces is of the order of 1 μm on a 200 μm grain. Moreover, the nature of the analysis for micro-roughness suggests a fruitful approach to disordered packing.

Let us assume that a nominally flat surface is rough. It has asperities with spherical summits all of radius, ε , which deform elasticity in accordance to equations 6-9. Following Greenwood and Williamson (1966), as the rough surface approaches to a distance h from a truly flat plane, the probability of making contact at any given asperity of height, ℓ is

$$\text{prob } (\ell > h) = \int_h^\infty \phi(\ell)\, d\ell \tag{29}$$

where ϕ is the probability distribution of asperity heights. If one further assumes that the asperities do not interact and defines s to be the standard deviation of asperity eights or roughness, η to be the density of asperities, and $\tilde{A}$ to be the nominal macroscopic contact area we obtain

$$\begin{aligned} m &= \eta \tilde{A}\, F_0(h/s) \\ A &= \pi \eta A \varepsilon s\, F_1(h/s) \\ n &= \frac{16\mu}{3(1-\nu)} \eta A\, \varepsilon^{1/2}\, s^{3/2}\, F_{3/2}(h/s) \end{aligned} \tag{30}$$

where m is the number of contact sites, A is the actual contact area,

and

$$F_k(h/s) = \int_z^\infty (u - \frac{h}{s})^k \phi^*(u)\, du \quad . \tag{31}$$

$\phi^*(u)$ is the height distribution scaled such that its standard deviation is 1.

Two particular distributions are of interest. Measured height distributions tend to be Gaussian (Greenwood and Williamson, 1966). However an exponential distribution is a fair approximation to the uppermost 25% of the asperities and gives a simple analytic solution. This solution yields results very close to those obtained numerically for the Gaussian distribution by Greenwood and Williamson (1966).

Given an exponential distribution of heights, i.e. $\phi^*(u) = e^{-u}$, then the functions $F_k(h/s)$ are just $k!e^{-h/s}$. Equations (30) reduces to

$$\begin{aligned} m &= \eta\tilde{A}\, e^{-h/s} \\ A &= \pi(\eta\varepsilon s)\tilde{A}\, e^{-h/s} \\ n &= \frac{4\mu\pi}{1-\nu}^{1/2} (\eta\varepsilon s)\, (s/\varepsilon)^{1/2}\, A\, e^{-h/s} \quad . \end{aligned} \tag{32}$$

Eliminating the separation (h/s), we find that both the number of contact sites and the area of contact are exactly proportional to the normal force. Thus, the average size of the contact, and the contact pressure are independent of the load. Of course, a given individual contact grows in area with load, but simultaneously new smaller contacts are being formed. There exists a balance which leaves the average unchanged.

The calculations for a Gaussian distribution show a similar behavior except that the proportionalities, which were exact for the exponential distribution, now vary slowly with load.

In the case of the approach of two rough spheres, the global curvature of the bodies limits the apparent contact area. The asperities can no longer be assumed to be independent, for the force on one contact may change the height of its neighbors. Greenwood and Tripp (1967) have numerically solved this problem for a Gaussian distribution of asperity heights. Hertzian contact theory (equations 6-9) is found to be the high load limit for rough spheres. At low loads, the pressure distribution strongly contrasts with the Hertz predictions. The nominal contact area is an order of magnitude larger, and the maximum pressure is 1/3 smaller. Of course, the actual contact area is much smaller than the Hertzian value. And the pressures on the microcontacts are much higher than Hertzian pressures. They are in fact of the same order as those for nominally flat surfaces, and again are proportional to $\frac{2\mu}{1-\nu}(s/\varepsilon)^{1/2}$. The proportionality factor varies slowly with the magnitude of the load.

Some asperities may suffer plastic deformation. The plasticity index, ζ, which combines the material and topographic properties of a surface has been shown to be an accurate criterion for the onset of plasticity (Greenwood and Williamson, 1966). ζ is

$$\zeta = \frac{\mu}{H(1-\nu)}(s/\varepsilon)^{1/2} \tag{33}$$

where H is the hardness of the material. 5.15×10^{10} kg/m^2 is the hardness reported by Potters Industries Inc. (1980) for the glass beads. Sharp and rough grains with ζ above 1 will almost certainly

have some plastic deformation, while round and smooth grains with ξ below 0.6 will strain elasticity.

The general result however does not rest on the particular constitutive model governing the contacts. The behavior at low loads is not determined by the mechanics of the asperities but rather by the statistics of the surface roughness. If increasing the load creates new contact sites, then $A \propto n$. At high loads where increasing the load simply enhances the size of the existing contacts, the micromechanics takes over, and in the elastic case, $A \propto n^{2/3}$.

Permit one further point for completeness. Surface roughness may inhibit adhesion (Fuller and Tabor, 1974). Consider a dimensionless adhesion parameter, ξ ,

$$\xi = \frac{2\mu(1+\nu)\, s^{2/3} R^{1/2}}{\gamma\varepsilon} \quad . \tag{34}$$

The demoninator is a measure of the adhesive force experienced by a sphere of radius, ε . The numerator is a measure of the elastic force needed to push a sphere of radius ε to a depth s into a solid of modulus, $2\mu(1+\nu)$. ξ is the ratio of the compressive elastic forces exerted by the higher asperities which are attempting to separate the surfaces and the adhesive forces which are attempting to hold the surfaces together. When the adhesion parameter is small, the adhesion is high. As the surface roughens the adhesion parameter increases. When the asperities are sufficiently high, the surfaces are effectively pried apart and the adhesion falls to a small value.

8. DISORDERED PACKINGS OF UNIFORM SPHERES

In crystallographic arrays, the porosity and coordination number are fixed, microscopically uniform, and known. But in natural and artificial sediments, the packing is disordered. Porosity and coordination are undetermined. They vary microscopically, and their continuum values are averages or probability densities. Porosity can be measured. Coordination number is more difficult to obtain. Most relevant to our interest, porosity and coordination number, especially coordination number, are dependent on pressure.

Without any exaggeration, it is the relation between coordination number and effective pressure which controls the dynamic frame moduli in marine sediments. In this section we continue our analysis of compacted artifical materials, carefully building a solid understanding of the physics. We shall show in Section 11 that the theoretical framework proposed in this section fits a compiled set of in situ data remarkably well.

Virtually no previous work has focused on the effects of disorder on velocities. Gangi (1981) reflects the state-of-the-art.

Brandt (1956) derived a model for the random packing of elastic spheres in Hertzian contact. Coordination number was assumed independent of pressure and fixed at 8.84. V_p was found to vary with $p^{1/6}$.

We find that the change in coordination number with pressure successfully explains our glass bead results. The process involved is similar to that in the case of grain roughness. At low pressures, the increase of contact area due to the creation of new contact sites dominates the pressure dependence, yielding $V \propto p^{1/4}$. At high pressures, coordination number becomes independent of pressure, and the Hertz-

Mindlin $p^{1/6}$ dependence takes over.

Smith et al. (1927) and Bernal and Mason (1960) have studied the porosity ϕ, coordination number ψ, and their relationship, $\phi = f(\psi)$, in random packings of uniform spheres. Recall that the hcp and fcc packings are the densest possible for uniform spheres with $\phi = 0.2596$ and $\psi = 12$; while, the sc packing is the loosest possible ordered packing with $\phi = 0.4795$ and $\psi = 6$. Random packings have a narrower range of porosities. Random close packing, rcp, yields $\phi = 0.36$. Random loose packing, rlp, has $\phi = 0.40$ (Scott, 1960). Bernal and Mason (1960) were able to measure the distribution of coordination numbers in random packings of uniform spheres. More importantly, they were able to distinguish between those grains which were actually in contact and those which were near to contact. In rcp, the mean actual contacts are 6.4 per grain. While the total coordination, adding actual plus near, is 8.5. The mean actual contacts in rlp are 5.5, and total coordination is 7.1 These results are plotted in figure 14 along with measurements from Smith et al. (1927).

The solid line curve in figure 14 corresponds to the mean total coordination at a given porosity. The porosities measured at 0.1 MPa in our glass bead experiments were roughly 0.40. Measured at 35 MPa, the porosity approached 0.37. The pressure increase decreases porosity, and in figure 13 we move up the solid line curve from 8.2 at 0.40 to 8.8 at 0.37. Yet this is the weak component of the effect. The actual number of contacts at low pressures is far beneath the line, perhaps below 5. The displacements associated with low uniaxial pressure cause the near contacts to progressively come into actual contact. Thus in figure 14, low uniaxial pressures (<10 MPa) drive the rlp

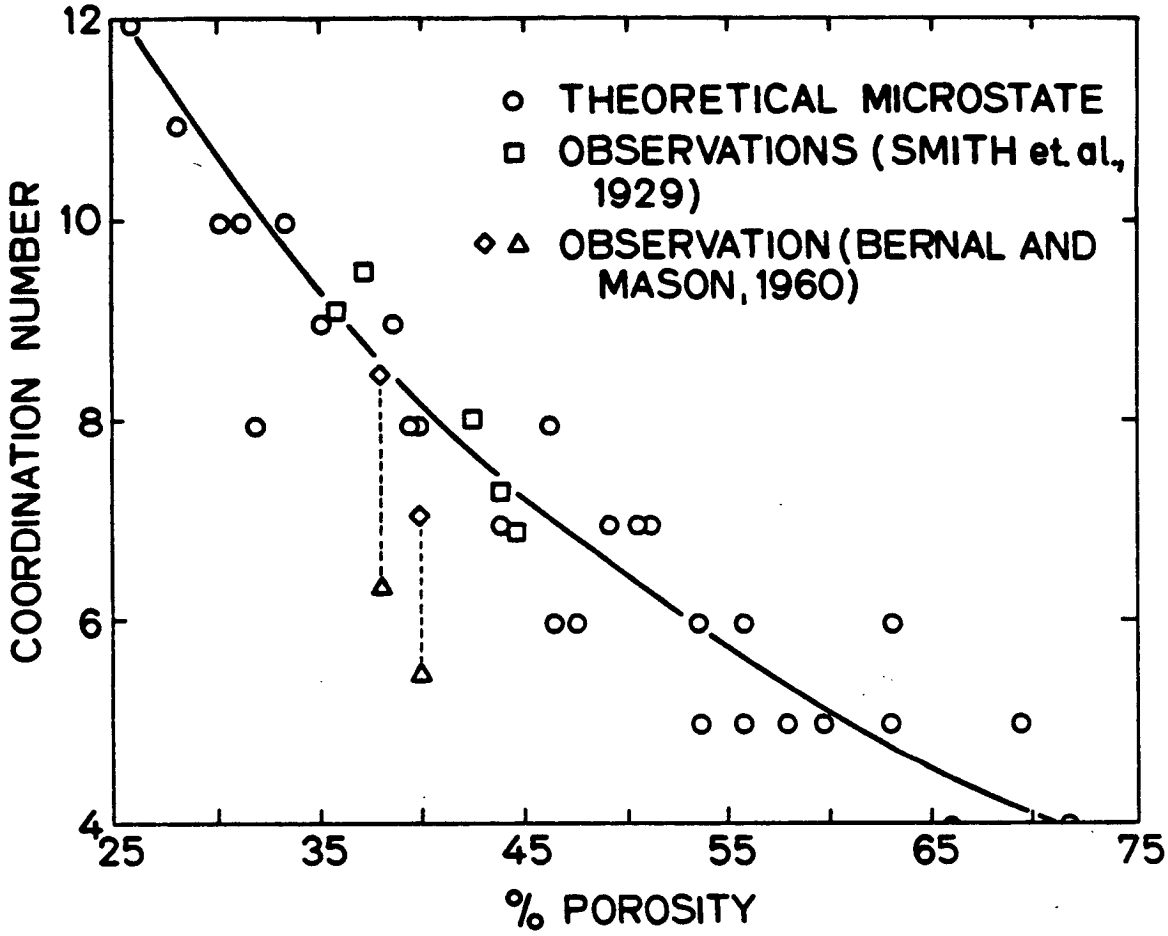

Fig. 14. Coordination vs. porosity. The actual number of contacts in Bernal and Mason's (1960) packings denoted by (△). The total number of contacts, actual plus near, are denoted by (◇). The theoretical microstates represent twenty-eight possible arrangements of ordered and disordered unit cells.

actual contact number nearly vertically to the solid line. This is the dominant mode of contact area increase at low pressures. By 15 MPa the coordination varies with porosity solely along the solid line.

The argument may be readily formulated in terms of roughness. Consider two layers of spheres, separated by a small distance where the roughness elements assume the radius of the spheres. The centers of the spheres in the "flat" layer are fixed at a depth R below the surface. The centers of the spheres in the approaching plane are distributed in depth between 0 and R according to $\Phi(w)$. The governing equations then become equations (30), if we substitute R for ε.

In the case of an exponential distribution of sphere heights above the nominal plane, we find that the displacement, α , for two layers of distributed heights is

$$\alpha = 2s \ln\left[\frac{(1-\nu)n}{\mu\eta\pi^{1/2}\tilde{A}(s/R)^{1/2}} \right] \qquad (35)$$

where s is the standard deviation of heights or roughness, $\eta = 1-\phi$, the density of spheres, and $\tilde{A}$ is the nominal area, say the area of a horizontal section in the sample. The normal compliance of two layers of distributed heights is

$$J_n = \frac{d\alpha}{dn} = \frac{2s}{n} \quad . \qquad (36)$$

The contact area, A , can be similarly determined. Eliminating the separation, it is clear that A is proportional to n.

An other case of interest is a random or uniform distribution of heights 1/R above the nominal plane. Physically, such a distribution corresponds to a contant rate of increase in contact sites per unit

displacement. The displacement, , is given by

$$\alpha = \left[\frac{15(1-\nu)\, n}{4\mu\nu\tilde{A}\sqrt{2}\, R^{1/2}} \right]^{2/5} , \qquad (37)$$

and the normal compliance is

$$J_n = \frac{d\alpha}{dn} = .68 \left[\frac{1-\nu}{\mu\nu\tilde{A}\sqrt{2}\, R^{1/2}} \right]^{2/5} n^{-3/5} \qquad (38)$$

The contact area can be shown to be proportional to $p^{4/5}$.

Defining p to be $\frac{n}{4\eta\tilde{A}R^2}$, velocities and contact area may be related to pressure. The results are given in Table 4 along with the corresponding Hertz-Mindlin predictions

TABLE 4

	Exponential Distribution	Random Distribution	Hertz-Mindlin
$V \propto$	$p^{1/2}$	$p^{1/3.3}$	$p^{1/6}$
	$A^{1/2}$	$A^{5/12}$	$A^{1/4}$
	$A \propto p$	$A \propto p^{4/5}$	$A \propto p^{2/3}$

The behavior is strongly determined by the probability distribution chosen. A satisfactory description of a compacted sphere pack would include a 1/4 dependence at low pressures which implicitly flattens to Hertz-Mindlin behavior at high pressures. The exponential distribution is obviously to disperse for a compacted sphere pack. Neither is the random distribution a satisfactory model. It is however instructive. Again, it implies a constant rate of increase in contact sites per unit displacement. Following the trends in Table 4, some interesting points

may be drawn about the character of a satisfactory model. Obviously, $V \propto p^{1/4}$ falls between the random distribution and the Hertz-Mindlin predictions. The corresponding proportionalities among the other variables calculated from the trends in the table would be $V \propto A^{1/3}$ and $A \propto p^{11/15}$. In terms of the statistical microprocess involved, we may speculate that the rate of increase in contact sites must fall off faster with load than does the displacement.

Recall from the previous section that Greenwood and Tripp (1967) found that a Gaussian distribution of roughness heights on a sphere behaved like an exponential at very low pressures, but at higher pressures approached a Hertz-Mindlin limit. In fact, we find in Section II that in self-loaded, uncompacted, in situ continental shelf sands, the velocities are well described by our model based on the exponential distribution in the first 50 m of depth. Then, from 50 m to 100 m, the velocities follow the predictions based on the random distribution. Presumably, with continuing depth, the velocities would pass through a behavior associated with the 1/4 power dependence before reaching the Hertz-Mindlin state at some greater depth.

The Gaussian distribution actually corresponds in granular sediments to the radial probability density of nearest neighbors. A physical interpretation of the compaction process is given with the aid of figure 15. The probability of finding a grain center at a radial distance, $2R-\Lambda < r < 2R+\Lambda$, is represented by a Gaussian distribution. The actual number of contacts per grain is given at the intersection of the cumulative distribution with the vertical line 2R. At very low pressures, the grains are disperse. The mean is outside the distance, 2R (figure 15a). Fewer neighboring grains are in contact now than are

likely to come into contact in the future (with the application of pressure). That is, the liklihood of an increase in the number of contacts resulting from an increment in pressure is very high. The shape of the segment of the Gaussian distribution which intersects 2R is well approximated by an exponential distribution. With the application of small loading the packing will tighten. The distribution will narrow and will displace towards the origin. At some small applied pressure, the mean will lie on 2R (figure 15b). At this point, the number of grains which are in contact is equivalent to those which are likely to come into contact in the future. Here, the uniform or random distribution is a good approximation. With increased pressure, the mean is now driven inside 2R (figure 15c). That is, more grains are currently in contact than are likely to come into contact in the future. The distribution now intersects 2R on the down side of the distribution. Here, $V \propto p^{1/4}$. And at some higher pressure still, the distribution is almost entirely within 2R (figure 15d). It is now highly unlikely that a grain will gain any new contacts with additional increments of pressure. The sediment is now a Hertz-Mindlin material.

We can summarize this model by saying that the frame moduli in a granular sediment qualitatively evolve with the state of compaction. This model would suggest that the evolution we observe in the laboratory samples is truncated due to pre-compaction.

The model also implies specific predictions about the velocity depth gradients in uncompacted, self-loaded, granular sediments. These predictions differ strongly with standing empirical models. In particular, the standing models predict a fixed pressure dependence with depth. The competing predictions are tested against in situ data in Section II.

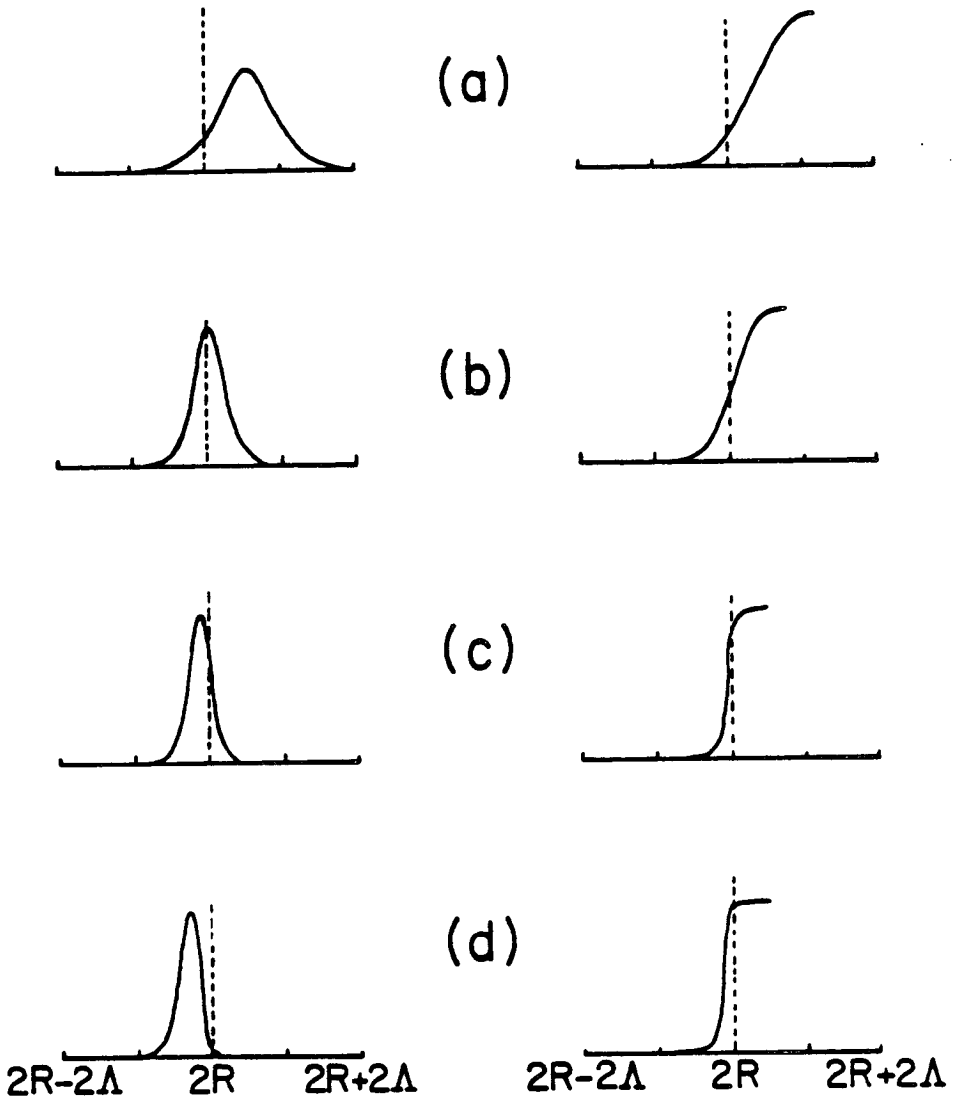

Fig. 15. Schematic micromechanical model of compaction, depicting the transformation of the Gaussian radial distribution with pressure. See text for explanation.

9. EFFECTS OF GRAIN ANGULARITY

We find that grain angularity produces three distinct effects on velocities: two through the micromechanics of the grain contacts, and the other on the packing. Each effect is separable.

First, recall that a principle assumption in the Hertz-Mindlin contact theory is that the radius of the contact is small compared to the radius of curvature of the grains. When a sharply angular grain comes into contact with another surface (figure 16), this assumption fails. (A similar situation prevails in the case of conformable bodies in contact, which is applicable to sandstones with large secondary quartz overgrowths.) The surfaces in the vicinity of the contact can no longer be modeled as quadric surfaces, and a higher order theory is required. The analysis has been developed for a number of special cases, and approximate solutions have been found by Cattaneo (1947), Deresiewicz (1961), Steurmann (1941, 1943), Lunberg (1939), and Goodman and Keer (1965). Galin (1961) surveys an extensive Russian literature on the subject. The general, relevant conclusion that may be drawn from this work is that the higher order load-displacement relations are stiffer. That is, elastic contact compliances between angular grains are predicted to be stiffer than those between round grains.

Perhaps, another way to visualize this effect is more readily understood. In figure 17, we now focus on a cross-section of the contact gap between grains. In the case of spherical grains, the gap may be thought of as a flat Mavko and Nur (1979) type crack. Near the contact circumference, the contact gap is very compliant. In contrast when two angular grains meet in contact, the geometry of the

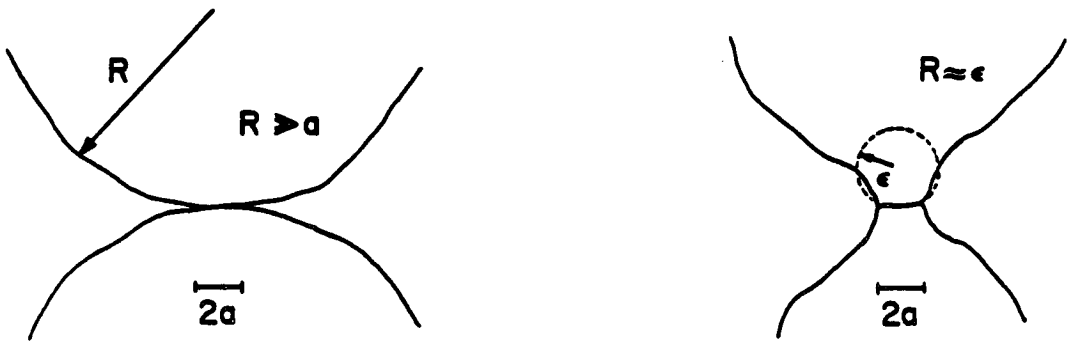

Fig. 16. Sketch contrasting the contact between two round grains (a) with that between two angular grains (b).

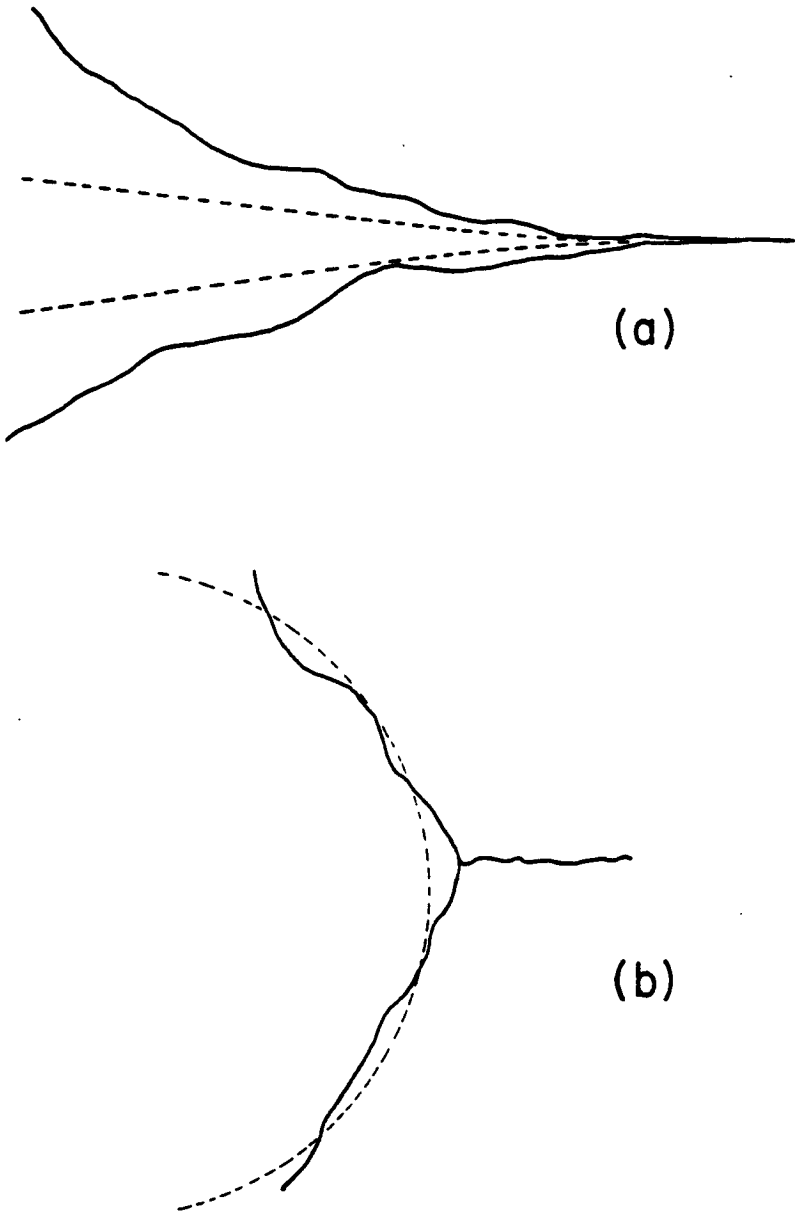

Fig. 17. Sketch contrasting the near-contact gap between two round grains in contact (a) with that between two angular grains in contact (b).

pore is more closely approximated by a Walsh (1965) type spherical or elliptical crack. This configuration is relatively stiff at the contact perimeter.

We have measured V_p and V_s in 149-174 μm, crushed and sieved glass beads as a function of uniaxial pressure. The sample was compacted to a porosity of ~0.40 at 0.1 MPa. The results are then compared in figure 18 to those for spherical glass beads. The velocities in the angular grains are consistently 15% higher. The V_p/V_s in the crushed glass is particularly high at 0.1 MPa.

The second effect of angularity on micromechanics is also evident in figure 18. Above 20 MPa, velocities in the crushed grains are nearly independent of pressure. The grains are so sharp; the radius of curvature of the grains, ε, at the grain contact is so small that the plasticity criterion in equation (33) has been exceeded. The micromechanics at the contact is plastic because ζ becomes greater than 1 above 15 MPa. At low pressures, V_s is proportional to $p^{1/6}$, while V_p goes as $p^{1/5}$. Apparently, the compaction was sufficient to close most of the near contacts. And at low pressures, the sample seems to behave elastically.

We have also measured V_p and V_s in three, 106-125 μm, quartz sands of differing angularities. The grains in Ottawa sand are round; those in Simplot sand are sub-angular; and Oceanside sand is angular. The results are plotted in figure 19. The porosities vary with pressure from 0.1 to 35 MPa. Those variations in the Ottawa, Simplot, and Oceanside samples are 0.408 to 0.396, 0.412 to 0.398 and 0.415 to 0.397, respectively. We observe virtually no effect of angularity

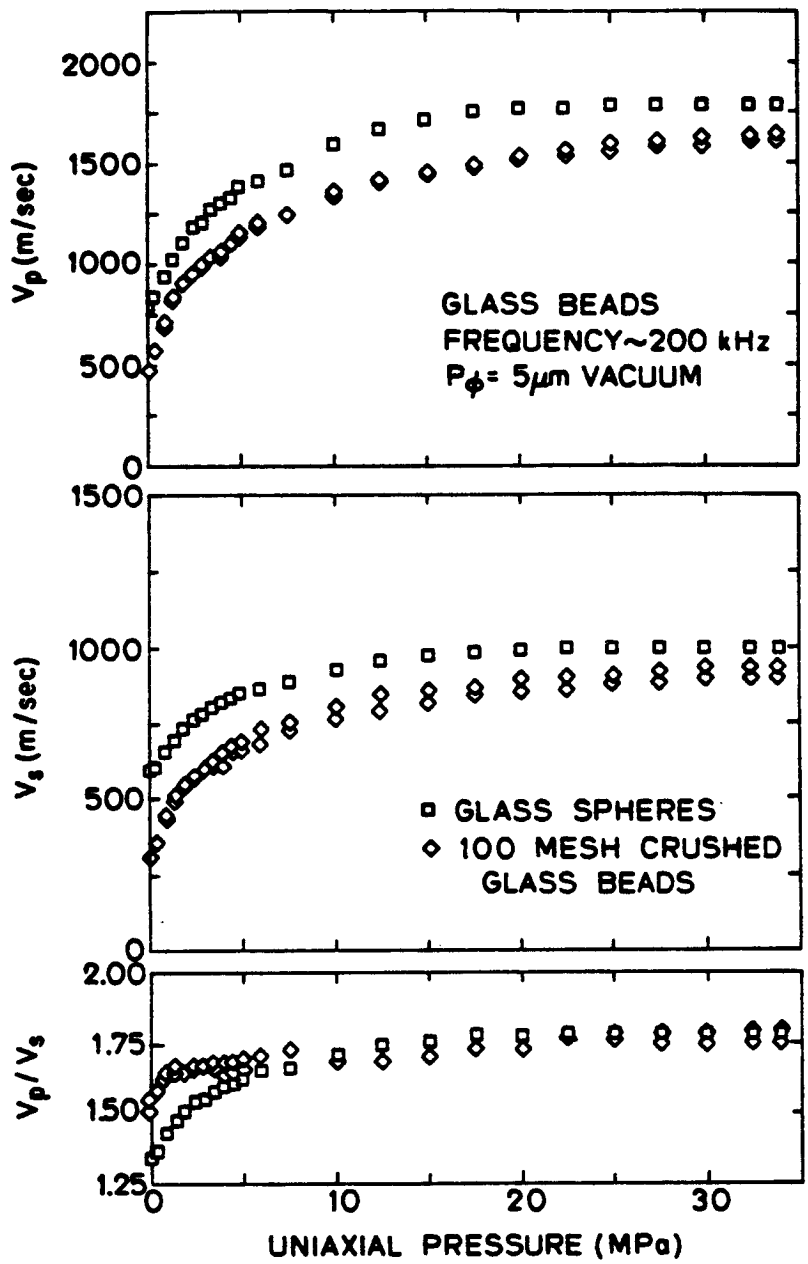

Fig. 18. V_p , V_s , and V_p/V_s vs. uniaxial pressure in 100 mesh crushed and screened glass beads, plotted along with data for spherical glass beads from figure 9.

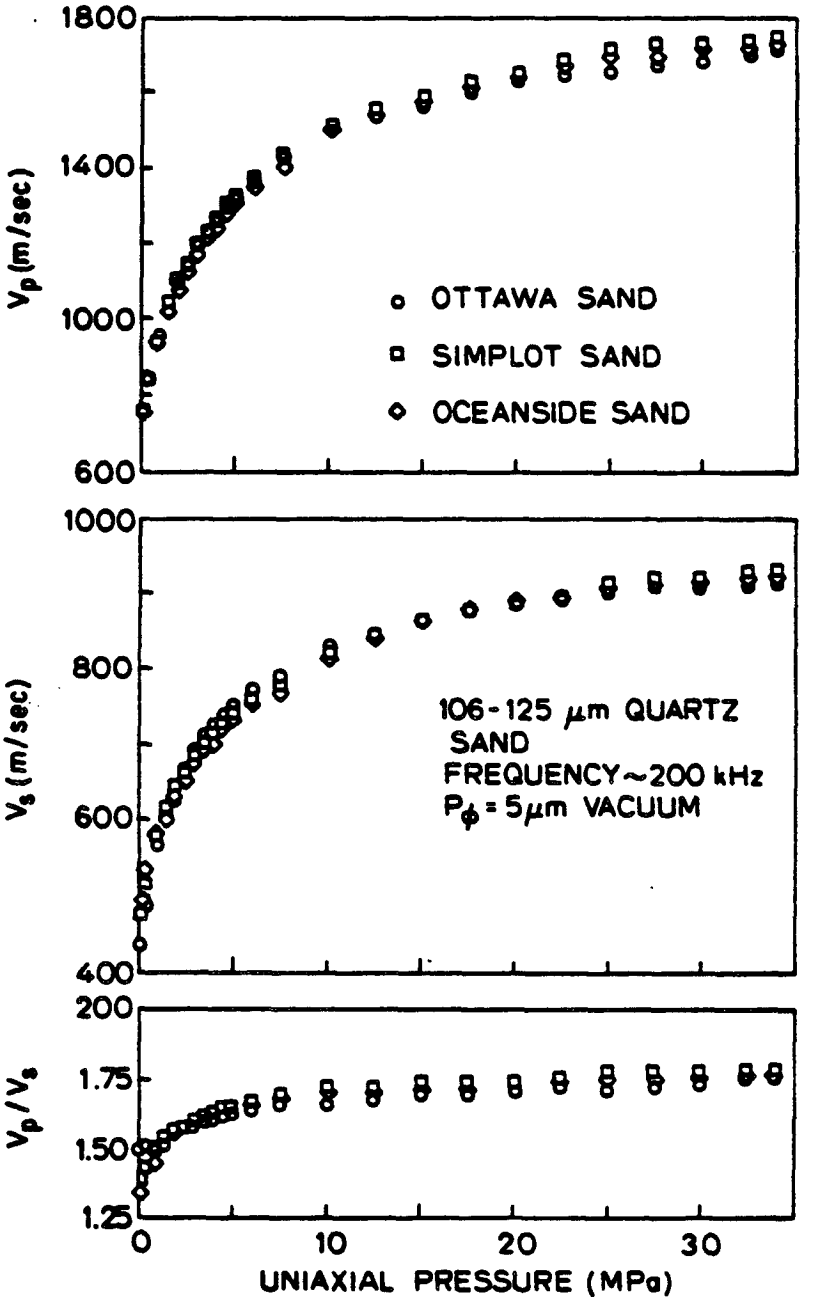

Fig. 19. V_p, V_s, and V_p/V_s vs. uniaxial pressure three vacuum dry sands of differing angularities.

except a relatively pronounced, ~10-15% increase in V_s at very low pressures.

In figure 20, we have replotted the V_p data along with a best fit power law. The expression, 920 $p^{1/6}$, is the same as the high pressure fit for the glass beads. The fact that it fits the entire pressure range so well indicates that again compaction had closed most of the near contacts. A better fit is obtained by the combination of 800 $p^{1/5}$ and 1000 $p^{1/7}$, suggesting that some plastic deformation is occurring at high pressures. The V_s dependence on pressure is very flat, again indicating plasticity.

The third effect of angularity is on the packing, and it is perhaps the most important in natural sediments. Consider an rlp of round grains and another of angular grains as sketched in figure 21. The rlp of round grains may assume a porosity between 0.40 and 0.42; while, the rlp of the angular grains achieves porosities between 0.45 and 0.58 (Brown and Richards, 1966). This result is plotted on a line graph in figure 22. The implications for natural sediments shall be discussed in the next section.

We would also like to suggest that a regular honeycomb of uniform and equant six-point grains would be a good candidate for an ordered packing of angular grains and exact analysis.

10. NATURAL GRAIN SIZE DISTRIBUTIONS AND POROSITY

Up to this point, we have considered packings of grains which have had uniform radii. In this section, we relax this constraint and investigate how natural grain size characteristics affect the frame moduli.

Grain size distributions in natural graunular sedimentar materials

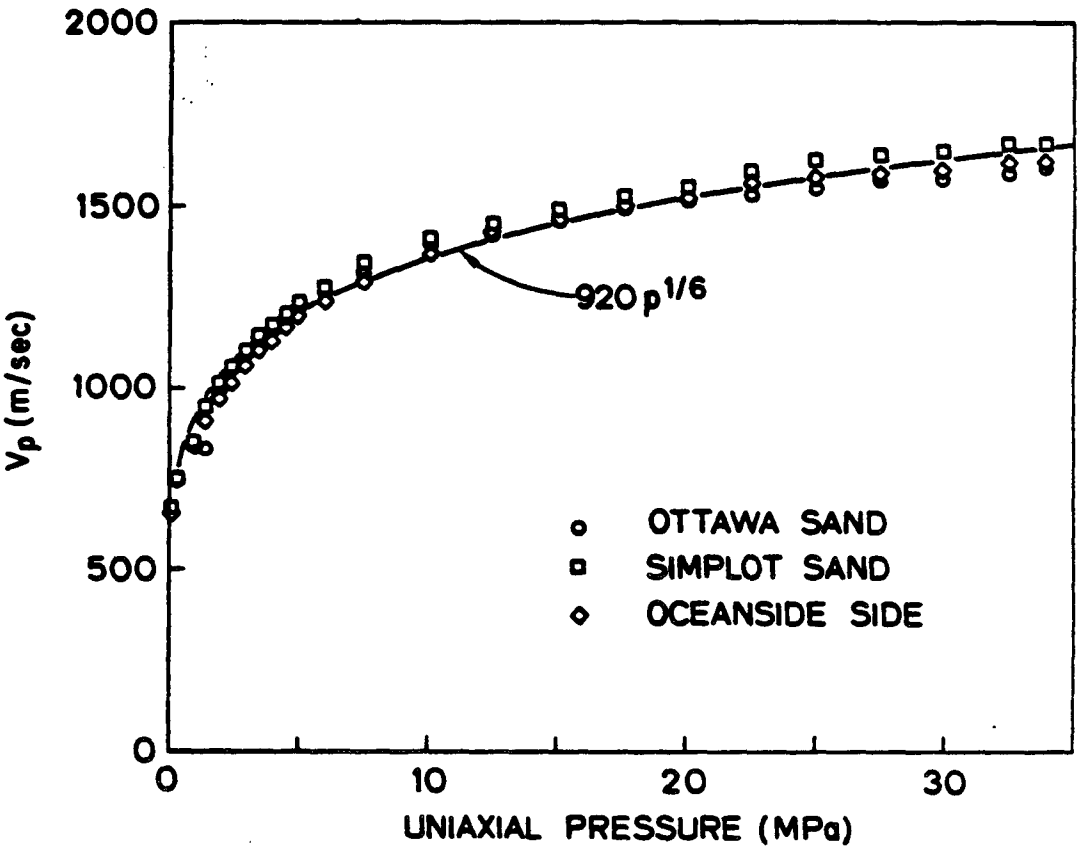

Fig. 20. 920 $p^{1/6}$ plotted against the V_p vs. uniaxial pressure data from figure 19.

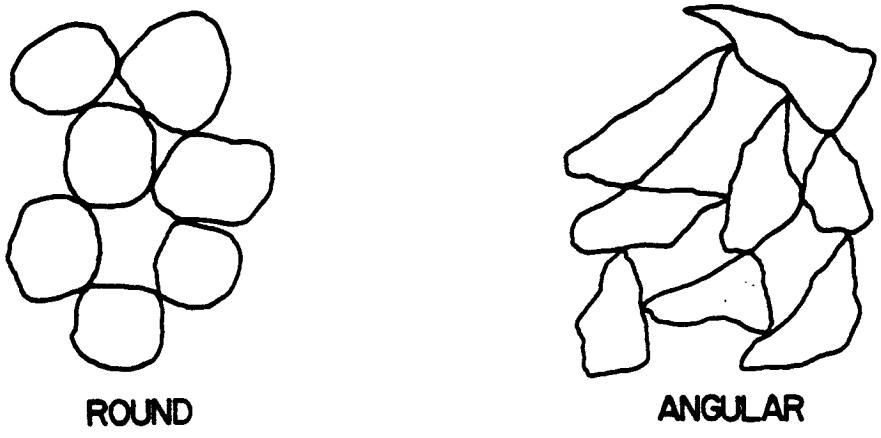

Fig. 21. Sketch contrasting the random loose packing of round grains with that of angular grains. The packing of angular grains has a higher porosity.

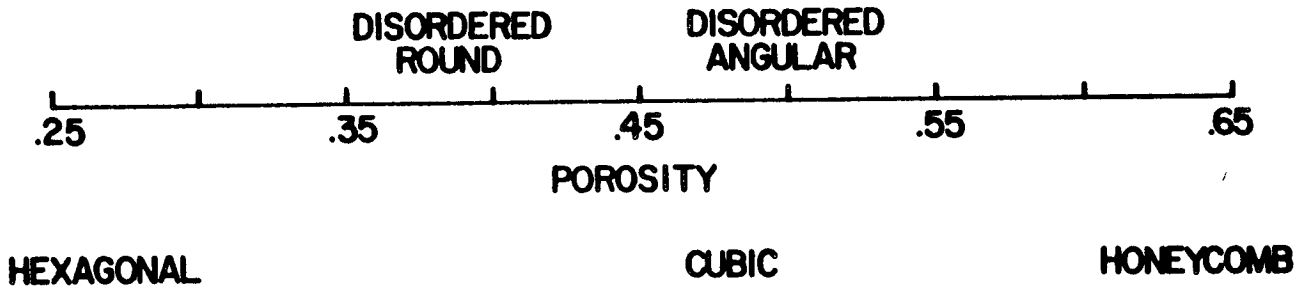

Fig. 22. Porosity for ordered and disordered packings of uniformly sized, yet differently shaped, grains.

are well described as sums of discrete log-normal components (Vischer, 1969). The first moment of the total distribution is the mean, $\bar{x}$. In phi (negative logarithm to the base 2) units, it is given by

$$\bar{x} = \sum_{i=1}^{n} f_i x_i \quad , \tag{39}$$

where f_i is the frequency in percent for each phi size fraction and x_i is the midpoint of each phi size fraction. The second moment or standard deviation, s , is a measure of the sorting.

$$s = \sum_{i=1}^{n} f_i (x_i - x^2)^{1/2} \quad . \tag{40}$$

If the grains are all spherical and surface effects are negligible, porosity declines with a decrease in grain sorting. This is a well-known fact based on the experimental measurements of Westman and Hugill (1930), Furnas (1931), Graton and Fraser (1935), Sohn and Moreland (1968), and Dexter and Tanner (1971). Norman et al. (1971) reached the same conclusion by computer simulation of circle coverings and sphere packs. The mechanism is obvious. The small sphere sizes are able to fill the intersitial pores between the larger grains. If such a model were relevant, the velocities would increase with decreasing sorting because of the increase in the number of contacts per grain.

Grains in natural sediments are not spherical. Indeed, the smaller the grains are, the more angular they become. As grain size diminishes, clevage, mineralogic habit, and crystallographic properties grow in relative importance. Therefore, implicit in any grain size variation in natural sediments is a change in grain shape.

We have gathered data for porosity in uncompacted sands as a

function of mean grain size and standard deviation from two sources: Pryor (1972) and Beard and Weyl (1973). A map of contours of constant porosity is given in figure 24. Of course, if the grains were all spherical, the contours would be horizontal lines of constant sorting. They are not. Mean grain size controls the porosity in uncompacted sediments with a significant variation due to the sorting (figure 4). Symbolically, we may write that

$$\phi \leftarrow \bar{x} | s \tag{41}$$

where $\leftarrow$ denotes an unspecified function and is read "is determined by".

We have also gathered data on coordination vs. porosity in granular materials. The compilation is plotted in figure 24. It is clear that broadly speaking, coordination number varies logarithmically with $1 - \phi$. Recall that the frame moduli are determined by the grain contact area, and that the contact area is most sensitive to a change in the number of actual contacts per grain, ψ . Thus, we may write that in uncompacted sediments at very shallow effective pressures,

$$V \propto A^{1/2} \leftarrow \psi \leftarrow e^{1-\phi} \tag{42}$$

The proportionality in relation (42) assumes that at very low effective pressures, the limit is well described by our model with an exponential radial distribution function. Relation 43 qualitatively explains the decrease in V_p with porosity in figure 2. The increase in porosity lowers the coordination number. The decline in coordination number reduces the grain contact area causing the frame moduli to soften. Consequently, V_p drops. Relation 42 indicates that a reduction in mean grain size was initially responsible for the entire process.

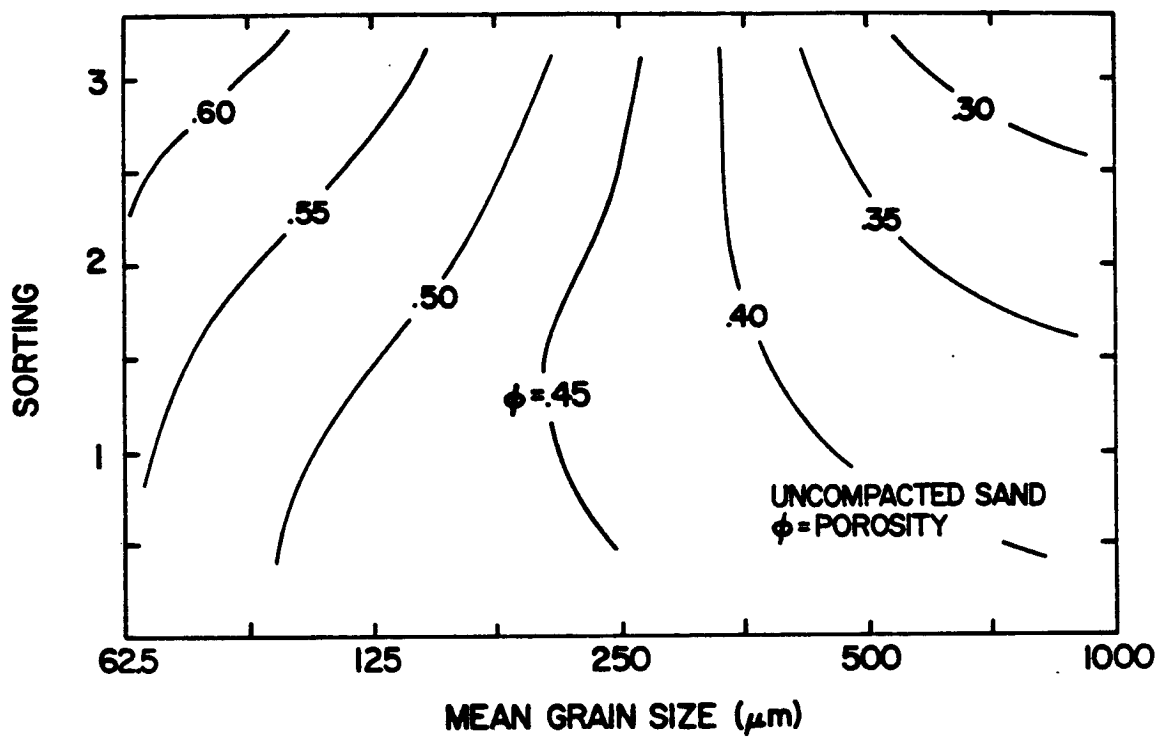

Fig. 23. Porosity as a function of mean grain size and sorting. Contours are rough, hand-drawn fits to data from Pryor (1972) and Beard and Weyl (1973).

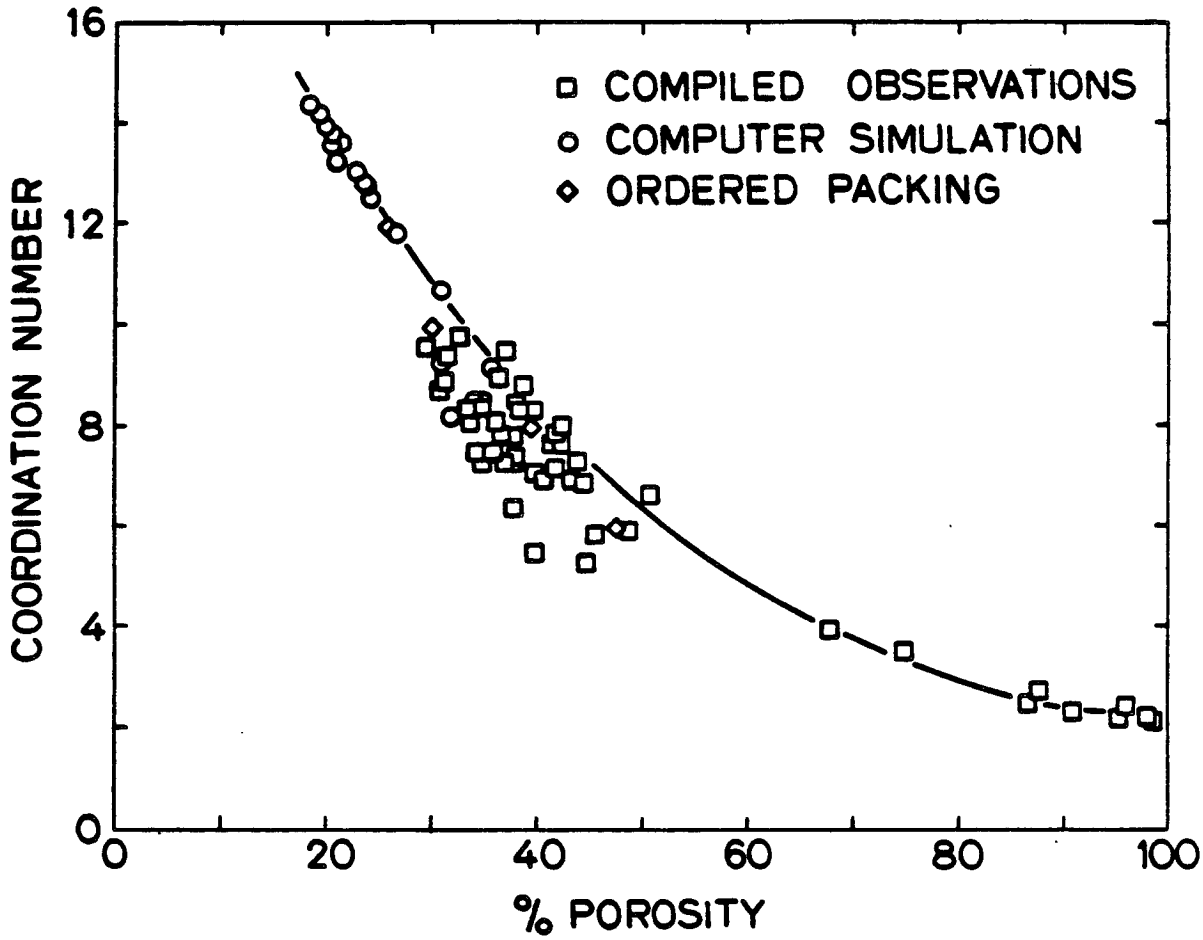

Fig. 24. Coordination number vs. porosity. The computer simulation results for random packing of spheres is from Norman and others (1971). Compiled observations are from Smith et al. (1927), Westman and Hugill (1930), White and Walton (1937), Oda (1977), Meissner et al. (1964), Yanagisawa (1978), and Marsal (1977).

The problem of shear wave velocities in figure 3 may now be resolved. We had sought in compacted sands a micromechanical effect which would significantly distinguish the behavior of the shear frame modulus from that of the bulk frame modulus. The data in figure 2 are considered to be reliable, and the Hamilton (1971, 1974b) and Smith (1974) shear velocity data are problematic. Our experiments have revealed only a small effect due to anularity, ~10-15% on V_s. In uncompacted sands, such an effect would be swamped by the effect represented by relation (42). Therefore, without equivocation, we remove the problematic "data" from figure 3, leaving figure 25.

11. VELOCITIES VERSUS DEPTH

Hardin and Richart (1963), Gardner et al. (1964), and Domenico (1977) have measured V_s in compacted sands varying with the 1/4 power of confining pressure. Seed and Idriss (1970), Hardin and Drnevich (1972a), Ohsaki and Iwasaki (1973), and Iwasaki and Tatsuoka (1973), Sherif and Ishibabi (1976), and Yanagiswa (1978) propose empirical equations for in situ sands of the general form

$$\rho V_s = c \cdot fcn(\phi) \cdot p_c^m \qquad (43)$$

where m is constant and close to 1/4. Hamilton (1980) settles on a simple power law for water saturated fine sand, $V_s = 128h^{0.28}$, where h is the depth. He also suggests another similar relationship, $V_s = 104.33h^{0.312}$, as a better fit to the data of Ohta and Goto (1978).

For compressional wave velocity, Hamilton (1978, 1980) proposed $V_p = 1805h^{0.015}$.

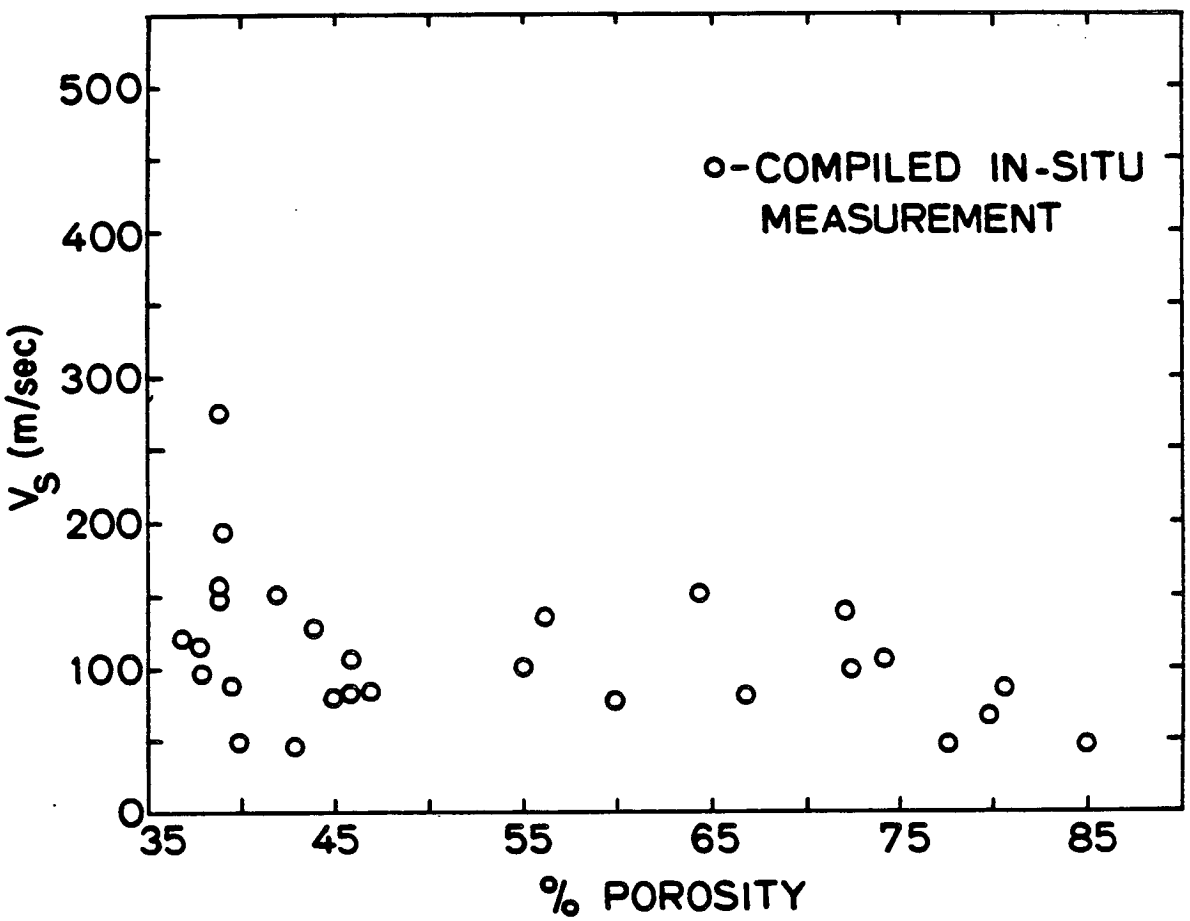

Fig. 25. V_s vs. porosity in in situ sediments.

We have compiled in situ measurements of V_s versus depth in water saturated sands from Barkan (1962), Kudo and Shima (1970), Stokoe and Woods (1972), Stokoe and Richart (1973), Cunny and Fry (1973), Hamilton (1976), Anderson et al. (1978), and Arango et al. (1978). The data are presented in figures 26 and 27.

In figure 26, Hamilton's predictions are plotted against the data. The predictions from our compaction model based on the Gaussian radial distribution function are plotted against the data in figure 27. The three curves presented are for the limiting cases of exponential and random distributions and the "1/4 power" behavior. The wetted shear frame moduli in the respective cases vary as p, $p^{3/5}$, and $p^{1/2}$. We substitute the proportionalities for μ_{wr} in the Biot-Gassman equations (equation 3). Time constraints have as yet precluded quantitative development of the model, and so the coefficients were determined by best fit.

No one curve describes the data accurately. The curve, 75 $p^{1/2}$, describes the very shallow, lower velocity data - presumably the most disperse sands - very well. The curve, 160 $p^{1/3.3}$, quite accurately describes the upper bound for the higher velocity, very shallow data, as well as most of the data between 50 and 80 m. The curve, 200 $p^{1/4}$, satisfactorily describes the data above 80 m. In other words, each curve is successful depending on the state of compaction. Perhaps shear velocity depth profiles rather than just shear velocity may be a useful tool for determining the extent of compact in a granular sediment.

This result strongly suggests that a rigorous development of a compaction model based on a Gaussian distribution function may

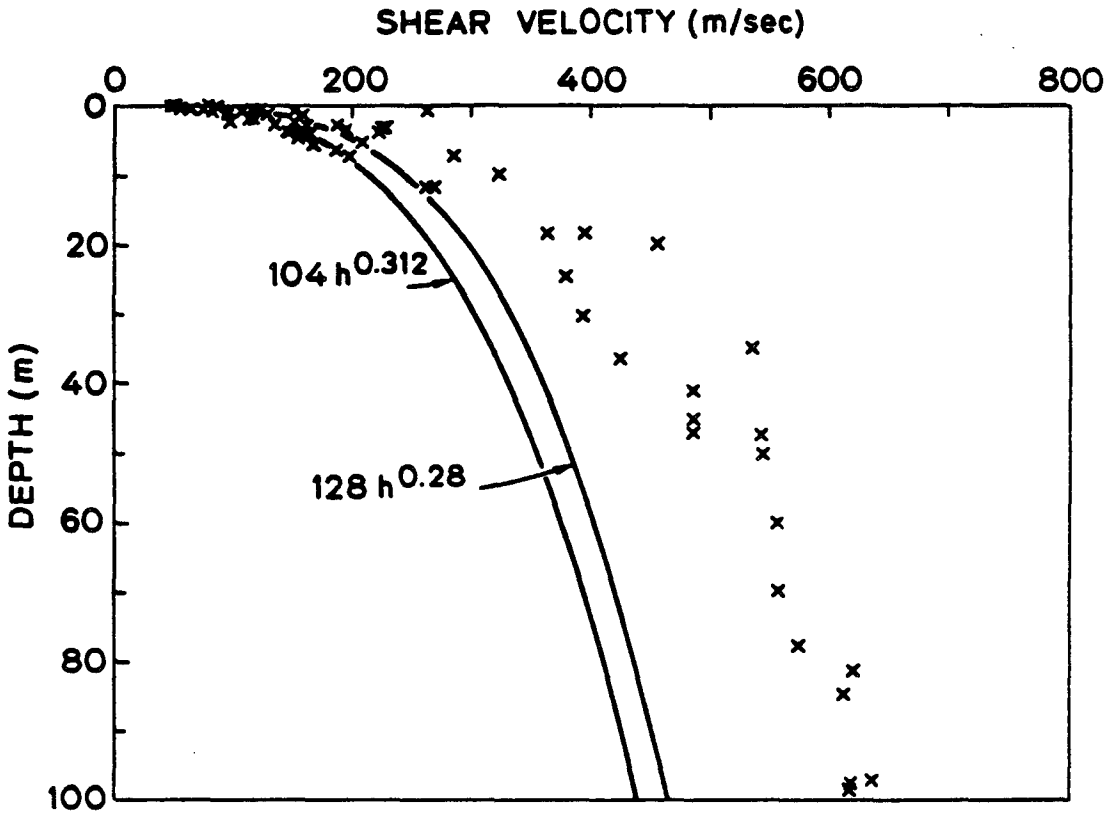

Fig. 26. Hamilton's curves for V_s as a function of depth plotted against compiled in situ data.

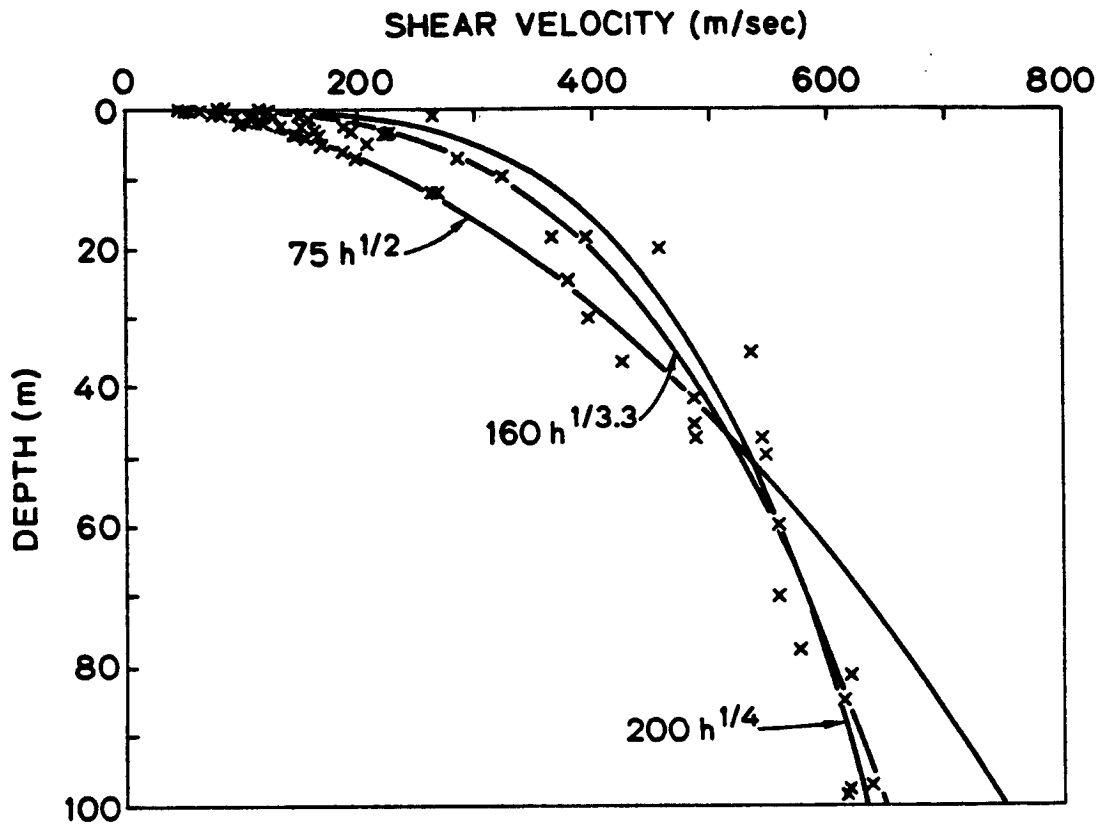

Fig. 27. Three limiting case proportionalities from the compaction model based on a Gaussian radial distribution fit to compiled in situ data.

accurately describe shear velocities in granular sediments.

We expect similar success with V_p. The wetted bulk frame modulus may be similarly determined. Substituting both the bulk and shear proportionalities into the Biot-Gassman equations (equation 2), we can predict the compressional wave dependence on pressure. Unfortunately, we have been unable to gather V_p data for water saturated sands at such shallow depths.

12. CONCLUSIONS

1) Frame moduli in granular sediments are determined by the grain contact area.

2) In the limit of high pressure or strong compaction where the coordination number is independent of pressure, glass beads and quartz sands are well described as a disordered packing of elastic grains in Hertz-Mindlin contact. Velocities vary with a confining pressure to the 1/6 power and contact area to the 2/3 power.

3) Grain contact area in uncompacted materials is dominated by the number of actual contacts per grain. A compaction model is proposed in which the radial distribution of nearest neighbors is Gaussian. The model predicts a strong dependence on the statistics of the packing, and a qualitative evolution of the frame moduli which fits in situ data remarkably well. The high pressure or strong compaction limit is a Hertz-Mindlin material.

4) In vacuum dry materials, adhesion between grain surfaces contracts contacts and significantly increases the area of each contact. Wetting the grains with water eliminates the adhesion. Moduli drop and the material expands measurably. Strain amplitude independence effectively refutes the significance of frictional grain sliding.

5) In uncompacted, disperse, self-loading sediments, velocities vary with the contact area to the 1/2 power. Contact area is dominated by the actual number of contacts which in turn is logarithmically related to 1 minus the porosity. Thus, compressional and shear wave velocities decrease with increasing porosity.

6) Grain size per se has no effect on frame moduli. However, in natural sediments increased grain angularity accompanies a decrease in mean grain size. Grain angularity in uncompacted materials increases the porosity. Therefore, in granular sediments, decreasing grain size generally lowers the frame moduli.

7) Contrarily, grain angularity in compacted materials increase the frame moduli. Grain contacts may be plastic at high pressure.

ACKNOWLEDGEMENTS

Amos Nur is director of the Stanford Rock Physics Program. This paper constitutes the second chapter of a doctoral dissertation. Joel Walls and Peter Gordon were instrumental in the design and construction of the uniaxial pressure vessel. Mary Kovacs sieved sand with remarkable patience, persistence, and good humor. George Parks lead me to the surface chemistry literature. This research was supported by the Office of Naval Research under contract N00014-77-C-0390 with the Marine Geology and Geophysics Program.

WORKS CITED

Anderson, A.L., and L.D. Hampton, Acoustics of gas bearing sediments, I. Background, J. Acoust. Soc. Am. 67, 1865-1889 (1980).

Anderson, A.L., and L.D. Hampton, Acoustics of gas bearing sediments, II. Measurements and models, J. Acoust. Soc. Am. 67, 1890-1903 (1980).

Anderson, D.G., C. Espana, and V.R. Lamore, Estimating in situ shear moduli at competent sites, Proc. Eq. Engr. Soil. Dyn. I, 181-197 (1978).

Aronson, M.P. and H.M. Princen, Aqueous films on silica in the presence of catonic surfactants, Colloid Polym. Sci. 256, 140-149, 1978.

Bea, R.G., Engineering fixed offshore platforms to resist earthquakes, Proc. Eq. Eng. Soil Dyn. III, 1357-1385 (1978).

Beard, D.C., and P.K. Weyl, Influence of texture on porosity and permeability of unconsolidated sand, Bull. AAGP 57, 349-369 (1973).

Bernal, J.D. and J. Mason, Coordination of randomly packed spheres, Nature 188, 910-911 (1960).

Biot, M.A., Theory of propagation of elastic waves in a fluid-saturated porous solid, I. Low frequency range, J. Acoust. Soc. Am. 28, 168-178 (1956).

Biot, M.A., Theory of propagation of elastic waves in a fluid saturated porous solid, II. High frequency range, J. Acoust. Soc. Am. 28, 179-191 (1956),

Brandt, H., A study of the speed of sound in a porous granular media, J. Appl. Mech. ASME 22, 497-486 (1955).

Brandt, H., Factors affecting compressional wave velocity in unconsolidated marine sediments, J. Acoust. Soc. Am. 32, 171-179 (1960).

Brown, R.J.S., and J. Korringa, On the dependence of the elastic properties of a porous rock on the compressibility of the pore fluid, Geophys. 40, 608-616 (1975).

Brown, R.L. and J.C. Richards, Principles of Power Mechanics, Chapt. 2, 13-39, Pergamon, Oxford (1966).

Brunauer, S., D.L. Kantro, and C.H. Weise, The surface energies of amorphous silica and hydrous amorphous silica, Can. J. Chem. 34, 1483-1496 (1956).

Cataphote Division-Ferro Corporation, World's largest catalog of small glass beads: microscopic glass beads for industrial, scientific, optical, and reflective purposes, Jackson, Miss. (1977)

Cattaneo, C., Teoria del contatto elastico in seconda approssimazione, Rc. Mat. Applic. 6, 504-512 (1947).

Christensen, R.E., J.A. Frank, and W.H. Geddes, Low-frequency propagation via shallow refracted paths through deep ocean unconsolidated sediments, J. Acoust. Soc. Am. 57, 1421-1426 (1975).

Clark, V.A., B.R. Tittmann, and T.W. Spencer, Effects of volatiles on attenuation (Q^{-1}) and velocity in sedimentary rocks, J. Geophys. Res. 35, 5190-5198 (1980).

Deresiewicz, H. Stress-strain relations for a simple model of a granular medium, J. Appl. Mech. ASME 25, 402-405 (1958).

Deresiewicz, H., A note on second-order Hertz contact, J. Appl. Mech. ASME 28, 141-142 (1961).

Dexter, A.R. and D.W. Tanner, Packing density of ternary mixtures of spheres, Nature 230, 177-179 (1971).

Digby, P.J., The effective elastic moduli of porous granular rocks, J. Appl. Mech. ASME 48, 803-808 (1982).

Domenico, S.N., Elastic properties of unconsolidated porous sand reservoirs, Geophys. 42, 1339-1368 (1977).

Duffy, J., A differential stress-strain relation for the hexagonal close-packed array of elastic spheres, J. Appl. Mech. ASME 26, 251-258 (1959).

Duffy, J. and R.D. Mindlin, Stress-strain relations of a granular medium, J. Appl. Mech. ASME 24, 585-593 (1957).

Edil, T.B. and G.F. Luh, Dynamic modulus and damping relationships for sands, Proc. Eq. Eng. Soil Dyn. I, 394-409 (1978).

Elliott, S.E. and B.F. Wiley, Compressional velocities of partially saturated unconsolidated sands, Geophys. 40, 949-954 (1975).

Fryer, G.J., Compressional-shear wave coupling induced by velocity gradients in marine sediments, J. Acoust. Soc. Am. 69, 647-660 (1981).

Fuller, K.N.G. and D. Tabor, The effect of surface roughness on the adhesion of elastic solids, Proc. Roy. Soc. A 345, 327-342 (1975).

Furnas, C.C., Mathematical relations for beds of broken solids of maximum density, Indust. Eng. Chem. 23, 1052-1058 (1931).

Galin, L.A., Contact Problems in the Theory of Elasticity (English trans.), Appl. Math. Res. Group, North Carolina State, 233 pp. (1961).

Gangi, A.F., Pressure dependence of the velocity of lunar soil: the velocity/depth variation in the shallow lunar crust, J. Geophys. Res. 86, 9562-9566 (1981).

Gardner, G.H.F., M.R.F. Gardner, and D.M. Droshak, Effects of pore pressure and saturation on the attenuation of elastic waves in sand, J. Petr. Tech. 16, 189-198 (1964).

Gassman, F. Ueber die elastizitat poroser median, Vierteljahrsschr. Naturforsch. Ges. Zuerich, Heft I, (1951a).

Gassman, F., Elastic waves through a packing of spheres, Geophys. 16, 673-685 (1951b).

Geertsma, J., and D.C. Smit, Some aspects of wave propagation in fluid saturated porous solids, Geophys. 26, 169-181 (1961).

Goodman, L.E. and L.M. Keer, The contact stress problem for an elastic sphere indenting an elastic cavity, Int. J. Solids Struct. 1, 407-415 (1965).

Graton, L.C. and H.J. Fraser, Systematic packing of spheres - with particular relation to porosity and permeability, J. Geol. 43, 785-909 (1935).

Greenwood, J.A. and J.B.P. Williamson, Contact of nominally flat surfaces, Proc. Roy. Soc. A. 97, 300-316 (1966).

Greenwood, J.A. and J.H. Tripp, The elastic contact of rough spheres, J. Appl. Mech. ASME 89, 153-159 (1967).

Hamilton, E.L., Sound velocity and related properties of marine sediments, J. Geophys. Res. 75, 4423-4446 (1970).

Hamilton, E.L., Elastic properties of marine sediments, J. Geophys. Res. 76, 579-604 (1971).

Hamilton, E.L., Geoacoustic models of the seafloor, in Proc. Symp. Phys. Sound in Mar. Sed. (L.D. Hampton, ed.), 181-221 (1974a)

Hamilton, E.L., Prediction of deep-sea sediment properties: state-of-the-art, in Proc. Symp. Phys. Engr. Prop. Deep-Sea Sed., (A.L. Inderbitzen, ed.), 1-43 (1974b).

Hamilton, E.L., Shear-wave velocity versus depth in marine sediments: a review, Geophys. 37, 520-646 (1976a).

Hamilton, E.L., Variations of density and porosity with depth in deep sea sediments, J. Sed. Pet. 46, 28-300 (1976b).

Hamilton, E.L., Sound velocity-density relations in sea-floor sediments and rocks, J. Acoust. Soc. Am. 63, 366-377 (1978).

Hamilton, E.L., Sound velocity gradients in marine sediments, J. Acoust. Soc. Am. 65, 909-922 (1979a).

Hamilton, E.L., V_p/V_s and Poisson's ratios in marine sediments and rock, J. Acoust. Soc. Am. 66, 1093-1101 (1979b).

Hamilton, E.L., Geoacoustic modeling of the sea floor, J. Acoust. Soc. Am. 68, 1313-1340 (1980a).

Hamilton, E.L., Compressional and shear wave gradients in marine sediments, J. Acoust. Soc. Am. 64, Suppl. 1, S141 (abstract) (1980b).

Hara, G., Theorie der akustischen Schwingungsausbreitung in gekörnten Substanzen und experimentalle Untersuchungen an Kohlepulver, Elektrische Nachr. Techn. 12, 191-200 (1935).

Hardin, B.O., The nature of stress-strain behavior for soils, Proc. Eq. Engr. Soil Dyn. I, 3-90 (1978).

Hardin, B.O. and V.P. Drnevich, Shear modulus and damping in soils, measurements and parameter effects, J. Soil. Mech. Fdn. Div. ASCE 98, 603-624 (1972a).

Hardin, B.O., and V.P. Drnevich, Shear modulus and damping in soils: design equations and curves, J. Soil Mech. Fdn. Div. ASCE 98, 667-692 (1972b).

Hardin, B.O., and F.E. Richart, Elastic wave velocities in granular soils, J. Soil Mech. Fdn. Div. ASCE 89, 33-65 (1963).

Iida, K., The velocity of elastic waves in sand, Bull. Eq. Res. Inst., Tokyo Univ. 27, 131-144 (1938).

Iida, K., Velocity of elastic waves in a granular substance, Bull. Eq. Res. Inst., Tokyo Univ. 17, 783-808 (1939).

Israelachivili, J.N. and G.E. Adams, Measurement of forces between two mica surfaces in aqueous electrolyte solutions in the range 0 to 100 nm, J. Chem. Soc., Faraday Trans. I, 74, 975-1001 (1980).

Israelachivili, J.N. and D. Tabor, Van der Waals forces: Theory and experiment, in Progress in Surface and Membrane Science (J.F. Danielli, M.D. Rosenberg, and D.A. Cadenhead, eds.), v. 7, 1-55, Academic Press, N.Y. (1973).

Iwasaki, T., and F. Tatsuoka, Dynamic soil properties with emphasis on comparison of laboratory tests and field measurements, Proc. Fifth Conf. Eq. Eng. 1, 2303-2308 (1973).

Johnson, D.L., Equivalence between fourth sound in liquid He 11 at low temperatures and the Biot slow wave in consolidated porous media, Appl. Phys. Lett. 37, 1065-1067 (1981).

Johnson, D.L. and P. Sen, The multiple scattering of acoustic waves with application to the index of refraction of 4th sound, Phys. Rev. B, 24, 2486-2496 (1981).

Johnson, D.M., A.L. Frisillo, J. Dorman, G.V. Latham and D. Strangway, Compressional wave velocities of a lunar regolith sample in a simulated lunar environment, J. Geophys. Res. 87, 1899-1902 (1982).

Johnson, K.L., Surface interaction between elastically loaded bodies under tangential forces, Proc. Roy. Soc. A. 230, 531-549 (1955).

Johnson, K.L., K. Kendall, and A.D. Roberts, Surface energy and the contact of elastic solids, Proc. Roy. Soc. A. 324, 301-313 (1971).

Kudo, K., and E. Shima, Attenuation of shear waves in soil, Bull. Eq. Res. Inst., Univ. Tokyo, 48, 145-159 (1970).

Lunberg, G. Elastische Beriihrung zweier Halbraume, Forsch. Geb. Ingenieurw. 10, 201-211 (1939).

Marsal, R., Mechanical properties of rockfill, in Embankment - Dam Engineering, 109-208, Wiley, N.Y. (1973).

Mavko, G.M. and A. Nur, The effect of non-elliptical cracks on the compressibility of rocks, J. Geophys. Res. 83, 4459-4468 (1978).

McFarlane, J.S. and D. Tabor, Adhesion of solids and the effect of surface films, Proc. Roy. Soc. A. 202, 224-243 (1950).

Meissner, H.P., A.S. Michaels and R. Kaiser, Crushing strength of zinc oxide agglomerates, I. and E.C. Design Develop. 3, 202-205 (1964).

Mindlin, R.D., Compliance of elastic bodies in contact, J. Appl. Mech. ASME 16, 259-268 (1949).

Mindlin, R.D. and H. Deresiewicz, Elastic spheres in contact under varying oblique forces, J. Appl. Mech. ASME 20, 327-344 (1953).

Mindlin, R.D., W.P. Mason, T.F. Osmer and H. Deresiewicz, Effects of an oscillating tangential force on the contact surfaces of elastic spheres, Proc. First Nat. Cong. Appl. Mech., 203-208 (1956).

Morse, P.M. and K.V. Ingard, Theoretical Acoustics, McGraw-Hill, N.Y. 927 pp. (1968).

Murphy, W.F., Effects of partial water saturation on attenuation in Massilon sandstone and Vycor porous glass, J. Acoust. Soc. Am. 71, 6 (in press) (1982a). Also Chapt. III in this volume.

Murphy, W.F. and A. Nur, On velocities and attenuation as a measure of partial gas saturation on tight sandstones at borehole and ultrasonic frequencies, Geophys. (subm. in July) (1982a). Also Chapt. IV in this volume.

Murphy, W., and A. Nur, On the acoustic properties of the shallow lunar crust, J. Geophys. Res. (in preparation) (1982b).

Norman, L.D., and other, Computer simulation of particular systems, U.S. Bureau of Mines Bull. 658, 55p. (1971).

Oda, M. Co-ordination number and its relation to shear strength of granular material, Sols Fdn. 17, 29-42 (1977).

Oda, M., J. Konishi, and S. Nemat-Nasser, Some experimentally based fundamental results on the mechanical behavior of granular materials, Geotechnique 30, 479-495 (1980).

Ohsaki, V. and R. Iwasaki, On dynamic shear moduli and Poisson's ratio of soil deposits, Soils Fdn. 13, 61-73 (1973).

Ohta, V. and N. Goto, Empirical shear wave velocity equations in terms of characteristic soil indexes, Eq. Engr. Struct. Dyn. 6, 167-187 (1978).

Pillbeam, C.C. and J.R. Vaisnys, Acoustic velocities and energy losses in granular aggregates, J. Geophys. Res. 78, 810-824 (1973).

Potters Industries, Inc., Technical quality solid glass spheres for industrial and scientific applications, Hasbrouck Heights, N.J. (1980).

Pandit, B.I. and M.S. King, The variation of elastic wave velocities and quality factor Q of a sandstone with moisture content, Canad. J. Earth Sci. 16, 2187-2195 (1979).

Pashley, R.M. and J.N. Israelachivili, A comparison of surface forces and interfacial properties of mica in purified surfactant solutions, Colloid. Surf. 2, 169-187 (1981).

Pryor, W.A., Reservoir inhomogeneities of some recent sand bodies, Soc. Pet. Eng. J. 253, 229-245 (1972).

Sherif, M.A. and I. Ishibashi, Dynamic shear moduli for dry sands, J. Geotech. Div. ASCE 102, 1171-1184 (1976).

Seed, H.B. and I.M. Idriss, Soil moduli and damping factors for dynamic response analyses. EERC 70-10, Eq. Engr. Res. Center, U.C., Berkeley (1970).

Smith, D.T., Acoustic and mechanical loading of marine sediments, in Proc. Symp. Phys. Sound Mar. Sed. (L.D. Hampton, ed.), 41-61 (1974).

Smith, W.O., P.D. Foote, and P.F. Busang, Packing of homogeneous spheres, Phys. Rev. 34, 1271-1274 (1927).

Sohn, H.Y., and C. Moreland, The effect of particle size distribution on packing density, Can. J. Chem. Eng. 46, 162-167 (1968).

Sonntag, H., and K. Strenge, Coagulation and Stability of Disperse Systems, Wiley, NY, 139 pp. (1970).

Spencer, J.W., Stress relaxations at low frequencies in fluid-saturated rocks: attenuation and modulus dispersion, J. Geophys. Res. 86, 1803-1812 (1981).

Steurmann, E., On Hertz's theory of local deformations in compressed elastic bodies, C.R. Acad. Sci. URSS 25, 359-361 (1941).

Steurmann, E., On the question of local deformations in elastic bodies pressed against one another, C.R. Acad. Sci. URSS 31, 738-741 (1941).

Steurmann, E., Some special cases of the contact problem, C.R. Acad. Sci. URSS 38, 197-200 (1943).

Stokoe, K.H., D.G. Anderson, R.J. Hoar, and W.H. Isenhower, Discussion of in situ and laboratory shear velocity and modulus, Proc. Eq. Eng. Soil Dyn. III, 1498-1502 (1978).

Stokoe, K.H., and F.E. Richart, Shear modulus of soils: in situ and laboratory measurements, Proc. Fifth World Cong. Eq. Engr. 1, 356-359 (1973).

Stoll, R.D., Experimental studies of attenuation in sediments, J. Acoust. Soc. Am. 66, 1152-1160 (1979).

Stoll, R.D., Theoretical aspects of sound transmission in sediments, J. Acoust. Soc. Am. 68, 1341-1350 (1980).

Talwani, P., A. Nur and R.L. Kovach, Compressional and shear wave velocities in granular materials to 2.5 kilobars, J. Geophys. Res. 78, 6899-6909 (1973).

Telford, W.M., L. P. Geldart, R.E. Sheriff, and D.A. Keys, Applied Geophysics, Cambridge Univ., 860 pp. (1976).

Timoshenko, S. and J.N. Goodier, Theory of Elasticity, McGraw-Hill, N.Y., 372 pp. (1951).

Tittmann, B.R., M. Abdel-Gawad, and R.M. Housely, Elastic velocity and Q factor measurements on Apollo 12, 14, and 15 rocks, Proc. Lunar Sci. Conf. 3, 2565 (1972).

Tittmann, B.R., L. Alberg, and J. Curnow, Internal friction and velocity measurements, Proc. Lunar Sci. Conf. 7, 3123-3132 (1976).

Tittmann, B.R., L. Alberg, H. Nadler, J. Curnow, T. Smith, and E.R. Cohen, Internal friction quality-factor Q under confining pressure, Proc. Lunar Sci. Conf. 8, 1209-1224 (1977).

Tittmann, B.R., H. Nadler, J.M. Richardson, and L. Ahlberg, Laboratory measurements of P-wave seismic Q on lunar and analog rocks, Proc. Lunar Sci. Conf. 9, 3627-3637 (1978).

Tittmann, B.R., H. Nadler, V. Clark and L. Coombe, Seismic Q and velocity at depth, Proc. Lunar Sci. Conf. 10, 2131-2147 (1979).

Van Voorhis, J.J., R.G. Craig, and F.E. Bartell, Free energy of immersion of compressed powders with different liquids, II. Silica powder, J. Phys. Chem. 61, 1513-1519 (1957).

Verwey, E.J.W., and J. Th. G. Overbeek, Theory of the stability of lyophobic colloids, Elsevier, Amsterdam (1948).

Vischer, G.S., Grain size distributions and depositional processes, J. Sed. Pet. 39, 1074-1106 (1969).

Walsh, J.W., The effects of cracks on the compressibility of rocks, J. Geophys. Res. 70, 381-389 (1965).

Walton, K., The effective elastic moduli of model sediments, Geophys. J. R. Astr. Soc. 43, 293-306 (1975).

Warren, N., O.L. Anderson, and N. Saga, Applications to lunar geophysical models of the velocity-density properties of lunar rocks, glasses, and artificial lunar glasses, Proc. Lunar Sci. Conf. 3, 2587-2598 (1972).

Warrick, R.E., Seismic investigation of San Francisco Bay mud site, Bull. SSA 64, 375-385 (1974).

Watt, J.P., The elastic properties of composite materials, Rev. Geophys. Space Phys. 14, 541-563 (1976).

Westman, A.E.R., and Hugill, H.R., The packing of particles, J. Am. Ceramic Soc. 13, 767-779 (1930).

White, H.E., and S.F. Walton, Particle packing and particle shape, J. Am. Ceramic Soc. 20, 155-166 (1937).

White, J.E., Seismic Waves: Radiation, Transmission and Attenuation, McGraw-Hill, N.Y., 302 pp. (1965).

Wilson, R.C., R.E. Warrick, and M.J. Bennett, Seismic velocities of San Francisco Bayshore sediments, Proc. Eq. Eng. Soil Dyn. II, 1007-1023 (1978).

Woods, R.D., Measurement of dynamic soil properties, Proc. Eq. Engr. Soil Dyn. I, 91-178 (1978).

Wyllie, M.R.J., A.R. Gregory, and L.W. Gardner, Elastic wave velocities in heterogeneous and porous media, Geophys. 21, 41-70 (1956).

Wyllie, M.R.L., A.R. Gregory, and G.H.F. Gardner, Elastic wave velocities in heterogeneous and porous media, Geophys. 21, 41-70 (1958).

Yanagisawa, E., Relation between the dynamic shear modulus and void ratio in granular media, in Proc. Cont. Mech. Stat. Approaches Mech. Granular Mat., (S.C. Cowin and M. Satake, eds.), 64-70 (1978).

ADDITIONAL REFERENCES

Abramowitz, M., and I.A. Stegun, Handbook of Mathematical Functions, Dover, NY, 1046 pp. (1965).

Beran, M.J., Statistical Continuum Theories, Wiley, N.Y., 424 pp. (1968).

Beresford, R.H., Statistical geometry of random heaps of equal hard spheres, Nature 224, 550-553 (1969).

Bjerrun, L., Geotechnical problems involved in the foundations of structures in the North Sea, Geotechnique 23, 319-358 (1973).

Brown, C.B., The use of maximum entropy in the characterization of granular media, in Proc. Cont. Mech. Stat. Approaches Mech. Granular Mat. (S.C. Cowin and M. Satake, eds.), 98-109, (1978).

Burns, G., and A.M. Glazer, Space Groups for Solid State Scientists, Academic, N.Y. 278 pp. (1978).

de Pater, A.D., and J.J. Kalker (eds.) The Mechanics of Contact Between Deformable Bodies, Delft Univ., 414 pp. (1975).

Deresiewicz, H., Mechanics of granular matter, Adv. Appl. Mech. 5, 233-306 (1958).

Deresiewicz, H., Bodies in contact with applications to granular media, in R.D. Mindlin and Applied Mechanics (G. Hermann, ed.), Pergamon, N.Y., 105-143 (1974).

Gardner, G.H.F., and M.H. Harris, Velocity and attenuation of elastic waves in sands, Trans. Ninth Ann. Log. Symp. M1-M19 (1968).

Gray, W.A., The Packing of Solid Particles, Chapman and Hall, Lond., 134 p. (1968).

Hashim, Z., Theory of composite materials, Proc. Fifth Symp. Naval Struct. Mech., 201-242 (1970).

Iwasaki, T., F. Tatsucka, and V. Takagi, Shear modulus of sands under cyclic torsional shear loading, J. Japan Soc. Soil Mech. Fdn. Eng. 17, 19-35 (1977).

Jaynes, E.T., Information theory and statistical mechanics, Phys. Rev. 106, 620-630 (1957).

Kendall, K., Sticky solids, Contemp. Phys. 21, 277-297 (1980).

Krinsely, D.H. and J.C. Doornkamp, Atlas of Quartz Sand Surface Textures, Cambridge Univ., 91 pp. (1973).

Kroner, E., Statistical Continuum Theories, ICMS 92, Springer-Verlag, 157 pp. (1971).

Ladd, R.S., Specimen preparation and the liquefaction of sands, J. Geotechn. Eng. Div. ASCE 100, 1180-1184 (1974).

Ludwig, W.J., J.E. Nafe and C.L. Drake, Seismic refraction, in The Sea 4, (A.E. Maxwell, ed.), 53-84 (1970).

McCoy, J.J., Macroscopic response of continua with random microstructures, Mech. Today 6, 1-40 (1981).

Mindlin, R.D., Microstructure in linear elasticity, Arch. Rat. Mech. Anal. 16, 51-78 (1964).

Naar, J. and R.J. Wyal, Structures and properties of unconsolidated aggregates, Canad. J. Phys. 40, 818-831 (1962).

Nafe, J.E. and C.L. Drake, Physical properties of marine sediments, in The Sea 3, (M.N. Hill, ed.), Wiley, N.Y., 794-815 (1963).

Paterson, N.R., Seismic wave propagation in porous granular media, Geophys. 21, 691-714 (1956).

Pyke, R., Discussion of measurement of dynamic soil properties, Proc. Eq. Eng. Soil Dyn. III, 1474-1477 (1978).

Richart, F.E., D.G. Anderson and K.H. Stokoe, Predicting in situ strain-dependent shear moduli of soil, Proc. Sixth World Cong. Eq. Eng. 6, 159-164 (1977).

Richart, F.E., J.R. Hall, and R.D. Woods, Vibration of Soils and Foundations, Prenctice-Hall, Englewood Cliffs, 414 pp. (1970).

Shirely, D.J., and L.D. Hampton, Shear-wave measurements in laboratory sediments, J. Acoust. Soc. Am. 63, 607-613 (1978).

Shumway, G., Sound speed and absorption studies of marine sediments by a resonance method, Part I, Geophys. 25, 451-467 (1960). Part II, Geophys. 25, 659-682 (1960).

Spence, D.A., Self similar solutions to adhesive contact problems with incremental loading, Proc. Roy. Soc. A. 305, 55-80 (1968).

Spence, D.A., A Wiener-Hopf equation arising in elastic contact problems, Proc. Roy. Soc. A. 305, 81-92 (1968).

Truell, R. C. Elbaum and B.B. Chick, Ultrasonic methods in solid-state physics, Academic, N.Y., 464 pp. (1969).

Vaisnys, J.R. and C.C. Pilbeam, Mechanical properties of granular media, Ann. Rev. Earth Sci. 3, 345-360 (1975).

Vermeulen, P.J. and K.L. Johnson, Contact of non-spherical elastic bodies transmitting tangential forces, J. Appl. Mech. ASME 31, 338-340 (1964).

Winkelmolen, A.M., Critical remarks on grain parameters, with special emphasis on shape, Sedimentology 29, 255-266 (1982).

Chapter III

Effects of Partial Water Saturation on Attenuation in Massilon Sandstone and Vycor Porous Glass*

INTRODUCTION

Specific attenuation, Q^{-1}, is a dimensionless measure of the energy loss per cycle as a stress wave propagates through a dissipative material. It is preferably defined as[1]

$$\frac{1}{Q} = \frac{\Phi}{4\pi W} \tag{1}$$

where Φ is the energy loss per cycle and W is the average energy stored per cycle. Accurate estimates of Q^{-1} in sands and sandstones are necessary in order to reliably predict the path and decay of low frequency sound which travels through the ocean floor.[2-6] In geophysical exploration, an understanding of how acoustic energy loss depends on pore structure and water saturation may advance the interpretation of borehole sonic logs and high resolution seismic reflections.[7] Consider that much of the original technical motivation for the analysis of "bright spots" observed in seismic reflections, arose from a limited understanding of ultrasonic velocities as a function of partial water saturation.[7-12]

Despite the pioneering results of Biot,[13-17] Winkler,[18,19] and others,[20-23] I think it safe to say that in geophysics as a whole, frictional grain sliding is still widely regarded as the dominant

---

*Accepted by the Journal of the Acoustical Society of America, to appear in volume 71, number 6, June, 1982. Copyright held by the Acoustical Society of America.

mechanism of stress wave attenuation in porous sands and sandstones.[2,3,24-26] This perception is due, in no small part, to the fact that Q^{-1} is generally considered to be independent of frequency from 10^{-3} Hz (i.e. the earth's free oscillations) to 10^{6} Hz (i.e., laboratory ultrasonic testing).[2,3,24-27] Results presented in this paper substantially refute both the premise that Q^{-1} is independent of frequency and the conclusion that frictional grain sliding is the dominant mechanism. Significant frictional losses[28,18] are restricted to situations where strain amplitudes exceed 10^{-6}; they are not important in far-field seismic exploration, echo sounding, or borehole sonic logs. Q^{-1} is an independent or a weak function of frequency only in very dry rocks or over a limited band width in wetted rocks. It is now clear that pore fluids control energy dissipation in porous sands and sandstones. Indeed, energy dissipation is a strong function of frequency throughout the acoustic range.

In this paper, we report a set of experimental results which demonstrate the effect of continuously varying partial water saturation, S_w , on extensional and shear wave velocities and their attenuation in Massilon sandstones (porosity = 23%) and Vycor porous glass (porosity = 28%). Frequency dependence is observed from 25 Hz to 14 kHz (fig. 1) as a function of S_w(0.92-0.90, 0.76-0.74, 10^{-3}, dry). The experiments were originally designed in order to demonstrate the various effects involved. However, certain implications regarding loss mechanisms have obviously emerged. These implications are discussed qualitatively. Theoretical analysis is deferred to a subsequent paper.

Perhaps the central point to be derived from this paper is that the acquisition of compressional and shear wave velocities and their

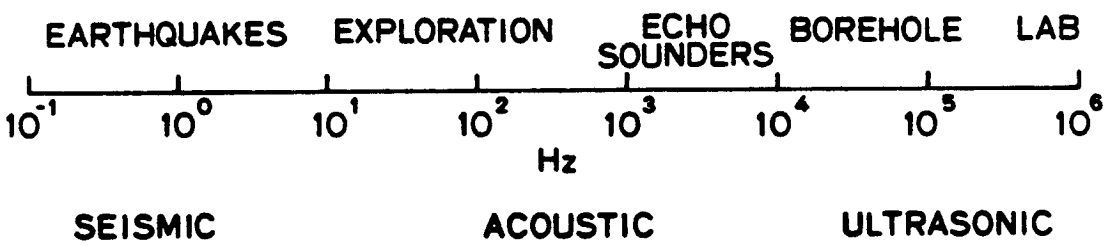

Fig. 1. Frequency spectrum of geoacoustic interest. Our experiments cover the range from roughly 10^{1} to 10^{4} Hz.

attenuation provides significant information about pore fluids and their mobility in porous granular materials.[14,15] Most exciting is that attenuation is found to be very sensitive to partial gas saturation. Thus predictive knowledge of acoustic properties in sands and sandstones may be increasingly useful in the search for economic natural gas reservoirs.

1. EXPERIMENTAL METHODS

Extensional velocity, V_e, shear velocity, V_s, extensional specific attenuation, Q_e^{-1}, and shear specific attenuation, Q_s^{-1}, were measured in Massilon sandstone and Vycor porous glass using a resonant bar technique. Sample descriptions are given in Table 1. Massilon is generally accepted to be representative of quartz-rich, high porosity sandstones.[19] In those cases where corresponding measurements were made, homologous behavior has been observed in Berea 600 (which is also a standard, quartz-rich, high porosity sandstone).

Our resonance system is similar to that used by Gardner et al.[23] and is described in detail by Winkler.[29] The length of the sample 1 m to 20 cm, puts the fundamental resonance, in each mode, roughly between 300 to 5000 Hz, depending on the saturation. Wave lengths are the order of 1 m, and grain sizes are the order of 100 μm or less. Scattering losses therefore are negligible. Resonant frequencies are measured to 1 part in 10^3 and converted to velocities using the relation $V = 2cLf$, where L is the length of the sample, f is the frequency, and c is the geometric correction factor given by Spinner and Tefft.[30] Strain amplitudes are measured with crystal phonograph pickups calibrated against semiconductor strain gauges. Attenuation

TABLE 1. Sample Descriptions

Name	Classification	Composition	Grain Density g/cm^3	Porosity %	Pore Dia. μm	Grain Size μm	Pore Surface Area m^2/g	Permeability milli-darcy	Sample Dimensions cm
Massilon Sandstone	sub-quartz arenite	88% quartz 4% amorphous silica 5% kaolinite 3% feldspar	2.66	23	30	150-200	~1	737	100 x 2.2 x 2.2
Vycor Porous Glass	Corning Glass #7930	96% amorphous silica 4% boric acid	2.40	28	0.005	0.050	200	~0.01	91 x 1.4

data can be obtained either by plotting resonance peaks ($Q^{-1} = \Delta f/f$) or by measuring the time constant of resonant decays ($\tau = Q/\pi f$). In practice, the decay technique is used almost exclusively. However, prior to each measurement, resonant peak shapes are carefully observed to insure the purity of the resonance. Relative precision is within 2%. We estimate the accuracy of the attenuation measurements to be 5-10%. The upper limit on Q^{-1} measurements is 0.125. Thereafter, the decays are considered too sparse for the required accuracy.

Velocities and attenuation are measured as a function of S_w by a drying experiment. A fully saturated sample[31] is mounted in the measurement frame, which is located in a humidity chamber. As the Massilon dries, V_e, V_s, Q_e^{-1}, and Q_s^{-1} are measured at 5 min, then progressively longer intervals. S_w is monitored by weighing a similar sample, which is drying simultaneously on a thermally buffered digital scale, also in the humidity chamber. S_w is determined to within 2% accuracy. The rate of drying is controlled by the relative humidity in the chamber, which is set using a commercial humidifier.

Upon reaching equilibrium at a relative partial pressure of water vapor, $P/P_0(H_2O)$, of 0.45, the bar is designated "dry". Subsequently, $P/P_0(H_2O)$ is lowered in steps of 0.15 by placing predetermined amounts of a commercial desiccant into the chamber. The condition designated "very dry" refers to that state at which the sample equilibrates with $P/P_0(H_2O) < 0.01$.

Results of the drying experiments in Massilon sandstone have been reproduced successfully in several different ways. First, the same Massilon bar was dried at the same rate. Secondly, we dried the specified Massilon bar again, but at a slower rate. This experiment

includes drying to certain degrees of saturation and holding at equilibrium for several hours. Lastly, a different Massilon bar was dried at the original rate. Qualitatively similar results were observed. The quantitative discrepancy between two bars in both velocities and attenuation was systematic and less than 12% and 4%, respectively.

A frequency range of 300 Hz to 14 kHz was achieved with the resonant bar system by i) using samples of various lengths, 20 to 100 cm, and ii) exciting higher odd harmonics. A supposed particularly uniform suite of Massilon bars -- cut from a single block at the quarry -- were tested. At a given frequency and under ambient conditions, variation among the bars in this suite does not exceed 15% in velocities and 6% in attenuation. This variation precludes the measurements of velocity dispersion. On the other hand, it poses merely a small problem for attenuation frequency dependence because the magnitude of the effect is roughly a factor of 7 or so. Signal to noise problems arise with the combination of high loss ($Q^{-1} > 0.05$), higher harmonics, and high frequency ($f > 4$ kHz). In fact, measurements in Massilon at the higher degrees of saturation must be truncated at 7 kHz.

A torsional pendulum technique similar to that described by Peselnick and Outerbridge[32] was implemented in order to measure Q_s^{-1} at low acoustic frequencies. The apparatus is housed in a humidity chamber similar to the resonant bar system. Frequency is varied simply by changing the inertial mass at the base of the sample. Q_s^{-1} has been successfully measured at several degrees of saturation from 25 to 400 Hz in a cylindrical Massilon sample, 25.4 cm in length and 2.54 cm in diameter.

II. EXPERIMENTAL RESULTS

In all figures Q^{-1} is plotted as 1000/Q because the magnitudes of 1000/Q for sands and sandstones fall conveniently at 10 for small loss and 100 for large loss.

A. The Effects of Moisture

Observations

Our data for S_w varying from 0.10 down to 0 in a 1 m Massilon bar is shown in figures 2, 3, and 4. This data includes a set of measurements for $P/P_0(H_2O)$ varying from 0.98 to less than 0.01.

In figure 2, a velocity increase totaling 60% in extension and 70% in shear is observed as the degree of water saturation declines from 0.10 to the very dry state [$S_w = 0$, $P/P_0(H_2O) < 0.01$]. From 0.10 down to 0.015 S_w, only a 5% increase occurs in both V_e and V_s. The dramatic increase, roughly 2/3 in both modes, occurs with a very small change in moisture content, from 0.015 S_w to the very dry state. V_e ~ 1600 m/sec and V_s ~ 1200 m/sec in a dry [$S_w = 10^{-4}$, $P/P_0(H_2O)$ 0.45] Massilon bar. Therefore, half of this remarkable increase (i.e. 1/3) was recorded before the sample became "dry"; the other 1/3 was measured at the $P/P_0(H_2O)$ was lowered to less than 0.01 (the very dry state).

Figure 3 demonstrates the corresponding effects on attenuation. As the saturation declines, 1000/Q decreases by a total of 75% in extension and 60% in shear. $1000/Q_e$ ~ 18 and $1000/Q_s$ ~ 15 in a dry Massilon bar. Thus although most of the reduction in attenuation occurs before the dry state, the effect of humidity is substantial. An unexpected minor peak is observed at roughly 0.005 to 0.01 S_w. The

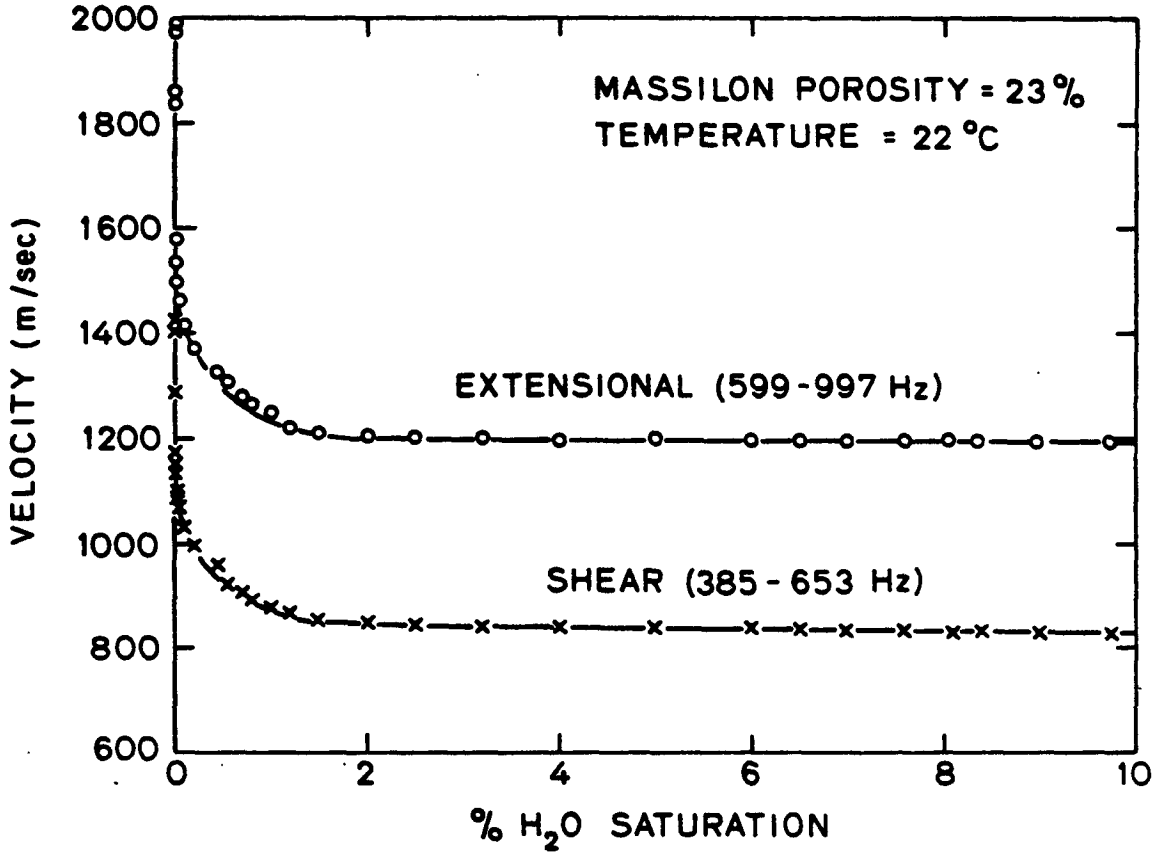

Fig. 2. E and S velocities vs. moisture content (S_w = 0 - 0.10) in Massilon sandstone.

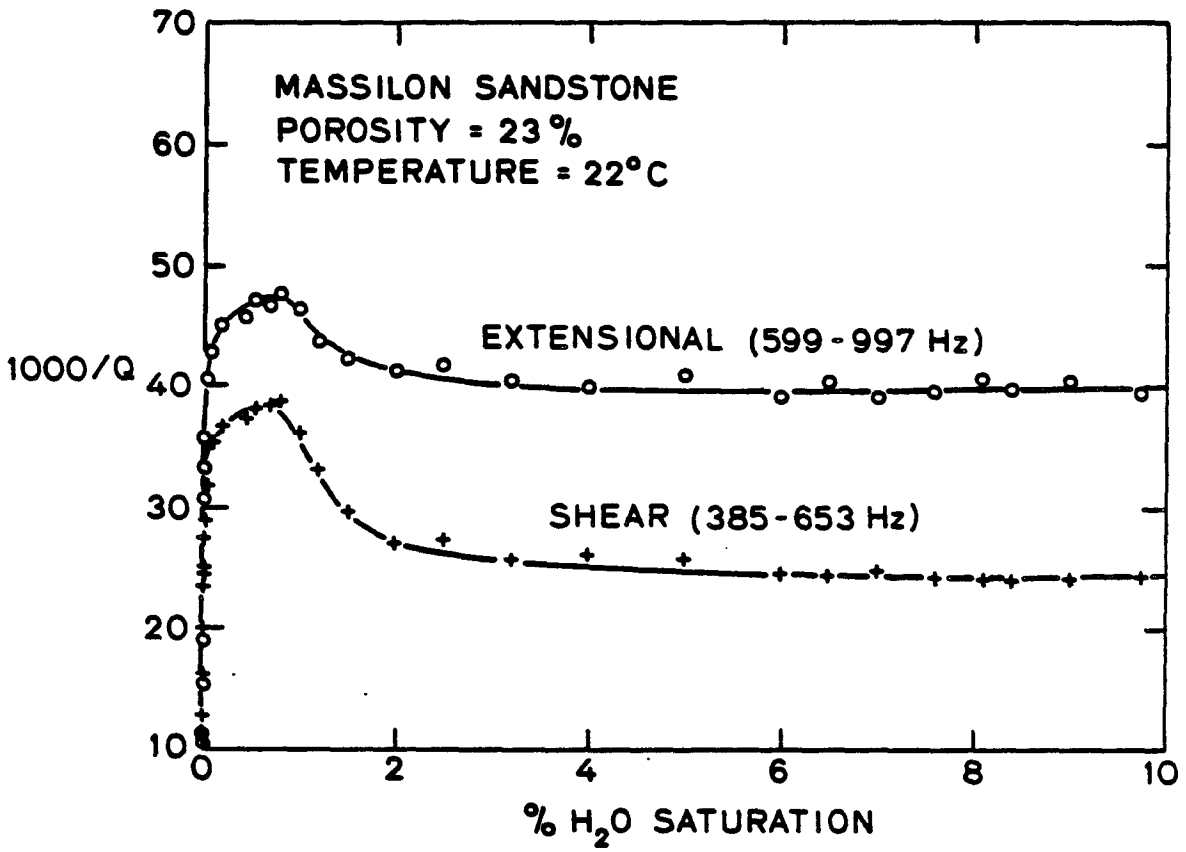

Fig. 3. $1000/Q_e$ and $1000/Q_s$ vs. moisture content (S_w = 0 - 0.10) in Massilon sandstone.

peak constitutes a 15% increase in extension and 40% increase in shear. The dependence is very weak from 0.10 down to 0.02 S_w.

Our standard measurements are made at wave strain amplitudes which are less than 10^{-7}. Figure 4 demonstrates the effect of increasing the strain amplitude on shear velocity and attenuation at two levels of $P/P_0(H_2O)$. We observe that increasing the level of strain has no effect on V_s or $1000/Q_s$ until strains approach 10^{-6}. Contrarily, a decrease of 0.60 in relative humidity affects a 16% overall increase in V_s and a 43% overall decline in specific attenuation.

Discussion

Wyllie et al.,[20] Hardin and Richart,[33] and Clark et al.[34] have observed similar velocity reductions in sands and sandstones with the addition of small amounts of water. The effect of moisture on attenuation has been studied by Tittmann et al.,[21] and Pandit and King.[35] While our results are qualitatively similar to the previous work, the coherence of our experiments leads to further understanding.

In the low-frequency limit, which applies to our measurements, V_e and V_s are inversely related to the square root of the composite density, ρ_c, given by

$$\rho_c = (1 - \phi)\rho_s + \phi S_w \rho_w \qquad (2)$$

where ϕ is the porosity (i.e. 0.23 for Massilon, ρ_s is the density of the individual grains (i.e. 2.66 g/cm^3 for Massilon), and ρ_w is the density of water (1.0 g/cm^3). The 0.5% velocity increase observed from 0.10 to 0.02 S_w is precisely explained by the decrease in the mass of water. However, the density effect from 0.02 to 0 S_w merely accounts for a 0.25% velocity increase, not the roughly 65% observed.

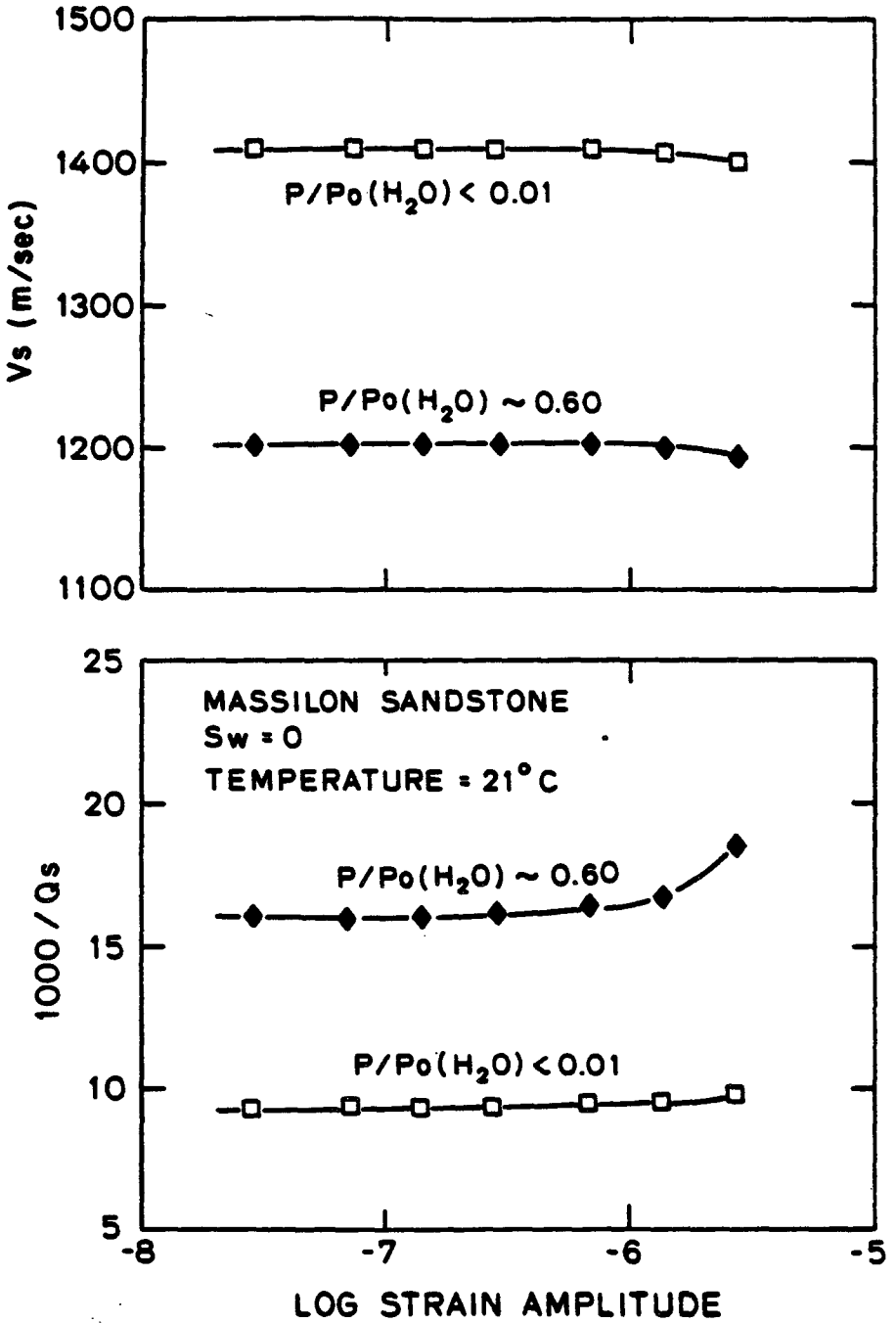

Fig. 4. Strain amplitude tests in Massilon sandstone at $P/P_0(H_2O)$ of < 0.01 and 0.60: (above) V_s vs. log strain amplitude; (below) $1000/Q_s$ vs. log strain amplitude.

Actually, the strong velocity increase reflects a 5 GPa increase in the extensional frame modulus and a 2.8 GPa increase in the shear frame modulus.

Clark et al.[34] attribute this effect to the dehydration and stiffening of detrital clays between grain contacts. This mechanism is brought into question when we consider Hardin and Richart's result. Hardin and Richart[33] found a 15% drop in velocities in Ottawa sand with the addition of a mere 0.0015 S_w. This effect, though not as large, is roughly similar to Clark's observations in Berea, Wingate, and Coconino sandstones and to our Massilon results (also observed in Berea 600 and Vycor). Ottawa sand is unconsolidated and has no clay. Another more general mechanism must be sought.

It is well known (e.g. Duffy and Mindlin[28]) that frictional attenuation in granular materials is inherently nonlinear in strain. Standard laboratory measurements in rock physics are conducted at strains below 10^{-6}.[18,22,33,36-38] For standard in situ techniques, seismic, sonar, and borehole sonic strains are around or below 10^{-7} in the far-field (i.e., a wavelength away from the source).[28] Winkler,[18] and Stoll[22] have each observed V and Q^{-1} independent of strain up to strains of 10^{-6}. The measurements shown in figure 4 reproduce their observation for our samples. Furthermore, Winkler et al.[18] observed that a confining pressure of 3 MPa significantly flattens the strain amplitude effect and may shift its onset to significantly higher strains. Therefore, frictional grain sliding is not an important mechanism for stress wave attenuation in porous sands and sandstones. Moreover, the magnitude of the humidity effect observed in figure 4 emphasizes the fact that pore fluids control attenuation even in

laboratory dry rocks.

Tittmann et al.[21] ascribe the energy loss in dry sandstones to stress-induced diffusion of adsorbed water. Each cycle redistributes water molecules (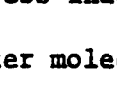) on the silanol (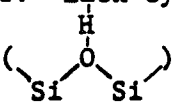) surface of the silicate grains. The energy is dissipated in the breakage of hydrogen bonds between the surface hydroxyls and the water molecules. Spencer proposes a similar model. Biot[17] and Spencer[33] further postulate that the absorbed water sufficiently reduces the surface free energy of the silicate framework in order to account for the observed modulus defect with the addition of small amounts of water.

Mason[36,37] suggests that attenuation in "dry" rocks results from the motion of dislocation kinks activated in the silicate surface. However, it is unlikely that dislocations in quartz are active at ambient temperature and pressure.[39]

At our present state of knowledge, we prefer the following working model. It is well known in chemical engineering literature[40] that the presence of small amounts of liquid in fine granular materials generates an adhesive force sufficient to densify the material. In sands and sandstones, discrete films of water, ~1 to 10 nm in thickness, maybe drawn into and held in fine capillaries by a strong capillary pressure. These films and their sensitivity to $P/P_0(H_2O)$ may affect the moduli in two ways. First, increasing adhesive force with decreasing $P/P_0(H_2O)$ increases the surface free energy and thereby stiffens the quartz at the grain contacts.

As the capillaries are compressed each cycle, the film must deform. We suggest that the energy losses be considered phenomonologically as a microcapillary hysteresis. The actual molecular mechanism may

be either bond breaking at the water-silanol interface, or viscous dissipation as the film moves over surface asperities.

At saturations above 0.02, a different dissipative mechanism takes control of the attenuation. This mechanism, which will be investigated in the following sections, is frequency dependent and is most likely pore fluid flow.

The attenuation peak at $S_w = 0.01$ (figure 3) is due to the combined effects of the surface and fluid flow mechanisms. In this range of saturation, the capillary processes begin to stiffen the sandstone (figure 2). The rise in velocity requires the frequency to increase (recall that $f = V/2cL$, where $2cL$ is fixed). Attenuation increases in this limited range because of the frequency dependence of the viscous flow mechanism (to be demonstrated in section II-C). By $S_w = 10^{-3}$, the viscous flow loss is eliminated, yielding control to the surface mechanism; and 1000/Q drops dramatically (figure 3). In other words, had this experiment been conducted at a fixed frequency, 1000/Q would simply roll over at 0.02 S_w, exhibiting no peak.

Remark

The dramatic variability observed in the moduli under the conditions usually referred to as "laboratory dry" requires a comment regarding the frame moduli. The frame moduli are elementary components of acoustic response of porous granular materials.[9,10,13-17,41] As noted by Biot,[17] the frame moduli of geophysical interest (i.e., in the range of water saturations from 0.10 to 1.00) are not the so-called "dry frame moduli". Rather, it is the "wetted" frame moduli which are appropriate. Laboratory measurements made at $S_w = 0$ would yield high values resulting from stiffening due to artificial laboratory drying. We suggest

that the "wetted" frame moduli be calculated from V vs. S_w plots such as figure 5.

B. The Effects of Partial Water Saturation

Observations

The dependence of velocities and attenuation on S_w varying from 1.00 to 0.10 in Massilon sandstone is plotted in figures 5 and 6.

In figure 5, V_s is observed to increase gradually as S_w decreases from 1.00 to 0.10. The total increase is about 5%. In contrast, V_e drops rapidly (i.e. 1354 to 1142 m/sec) as S_w goes from 0.9925 to 0.97. That is nearly a 16% velocity decrease with merely a 2% reduction in saturation. However, below $S_w = 0.97$, the dependence changes and roughly parallels that of V_s.

Figure 6 shows attenuation to be very sensitive to water saturation. At nearly full saturation, $1000/Q_s$ is 11% greater than $1000/Q_e$. However, as S_w is reduced to 0.80, the shear loss drops almost exponentially, about 55%; while the extensional loss increases 50% to a peak at $S_w = 0.85$. Below 0.80 S_w, $1000/Q_s$ decreases quite gradually. $1000/Q_e$ drops rapidly from its peak at $S_w = 0.80$. Below 0.60 S_w, the dependence weakens and roughly parallels that of $1000/Q_s$. The scatter of the data in figure 6 is attributed to errors in the hand digitizing of the resonance decays.

Discussion

The velocity behavior (figure 5) is well described by a simple extension to partially saturated materials of Biot's theory in the limit as $f \to 0$ and the fluid-solid coupling becomes infinite.[10] In shear, the velocity is determined by the frame rigidity, which is a

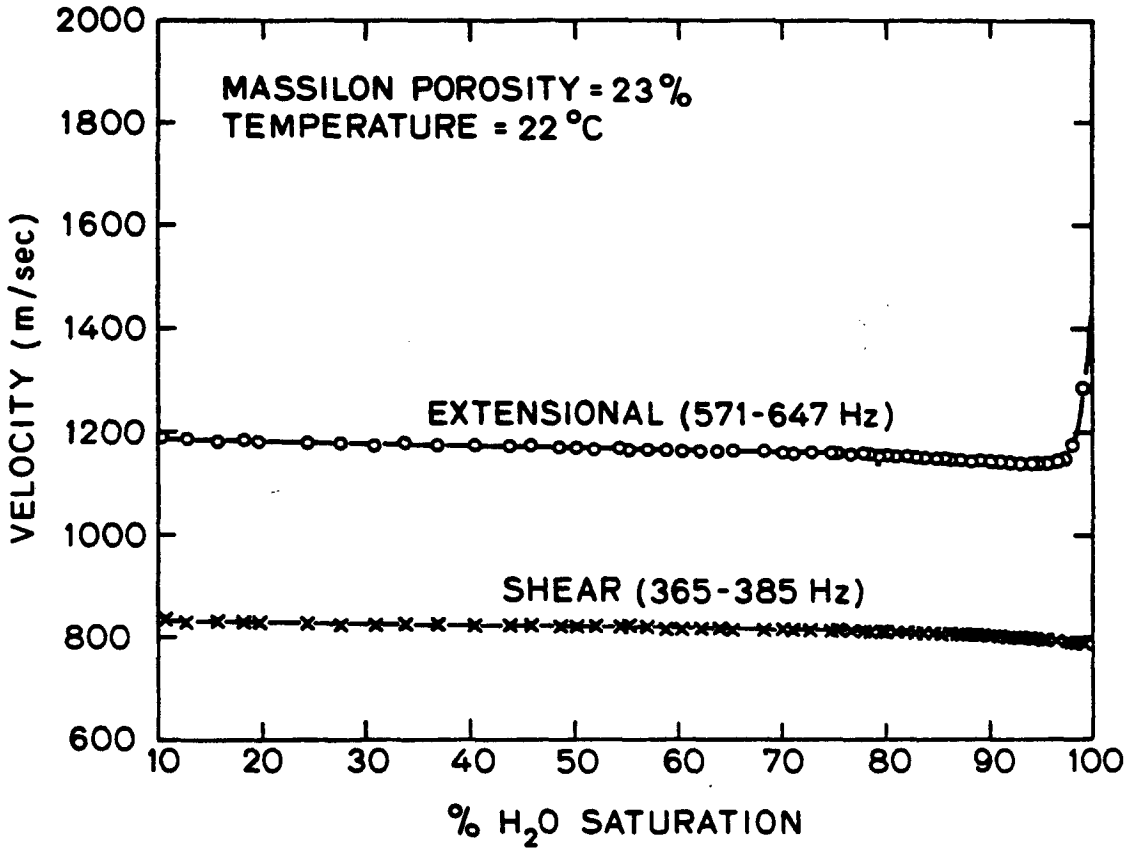

Fig. 5. E and S velocities vs. % H_2O saturation (S_w = 0.10 - 1.00) in Massilon sandstone.

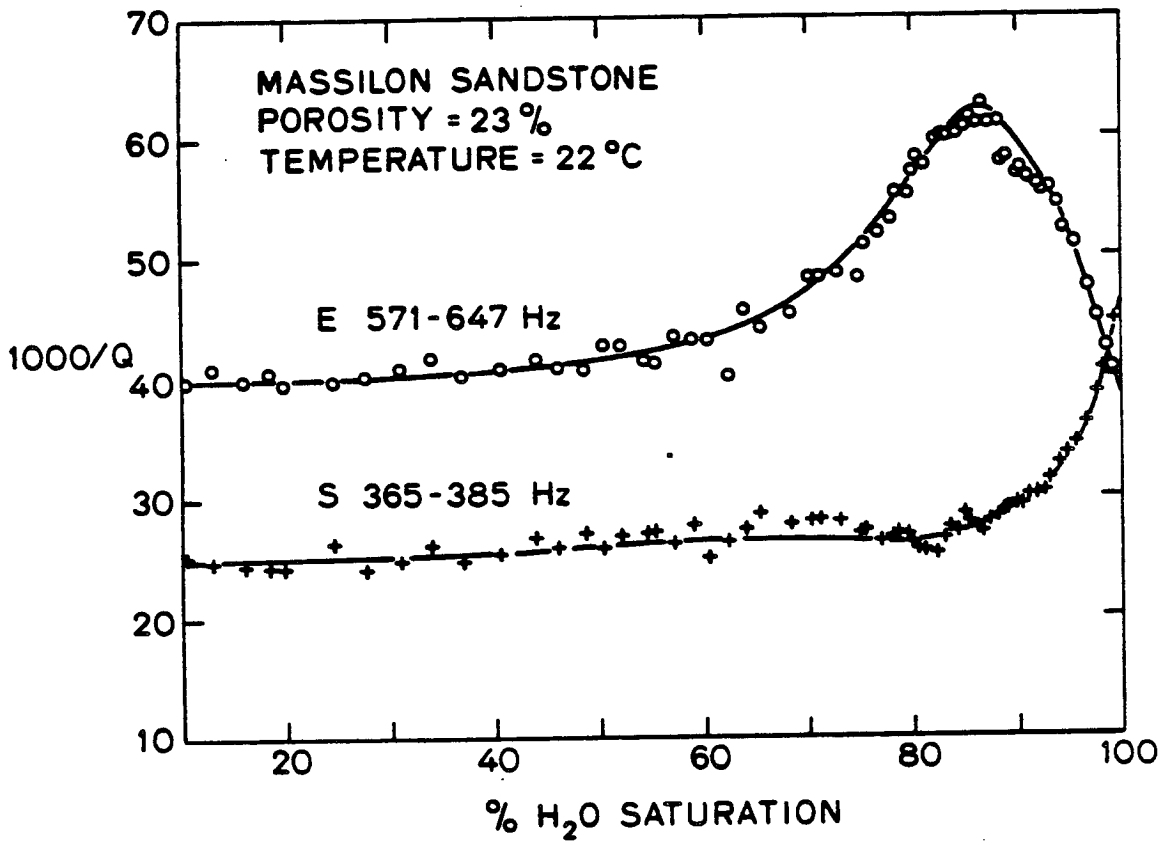

Fig. 6. $1000/Q_e$ and $1000/Q_s$ vs. % H_2O saturation (S_w = 0.10 - 1.00) in Massilon sandstone.

constant, and the composite density, which is a function of S_w given by equation (2). The dependence of V_s on S_w is thus purely a density effect. The bulk compressional contribution to V_e is determined by the composite density; the porosity, which is a constant; the bulk modulus of the individual grains, which is a constant; the frame bulk modulus, which is a constant; and the pore fluid bulk modulus. At full water saturation, the pore fluid bulk modulus is the same order of magnitude as the frame bulk modulus. However, the introduction of a significant amount of gas into the pores reduces the pore fluid bulk modulus effectively to 0. Thus the initial 16% drop in V_e (figure 5) is a modulus effect. The subsequent increase in V_e is a density effect.

Energy loss in partially saturated Massilon sandstone is controlled by viscous dissipation resulting from wave-induced pore fluid flow. Unfortunately, a fully satisfactory theory has not yet been published. We contend that the paucity of experimental data has precluded delineation of the micromechanics. Enough is known however to make several qualitative hypotheses here.

Two flow mechanisms have been proposed for fully saturated sands and sandstones. Biot[14] first noted that oscillation of a pore wall in its plane would entrain fluid, diffuse vorticity, and dissipate energy. The idealized case is known in fluid mechanics as "Rayleigh's problem" (Although it was originally solved by Stokes in 1851[42]). This mechanism predicts that for full saturation, $1000/Q_s > 1000/Q_e$, as observed in figure 6. However, it further predicts a strong frequency dependence centered at 10^4-10^5 Hz for Massilon sandstone. And at acoustic frequencies, the predicted losses are insignificant

compared to those we observe. The other flow mechanism has, in the geophysics literature,[43-45] been given the misnomer "squirt", which unwittingly implies a fluid jet. We prefer the less provocative term "squish" and a simple description: the compression of grain contacts and fine capillaries generates a local pore pressure field which drives dissipative fluid flow. Although comprehensive treatment of this mechanism is lacking, particular theoretical results[43-45] are quite encouraging. Phenomenologically, the "squish"-type mechanism yields a linear viscoelastic stress relaxation,[15] roughly similar to Zener's[46] standard linear solid. At full saturation, bulk compressional losses are small, because the hydrostatic compression of low-compressiblity pores generates relatively weak gradients in the pore pressure field. Shearing, however, provides stronger gradients between adjacent contacts and capillaries having different orientations and aspect ratios. Thus $1000/Q_s > 1000/Q_e$ at full saturation.[44] The predicted center frequency for the relaxation in high porosity sandstones lies in the range between 10^3-10^4 Hz.[45] And the predicted magnitudes of Q^{-1} are comparable to those we observe in Massilon at 500 Hz.

At partial saturation, the large compressibility of the gas-water mixture enhances local pore pressure gradients within individual pores. Thus in partially saturated sandstones, "squish" becomes essentially a bulk compressional mechanism, resulting in a $1000/Q_e$ much greater than $1000/Q_s$.[43] Extensional wave energy is absorbed most efficiently in the range 0.95 to 0.75 S_w (figure 6). In this saturation range, the loss occurs predominantly in the larger pores (i.e. 25 to 100 μm) and is very sensitive to changes in S_w. As indicated by the peak at $S_w \sim 0.85$, the conditions for dissipation in the large pores are

optimal at that given water saturation. Below S_w - 0.60, the losses appear to be weakly affected by the variation in saturation. In this saturation range, the larger pores are sufficiently drained and no longer contribute significantly to the losses. Here, it is the capillaries which provide the principle sites for spatial pore pressure gradients, water flow, and viscous dissipation. As the capillaries themselves remain water saturated down to S_w - 0.01, it is not surprising to find that Q^{-1} in both extension and shear is rough independent of S_w in this range.

C. Frequency Dependence

A major criticism of fluid flow mechanisms in the past has been the lack of supporting evidence for a strong frequency dependence. In this section, we report such evidence.

Observations

Figure 7 displays $1000/Q_e$ and $1000/Q_s$ versus S_w at two different sets of frequencies. In this figure, the data from figure 6 is replotted along with new data taken on a second Massilon bar, cut to 70 cm. In shear, the higher frequency data (525 Hz) demonstrates at least a 10%, and sometimes a 30%, increment in loss over the lower frequency (375 Hz) data. In extension, $1000/Q_e$ at 825 Hz is at least 4%, and sometimes 30%, greater than $1000/Q_e$ at 575 Hz. It had previously been established at a given wavelength under ambient conditions that the second Massilon sample is ~9% higher in V_e, ~12% higher in V_s, ~2% smaller in $1000/Q_e$, and ~4% greater in $1000/Q_s$ than the first Massilon sample. Thus, the increase with frequency observed in 1000/Q is significant throughout the saturation range tested.

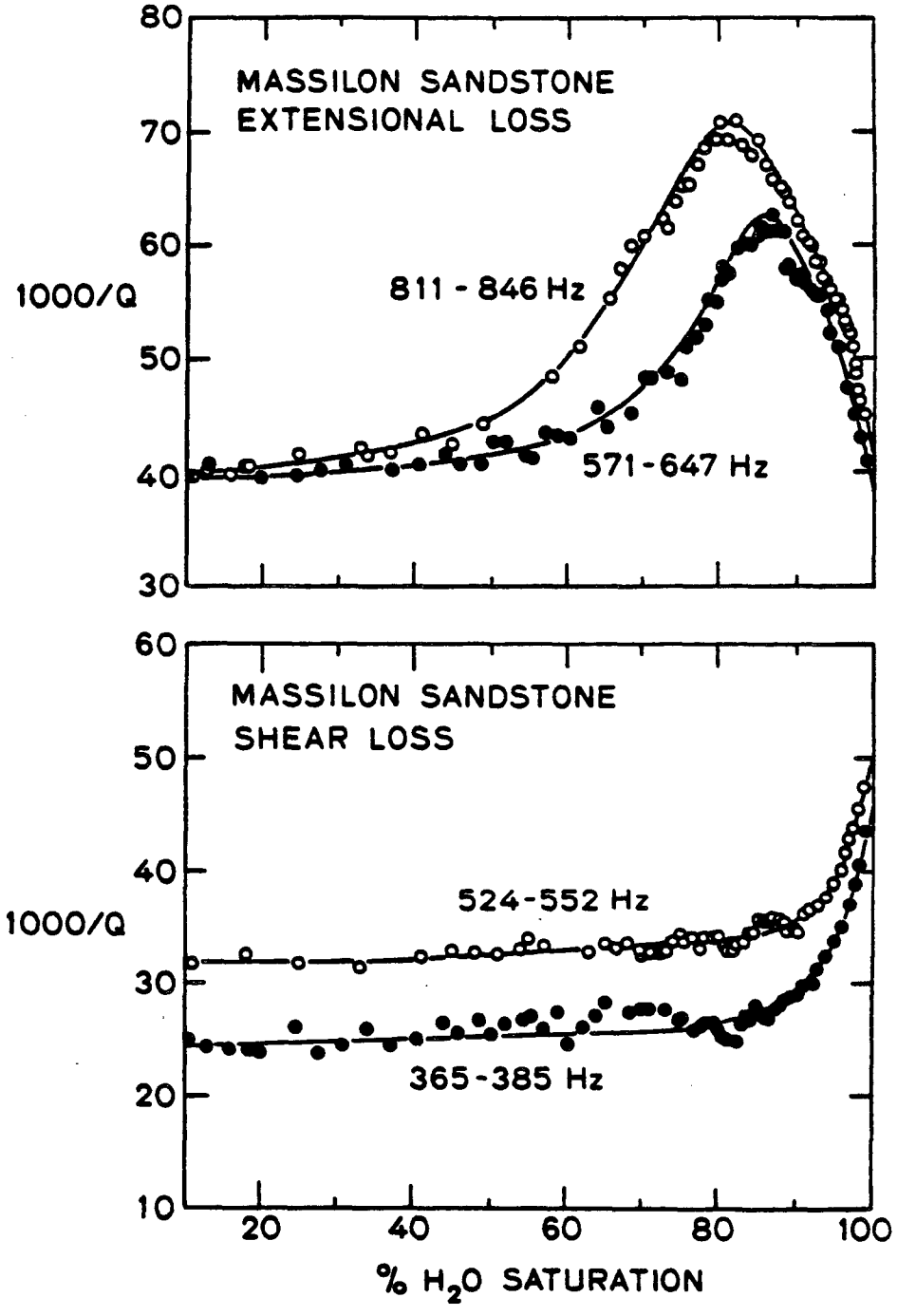

Fig. 7. $1000/Q_e$ and $1000/Q_s$ vs. % H_2O (S_w = 0.10 - 1.00) in Massilon sandstone at two different sets of frequencies: (above) E loss at 571-647 Hz and 811-846 Hz; (below) S loss at 365-385 Hz and 524-552 Hz.

Figures 8 and 9 demonstrate the frequency dependence of 1000/Q from 25 to 14,000 Hz in partially saturated Massilon sandstones at 0.92-0.90 S_w , 0.76-0.74 S_w , 10^{-3} S_w , and the very dry state. In very dry Massilon, 1000/Q in the acoustic range is independent of frequency. The extensional loss is slightly greater than the shear loss. At $S_w = 10^{-3}$, we observe in both modes an overall increase and a weak dependence with a small peak at about 5 kHz. At 0.92-0.90 S_w , a strong dependence (i.e., a factor of 5) is found. The data suggests a peak around 3-4 kHz. $1000/Q_e$ is greater than $1000/Q_s$, and the dependence in both modes looks remarkably similar. As S_w is decreased to 0.76-0.74 (figure 9), the E dependence becomes sharper, and S flattens slightly.

We wish to express caution with regard to the resolution of the peaks, particularly $1000/Q_e$ at 0.76-0.74 S_w. We reiterate that i) the observed dependence is an aggregate of 23 different bars from 13 different samples, measured at coarsely controlled S_w , and ii) the upper limit on 1000/Q measurable in our system is 125.

The frequency dependence of Vycor porous glass from 1 to 14 kHz is shown in figure 10. The data designated dry was taken on brand new, clean Vycor bars at $S_w = 0$ and $P/P_0(H_2O) \sim 0.30$. In these bars, which had not yet been hydrated, 1000/Q is independent of frequency in both modes; and $1000/Q_s$ is slightly higher than $1000/Q_e$. The saturation data were taken in a different set of bars, which had been used several times previously. When dry, these bars exhibit a light yellow color rather than the characteristic light blue. The glass is hydrated, and the pore surface may possibly be polluted by the absorption of organic components which are present in trace amounts in

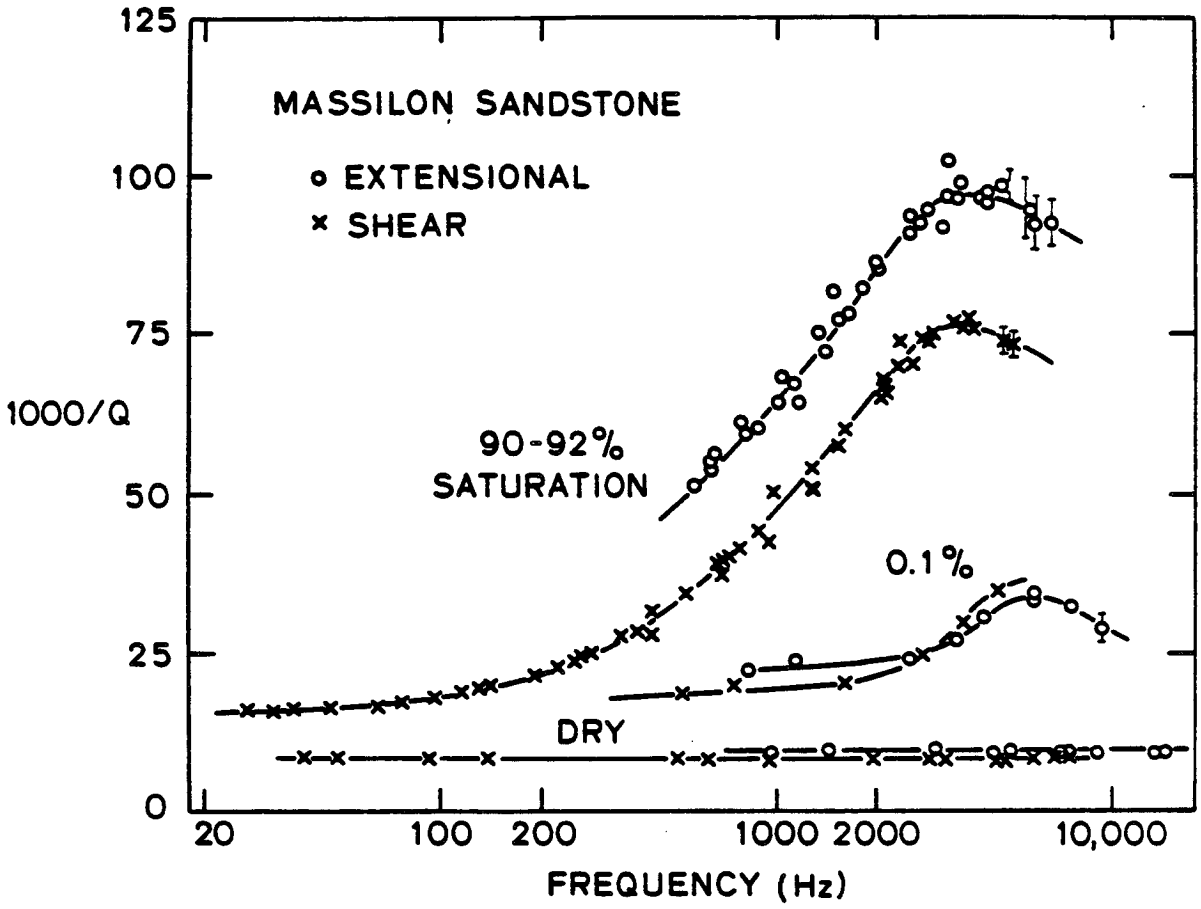

Fig. 8. $1000/Q_e$ and $1000/Q_s$ vs. frequency in Massilon sandstone at 0.92-0.90 S_w , 10^{-3} S_w , and the very dry state.

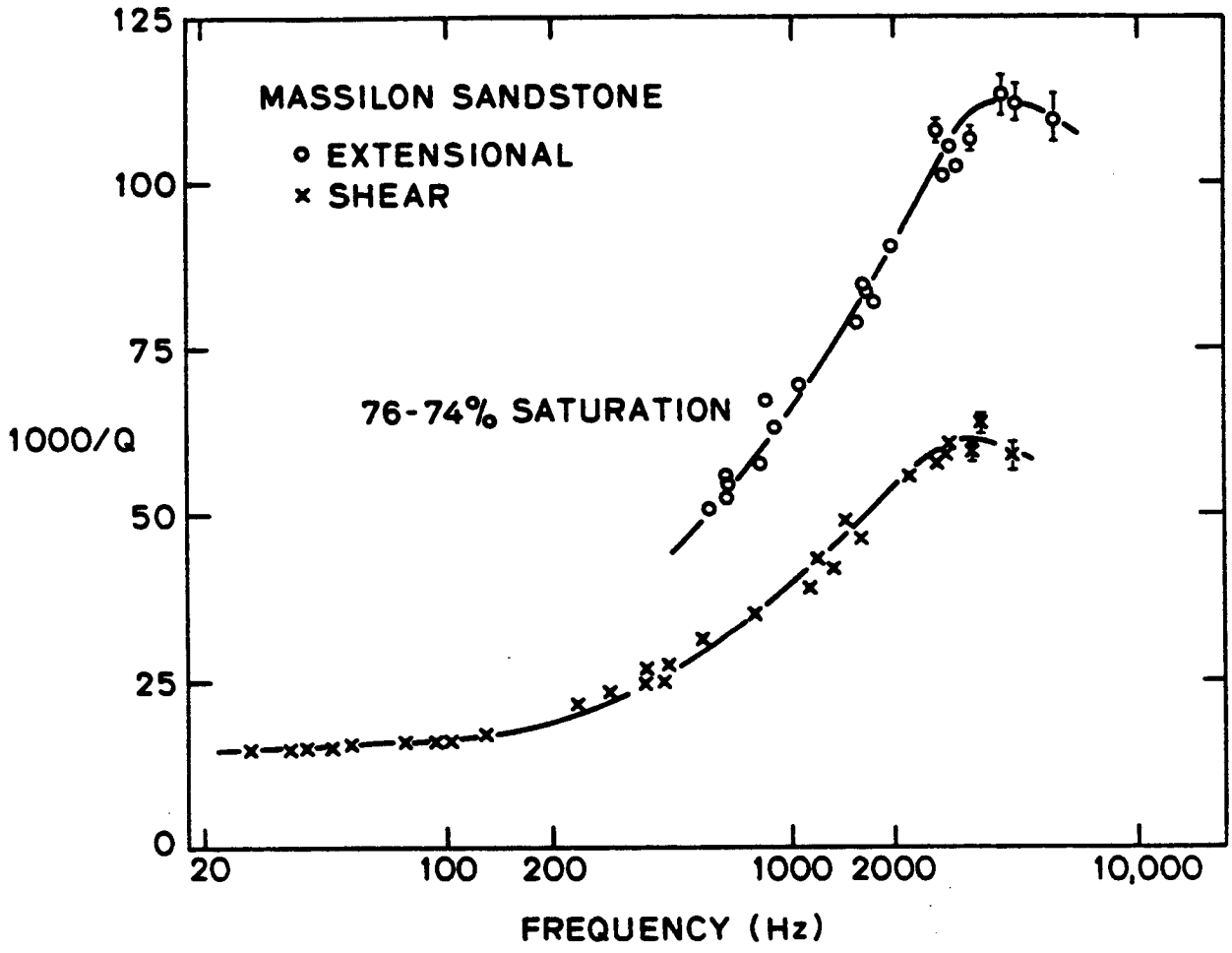

Fig. 9. $1000/Q_e$ and $1000/Q_s$ vs. frequency in Massilon sandstone at $S_w = 0.76 - 0.74$.

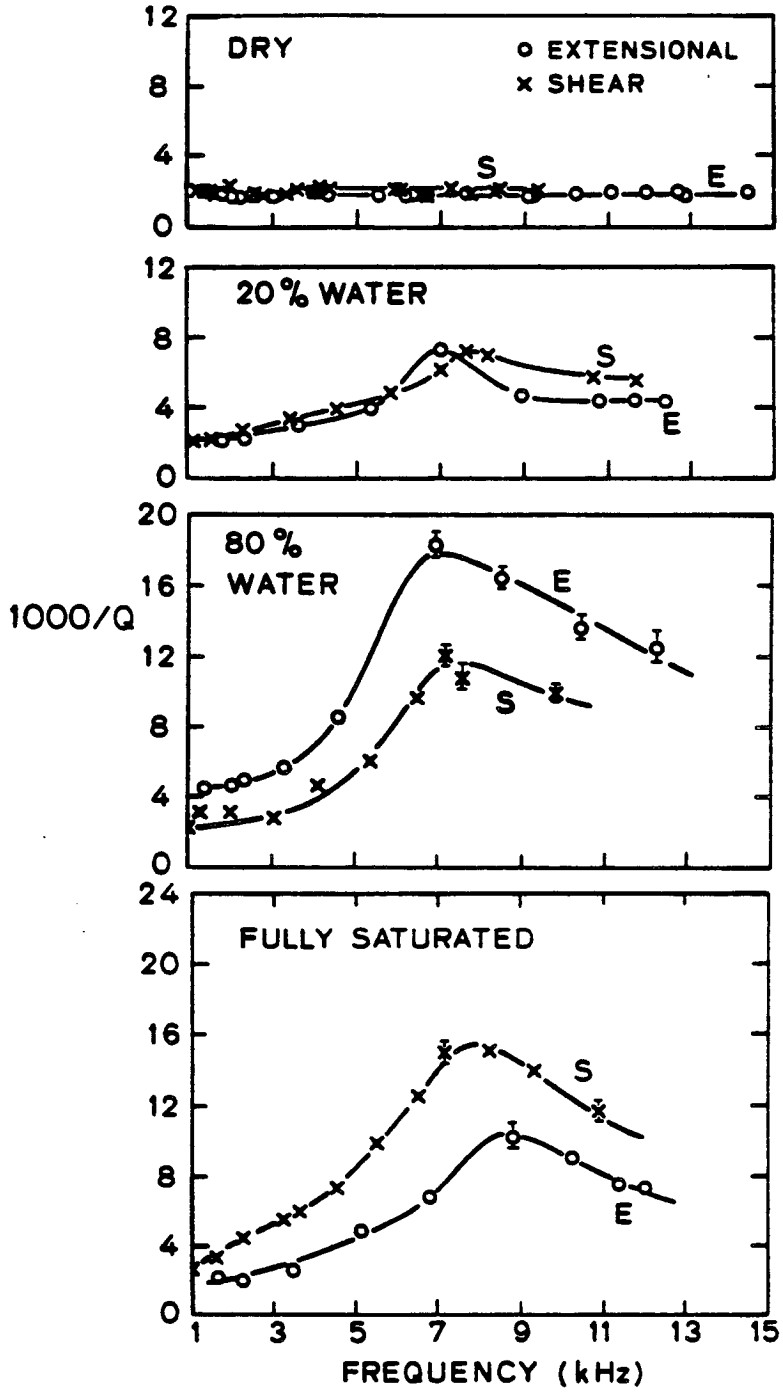

Fig. 10. $1000/Q_e$ and $1000/Q_s$ vs. frequency as a function of partial water saturation in Vycor porous glass.

the atmosphere. In the fully saturated Vycor, $1000/Q_s$ exhibits a peak at 7.5 kHz and is greater than $1000/Q_e$ throughout the frequency range tested. The extensional peak occurs closer to 8.5 kHz. At $S_w = 0.80$, $1000/Q_e$ is greater than $1000/Q_s$. The E dependence is very sharp and asymmetric. From 0.80 down to 0.20 S_w, the peaks progressively flatten with decreasing saturation.

Discussion

Partially saturated Massilon sandstone at S_w from 0.92 to 0.75 exhibits a strong frequency dependence with characteristic relaxation times the order of 0.5 to 0.2 msec. $1000/Q_e$ is consistently greater than $1000/Q_s$, and the E dependence is stronger than S. Both E and S demonstrate a sensitivity to S_w. Presumably, the E dependence is diminishing below $S_w \sim 0.85$-0.80. The observed frequency dependence, coupled with the observed sensitivity to S_w - particularly at these high saturations - is strongly indicative of the squish-type attenuation mechanisms.

Similar frequency responses have been observed in fully saturated materials over limited band widths. Stoll[22] and Brunsen and Johnson[47] have measured the S loss in fully saturated quartz sands. Tittmann et al.[48] and Spencer[36] have measured the E loss, while Winkler[28] has measured the S loss, in saturated quartz-rich sandstones. Although fully adequate evidence is still unavailable, existing data suggests that in fully saturated materials i) the loss in shear consistently exceeds that in extension, and ii) the shear frequency dependence is stronger than extensional dependence. With the gradual introduction of gas into the pore fluid, the pore compressibility jumps sharply. The topology of the two fluid phases varies within the

pores. The local stress fields change, and the flow configuration alters. At $S_w = 0.97$, $1000/Q_s$ at 560 Hz is smaller than $1000/Q_e$ at the same frequency (see figure 12). However, some preliminary data taken at 0.98-0.96 S_w suggests that the shear frequency dependence is still stronger at this saturation and protrudes above extension at ~1 kHz. Clearly, as the water saturation declines to ≤ 0.92, the extensional loss is stronger throughout the frequency range. This relationship is expected to hold down to $S_w \sim 0.01$.

The thermoelastic mechanism proposed by Kjartansson and Nur[49] also predicts a dependence of $1000/Q_e$ on both water saturation and frequency. It does not, however, account for losses in shear. The predicted peak in $1000/Q_e$ with S_w is spike-like at $S_w = 0.99$. And the magnitude of the predicted losses at ambient temperature and pressure are far too small to account for those observed in Massilon. Furthermore, the frequency dependences of 1000/Q at both 0.92-0.90 and 0.76-0.74 S_w are quite sharp. The narrowness of the observed relaxations are inconsistent with a diffusive process such as thermal relaxation.

Another important point may be gleaned from the observed frequency dependence (figure 8 and 9). At low acoustic frequencies (i.e., $f < 100$ Hz) the frequency dependent behavior is gradually yeilding to a frequency-independent background loss. A strain amplitude test (figure 11) taken at 78 Hz demonstrates that this frequency-independent loss - occurring at strains $<10^{-6}$ Hz - is not due to a nonlinear frame mechanism, such as friction grain sliding.[50,51] At these frequencies, the effect of S_w is small but significant. At 78 Hz, $1000/Q_s$ is 16.95 with $S_w = 0.90$, while it is 14.5 with $S_w = 10^{-3}$. This 18% increase

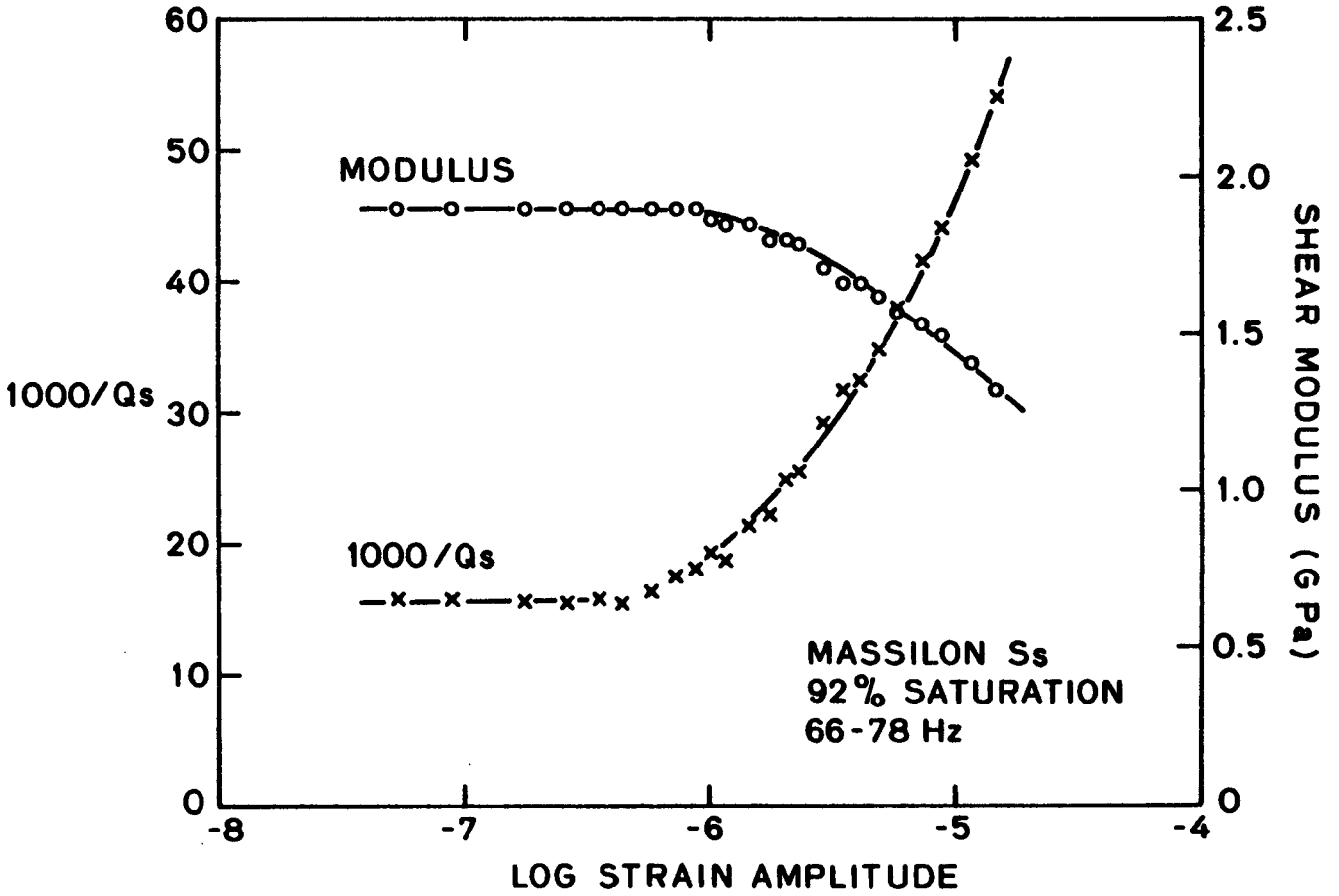

Fig. 11. Strain amplitude test at 66-78 Hz in Massilon sandstone at $S_w = 0.92$.

indicates that viscous dissipation is the controlling mechanism even at low acoustic frequencies where Q^{-1} is frequency independent. The actual flow process remains as yet unspecified.

An unusual model has been proposed by Spencer[35] to explain the acoustic frequency dependence in saturated sandstones. The attenuation mechanism is supposed to be hydrogen bond breakage between water molecules and surface hydroxyls. In this model, the loss is claimed to be independent of microstructure. Yet if the energy loss is indeed due to a surface (bond breaking) mechanism, it must be, by definition, a direct function of pore surface area. Vycor has very small pores, 5 nm in diameter, and a relatively large surface, 200 m^2/g. However, the observed loss is systematically 1/6 that of Massilon, which has 10-100 μm pores and a pore surface area roughly 1 m^2/g. Even though Vycor consists of 96% amorphous silica, while Massilon has 4% amorphous silica and 88% quartz, the disorder of the SiO_2 substrate should be insignificant in comparison to the surface area effect. Therefore, Spencer's model is inconsistent with our observations. Moreover, it is unclear how the bond breaking mechanism implies a frequency dependence for stress wave attenuation in the acoustic frequency band. Lastly, a surface mechanism is unable to explain the strong dependence of Q^{-1} on S_w in Massilon sandstone in the higher water saturation range.

To explain the smaller loss in Vycor relative to Massilon, we need to consider the effect of grain contact geometry on the squish mechanism.[45] SEM studies reveal that Vycor consists of a disordered packing of sintered glass beads. The sintered contacts are extremely regular and have relatively high aspect ratios. Massilon, on the

other hand, has a broad distribution of aspect ratios - some being very small - and many near contacts or thin gaps between grains. Smaller aspect ratio (i.e. flatter) contacts and near contact gaps are more compliant.[52] Their compression thus generates high local pore pressures and results in greater viscous dissipation.

We were initially surprised by the relaxation center frequencies between 7 and 9 kHz in Vycor. Yet Palmer and Traviolia[45] suggest that squish absorption may be independent of absolute grain size. These peaks, therefore, are not irreconcilable with squish, given improved formulation of the microfluid dynamics. The observed Q^{-1} dependence on water saturation is entirely consistent with our expectations for squish type fluid flow mechanisms.

In section II-A, we established the surface or capillary film mechanism, which is thought to control the loss in dry Massilon and Vycor, to be linear and very sensitive to humidity. In figure 8, we find that it is also independent of frequency, at least in the acoustic range. The onset of bulk viscous flow, as evidenced by a frequency dependence, is not observed until $S_w = 10^{-3}$. Similar conclusions may be drawn from Born's data on Amherst sandstone[53] and Pandit and King's measurements on Berea sandstones.[35]

The question remains that if Vycor has such a relatively large surface, then why does Massilon continue to have a larger loss in a correspondingly dry state? We think that the capillary film mechanism is strongly dependent on microstructure. Besides $P/P_0(H_2O)$ and other fluid properties (i.e. viscosity, surface tension, wettability, pH), the micro-capillary hysteresis should be sensitive to capillary surface roughness and capillary aspect ratio (i.e., half

width to half length ratio). The rougher surfaces generate greater viscous losses. The smaller aspect ratio (flatter) capillaries are more compliant;[52] thus more surface area is deformed each cycle and more bonds are broken. As seen under a SEM, Massilon has angular grains with very rough surfaces and very compliant capillaries between grain contacts. In contrast, Vycor has a very smooth surface, spherically isotropic pores, and sintered contacts.

The capillary film mechanism may exhibit a frequency dependence in the ultrasonic range. Mason[36,37] has observed, in laboratory dry slate and granite, a flat response from 10^4 - 10^5 Hz; then, a significant peak from 10^5 - 10^7 Hz. The response of dry Massilon at ultrasonic frequencies is unknown.

III. DISCUSSION OF COMPRESSIONAL WAVE ATTENUATION

One may calculate compressional wave and bulk compressional specific attenuation, Q_p^{-1} and Q_k^{-1}, having measured V_e, V_s, Q_e^{-1} and Q_s^{-1} at a single frequency respectively. Q_p^{-1} is given by

$$\frac{1000}{Q_p} = \frac{1000}{(1-\nu)(1-2\nu)} \left(\frac{1+\nu}{Q_e} - \frac{2\nu(2-\nu)}{Q_s} \right) , \tag{3}$$

and Q_k^{-1} is given by

$$\frac{1000}{Q_k} = \frac{1000}{(1-\nu)} \left(\frac{3}{Q_e} - \frac{2(1+\nu)}{Q_s} \right) , \tag{4}$$

Where ν is Poisson's ratio of the composite material,

$$\nu = \frac{1}{2} \left(\frac{V_e}{V_s} \right)^2 - 1 \tag{5}$$

Given equations (3) and (4) it is easy to show that when ν is positive, either

$$Q_s^{-1} > Q_e^{-1} > Q_p^{-1} > Q_k^{-1} \quad , \tag{6a}$$

$$Q_s^{-1} = Q_e^{-1} = Q_p^{-1} = Q_k^{-1} \quad , \tag{6b}$$

or

$$Q_s^{-1} < Q_e^{-1} < Q_p^{-1} < Q_k^{-1} \quad . \tag{6c}$$

Figure 12 shows the measured $1000/Q_e$ and $100/Q_s$ vs. S_w at roughly 560 Hz, along with the calculated values for $1000/Q_p$ and $1000/Q_k$. Errors are approximately 5% for P and 10% for K. Error bars are omitted so as not to clutter the figure. Relations (6a) are found to hold in a very limited range for the nearly fully saturated sandstone. Equation (6b) holds at a point near $S_w = 0.98$. And as expected, relations (6c) hold across nearly the entire range of partial saturation. In other words, bulk compressional losses dominate in partially saturated Massilon sandstone. Below $S_w = 0.98$, the P loss closely emulates the E loss because the Poisson's ratio is ~0.02 throughout that range of saturation.

Figure 13 represents our conception of the effect of partial water saturation on compressional specific attenuation as a function of frequency, based on our limited data. Several points may be drawn from this figure. Constant Q models[27] may, with caution, be a valid approximation for fully and partially water saturated, high porosity sandstones in the exploration range (i.e., 10-100 Hz). (This may not be the case, however, if high viscosity oil is present

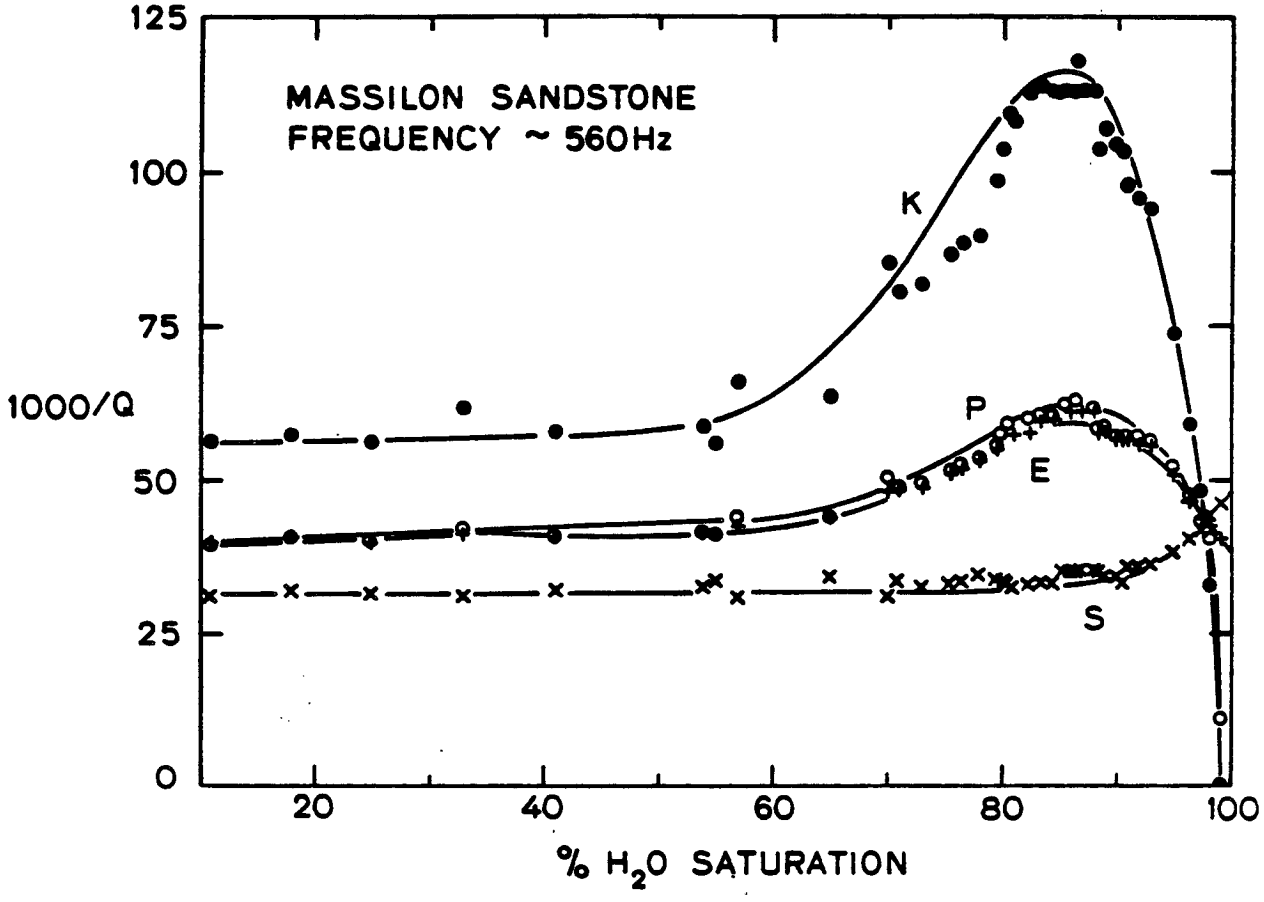

Fig. 12. Calculated $1000/Q_p$ and $1000/Q_k$, along with measured $1000/Q_e$ and $1000/Q_s$, at ~560 within Hz vs. % H_2O saturation in Massilon sandstone.

Fig. 13. Schematic $Q_p^{-1} - f - S_w$ surface for Massilon sandstone:

a) three dimensional conception;

b) corresponding contour map.

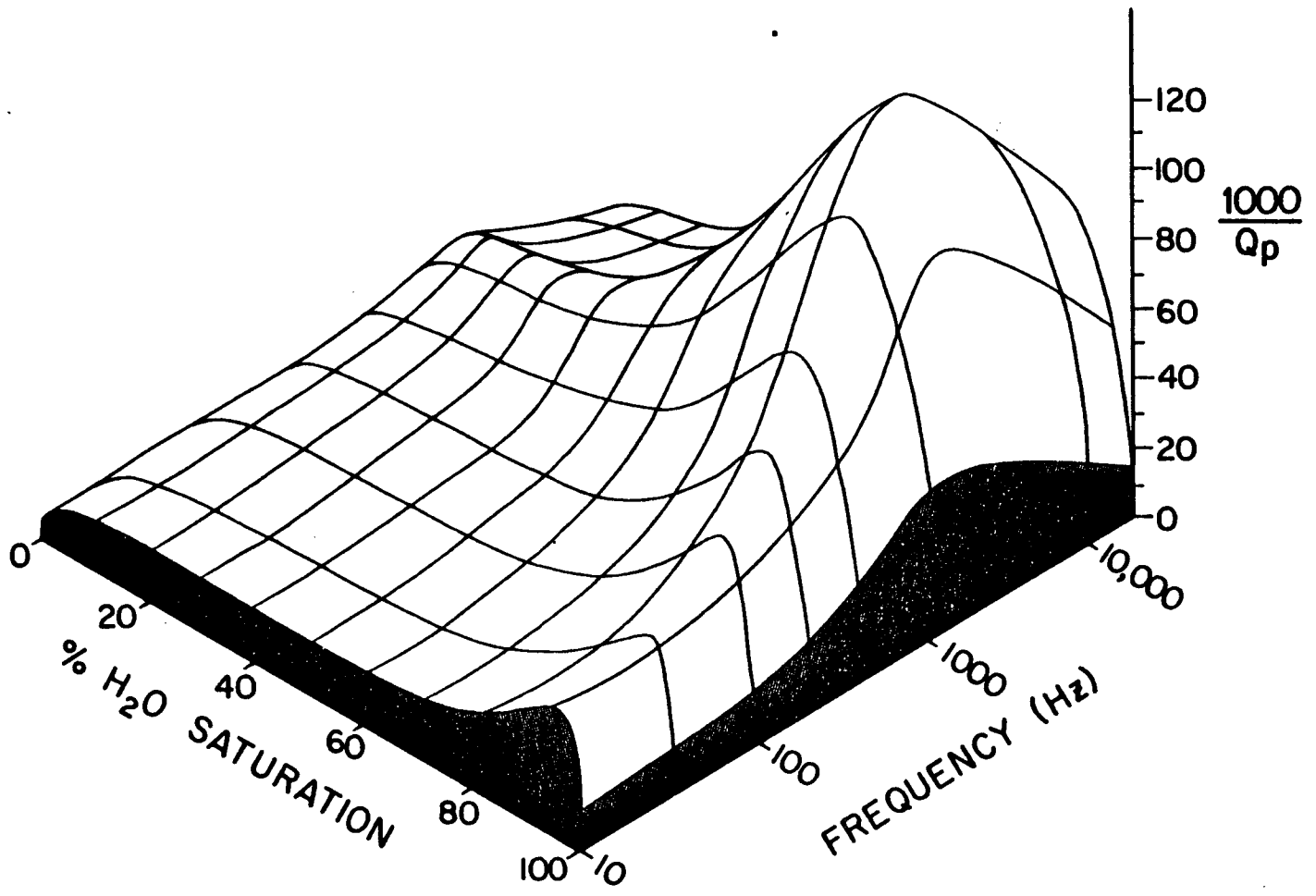
120
100
80
60
40
20
0
1000/Qp
0
20
40
60
80
100
% H2O SATURATION
10
100
1000
10,000
FREQUENCY (Hz)

Figure 13a.

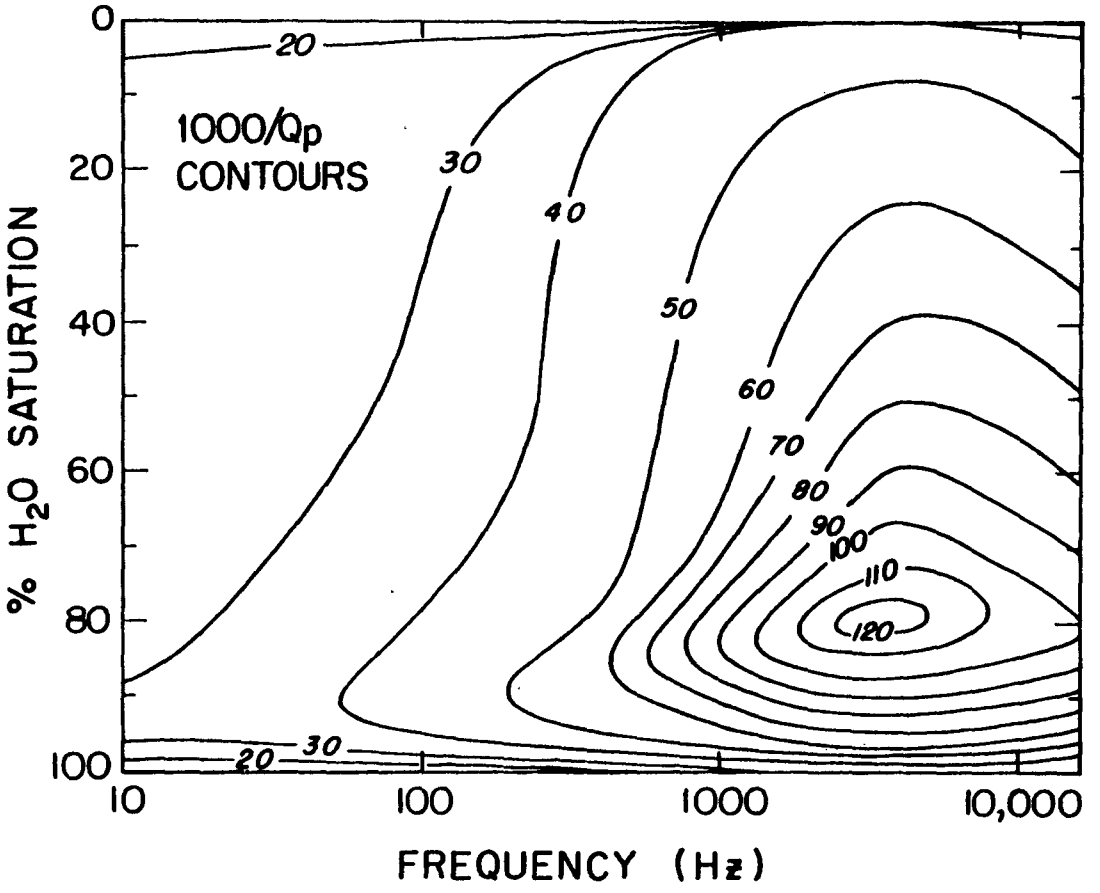
1000/Qp
CONTOURS
20
30
40
50
60
70
80
90
100
110
120
20
30
0
20
40
60
80
100
% H2O SATURATION
10
100
1000
10,000
FREQUENCY (Hz)

Figure 13b.

in the pores.) At full water saturation, compressional losses and frequency dependence may be relatively weak. Even so, Hamilton's in situ measurement of $Q_p \sim 32$ at 14 kHz in saturated shelf sands may approach $Q_p \sim 100$, as the frequency goes to 10 Hz. P velocity dispersion should not be expected to be very large in fully saturated granular materials. However, in partially saturated sandstones, the correlation of acoustic measurements taken at seismic frequencies (i.e. 10-100 Hz) with those measured in a borehole (i.e., taken at 10-30 kHz), may indeed require correction due to the frequency dependence.

In figure 14, we have plotted V_p/V_s and Q_p^{-1}/Q_s^{-1} vs. water saturation at 560 Hz. This figure shows that at 560 Hz, the acquisition of all four properties V_p, V_s, Q_p^{-1}, and Q_s^{-1}, yields sufficient information to distinguish between a fully and partially saturated Massilon. If $V_p/V_s > 2$ and $Q_p^{-1}/Q_s^{-1} < 1$, then the Massilon is fully saturated. The situation for determining the degree of partial saturation is far less promising. The effect observed in the attenuation ratios is not within the resolution of current field techniques.

IV. CONCLUSIONS

Resonance experiments on a high porosity, quartz-rich sandstone at ambient temperature and pressure have shown that in the acoustic frequency range:

i) Attenuation is very sensitive to partial water saturation.

ii) Q^{-1} in partially saturated sandstones is strongly frequency dependent. In dry sandstones, Q^{-1} is independent of frequency.

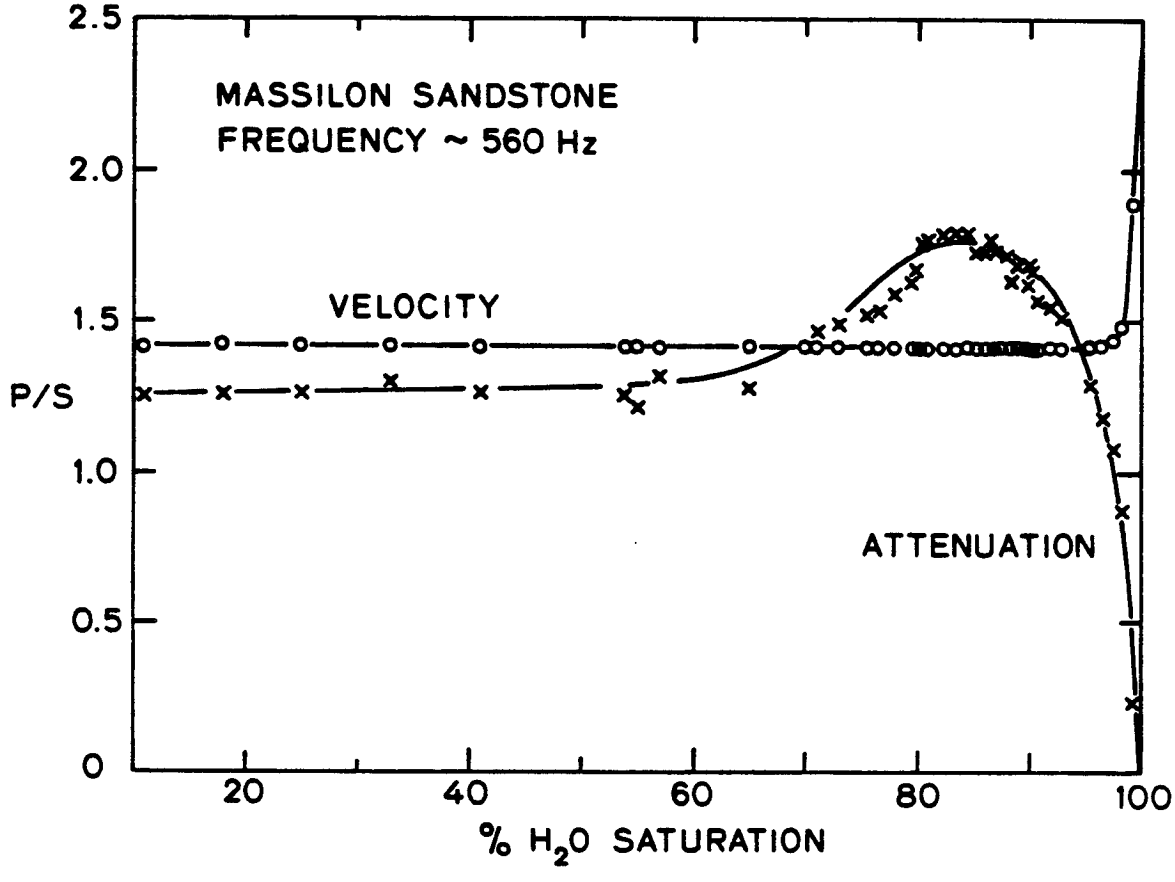

Fig. 14. V_p/V_s and Q_p^{-1}/Q_s^{-1} at ~560 Hz vs. % H_2O saturation in Massilon sandstone.

iii) Two distinct types of pore fluid mechanisms are significant: a surface, capillary film mechanism and viscous dissipation due to wave induced fluid flow in the pores. Viscous dissipation dominates at water saturations from 1 to 100%. Nonlinear mechanisms are not important at normal acoustic strains.

iv) Given the development of a satisfactory theory for wave propagation in porous granular materials, acoustic measurements may provide significant information about pore fluids and their mobility in sands and sandstones.

ACKNOWLEDGEMENTS

Amos Nur is the director of the Stanford Rock Physics Project. This paper constitutes the third chapter of a doctoral dissertation. Joel Walls is responsible for the torsional pendulum system, and throughout this work has been helpful in enumerable ways. Many aspects of this research have been discussed with Ken Winkler. Stephanie Williams drafted the figures. The Stanford Rock Physics Project is funded by a consortium of 15 oil companies and S.D.R. The author is supported as a graduate student by the Office of Naval Research under contract N00014-77-C-0390 with the Marine Geology and Geophysics Program.

References

1. R.J. O'Connell and B. Budanisky, "Measures of dissipation in viscoelastic media", Geophys. Res. Lett. 5, 5-8 (1978).
2. E.L. Hamilton, "Compressional wave attenuation in marine sediments", Geophys. 37, 620-646 (1972).
3. E.L. Hamilton, "Sound attenuation as a function of depth in the sea floor", J. Acoust. Soc. Am. 59, 528-535 (1976).
4. E.L. Hamilton, "Geoacoustic modeling of the sea floor", J. Acoust. Soc. Am. 68, 1313-1340 (1980).
5. A.L. Anderson and L.D. Hampton, "Acoustics of gas bearing sediments, I. Background", J. Acoust. Soc. Am. 67, 1865-1889 (1980) & II. "Measurements and models", J. Acoust. Soc. Am. 67, 1890-1903 (1980).
6. K.E. Hawker, W.E. Williams and T.L. Forman, "A study of the acoustical effects of sub-bottom absorption profiles", J. Acoust. Soc. Am. 65, 360-367 (1979).
7. A.L. Frisillo and T.J. Stewart, "Effect of partial gas brine saturation on ultrasonic absorption in sandstones", J. Geophys. Res. 85, 5209-5211 (1980).
8. S.N. Domenico, "Effect of water saturation on seismic reflectivity of sand reservoirs encased in shales", Geophys. 39, 759-769 (1974).
9. S.N. Domenico, "Effect of brine-gas mixture on velocity in an unconsolidated sand reservoir", Geophys. 41, 882-894 (1976).
10. S.N. Domenico, "Elastic properties of unconsolidated porous sand reservoirs", Geophys. 42, 1339-1368 (1977).
11. S.E. Elliott and B.F. Wiley, "Compressional velocities of partially saturated unconsolidated sand", Geophys. 40, 949-954 (1975).

12. T. Plona, "Observation of a second bulk compressional wave in a porous medium at ultrasonic frequencies", Appl. Phys. Lett. 36, 259-261 (1980).

13. M.A. Biot, "General theory of three dimensional consolidation", J. Appl. Phys. 12, 155-164 (1941).

14. M.A. Biot, "Theory of propagation of elastic waves in a fluid-saturated porous solid, I. Low frequency Range", J. Acoust. Soc. Am. 28, 168-178 (1956) & "II. High frequency range", J. Acoust. Soc. Am. 28, 179-191 (1956).

15. M.A. Biot, "Generalized theory of acoustic propagation in porous dissipative media", J. Acoust. Soc. Am. 54, 1254-1264 (1962).

16. M.A. Biot and D.G. Willis, "Elastic coefficients of the theory of consolidation", J. Appl. Mech. 24, 594-601 (1957).

17. M.A. Biot, "Nonlinear and semilinear rheology of porous solids", J. Geophys. Res. 78, 4924-4937 (1973).

18. K.W. Winkler, A. Nur, and M. Gladwin, "Friction and seismic attenuation in rocks", Nature 227, 528-531 (1979).

19. K.W. Winkler and A. Nur, "Pore fluids and seismic attenuation in rocks", Geophys. Res. Lett. 6, 1-5 (1979).

20. M.R.J. Wyllie, G.H.F. Gardner, and A.R. Gregory, "Studies of elastic wave attenuation in porous media", Geophys. 27, 569-589 (1962).

21. B.R. Tittmann, V.A. Clark, J.M. Richardson, and T.W. Spencer, "Possible mechanisms for seismic attenuation in rocks containing small amounts of volatiles", J. Geophys. Res. 85, 5199-5208 (1980).

22. R.D. Stoll, "Experimental studies of attenuation in sediments", J. Acoust. Soc. Am. 66, 1152-1160 (1979).

23. G.H.F. Gardner, M.R.J. Wyllie, and D.M. Droschak, "Effects of pressure and fluid saturation on the attenuation of elastic waves in sands", J. Petr. Tech. 15, 189-198 (1964).

24. D.H. Johnston, M.N. Toksoz and A. Timur, Attenuation of seismic waves in dry and saturated rocks, II. Mechanisms", Geophys. 44, 691-711 (1979).

25. D.H. Johnston and M.N. Toksoz, "Ultrasonic P and S wave attenuation in dry and saturated rocks under pressure", J. Geophys. Res. 85, 925-936 (1980).

26. R.S. Jacobson, G.G. Shor Jr. and L.M. Dorman, "Linear inversion of body wave data - Part II: Attenuation versus depth using spectral ratios", Geophys. 46, 152-162 (1981).

27. E. Kjartansson, "Constant Q-wave propagation and attenuation", J. Geophys. Res. 84, 4737-4748 (1979).

28. J. Duffy and R.D. Mindlin, "Stess-strain relations of a granular medium", J. Appl. Mech. 24, 585-593 (1957).

29. K.W. Winkler and A. Nur, "Seismic attenuation: the effects of pore fluids and frictional sliding", Geophysics (1982, in press).

30. S. Spinner and W.E. Tefft, "A method for determining mechanical resonance frequencies and for calculating elastic moduli from these frequencies", Proc. ASTM 61, 1221-1238 (1961).

31. Achieving full saturation in a rock is not a trivial procedure. The sample is first evacuated at 5 μm for 3 days. It is then flooded with 2 MΩ deionized H_2O which has been deaeriated by evacuation for 2 days. Subsequently, the sample and its pore fluid are pressurized to 20 MPa. After 5 days, the sample is removed from the vessel and immediately sealed in Saran Wrap. When the sample is securely

mounted in the measurement frame, the Saran Wrap is removed.

32. L. Peselnick and W.F. Outerbridge, "Internal friction in shear and shear modulus of Solenhofen limestone over a frequency range of 10^7 cycles per second", J. Geophys. Res. 66, 581-588 (1961).

33. B.O. Hardin and F.E. Richart, "Elastic wave velocities in granular soils", J. Soil Mech. Found. Div. 89, 33-65 (1963).

34. V.A. Clark, B.R. Tittmann, and T.W. Spencer, "Effect of volatiles on attenuation (Q^{-1}) and velocity in sedimentary rocks", J. Geophys. Res. 35, 5190-5198 (1980).

35. B.I. Pandit and M.S. King, "The variation of elastic wave velocities and quality factor Q of a sandstone with moisture content", Can. J. Earth Sci. 16, 2187-2195 (1979).

36. W.P. Mason, D.N. Beshers, and J.T. Kuo, "Internal friction in Westerly granite: relation to dislocation theory", J. Appl. Phys. 41. 5206-5209 (1970).

37. W.P. Mason and J.T. Kuo, "Internal friction in Pennsylvania slate", J. Geophys. Res. 76, 2084-2089 (1971).

38. J.W. Spencer, "Stress relaxations at low frequencies in fluid-saturated rocks: Attenuation and modulus dispersion", J. Geophys. Res. 86, 1803-1812 (1981).

39. D. Griggs, "Hydrolytic weakening of quartz and other silicates", Geophys. J.R. Soc. 14, 19-31 (1967).

40. W.D. Kingery, "Sintering in the presence of a liquid phase", in *Kinetics of High Temperature Processes*, edited by W.D. Kingery (Wiley, New York, 1959) pp. 187-194.

41. F. Gassmann, "Euber die elastizitat poroser medien", Vierteljahrsschr. Naturforsch. Ges. Zuerich, Heft I (1951).

42. G.G. Stokes, "On the effect of the internal friction of fluid on the motion of pendulums", Mathematical and Physical Papers 3, 1-154.

43. G.M. Mavko and A. Nur, "Wave attenuation in partially saturated rocks", Geophys. 44, 161-178 (1979).

44. R.J. O"Connell and B. Budanisky, "Viscoelastic properties of fluid-saturated cracked solid", J. Geophys. Res. 82, 5119-5736 (1977).

45. I.D. Palmer and M.L. Traviolia, "Attenuation by squirt flow in undersaturated gas sands", Geophys. 45, 1780-1792 (1980).

46. C.E. Zener, *Elasticity and Anelasticity of Metals*, (Univ. Chicago Press, Chicago, 1948), 1970 pp.

47. B.A. Brunsen and R.K. Johnson, "Laboratory measurements of shear wave attenuation in saturated sands", J. Acoust. Soc. Am. 68, 1371-1375.

48. B.R. Tittmann, H. Nadler, V.A. Clark, L.A. Ahlerg, and T.W. Spencer, "Frequency dependence of seismic dissipation in saturated rocks", Geophys. Res. Lett. 8, 36-38 (1981).

49. E. Kjartansson and A. Nur, "Attenuation due to thermal relaxation in porous rocks", Geophys (in press, 1982).

50. R.D. Stoll and G.M. Bryan, "Wave attenuation in saturated sediments", J. Acoust. Soc. Am. 47, 1440-1447 (1970).

51. R.D. Stoll, "Acoustic waves in ocean sediments", Geophys. 42, 715-725 (1977).

52. G.M. Mavko and A. Nur, "The effect of nonelliptical cracks on the compressibility of rocks", J. Geophys. Res. 83, 4459-4468 (1978).

53. W.T. Born, "The attenuation constant of earth materials", Geophys. 6, 132-148 (1941).

Appendix

Agreement with Spencer (1981)

The results of Spencer (1981) are very interesting. It has been remarked at several national meetings (e.g. AGU San Francisco in 1980; SEG Los Angeles in 1981) that the measurements of Murphy (1982) seem to be at variance with Spencer's data. The experimental techniques are quite different. Spencer (1981) used a quasi-static system and measured the phase angle between stress and strain, ϕ . Spencer's specific attenuation, Q_a^{-1}, is given by

$$Q_a^{-1} = \frac{\mathrm{Im}\ \bar{E}}{\mathrm{Re}\ \bar{E}} = \tan \phi \quad , \tag{1}$$

where $\bar{E}$ is the complex Young's modulus. Murphy (1982) used resonant bar and torsional pendulum techniques which measure the characteristic time of resonant decays, τ . Murphy's specific attenuation, Q_b^{-1} , is given by

$$Q_b^{-1} = (\tau \pi f)^{-1} \tag{2}$$

where f is the frequency. O'Connell and Budanisky (1978) were unable to derive a general relation between Q_a^{-1} and Q_b^{-1} . However, we may expect that

$$Q_b = Q_a - \frac{1}{4} Q_a^{-1} \quad . \tag{3}$$

The purpose of this short note is to provide experimental support for at least qualitative consistency between the two measurement

techniques for three materials of interest in the acoustic frequency range.

In figure 1, we see that Spencer's (1981) data for lucite plastic compares quite favorably with new measurement obtained with the resonance decay techniques.

We attempted the measurement of extensional Q_b^{-1} in a fully water saturated Navajo sandstone (provided by Jim Spencer) at three separate frequencies between 2 and 4 kHz. Because of the very low Q's we were able to obtain only a single measurement: $1000/Q_e$ is 286 at 2572 Hz. Yet when the Navajo samples were relatively dry we found

frequency	$1000/Q_e$
3885	13.5
4869	14.2
6778	11.5

These results are consistent with Spencer's (1981) findings.

We have made several measurements of extensional phase velocity and specific attenuation in a Sierra White granite. Sierra White has a porosity of 0.8% and may or may not be similar to Spencer's samples of Oklahoma granite, having a porosity of ~1.0% (Spencer's figure 9). Our measurements are shown in figures 2 and 3. Although the test is by no means conclusive, the broad qualitative agreement is encouraging.

References

Murphy, W.F., 1982, Effects of partial water saturation on attenuation in Massilon sandstone and Vycor porous glass, J. Acoust. Soc. Am. 71, (in press). Chapter III in this volume.

O'Connell, R.J. and B. Budanisky, 1978, Measures of dissipation in viscoelastic media, Geophys. Res. Lett. 5, 5-8.

Spencer, J.W., 1981, Stress relaxations at low frequencies in fluid saturated rocks: attenuation and modulus dispersion, J. Geophys. Res. 86, 1803-1812.

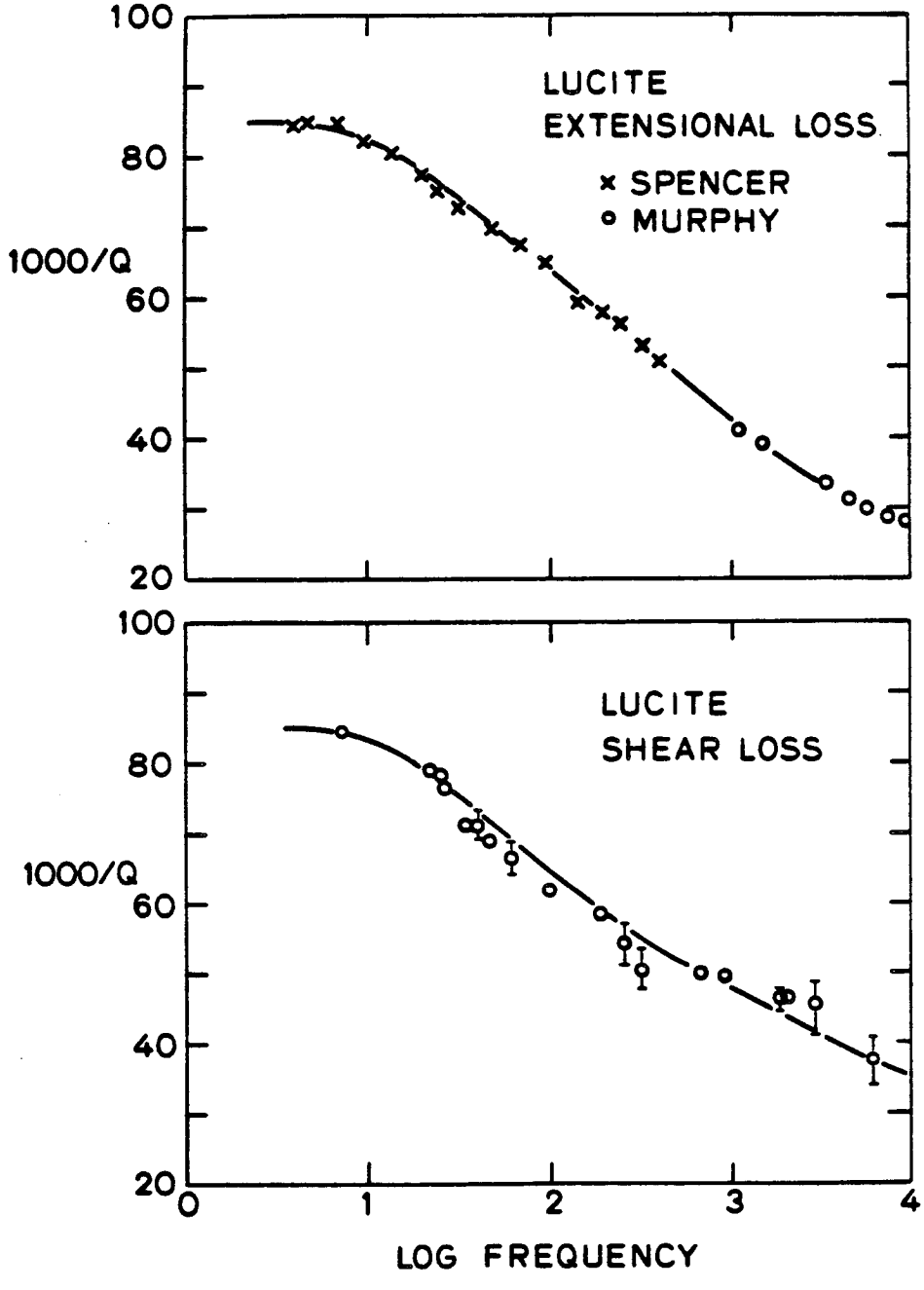

Fig. 1. $1000/Q_e$ and $1000/Q_s$ vs. frequency in lucite plastic.

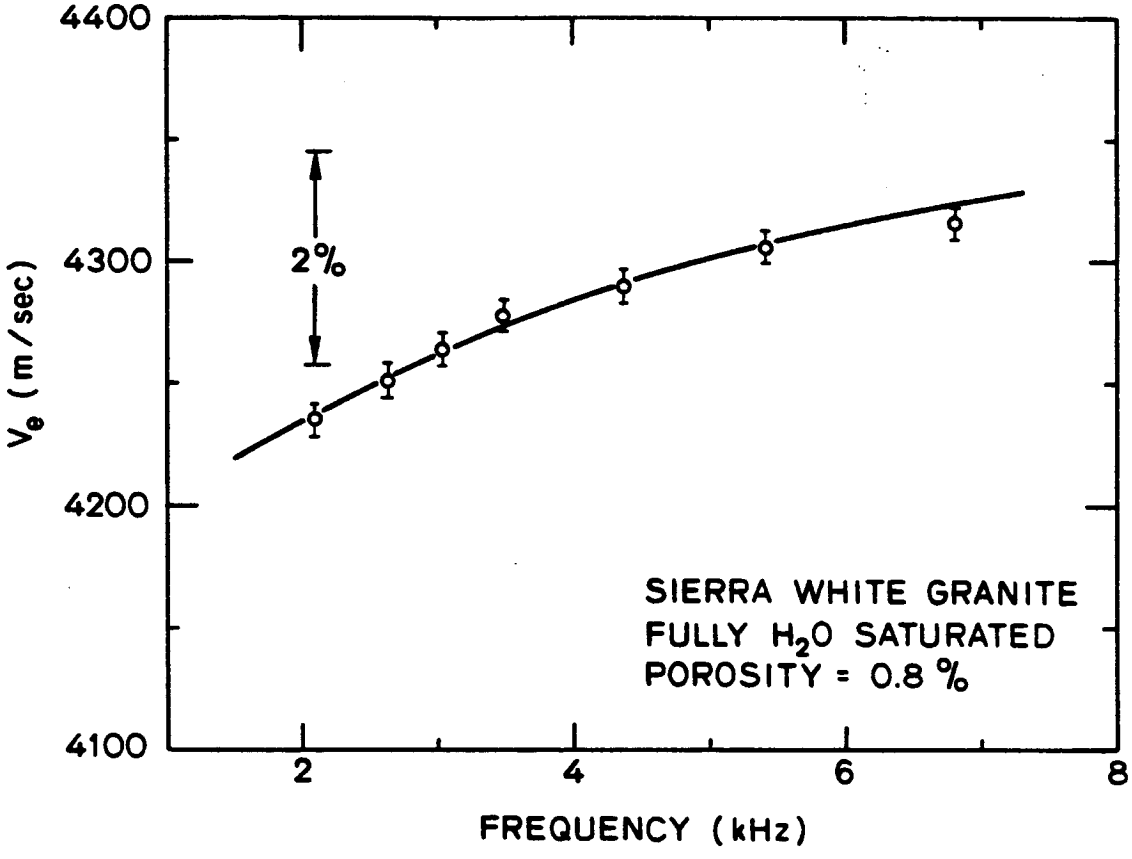

Fig. 2. V_e versus frequency in Sierra White granite.

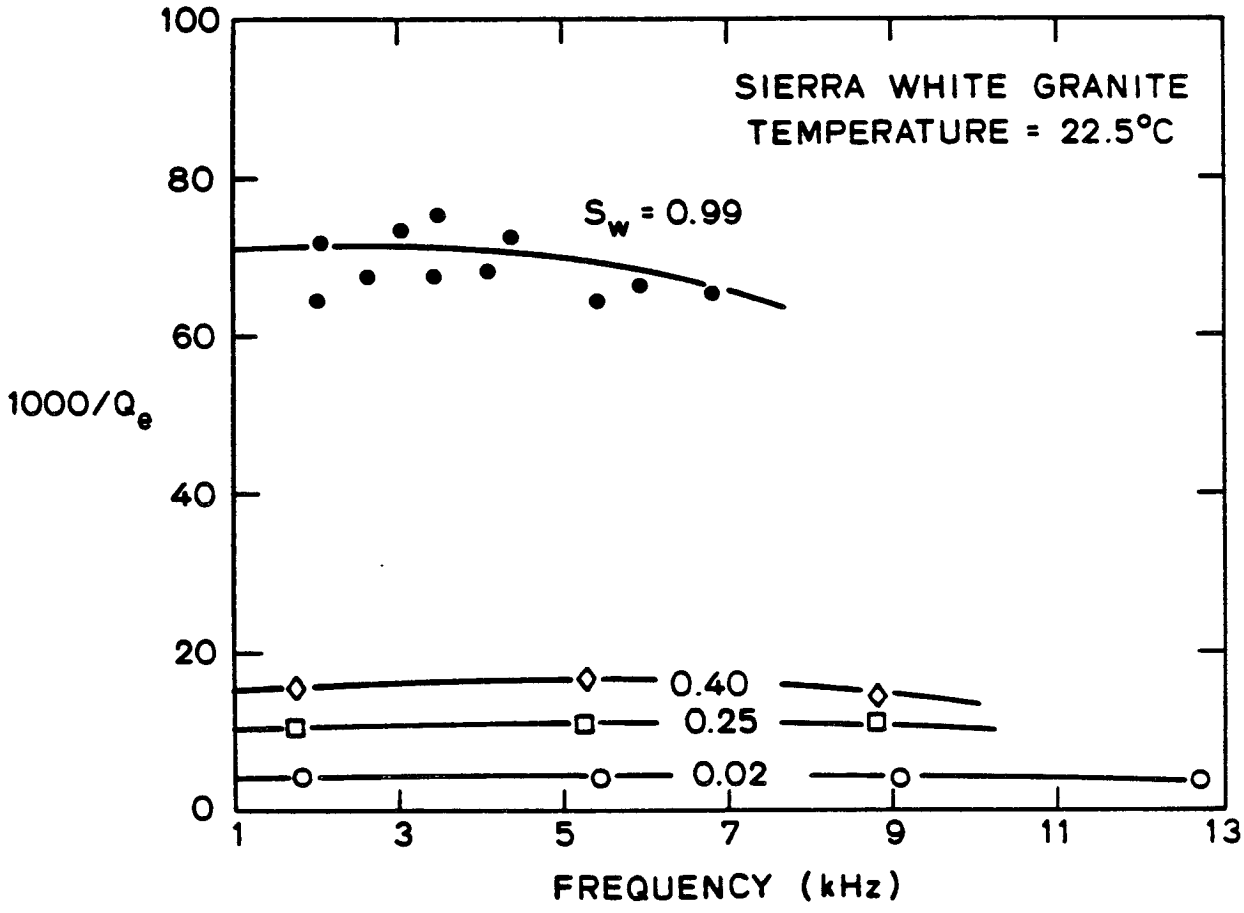

Fig. 3. $1000/Q_e$ vs. frequency in 99% water saturated Sierra White granite.

Chapter IV

On Velocities and Attenuation as A Measure of Partial Gas Saturation in Tight Sandstones at Borehole and Ultrasonic Frequencies*

Contents

1. INTRODUCTION

In recent years, small but significant progress has been achieved in understanding the acoustic velocities and attenuation of unconsolidated sands (Stoll, 1979; Murphy, 1982b) and high porosity (ϕ>10%) sandstones (Spencer, 1981; Winkler and Nur, 1982; Murphy, 1982a). Relatively little, however, is known about the acoustic properties of low porosity (ϕ<10%) sandstones. The exception is Gregory (1976). Those ultrasonic measurements on which he reported represent the only data available for tight sands regarding the sensitivity of velocities to partial gas saturation. We are aware of no published attenuation measurements in tight sandstones. As the production of natural gas

* Parts to be submitted to Geophysics and Journal of Geophysical Research in July 1982. A. Nur is to be co-author.

widens to ever more marginal reservoirs (such as tight gas sands with permeabilities as low as ~10-100 nd), increasing reliance is being placed on high resolution seismic reflections and borehole sonic logs to aid in reservoir evaluation (fig. 1). For tight sands techniques are required which not only reveal the presence of gas but also indicate to some extent the degree of partial gas saturation (Walls, 1981). More therefore needs to be learned about the acoustic properties of these rocks.

Gregory's (1976) results are singularly inauspicious. Not a single relevant effect of partial gas saturation appears sufficiently strong for resolution in in-situ. Our ultrasonic results are in agreement with Gregory. However, we shall demonstrate that at 3-6 kHz, compressional phase velocity, V_p , and the ratio of compressional phase velocity to shear phase velocity, V_p/V_s , are quite sensitive to undersaturation. Simultaneous measurement of V_p, V_s, Q_p^{-1}, and Q_s^{-1} may provide significant information not only about the presence of gas but also about the degree of gas saturation.

It is well established that in unconsolidated sands, V_p is very sensitive to the presence of small amounts of gas in the pores (Gassman, 1951; Domenico, 1974, 1976, 1977; Elliott and Wiley, 1975). This fact is of course the basis for the so-called 'bright spot' technology, which has made a significant contribution to the recovery of natural gas throughout the world. Knowledge of the sensitivity in P velocity was originally derived from a very rough linkage between theoretical considerations and laboratory measurements. The measurements were made at high ultrasonic (>0.5 MHz) frequencies (Elliott and Wiley, 1975; Domenico, 1976, 1977). Brown and Korringa (1979) have

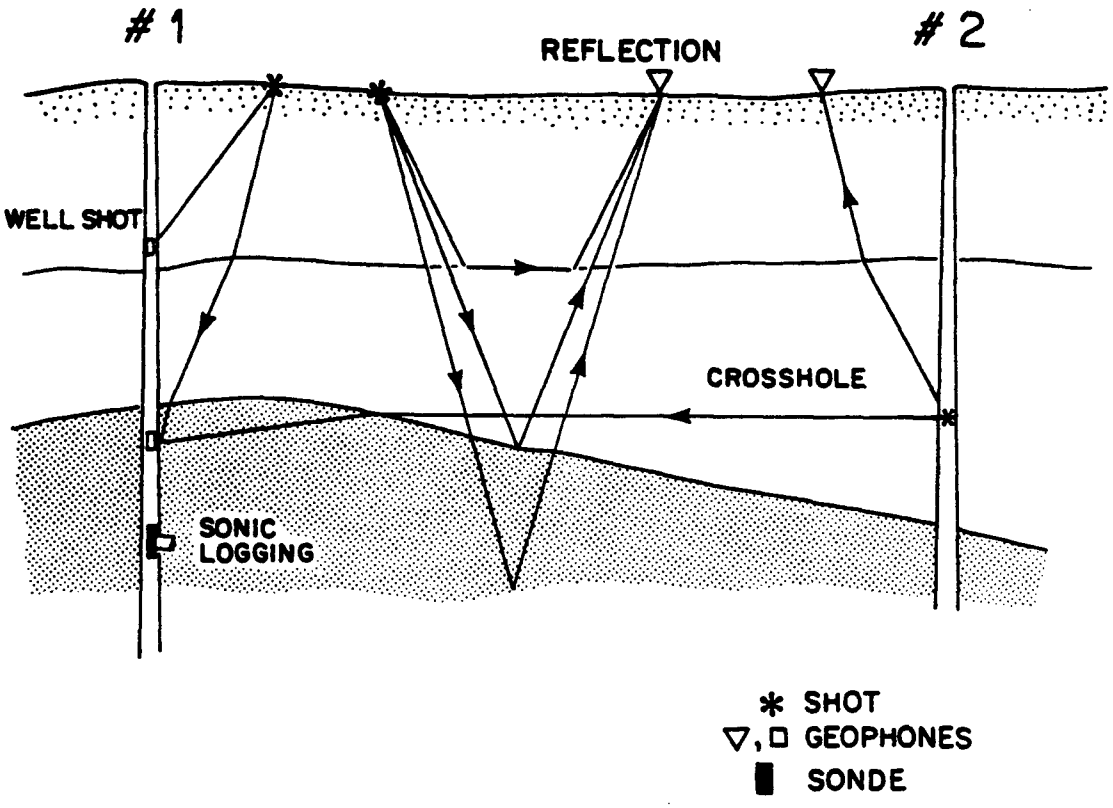

Fig. 1. Acoustic techniques for reservoir delineation.

subsequently shown that the Gassman-like extension of Biot's full (1956) frequency dependent theory is quantitatively inconsistent with these measurements. Nonetheless, the broad qualitative agreement between the measured dependence on gas saturation and the dependence predicted by the low frequency limit (the Biot-Gassman relations) is such that it has lead to the direct extrapolation of the ultrasonic results to seismic frequencies. Thus in practice, velocity dispersion has been considered inconsequential. Of course, the improved recovery rate underscores the sagacity of this assumption -- that is, at least in the case of unconsolidated sands.

The situation in tight sands is more subtle. Here, one may be easily misled by ultrasonic results. Gregory's (1976) measurements were made at 1 MHz. Dispersion was dismissed as without supporting evidence (p. 895), and the results were thus suggested to apply without correction to seismic frequencies (fig. 2). His measurements show the P velocity nearly unaffected by slight undersaturation and weakly dependent on partial water saturation, S_w, throughout the higher ranges (i.e. $S_w > 0.3$). The S velocity is observed to be roughly independent of S_w in the higher ranges. We now know that in sandstones, high ultrasonic measurements obtain relatively unrelaxed group velocities. In tight sandstones, consideration of frequency, attenuation, and dispersion is crucial for predicting from laboratory measurements with in situ response in borehole and seismic frequencies.

This paper presents an experimental study of tight sandstones. It extends the work on unconsolidated granular sediments (Murphy, 1982b) and on high porosity sandstones (Murphy, 1982a) to another microstructural extreme for granular sedimentary materials.

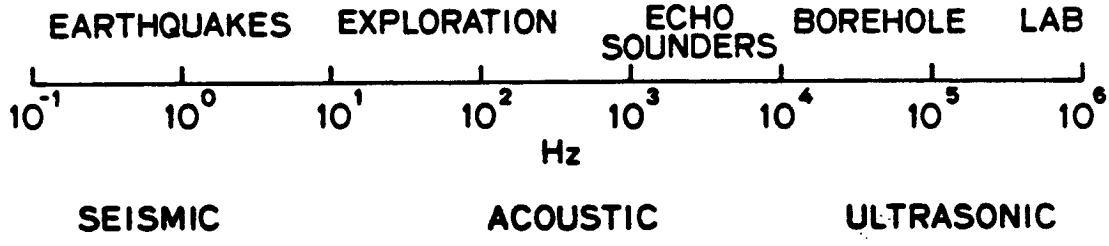

Fig. 2. Frequency spectrum of interest to geophysical exploration.

Section 2 in this paper compares and contrasts the less familiar grain contacts, pore structure, and relevant physical properties of tight sands with those more familiar from unconsolidated sands and high porosity sandstones.

In sections 3 and 4, we report on our 4-6 kHz measurements of V_e , V_s , Q_e^{-1}, and Q_s^{-1} as a function of continuously varying S_w in Fort Union sandstone, ϕ = 8.5% (where the subscript 'e' denotes the extensional mode). Several measurements of V_s and Q_s^{-1} in a Schuler-Cotton Valley sandstone (ϕ = 3.3%) and a Spirit River sandstone (ϕ = 5.4%) which were taken at frequencies ranging from 50 Hz to 7 kHz, are also given.

We have measured ultrasonic velocities as a function of S_w and effective pressure, P_e , in the Fort Union sandstone, two Spirit River sandstones (ϕ = 4.6 and 7.4%), and two Cotton Valley sandstones (ϕ = 3.3 and 5.1%). These results are discussed along with the general ultrasonic problem in sections 5 and 6.

2. BACKGROUND

Tight sandstones are a relatively unfamiliar class of granular sedimentary materials. It is most instructive to discuss them in a diagenetic context because we know significantly more about unconsolidated sands and high porosity sandstones (Murphy and Walls, 1981).

Descriptions of those samples to be examined in this paper are given in table 1.

Pore Network Geometry

During the primary stages of diagenesis, as sands consolidate and progressively lose porosity (fig. 3), the material usually increases total grain contact area, increases the number of contacts per grain,

TABLE I. SAMPLE DESCRIPTIONS

	AGE, LOCATION	CLASSIFICATION	POROSITY %	QUARTZ	QUARTZ OVERGROWTH	CHERT	FELDSPAR	CLAY	CALCITE	DOLOMITE	OTHERS	MEAN GRAIN SIZE μm	SORTING	GAS PERMEABILITY AT STP IN DARCIES
Schuler-Cotton Valley Ss. SCV9594	Late Jurassic Schuler Member Cotton Valley Formation East Texas Basin	Quartz Sub-arenite	5.1	71.9	12	3	2	1	4	1	-	100	moderately well sorted	1.6×10^{-5}
SCV10500		Quartz Sub-arenite	3.3	72	15	2	1	1	4	5	-	100	moderately well sorted	1.1×10^{-6}
Fort Union Ss.	Paleocene 10579.5-10574.7 ft. Pinedale Anticline Green River Basin	Fluvial Sub-Greywacke	8.5	42	10	-	5	11	10	10	12	125-150	poorly sorted	
Spirit River Ss. SR6556.5	Cretaceous Spirit River Member Falher Formation Deep Alberta Basin	Lith-arenite	7.1	48.8	14.3	13.3	-	2.9	-	7.3	-	100-125	poorly sorted	5.8×10^{-5}
SR6521.6		Lith-arenite	4.6	39.8	10	12.4	0.5	3.3	-	15.2	-	100-125	poorly sorted	1.9×10^{-5}
SR7227		Lith-arenite	5.4	41.1	10.8	23	0.5	6.6	-	10.4	2	125-150	poorly sorted	2.1×10^{-5}
St. Peter Ss.	Ordivician Missouri	Quartz arenite	8	91.9	8	-	-	0.1	-	-	-	200-250	well sorted	
Massilon Ss.	Mississippian Glenmont, Ohio	Quartz Sub-arenite	23	88	3	-	2	5	-	-	2	150-200	1.225	7.37×10^{-1}
Berea 100 Ss.	Mississippian Amherst, Ohio	Quartz Sub-arenite	19.8	82	4	-	0.5	4	-	-	1.5	150	1.335	5.2×10^{-3}
Ottawa Sand	Ordivician Ottawa Formation Ottawa, Illinois	Quartz sand	38	99.9	-	-	-	-	-	-	-	149-174	extremely well sorted	>10

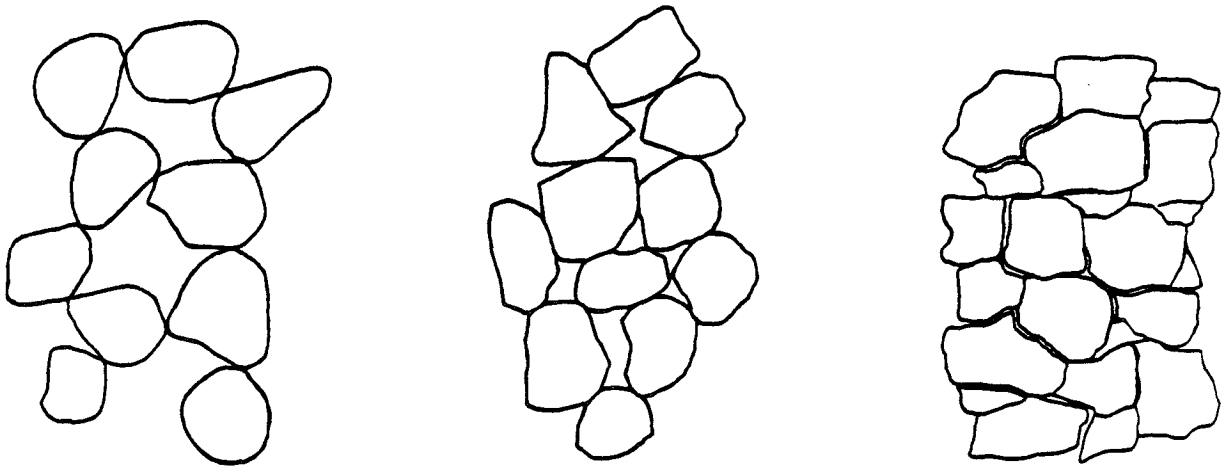

Fig. 3. Sketch of the fabric of the three general types of granular sedimentary materials:

a) unconsolidated sands,

b) high porosity consolidated sandstones, and

c) low porosity or tight sandstones.

and increases the pore network tortuosity. Consequently, in tight sands, the velocities are normally higher and the permeability is normally lower than in the higher porosity materials. Beyond these relatively continuous quantitative changes however, two qualitative events occur which clearly demark discrete differences in character among the three types of materials. The first change is not particularly relevant here. It occurs when the initial cement binds the loose sands and significantly increases the frame stiffness. The second change however, involves the local pore network geometry as a high ϕ sandstone becomes a low ϕ sandstone. As we shall see, this change controls the acoustic properties in tight sands.

In high ϕ sandstones, large (~20μm) high aspect ratio, spherically isotropic pores are well connected by large (>10μm) pore throats. This geometry results in nearly cylindrical pore channels (fig. 4, 5, and 6). These channels are relatively insensitive to effective pressure and dominate global permeability (Murphy and Walls, 1981). They also provide large capacitances for local pore pressure gradients which are generated during the passage of stress waves (Murphy, 1982c). Low aspect ratio near contact gaps (~1μm), which are more compliant, control the frame moduli (Mavko and Nur, 1979; Murphy, 1982b). Yet, they are merely offshoots on the pore channels. They contribute a small portion of the porosity, and are insignificant in global permeability.

In low ϕ sandstones, there may well remain some large rounded pores, either neglected during induration or opened during chemical erosion. But these large pores are sparsely distributed, and connectivity is provided by more compliant, low aspect ratio, sheet-like

Fig. 4. SEM photomicrographs of high porosity Massilon sandstone (a-b) and Schuler-Cotton Valley sandstone (c-d). The scale in microns is given by the bar at the base of each photomicrograph.

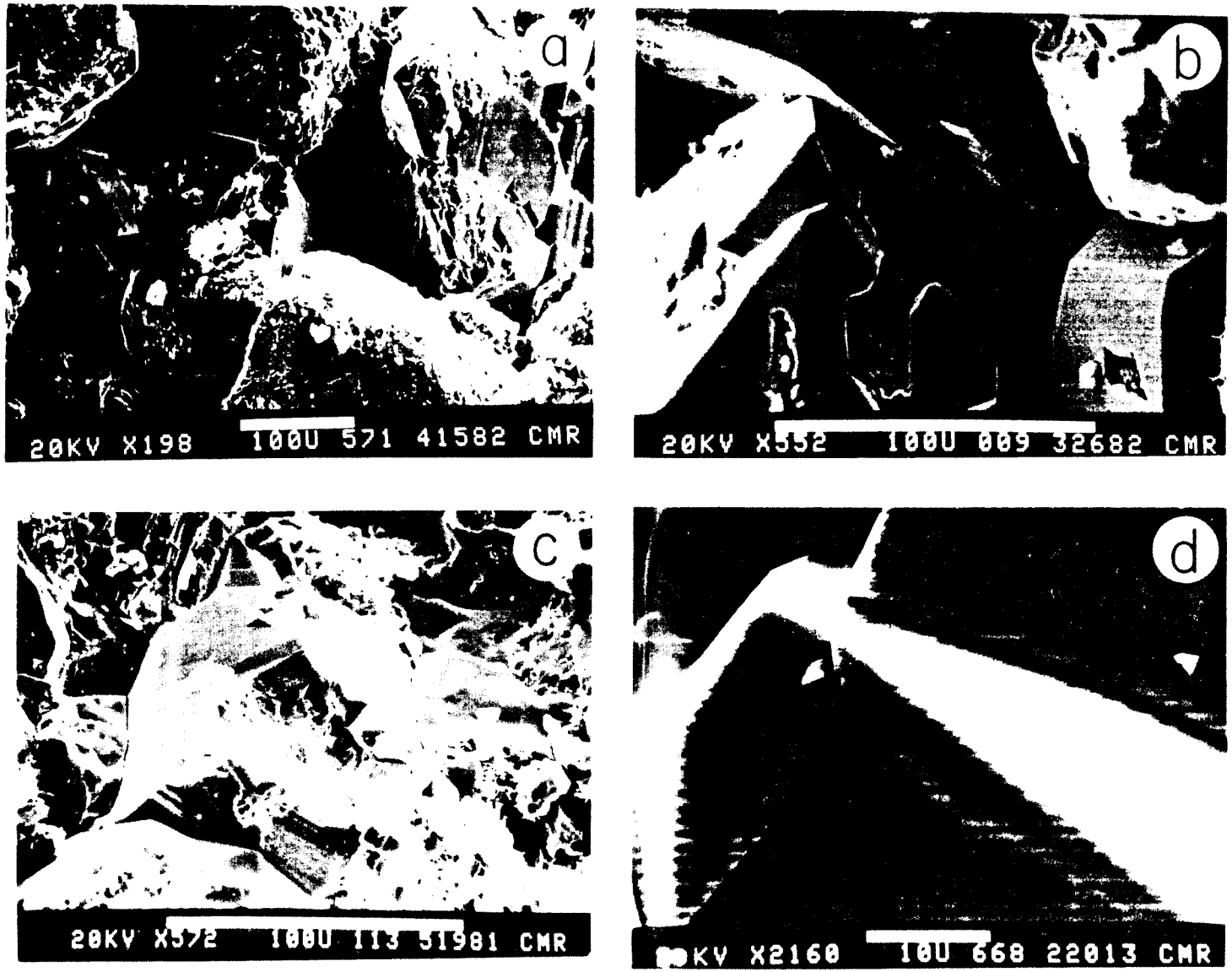
a
20KV X198 100U 571 41582 CMR
b
20KV X552 100U 009 32682 CMR
c
20KV X572 100U 113 31981 CMR
d
KV X2160 10U 668 22013 CMR

Fig. 5. Photomicrographs of thin sections impregnated with light blue epoxy. High porosity sandstones (a-b) and low porosity sandstones (c-d). a, b, c, and d are in the same positions as in figure 4. Grain size is roughly 100 microns in each photomicrograph.

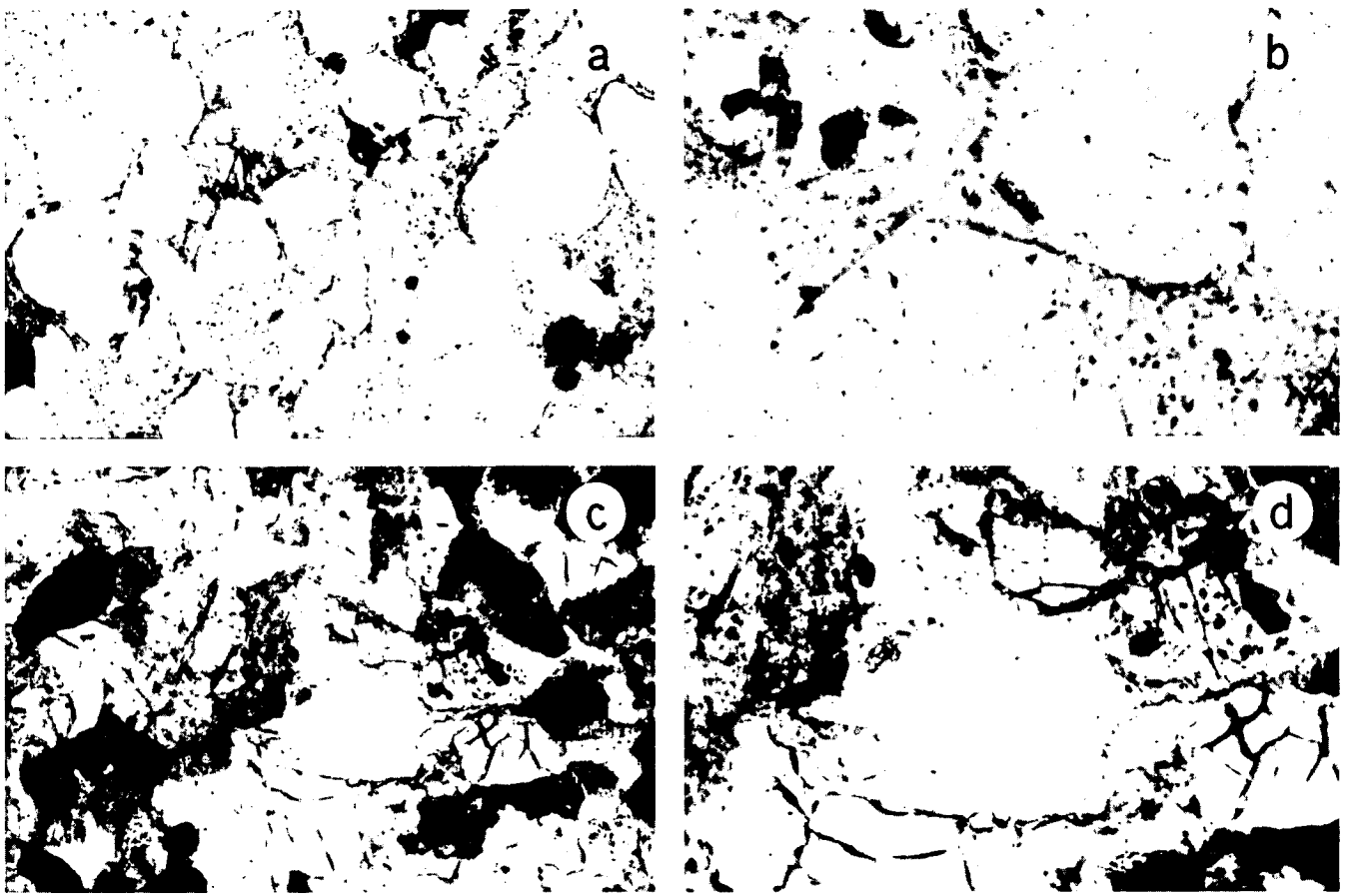
a
b
c
d

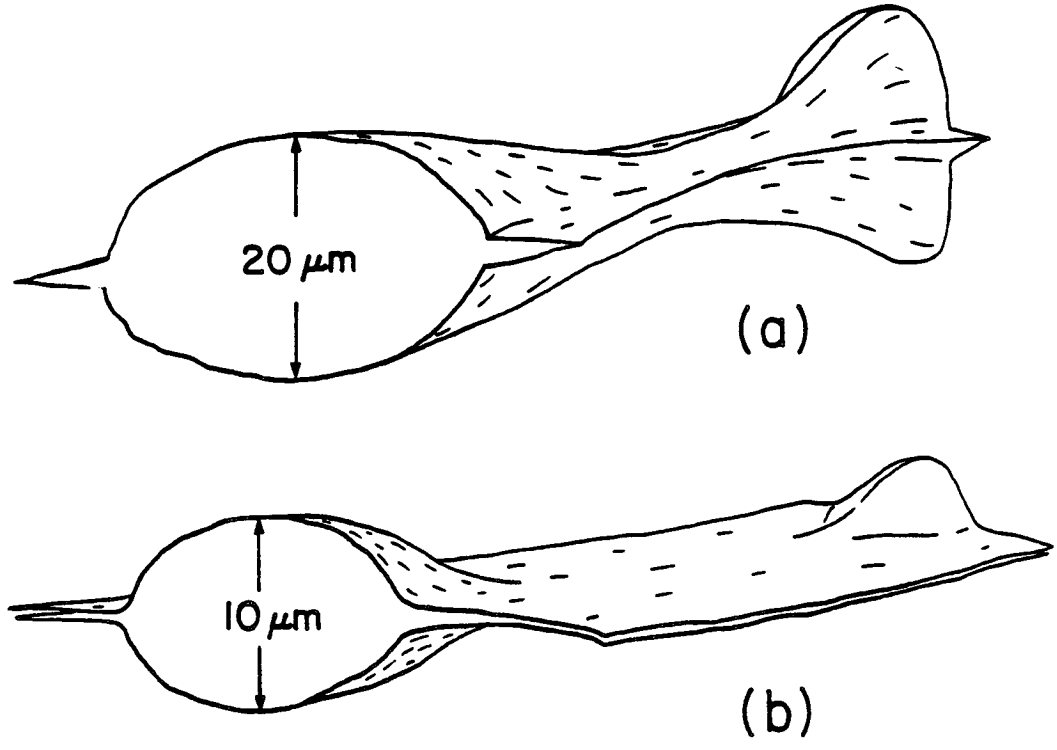

Fig. 6. The pore geometry of a high porosity sandstone may be thought of as a tortuous network of pores connected by open pore throats with near-contact gaps merely as anciliary wings (a), while the pore geometry of a low porosity sandstone may be thought of as a network of isolated pores in which the near-contact gaps provide the connectivity (b).

capillaries, <10μm in width (figs. 4, 5, and 6). These sheet capillaries now contribute a significant volume to the porosity, and they are the dominant microstructural factor for all properties in tight sands.

Figure 7 demonstrates in SR6521.6, a tight sandstone, the reduction in normalized pore volume with increasing confining pressure, P_e (measured by a pore fluid displacement technique in a "drained" experiment). We observe a 12.5% decline in pore volume as P_c goes from 0 to 25 MPa. Fatt (1953) has shown that the corresponding porosity decline is less than ϕ 3% or a factor of 4 less, in high ϕ sanstones.

Permeability

Figure 8 compares the dependence of gas permeability on P_e in two high ϕ sandstones and two low ϕ sandstones. (For a description of the experimental technique, see Walls, 1981). At 20 MPa, the high ϕ values exhibit less than a 10% reduction; while the low ϕ sandstones have dropped roughly an order of magnitude.

Another important effect has been discussed at length by Walls (1981). The Laplace-Young relations (c.f. Defay and Prigogine, 1966) dictate that in partially saturated sandstones, capillary forces will tend to drive the pore water into the narrow (<10μm) gaps between grains. Walls (1981) has shown that in a Spirit River sandstone, increasing S_w from 0 to 0.7 reduces gas permeability by nearly three orders of magnitude. As S_w increases, more and more the water is imbibbed into the sheet capillaries, progressively isolating the larger pores in which most of the gas resides. This effect on gas permeability is a principal reason why accurate

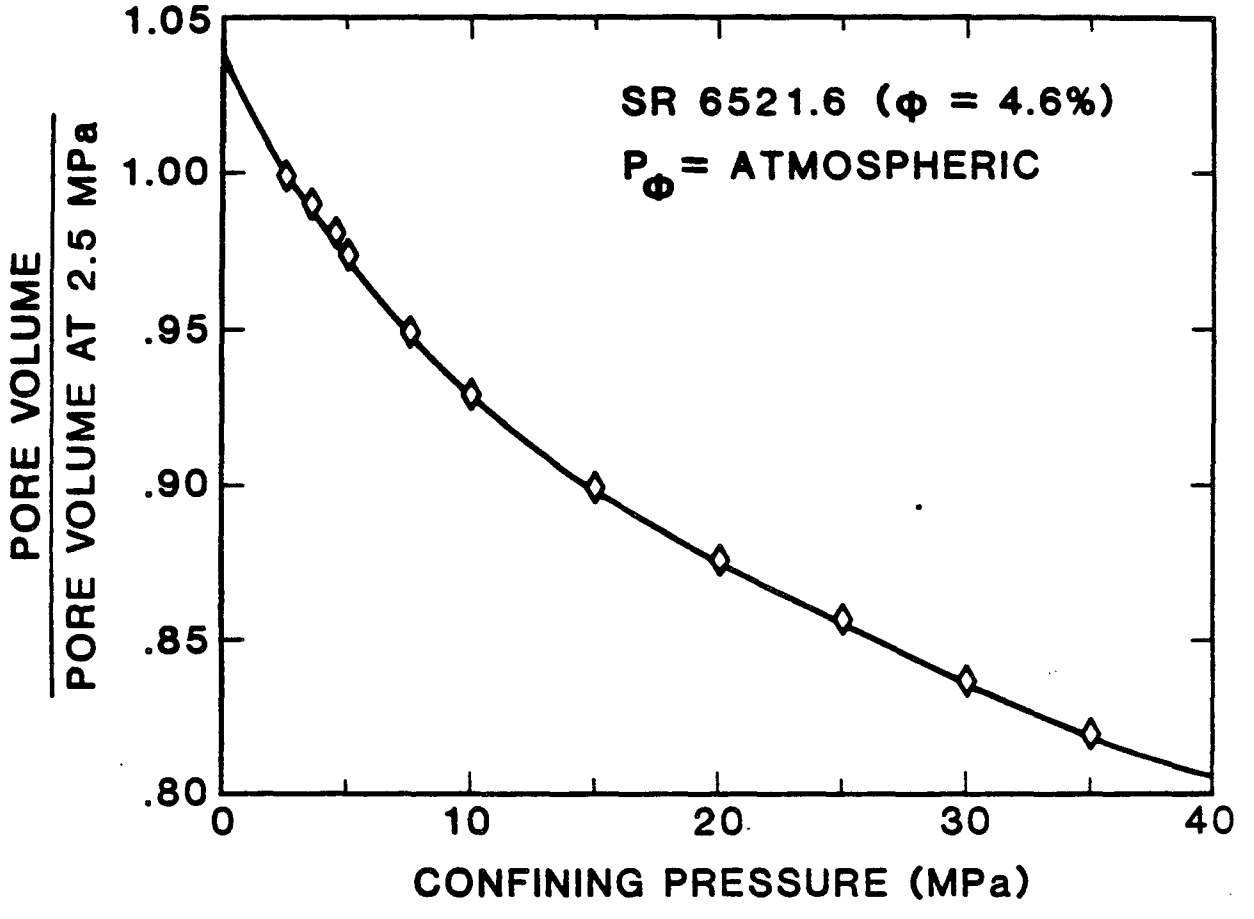

Fig. 7. Normalized pore volume change vs. confining pressure in SR 6521.6 low porosity sandstone.

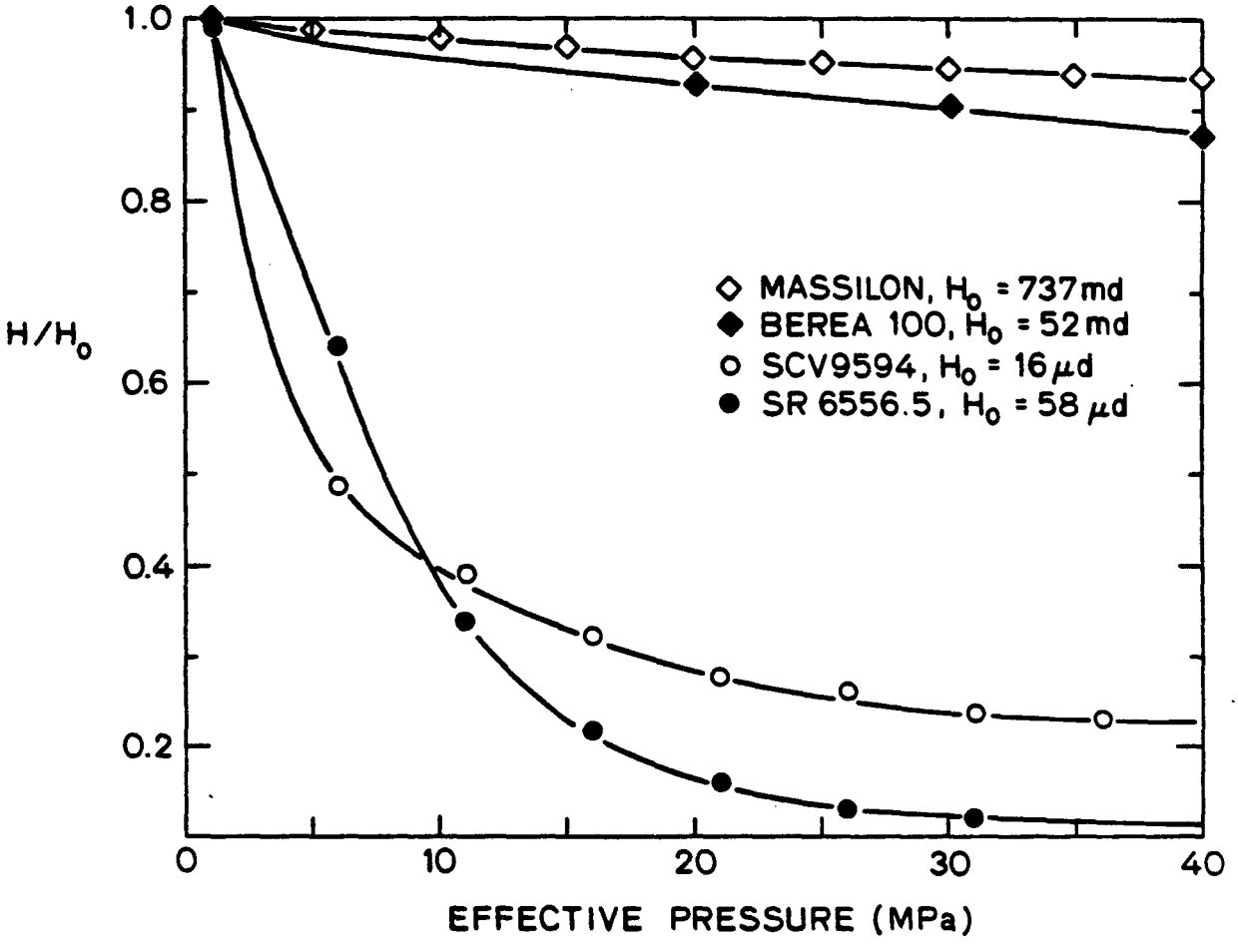

Fig. 8. Normalized permeability, H/H_0, vs. effective pressure in sandstones. Massilon and Berea sandstones are high porosity sandstones. SCV9594 and SR6556.5 are low porosity sandstones.

knowlege of S_w is so important in in situ tight gas and reservoir evaluation.

Velocities

Examples of P and S velocities for the three different materials in vacuum dry state are given in Figure 9 vs P_e. The measurements were obtained by a standard ultrasonic pulse transmission technique as described by Nur and Simmons (1969) or Gregory (1976). The pulse transmission technique yields P and S signal velocities, $\hat{V}_p$ and $\hat{V}_s$, respectively. In the case of a significantly dispersive media, $\hat{V}_p$ and $\hat{V}_s$ are equivalent to the P and S group velocities, $\overline{V}_p$ and $\overline{V}_s$, respectively. The group velocity is the velocity of "the center of gravity" o· a wave packet, in which the component waves differ somewhat in frequency (c.f. Morse and Ingard, 1968). The group velocities are related to the phase velocities by

$$\overline{V}_p = \left[\frac{d(\omega/V_p)}{d\omega} \right]^{-1}_{\omega_m} \quad \text{and} \quad \overline{V}_s = \left[\frac{d(\omega/V_p)}{d\omega} \right]^{-1}_{\omega_m} \qquad (1)$$

where $\omega = 2\pi f$ is the angular frequency, ω_m is the center angular frequency of the group of waves, and f is the frequency. If the phase velocity is independent of frequency, then $\hat{V}_p = \overline{V}_p = V_p$ and $\hat{V}_s = \overline{V}_s = V_s$. But if the phase velocity is a function of frequency, then

$$\overline{V}_p = V_p \left[1 - \frac{\omega_m}{V_p} \left(\frac{\partial V_p}{\partial \omega} \right)_{\omega_m} \right]^{-1} \qquad (2a)$$

and

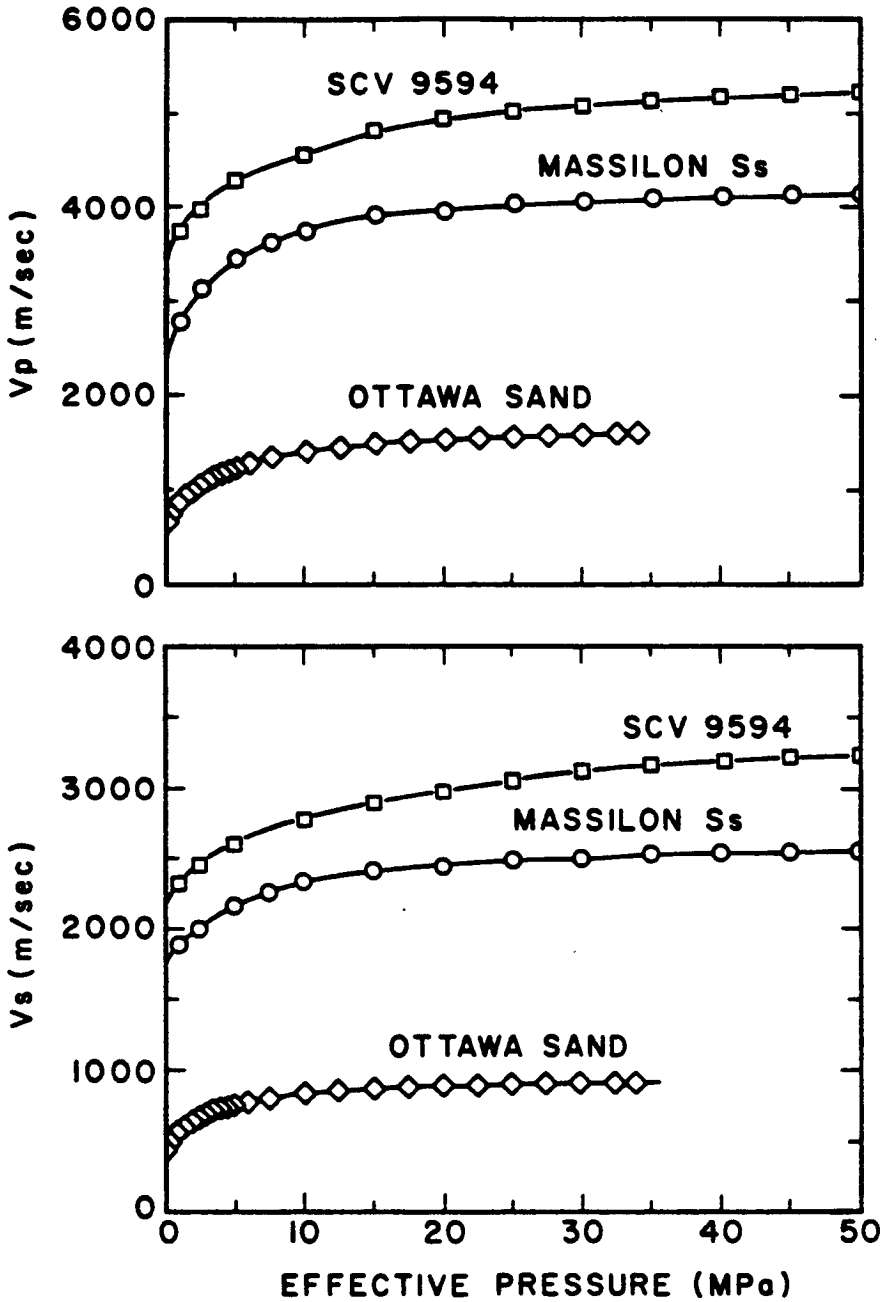

Fig. 9. Ultrasonic velocities vs. effective pressure in the three general types of granular sedimentary materials when they are vacuum dry.

$$\bar{V}_s = V_s\left[1 - \frac{\omega_m}{V_s}\left(\frac{\partial V_s}{\partial \omega}\right)_{\omega_m}\right]^{-1} . \qquad (2b)$$

Since we are aware of no evidence for velocity dispersion in vacuum dry granular sedimentary materials, we shall assume in this particular case that $\left(\frac{V_p}{\partial \omega}\right)_m = 0$ and $\left(\frac{V_s}{\partial \omega}\right)_m = 0$, thus $V_p = \bar{V}_p = V_p$ and $V_s = \bar{V}_s = V_s$. In figure 9, a factor of 2 jump in both V_p and V_s accompanies a 15% decrease in ϕ from Ottawa sand to Massilon sandstone; while a 25% velocity increase accompanies the 18% increase in ϕ from Massilon to Cotton Valley sandstone. Velocities in vacuum dry granular materials are given by Murphy (1982a),

$$V_p = \left(\frac{K_d + \frac{4}{3}\mu_d}{\phi \rho_s}\right)^{1/2} , \quad V_s = \left(\frac{\mu_d}{\phi \rho_s}\right)^{1/2} \qquad (3)$$

where K_d is the dry frame bulk modulus, μ_d is the dry frame shear modulus, and ρ_s is the density of the solid grains, ~ 2.65 g/cm^3 for quartz grains. As ϕ is reduced, the increase in velocity is contained in the dry frame modulus. The velocities in dry low ϕ sandstones are not always higher than those in high ϕ sandstones. Results for several tight sandstones are presented in figure 10. Note the relatively small velocity dependence on P_e in the St. Peter sandstone. This particular sample has a porosity of 8% and has extremely well cemented, ball-in-a-seat contacts (Murphy, 1982b).

In recent years, much has been made about the use of V_p/V_s in attempting to distinguish gas saturation or "true" bright spots from lithologic discontinuities (Ostrander, 1981). Moreover, Tatham (1982) has proposed using V_p/V_s to identify lithologies.

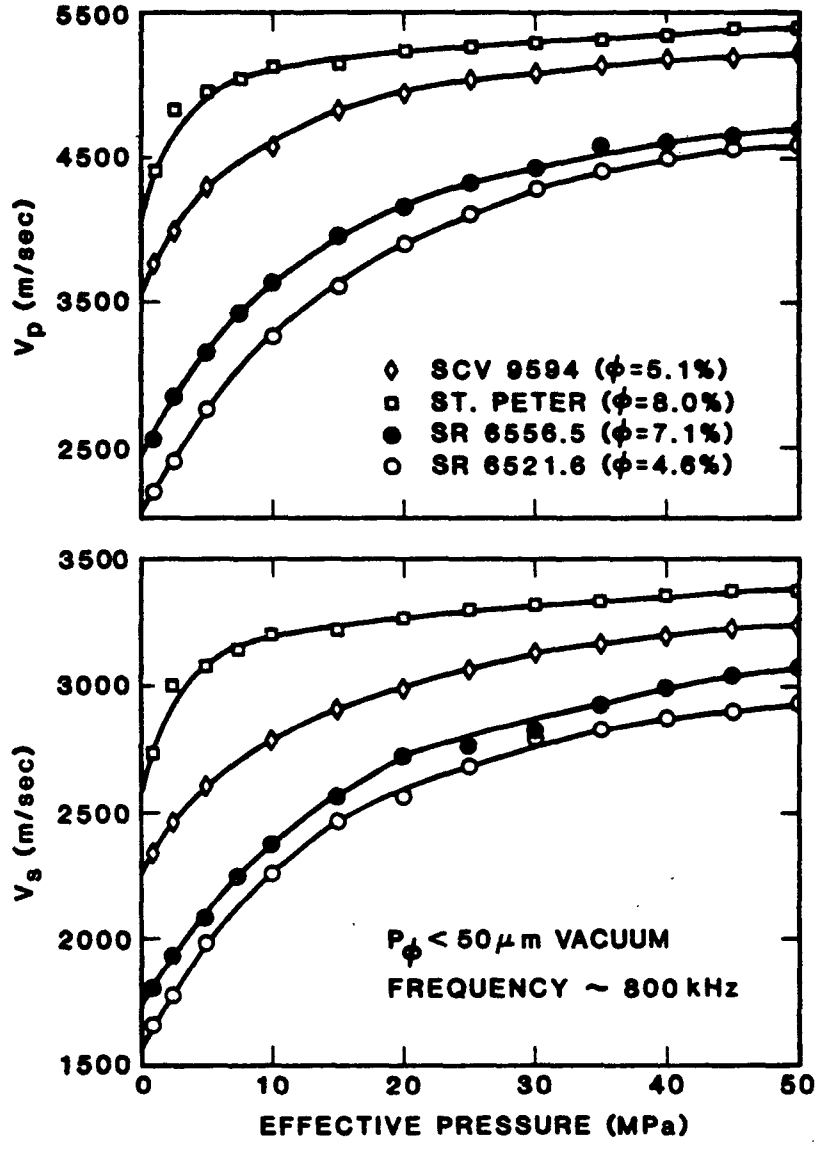

Fig. 10. Ultrasonic velocities vs. effective pressure in various vacuum dry, low porosity sandstones.

We have plotted V_p/V_s vs. V_p for vacuum dry materials in figure 11. The dry values for CV9594 straddle 1.6. Figure 11 does not show the values for the St. Peter sample which also lie along 1.6 nor those for SR6556.5 which converge on 1.6 with increasing pressure.

Figure 12 presents a similar plot for the materials in various states of saturation. Its aim is to demonstrate succinctly the problem which this paper addresses. We expect velocity dispersion in fully and partially saturated granular sedimentary materials. Spencer (1981) has demonstrated significant dispersion in a Navajo sandstone (ϕ = 11.0). And although experimental limitations precluded the direct measurement of velocity dispersion, Murphy (1982a) has observed a strong attenuation peak in Massilon sandstone; hence causality requires a significant dispersion. In general then, $(\frac{dV_p}{d\omega})_{\omega_m} > 0$ and $(\frac{dV_s}{d\omega})_{\omega_m} > 0$; thus, $\hat{V}_p = \overline{V}_p \neq V_p$ and $\hat{V}_s = \overline{V}_s \neq V_s$. The Ottawa sand data in figure 12 is more accurate than those of Domenico (1977); however, the large increase with full saturation is still clearly observed in $\overline{V}_p$ and $\overline{V}_p/\overline{V}_s$. These are the bright spot effects. In stark contrast, the data for the consolidated sandstones, particularly for the tight Cotton Valley, show a very small difference between values taken at $S_w = 0.7$ and full saturation in either $\overline{V}_p$ or $\overline{V}_p/\overline{V}_s$. This small saturation effect and its relationship to dispersion constitute our problem.

3. VELOCITIES AND ATTENUATION IN TIGHT SANDSTONES AT ACOUSTIC FREQUENCIES

Fort Union Sandstone

We have measured V_e and Q_e^{-1} at 5850 - 6286 Hz and V_s

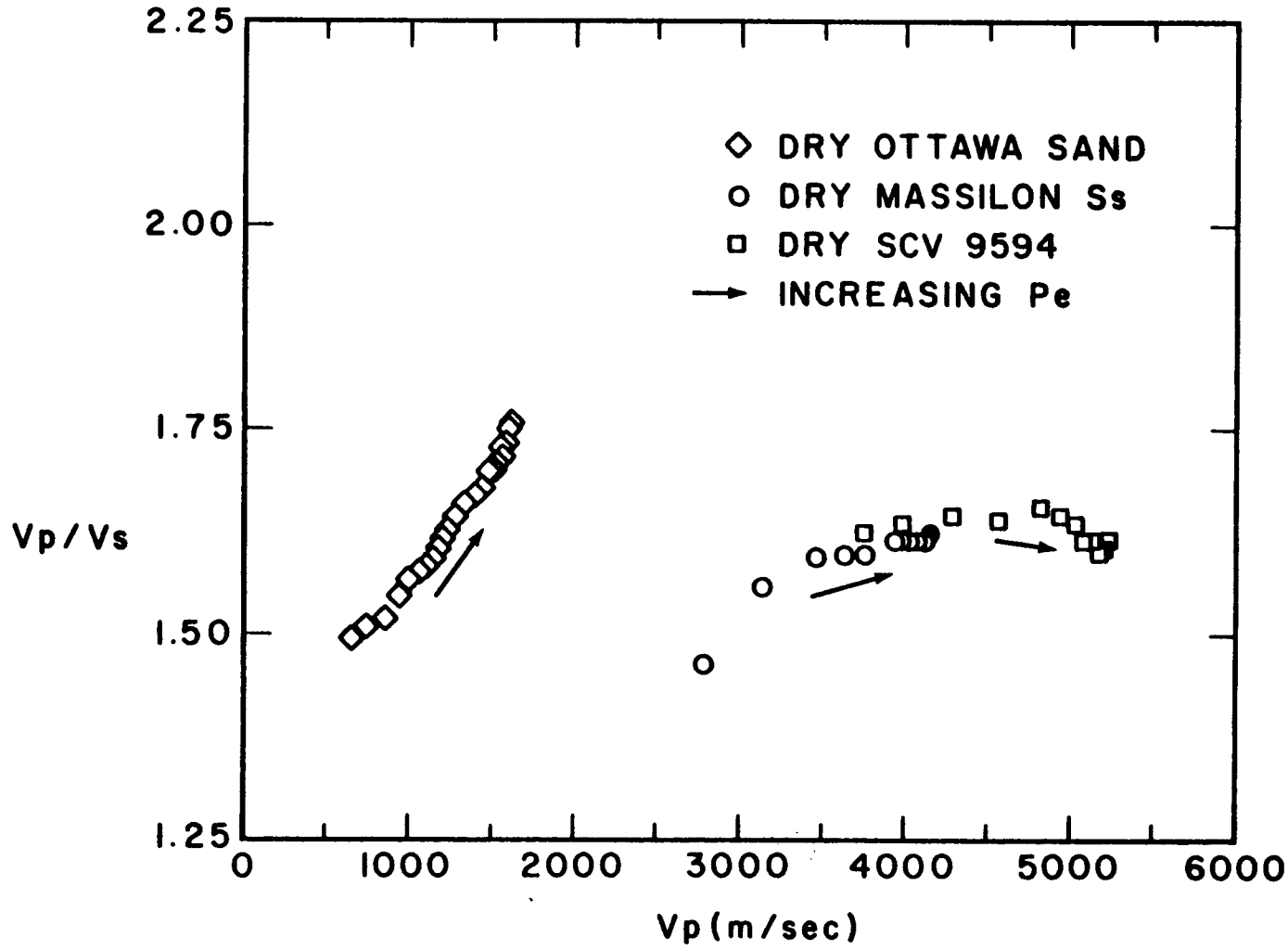

Fig. 11. V_p/V_s plotted against V_p as a function of effective pressure for the data from figure 9.

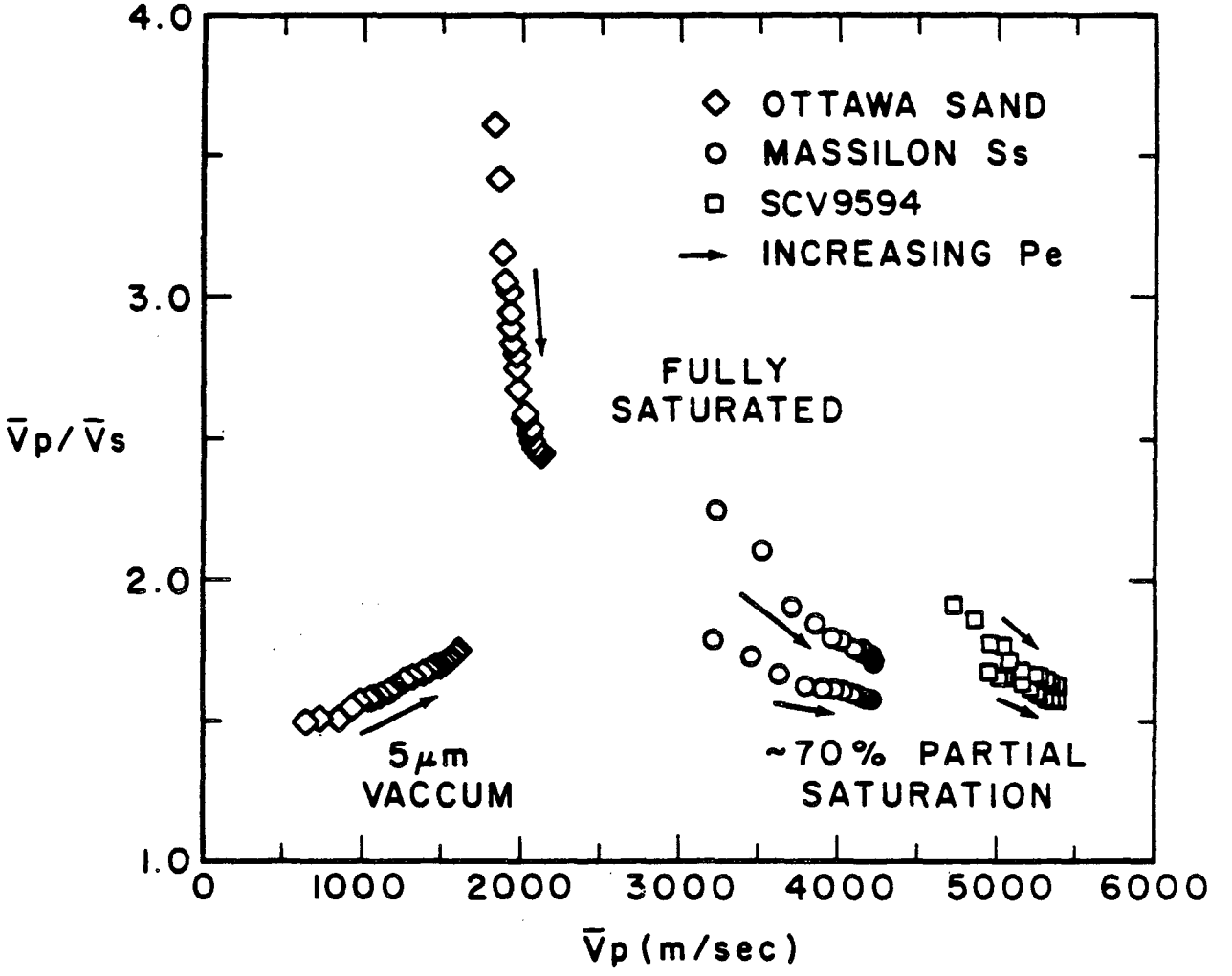

Fig. 12 V_p/V_s vs. V_p as a function of effective pressure in the three different material types at full water saturation and at 70% water saturation.

and Q_s^{-1} at 3892 - 4548 Hz in a Fort Union sandstone (ϕ = 8.5%) as a function of continuously varying S_w .

We use a resonant bar technique which is similar to Gardner et al. (1964) and described in detail by Winkler and Nur (1982). Resonant frequencies are measured to 1 part in 10^3 and converted to phase velocities using the relation $V = 2Lf$, where L is the sample length and f is the frequency. No geometric correction factor is required because the samples are cylindrical in crossection. Attenuation data are obtained by measuring the time constant of resonant decays ($\tau = Q/\pi f$). Relative precision is within 2%. We estimate the accuracy of the attenuation measurements to be 5-10%. The velocities and attenuation are measured as a function of continuously varying S_w by means of a drying experiment. Murphy (1982a) gives the details of the procedure. Basically, an unjacketed sample is monitored as it dries under atmospheric pressure in a humidity chamber. The saturating water is 2 MΩ H_2O which has been deaeriated by evacuation for 2 days. Temperature and relative humidity are held steady throughout the drying period at 22°C and 0.30, respectively. The only special features here with respect to those measurements described in Murphy (1982a) are that these samples are cylindrical with a crossectional diameter of 1.9 cm, that these samples are vertical cores, perpendicular to bedding, and that the sample length is 24 cm.

The results are given in figures 13-15. In figure 13, V_s increases 15% as water saturation decreases from full saturation to S_w = 0.1. A relatively sharp increase of 5% is observed before 0.9, followed by a relatively flat segment down to S_w = 0.4. A gradual steepening develops in the last segment from S_w = 0.3. V_e

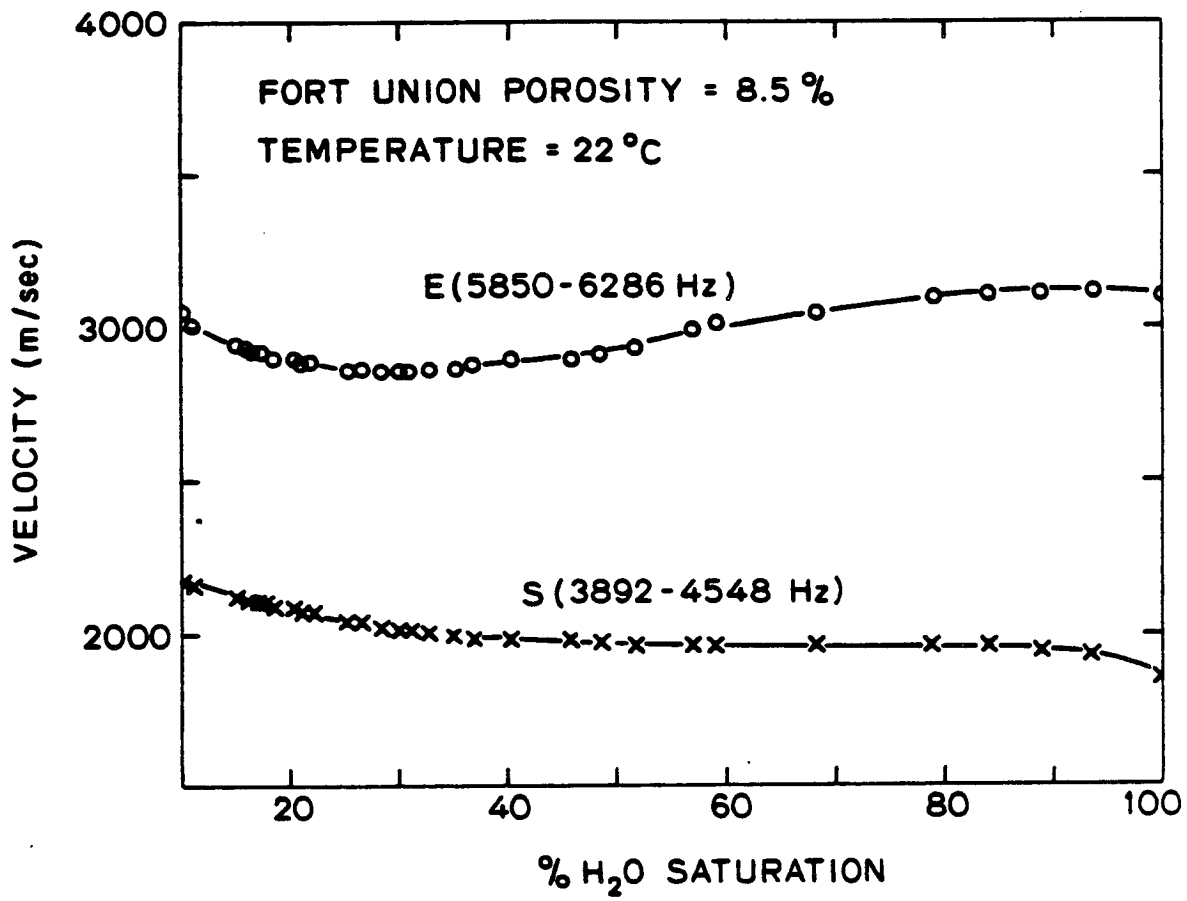

Fig. 13. V_e and V_s vs. % water saturation (S_w = 0.10 - 1.00) in Fort Union sandstone at ~ 5 kHz.

decreases 10% as S_w declines from 0.92 to 0.3. This occurs after a slight increase (i.e. 0.1%) with the initial undersaturation. From S_w = 0.3 to 0.1, V_e increases roughly 5%.

In figure 14, nearly a 15% increase is observed in both V_e and V_s from S_w = 0.03 to a dry state in which the samples have equilibrated with a relative humidity between 0.01 and 0.02.

The attenuation measurements in figure 15 are very interesting. We should emphasize the magnitude of the S loss at full saturation where Q is 5.3. $1000/Q_s$ drops linearly with decreasing water saturation from S_w = 1.0 to 0.3, with the exception of two steps in the data. A major step is observed between S_w = 0.85 and 0.7 and a minor blip occurs between S_w = 0.4 and 0.5. Q_e at full saturation is 9.6. $1000/Q_e$ rises to a peak at S_w = 0.79, crossing $1000/Q_s$ near 0.8. Thereafter, $1000/Q_e$ $1000/Q_s$, and the shape of the E dependence emulates that of the S dependence.

Cotton Valley Sandstone (Schuler Member)

A similar drying experiment was performed on a Schuler-Cotton Valley sandstone (SCV10500 = 3.3%) except that only shear data were taken. The samples are vertical, cylindrical cores, 20 cm in length. The frequency range is 6256 to 6603 Hz in figure 16. V_s exhibits a gradual 5% decline from full saturation to S_w = 0.5, then a gradual 5% increase to the dry state. Q_s is 6.7 at full saturation. The decrease in $1000/Q_s$ with S_w is nearly exponential from 149 at S_w = 1.0 to 58 at S_w = 0.69. The decline continues with a second exponential decrease from 51 at S_w = 0.63 to 7.4 at S_w = 0.

Schuler-Cotton Valley and Spirit River Sandstones

We were unable to measure the frequency dependence in tight sands

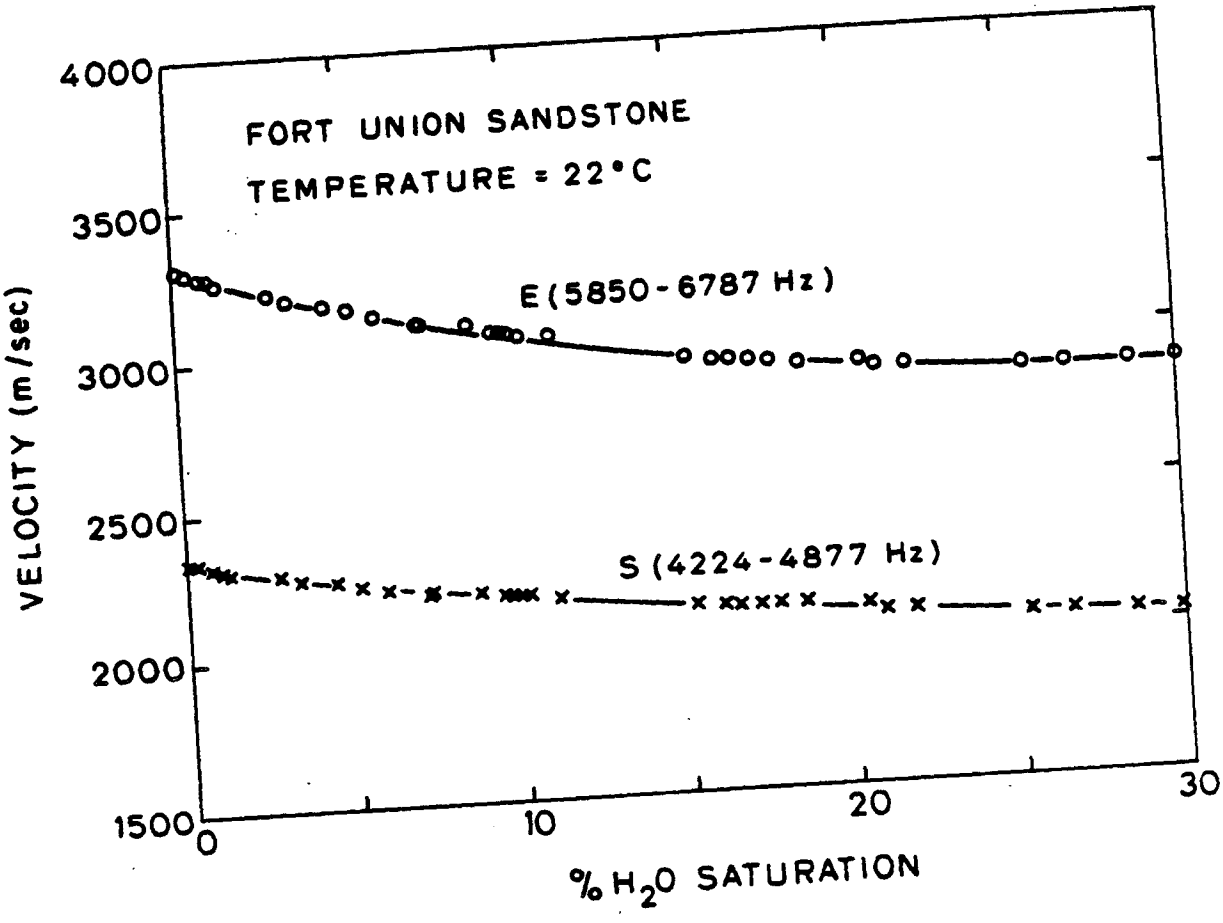

Fig. 14. V_e and V_s vs. moisture content (S_w = 0 - 0.10) in Fort Union sandstone at ~ 5 kHz.

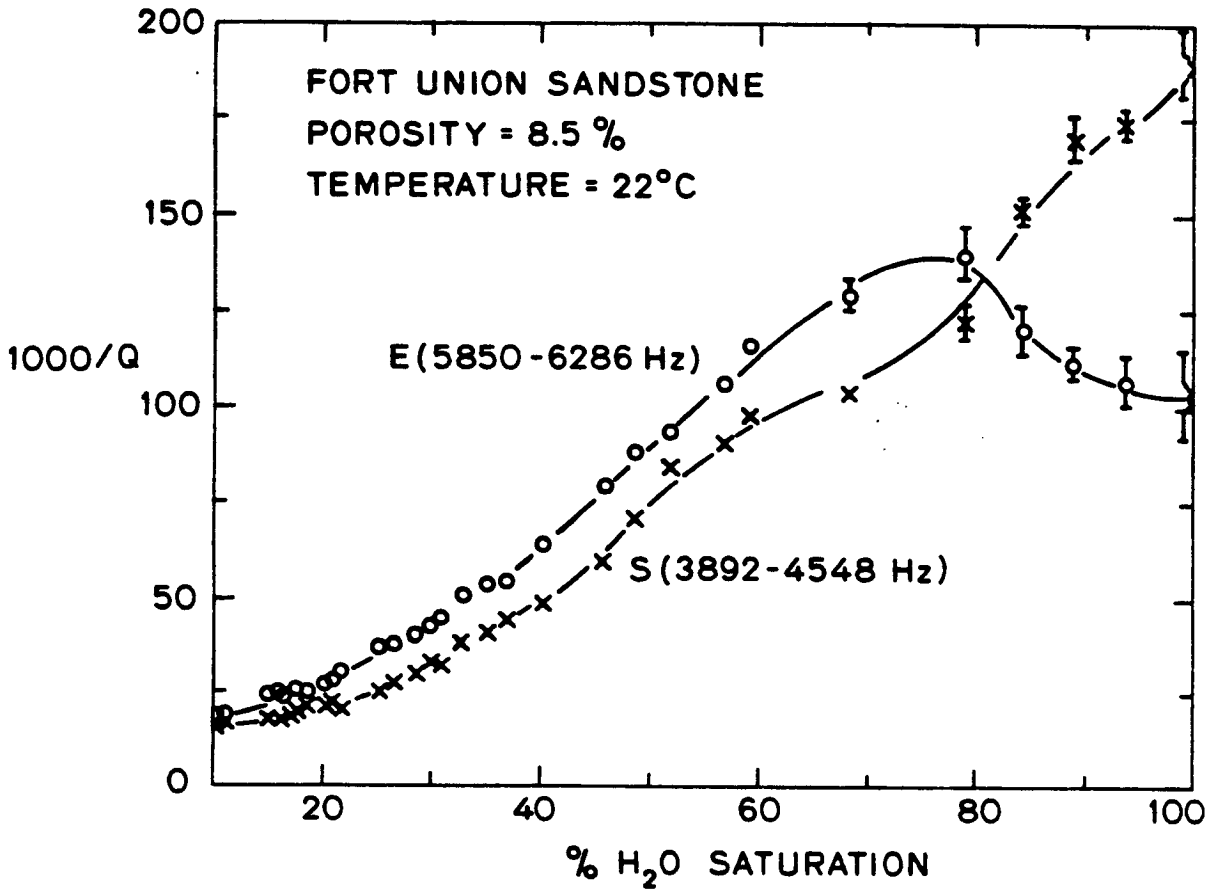

Fig. 15. $1000/Q_e$ and $1000/Q_s$ vs. % water saturation (S_w = 0.10 - 1.00) in Fort Union sandstone at ~5 kHz.

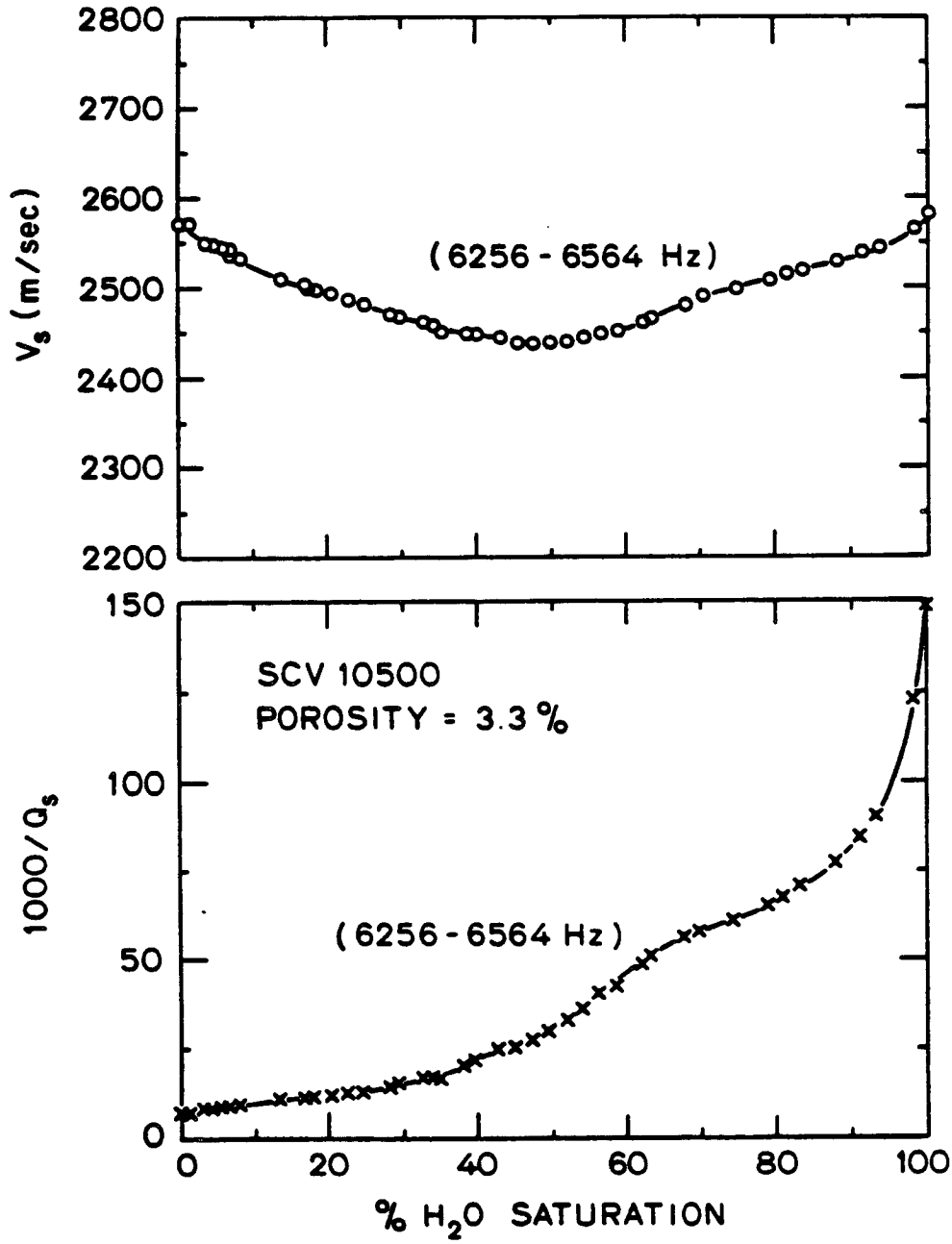

Fig. 16. Shear wave velocity and specific attenuation vs. % water saturation (S_w = 0 - 1.0) in SCV 10500 at ~ 6.5 kHz.

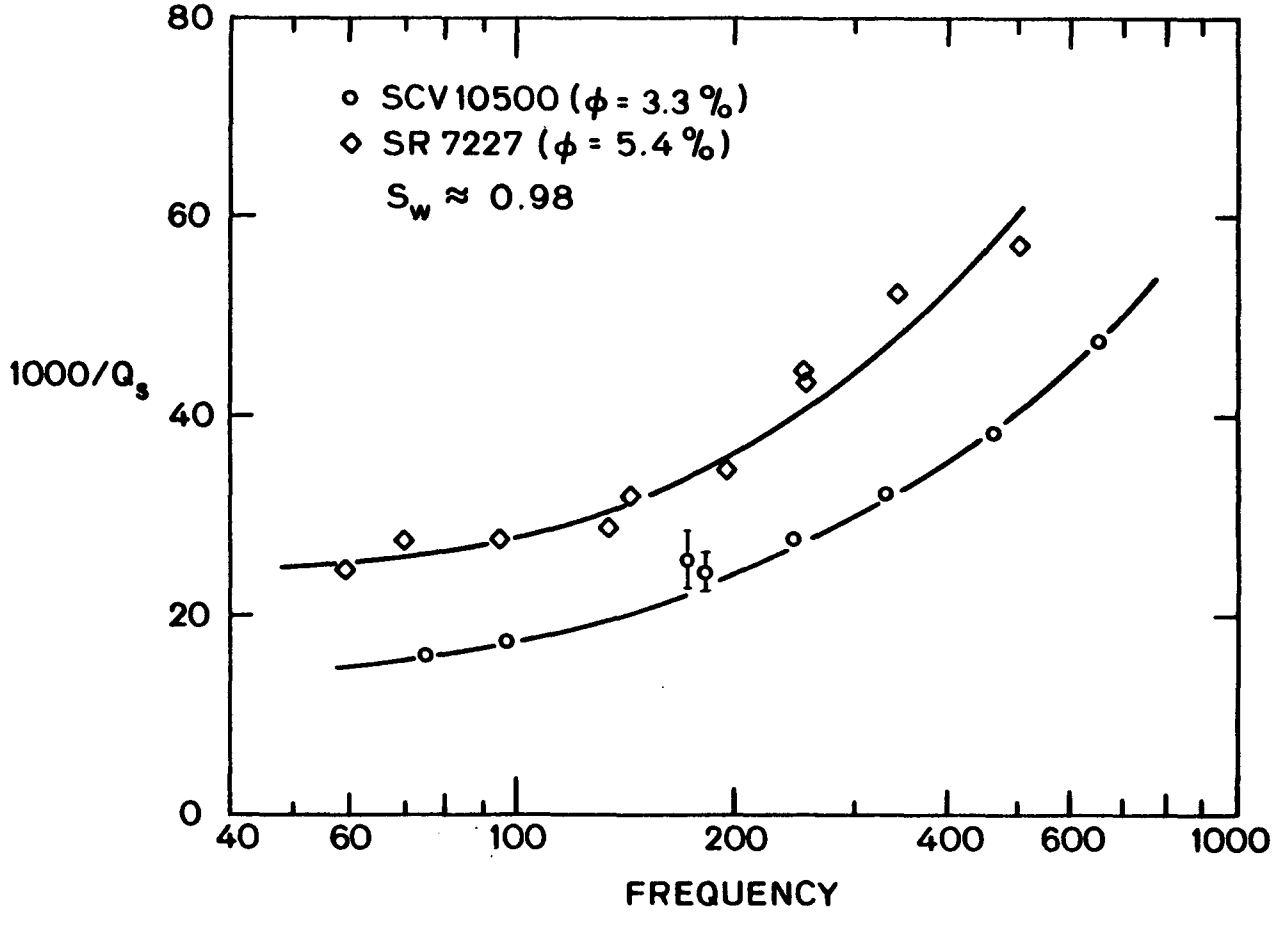

Fig. 17. $1000/Q_s$ vs. frequency from 50 to 700 Hz in SCV10500 and SR7227 at $S_w \approx 0.98$

by the resonant bar technique i) because the sample lengths are limited to short cores (< 30 cm) provided from wells; and ii) because the signal to noise ratio is too low in the higher harmonics for the required accuracy. In order to procure some information, we have measured $1000/Q_s$ in a 98% water saturated SCV10500 sandstone (ϕ = 3.3%) and a SR7227 (ϕ = 5.4%) using a torsional pendulum technique. The technique is similar to that of Peselnick and Outerbridge (1961). Frequencies are varied by simply changing the interial mass at the base of the sample. The apparatus is housed in a humidity chamber similar to the resonant bar. The fully saturated samples are jacketed with Saran Wrap. Slight undersaturation is expected to have occurred in the sourse of the sample mounting. Temperature is again held at 22°C, but relative humidity is pushed to 0.96 so as to impede drying.

In figure 17 the results are shown. We observe in SCV10500 a factor of 3 increase in $1000/Q_s$ from a frequency of 73 to 638 Hz. In SR7227, $1000/Q_s$ roughly doubles from 58 to 495 Hz.

4. DISCUSSION OF THE ACOUSTIC RESULTS

Having measured V_e, V_s, $1000/Q_e$, and $1000/Q_s$ in rock at a given frequency, one can calculate the compressional wave velocity, V_p, the compressional wave specific attenuation, $1000/Q_p$, and the bulk compressional specific attenuation, $1000/Q_k$, using the relations given in Murphy (1982a). Regretably, our sample limitations have precluded the measurement of E and S values in Fort Union sandstone at the same frequency. Strictly speaking, the observed frequency dependence (fig. 17) should render the following calculations invalid. Yet presently, we have neither the proper frequency-dependent constitutive

equations nor the characteristic relaxation times with which to perform the calculations rigorously. Most importantly, in the Fort Union case, where the maximum difference in E and S frequencies is from 3892 to 6378 Hz, the resulting error is expected to be less than 5% in both velocities and 1000/Q.

Velocities

Measured V_s is replotted in figure 18 along with the calculated values for V_p. We find that from full saturation to $S_w = 0.9$, V_p drops sharply, ~20%. Then, V_p decreases more gradually to a full 30% decline at $S_w = 0.4$. Below $S_w = 0.4$, $V_p = V_e$ due to the low Poisson's ratio, ν, in that range.

This is a very significant finding. It suggests two important conclusions. First, at frequencies below 10 kHz, an in situ tight sandstone having gas saturation, S_g, greater than 0.2 may be identifiable as an anomalous decline in the compressional sonic velocity log (~10 kHz) or as a strong horizon in a reflection seismogram (~10-100 Hz). Secondly, considering Gregory's (1976) data showing a weak gas saturation effect, we may hypothesize that ultrasonic measurements are giving unrelaxed group velocities, which must be corrected for application to borehole and seismic data.

Also plotted in figure 18 are the Biot-Gassmann predictions for the dependence of V_p and V_s on S_w. V_p and V_s are given by

$$V_p = \left(\frac{M_r}{\rho_c}\right)^{1/2} \quad \text{and} \quad V_s = \left(\frac{N_r}{\rho_c}\right)^{1/2} \tag{4}$$

respectively; where the low frequency or relaxed compressional modulus, M_r, is

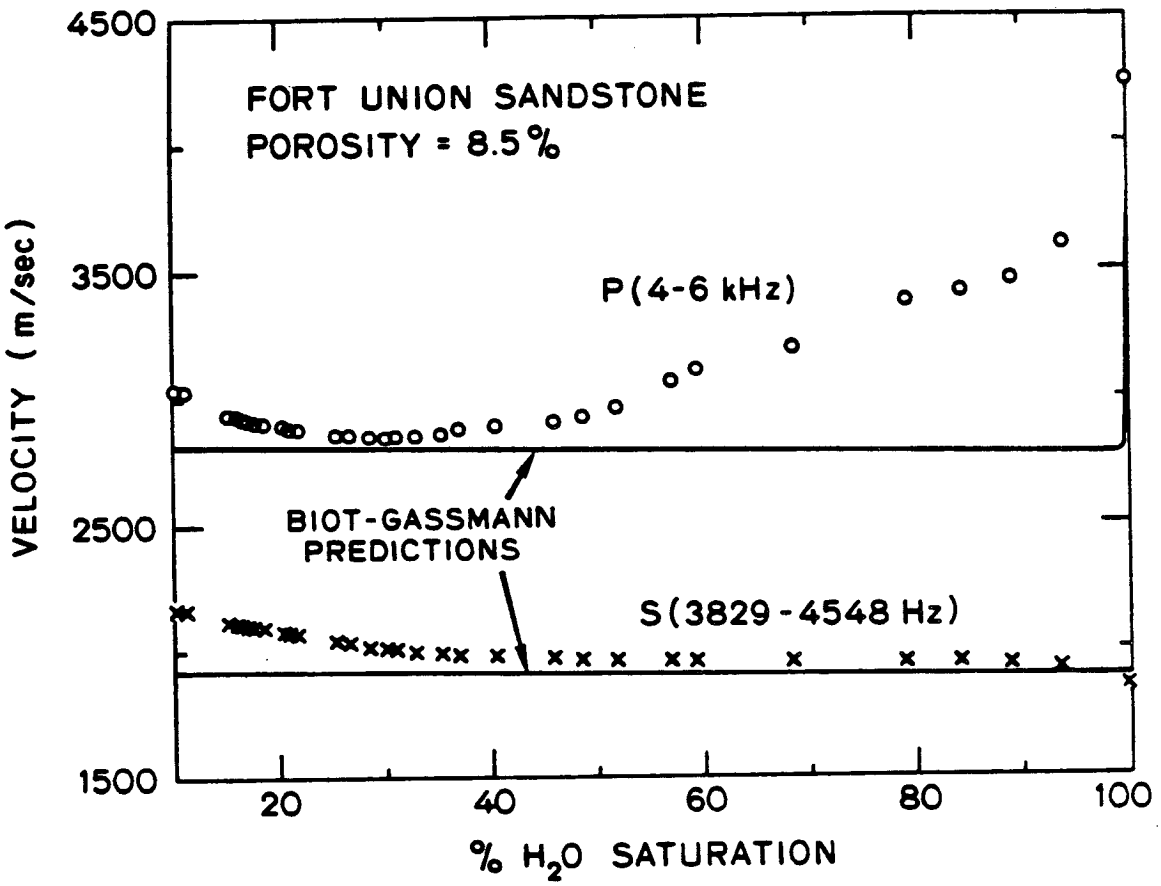

Fig. 18. Calculated V_p and measured V_s vs. % water saturation (S_w = 0.10 - 1.00) in Fort Union sandstone at ~5 kHz.

$$M_r = \frac{(K_s - K_{wr})^2}{K_s\left(1 - \phi - \frac{K_{wr}}{K_s} + \phi \frac{K_{wr}}{K_f}\right)} + K_{wr} + \frac{4}{3}\mu_{wr} , \quad (5)$$

the low frequency or relaxed shear wave modulus, N_r, is

$$N_r = \mu_{wr} , \quad (6)$$

and the composite density, ρ_c, is

$$\rho_c = (1 - \phi)\rho_s + \phi \rho_w S_w . \quad (7)$$

K_s is the bulk modulus of the solid grains, ρ_w is the density of the water, and K_f is the bulk modulus of the fluid given by

$$\frac{1}{K_f} = \beta_g(1 - S_w) + \beta_w S_w , \quad (8)$$

where β_g is the compressibility of the gas and β_w is the compressibility of the water. K_{wr} and μ_{wr} are the real past low frequency or relaxed water-wetted bulk and shear frame moduli, respectively.

The Biot-Gassmann relations (Gassmann, 1951; Geertsma and Smit, 1961; Domenico, 1974, 1977) are the low frequency limit of Biot's (1956) theory. Brown and Korringa (1975) have further shown that these relations govern the general low frequency or relaxed limit wherein the sufficiently long wave period provides water flow the necessary time required to equilibrate local wave-induced, pore pressure gradients in the fluid. The Biot-Gassmann relations have been shown (Murphy, 1982c) to describe successfully the dependence of V_p and V_s on S_w in Massilon sandstone at low acoustic frequencies (i.e. 20-600 Hz). Clearly, the Biot-Gassmann predictions for Fort Union sandstone

demonstrate qualitative and quantitative discrepancy from the 3-6 kHz data. Thus, figure 18 coupled with the $1000/Q_s$ frequency dependence observed in figure 17, suggests that these velocities, measured in the higher acoustic range (i.e. 1-20 kHz), are not entirely relaxed values for tight sandstones. This further supports the contention that ultrasonic measurements yield unrelaxed group velocities. It is perhaps important to emphasize that the V_p drop with undersaturation is expected to be even sharper in the low seismic frequency range where the velocities are completely relaxed, than that which we have measured at borehole frequencies.

The specific values input into the equations 4-7 for figure 18 are given in table II. In general, the bulk and shear frame moduli, $\overline{K}$ and $\overline{G}$ respectively are complex and strongly dependent on frequency and water saturation. The choice of K_{wr} and μ_{wr} in this particular case is somewhat arbitrary because i) measurements for the fully relaxed case have not been made, and ii) no satisfactory theory with predictive power has yet been published. A theoretical model having predictive potential is proposed in Murphy (1982c). In this paper, figure 19 suffices to demonstrate the relevant point. Figure 19 shows schematically the general, frequency-dependent, real part of the frame moduli normalized by the real part of the relaxed frame modulus plotted against frequency as a function of water saturation. As our measurements at 4-6 kHz are supposed to be near $\log(\omega\tau) \to 0$, we have chosen K_{wr} and μ_{wr} to be ~1% less than the lowest calculated values from both the E and S measurements. Consideration of the low value of V_s at full saturation was suppressed simply because we do not understand it.

Table II. Input parameters for Biot Gassman relations plotted in Figure 18.

	β_w	β_g	K_s	K_{wr}	μ_{wr}	ϕ	ρ_s	ρ_w
	$(GPa)^{-1}$		GPa			%	kg/m^3	
FORT UNION SANDSTONE	4.5×10^{-1}	7.6×10^{3}	35	7.14	9.06	8.5	2650	1000

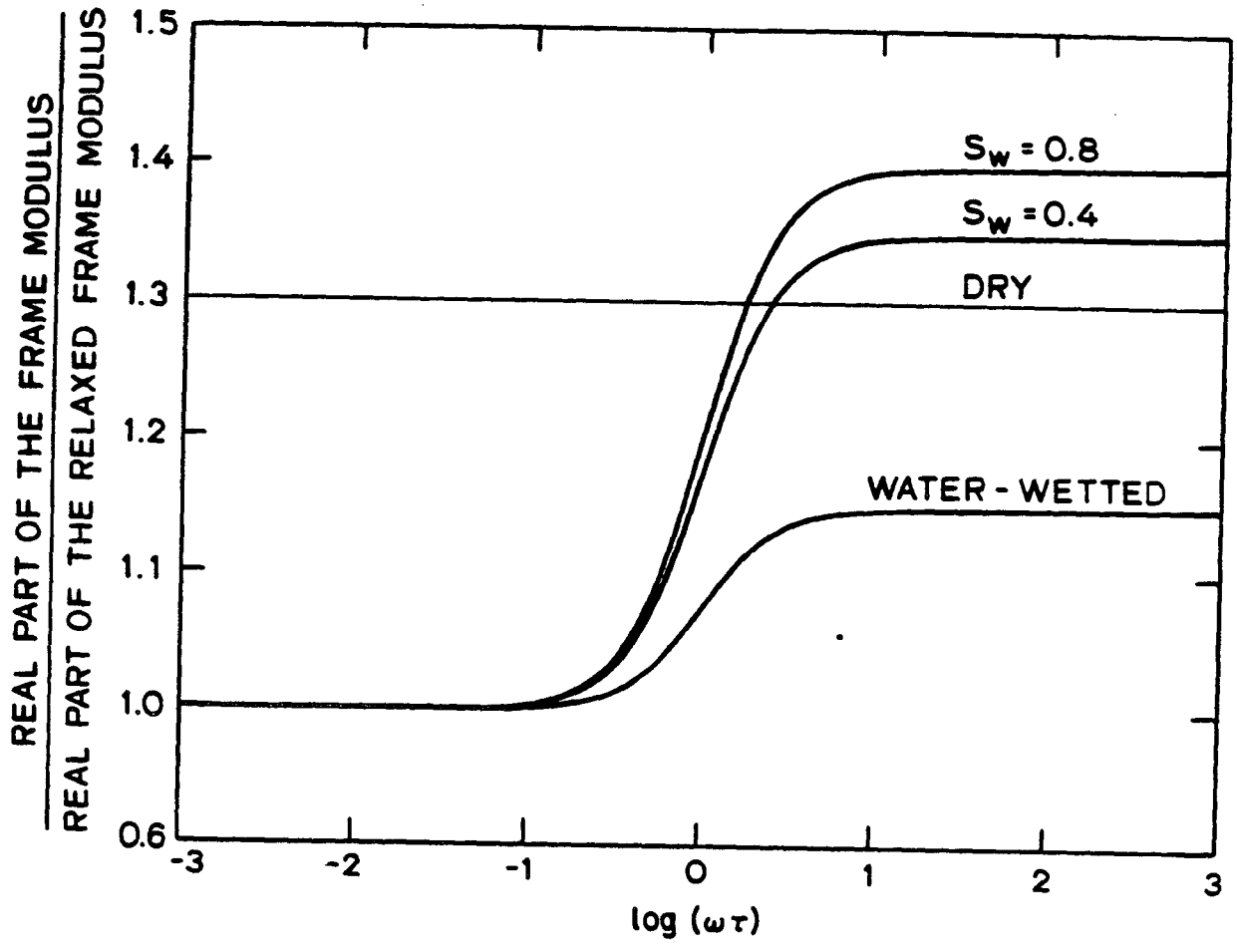

Fig. 19. Theoretical dispersion, as a function of water saturation, of the real part of the frame modulus normalized to the real part of the relaxed frame modulus.
$\tau \approx 10^{-3} - 10^{-4}$ sec.

Attenuation

Given the relations in Murphy (1982a), it is easily shown that when ν is positive either

$$Q_s^{-1} > Q_e^{-1} > Q_p^{-1} > Q_k^{-1} , \quad (9a)$$

$$Q_s^{-1} = Q_e^{-1} = Q_p^{-1} = Q_k^{-1} , \quad (9b)$$

or

$$Q_s^{-1} < Q_e^{-1} < Q_p^{-1} < Q_k^{-1} , \quad (9c)$$

Figure 20 shows the calculated $100/Q_k$ and $1000/Q_p$ plotted along with the measured $1000/Q_e$ and $1000/Q_s$. Errors may be 10% in P and 20% in K. Most error bars are omitted so as not to clutter the figure. Relations (9a) are seen to hold above $S_w = 0.8$. In this domain, the bulk compressional loss is negligible, and $1000/Q_p$ is very small compared to $1000/Q_s$. Relations (9b) hold at a point somewhere between $S_w = 0.84$ and 0.79. From that point down to $S_w = 0.1$, relations (9c) hold. Q_k at 0.79 is calculated to be 3.6. At this peak, $1000/Q_p$ is nearly twice as large as $1000/Q_s$.

Above $S_w = 0.90$, a positive $1000/Q_e$ and $1000/Q_s$ could not be calculated. We think that this is due to the fact that $1000/Q_e$ and $1000/Q_s$ were measured at different frequencies. The $1000/Q_s$ measured at 4 kHz is expected to be near the apex of the frequency peak. The $1000/Q_e$ at 6 kHz is supposed to be on the high side of the peak, therefore having an artificially low $1000/Q_e$.

Study of the micromechanisms causing the energy loss is the specific purpose of another paper (Murphy, 1982c). However, a few points ought to be emphasized here.

Q is a fully and partially saturated tight sandstone and is

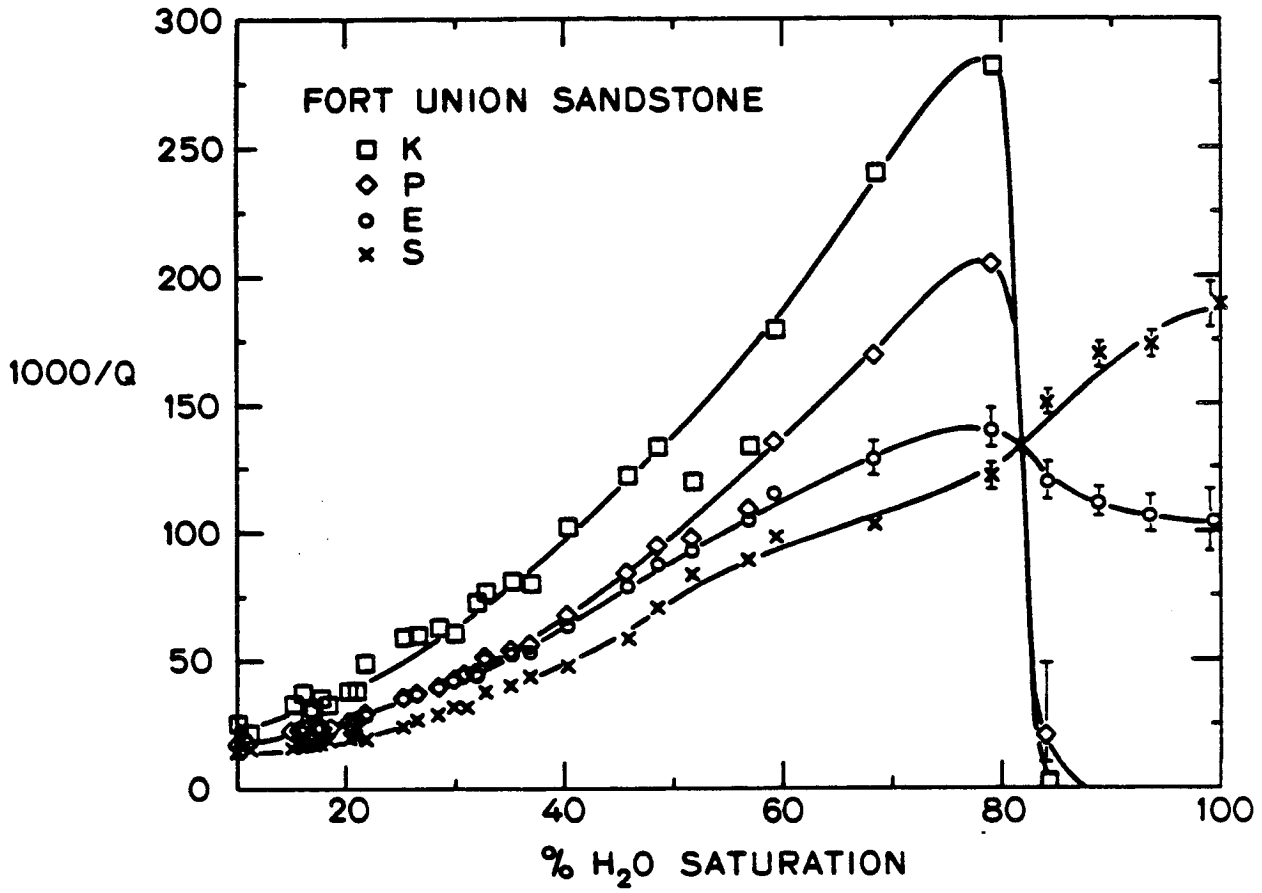

Fig. 20. Calculated $1000/Q_k$ and $1000/Q_p$, along with measured $1000/Q_e$ and $1000/Q_s$, vs. % water saturation (S_w = 0.10 - 1.00) at ~ 5 kHz.

frequency dependent in the acoustic frequency range (fig. 17).

In a very broad qualitative sense, Fort Union's dependence on S_w is similar to that observed in Massilon sandstone (Murphy, 1982a). That is, V_p and $1000/Q_s$ are maximum at full saturation; V_p declines and $1000/Q_p$ rises to a peak near $S_w = 0.8$; and $1000/Q_p < 1000/Q_s$ in fully saturated sandstone, and $1000/Q_p > 1000/Q_s$ in partially saturated sandstone. We have argued (Murphy, 1982a), in part of the basis of these water saturation and frequency effects, that in Massilon sandstone, the dominant dissipation mechanism is viscous water flow driven by local pore pressure gradients.

Several quantitative and specific qualitative features of the Fort Union measurements differ strongly with the Massilon data (even after correction for the difference in frequency between the two data sets). First, the losses above $S_w = 0.40$ in the Fort Union sandstone are greater. Secondly, the Massilon Q^{-1} data shows distinctly different behavior in various segments of its dependence on S_w. In the range from full saturation to $S_w = 0.1$, $1000/Q_s$ is sensitive to water saturation only above $S_w = 0.85$. $1000/Q_p$ shows a strong peak, but is weakly dependent on water saturation below $S_w = 0.6$. In contrast, $1000/Q_s$ vs. S_w in Fort Union sandstone exhibits nearly a uniform slope above $S_w = 0.3$; and $1000/Q_p$, although having a strong peak, depends quite smoothly on S_w throughout the range of water saturations.

Biot's (1956) inertial coupling mechanism predicts for Fort Union sandstone a center frequency of 1 MHz. The predicted S loss is too small at 5 kHz. The thermoelastic mechanism of Kjartansson and Nur (1982) is similarly refuted by the large loss in shear. Surface

mechanisms (Spencer, 1981; Murphy, 1982a), which are quite likely operative at high saturations and are especially important at very low saturations, cannot explain the strong dependencies on S_w in the higher saturation ranges.

Frame relaxation controlled by local water flow to and from near-contact gaps depends on two microstructural factors: i) compliant sites for pore pressure generation and ii) the admittance or local permeability of the pore neighborhoods in close proximity to the sites. The higher losses in both P and S follow from a higher percentage population of low aspect ratio pores in Fort Union than in Massilon sandstone (cf. Palmer and Traviolia, 1980). The loss in S is strong at full saturation in Massilon sandstone and declines sharply with slight undersaturation. In the higher partial saturation ranges in Fort Union sandstone, sufficiently low local permeability and high capillary forces cause the local pore neighborhoods to behave as if the rock were fully saturated. As these neighborhoods progressively drain, $1000/Q_s$ declines gradually. The continuing gradual decline below $S_w = 0.4$, now below that in Massilon, results from the removal of water from the silanol grain surfaces. This effect does not transpire in Massilon until low moisture contents (Murphy, 1982a) because Massilon has a much lower pore surface to pore volume ratio.

The attenuation dependence on S_w may provide an indication of the degree of partial saturation in situ. Relative values are more easily acquired. In figure 21 we have plotted V_p/V_s and Q_p^{-1}/Q_s^{-1} vs. S_w. This figure shows that the measurement of V_p/V_s is sufficient to distinguish full from partial water saturation. If V_p/V_s

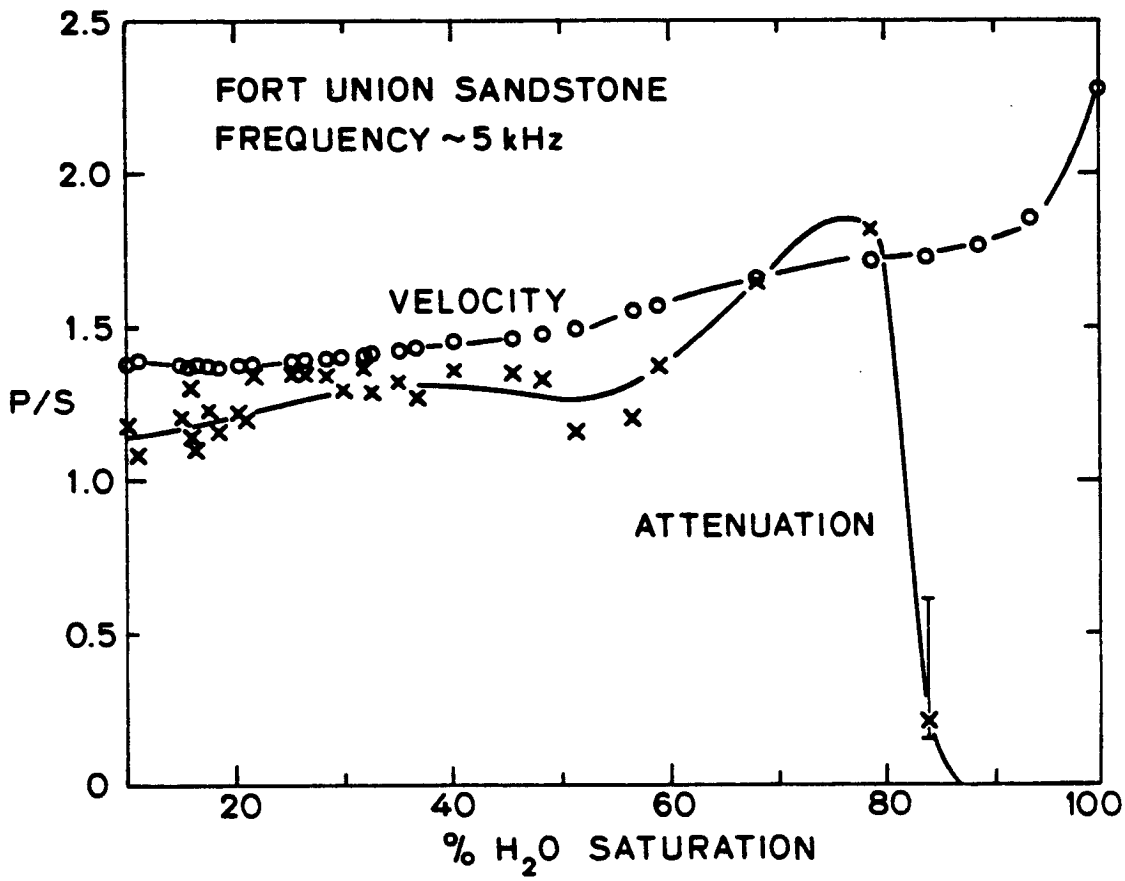

Fig. 21. V_p/V_s and Q_p^{-1}/Q_s^{-1} vs % water saturation (S_w = 0.10 to 1.00) in Fort Union sandstone at ~5 kHz.

is greater than 2, the rock is fully water saturated. Together figures 14 and 19 show that the acquisition of all four properties V_p, V_s, Q_p^{-1}, and Q_s^{-1}, is sufficient to distinguish three different ranges of partial water saturation. If $1.5 < V_p/V_s < 2$ and $Q_p^{-1}/Q_s^{-1} < 1$, then $0.8 < S_w < 1.0$. If $1.5 < V_p/V_s < 2$ and $Q_p^{-1}/Q_s^{-1} > 1$, then $0.6 < S_w < 0.8$. And if $V_p/V_s < 1.5$, $1000/Q_p$ and $1000/Q_s < 100$ and $Q_p^{-1}/Q_s^{-1} < 1.5$, then $S_w < 0.6$. Of course, these bounds must be reset for in situ temperature and pressure conditions, but the point remains that such an algorithm may be feasible for tight sandstones.

5. ULTRASONIC MEASUREMENTS

In order to test the hypothesis that ultrasonic pulse transmission measurements yield unrelaxed group velocities for fully and partially saturated tight sandstones, several ultrasonic experiments were performed. We shall demonstrate that the ultrasonic signal velocities, V_p and V_s, show a markedly different dependence on S_w than do the acoustic phase velocities, V_p and V_s, measured from 4 to 6 kHz. All samples are vertical cores whose axes are perpendicular to bedding.

Fort Union Sandstone

We have measured ultrasonic P and S velocities in Fort Union sandstone. The samples were taken from the same 25 cm x 10 cm well core as were those in the acoustic measurements. A pulse transmission technique was used in which P and S transducers were clamped with axial pressures less than 0.5 MPa at opposite ends of the 2.2 cm cylindrical sample. Frequencies were roughly 200 kHz. Measurements were obtained as a function of continuously varying S_w in a drying

experiment. The sample was unjacketed. The pressure was atmospheric. The temperature was 22°C. And the relative humidity was held at 0.3 in the humidity chamber.

Results are shown in figure 22. The P group velocity, $\overline{V}_p$, declines 12.5% very gradually from full saturation to $S_w = 0.7$. Between $S_w = 0.7$ and 0.4, the dependence is flat. And below $S_w = 0.4$, $\overline{V}_p$ drops again roughly 15%. After a 5% increase from full saturation to $S_w = 0.9$, the S group velocity, $\overline{V}_s$, is observed to be roughly independent of S_w.

In figure 23 we have plotted the P/S velocity ratios for the values taken at both acoustic and ultrasonic frequencies. Note that at full saturation, the acoustic V_p/V_s is 2.08, while the ultrasonic $\overline{V}_p/\overline{V}_s$ is 1.9.

Schuler-Cotton Valley Sandstone

An identical experiment was conducted in a 2.2 cm sample of SCV10500 ($\phi = 3.3\%$). Results are shown in figure 24. $\overline{V}_s$ is virtually independent of water saturation. $\overline{V}_p$ declines 6% from full saturation to $S_w = 0.85$, is flat between 0.8 and 0.6, and decreases gradually 15% from $S_w = 0.60$ to a laboratory dry condition.

Pressure Dependence as a Function of Saturation

We have measured $\overline{V}_p$ and $\overline{V}_s$ in SCV9594 ($\phi = 5.1\%$), St. Peter sandstone ($\phi = 8.0\%$), SR6556.5 ($\phi = 7.1\%$), and SR6521.6 ($\phi = 4.6\%$) under effective pressures ranging from 0 to 50 MPa. The measurements were made in samples, 5.1 cm in diameter, in three discrete states of saturation: vacuum (< 25 μm), dry ($S_w \sim 0$), partially saturated ($S_w = 0.7$), and fully water saturated ($S_w = 1.0$). The pulse transmission technique we used is similar to those described in Nur and

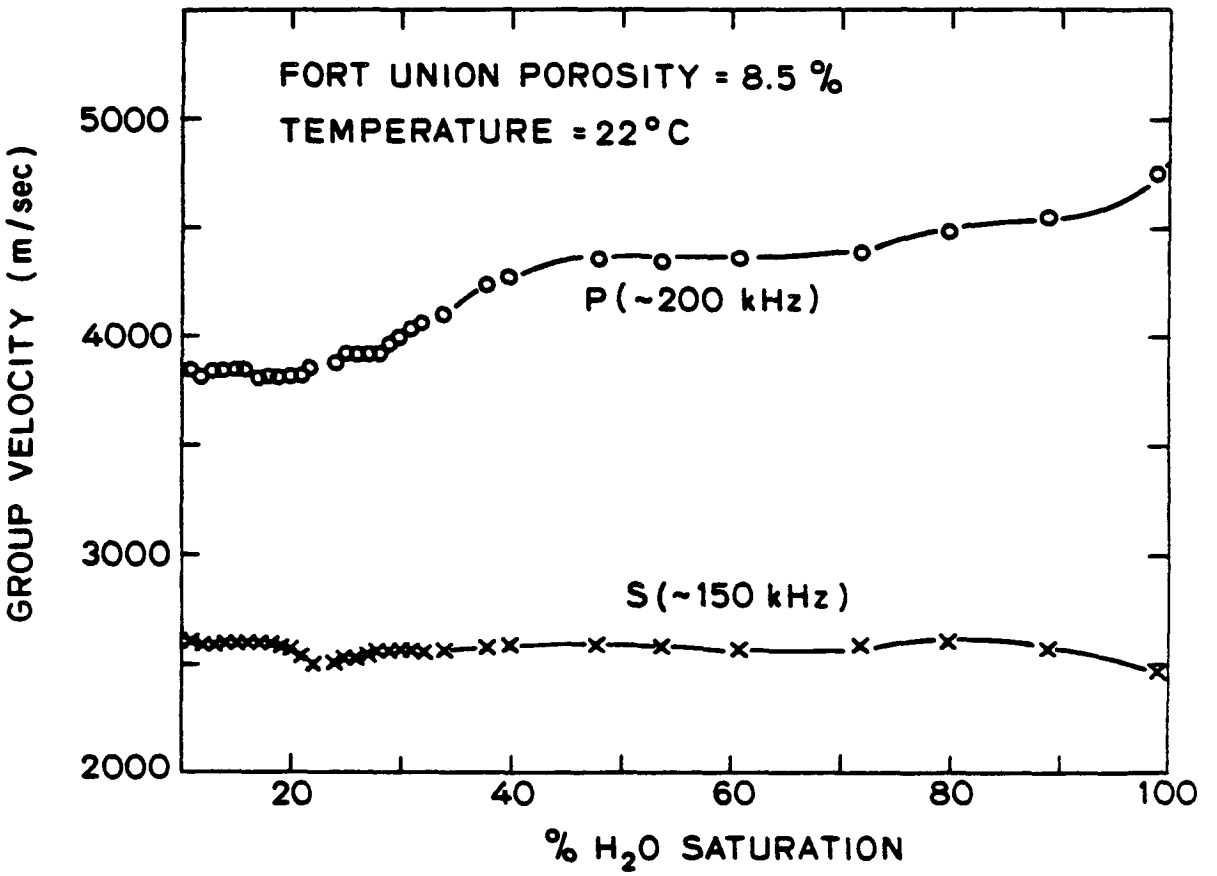

Fig. 22. Ultrasonic $\overline{V}_p$ and $\overline{V}_s$ vs. % water saturation (S_w = 0.10 - 1.00) in Fort Union sandstone.

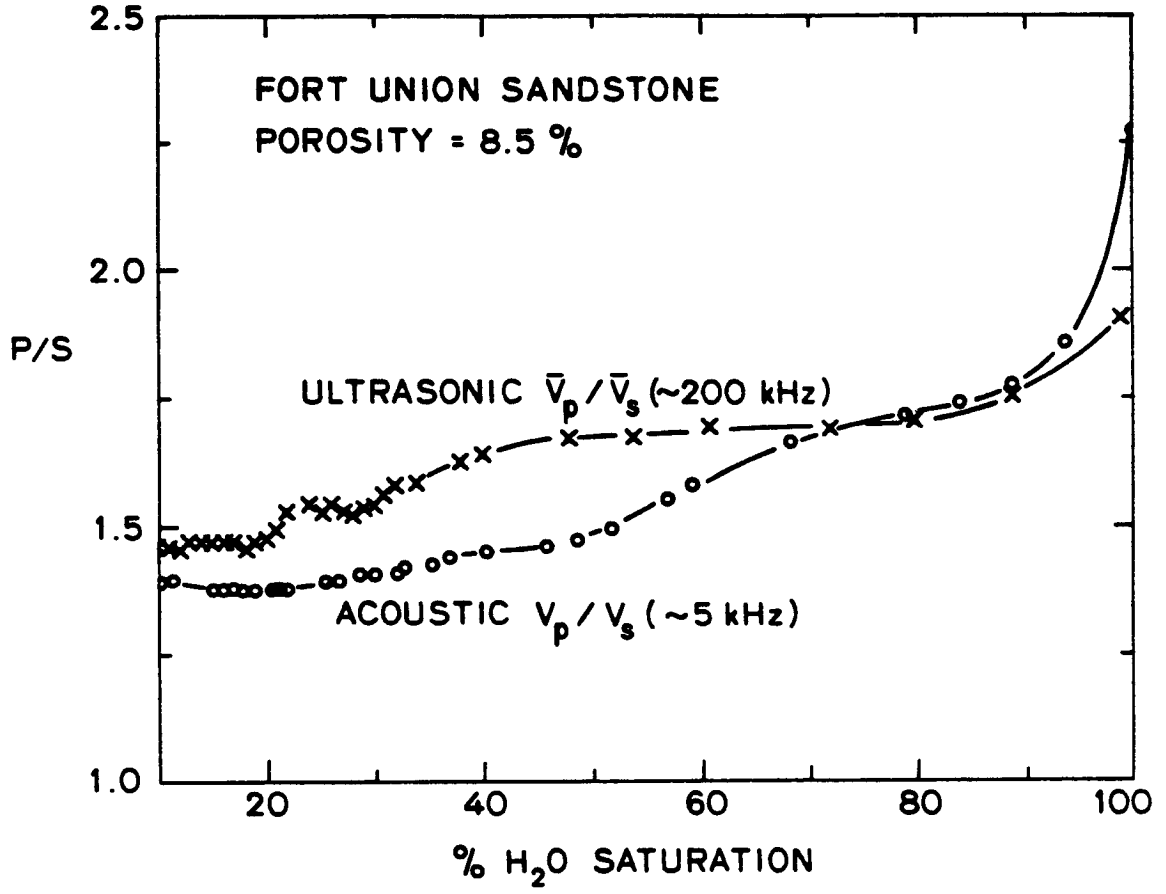

Fig. 23. Comparison of ultrasonic $\bar{V}_p/\bar{V}_s$ and acoustic V_p/V_s vs. % water saturation in Fort Union sandstone.

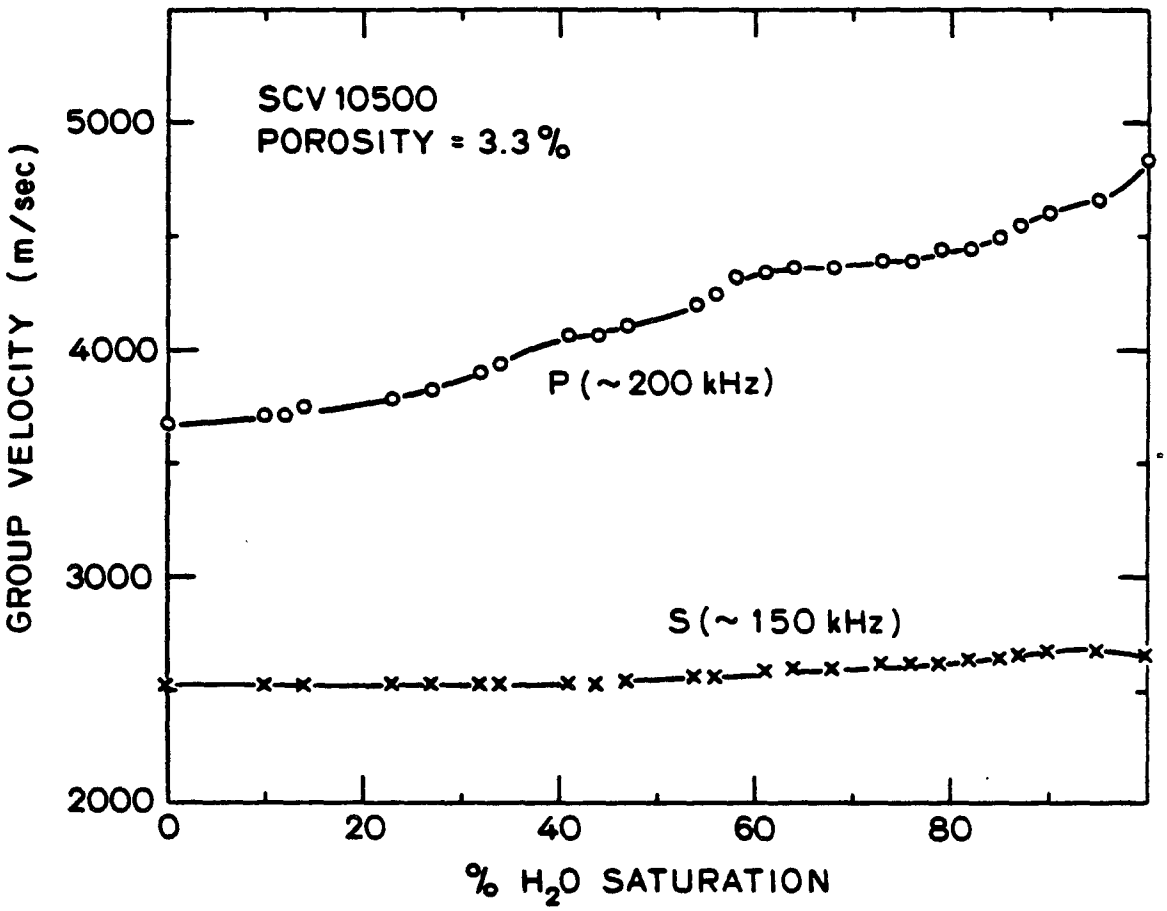

Fig. 24. Ultrasonic $\overline{V}_p$ and $\overline{V}_s$ vs. % water saturation (S_w = 0 to 1.0) in SCV 10500.

Simmons (1969) and Gregory (1976). Frequencies were roughly 800 kHz.

Results are presented in figure 25.

Neglecting details, we find in all cases that $\overline{V}_p(S_w = 1.0) > V_p(S = 0.7) > \overline{V}_p(S_w \simeq 0)$, and that the difference between fully and 70% partially water saturated $\overline{V}_p$ is less than 4%. In most cases, $\overline{V}_s(S_w = 0.7) > \overline{V}_s(S_w = 1.0) > \overline{V}_s(S_w \simeq 0)$. In SR6556.5 a relatively strong confining pressure effect pushes $\overline{V}_s(S_w \simeq 0)$ across the fully and partially saturated values at a pressure near -25MPa. St. Peter, an 8% porosity sandstone with relatively high aspect ratio and spherically isotropic pores, exhibits $\overline{V}_s(S_w \simeq 0) > \overline{V}_s(S_w = 0.7) > \overline{V}_s(S_w = 1.0)$.

6. DISCUSSION OF DISPERSION

Mounting evidence suggests that fully and partially saturated sandstones respond to small stress waves as linear viscoelastic materials (Spencer, 1981; Murphy, 1982a; Brennan and Stacey, 1981; Strick, 1981). The dominant relaxation mechanism appears to behave macroscopically as a standard linear solid (Zener, 1948) having a narrow distribution of relaxation times in a high porosity sandstone (Spencer, 1981; Murphy, 1982a), and a somewhat broader distribution of relaxation times in a tight sandstone (Murphy, 1982c). Scrupulously avoiding detail, let us briefly review the relations in a standard linear solid among phase velocity, specific attenuation, and frequency, as sketched in figure 26.

The phase velocities are given by

$$V_p = V_{pu}\left(1 - \frac{\Delta M/M_u}{1 + \omega^2\tau^2}\right) \qquad (10a)$$

Fig. 25. Ultrasonic $\overline{V}_p$ and $\overline{V}_s$ vs. effective pressure at three states of water saturation: dry (◇) , 70% partially saturated (○) , and full saturated (□). Measurements are shown for four low porosity sandstones:

a) SCV9594,

b) St. Peter Ss,

c) SR 6556.5, and

d) SR5421.5

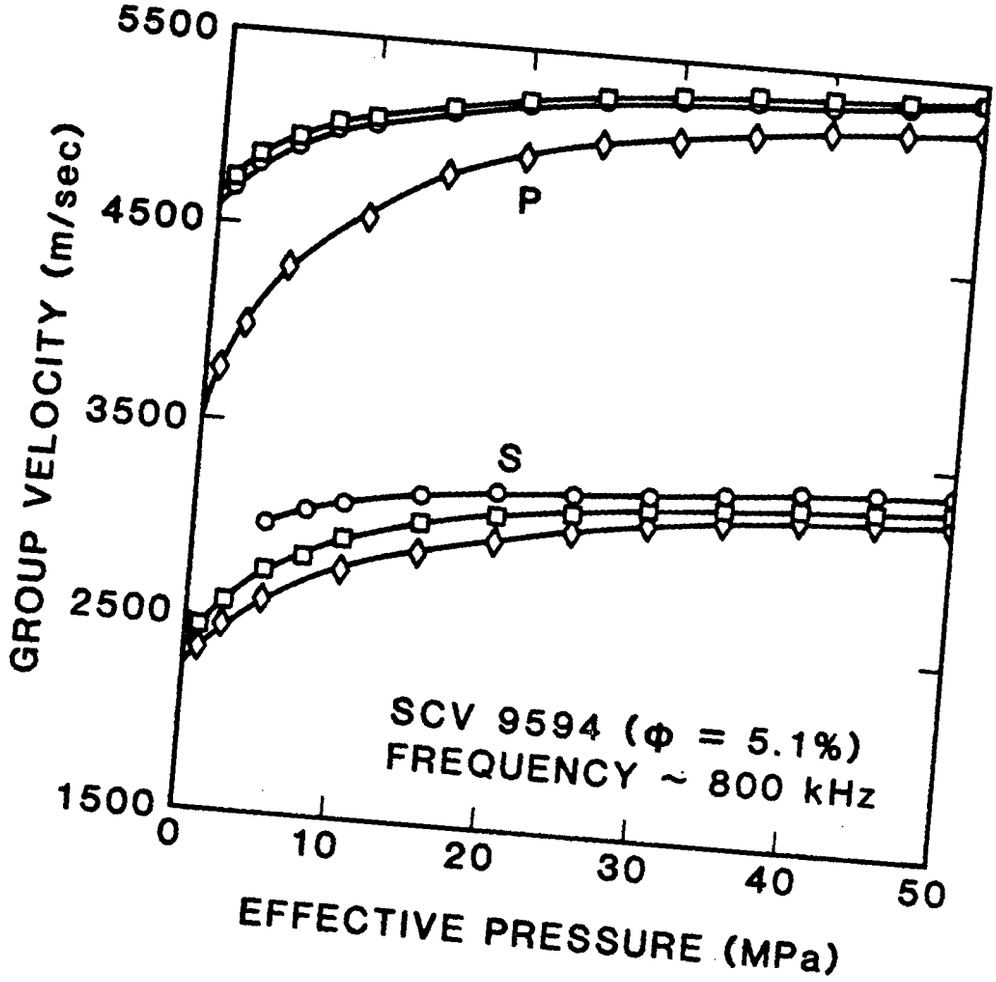
5500
4500
3500
2500
1500
GROUP VELOCITY (m/sec)
P
S
SCV 9594 (Φ = 5.1%)
FREQUENCY ~ 800 kHz
0
10
20
30
40
50
EFFECTIVE PRESSURE (MPa)

Figure 25a.

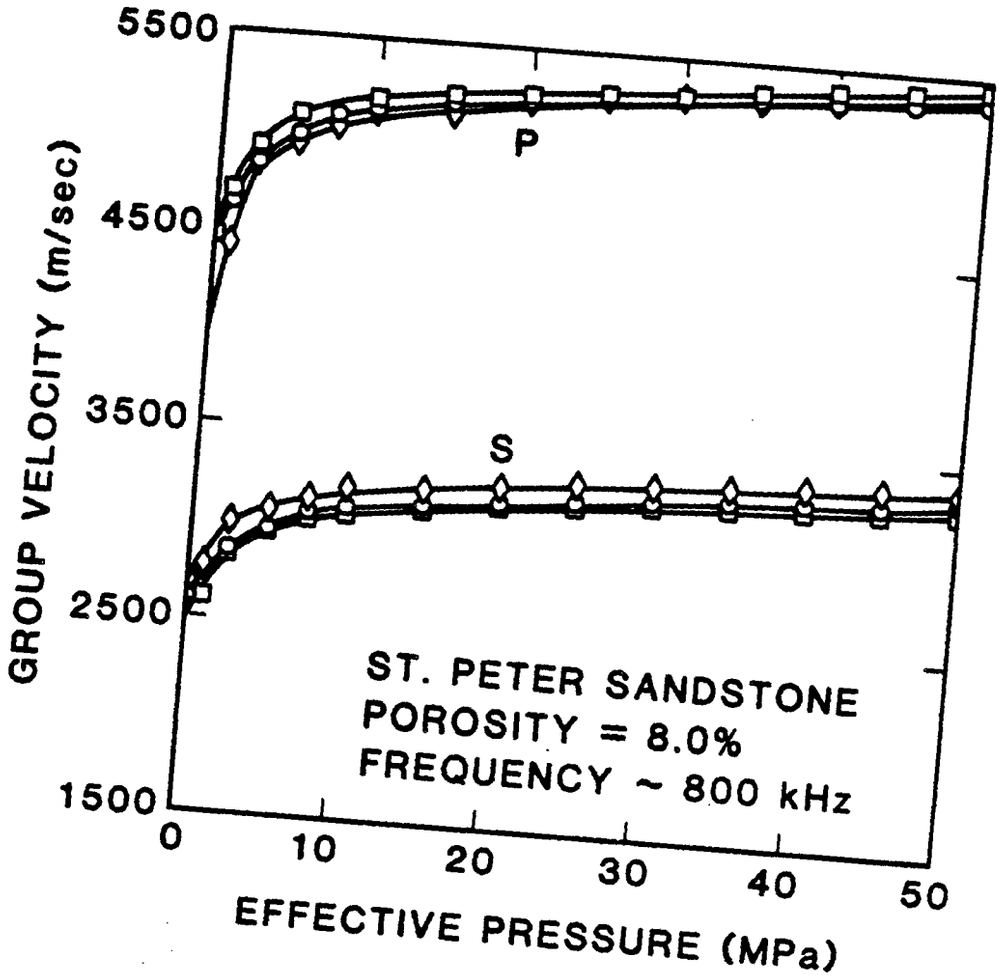
5500
4500
3500
2500
1500
GROUP VELOCITY (m/sec)
P
S
ST. PETER SANDSTONE
POROSITY = 8.0%
FREQUENCY ~ 800 kHz
0
10
20
30
40
50
EFFECTIVE PRESSURE (MPa)

Figure 25b.

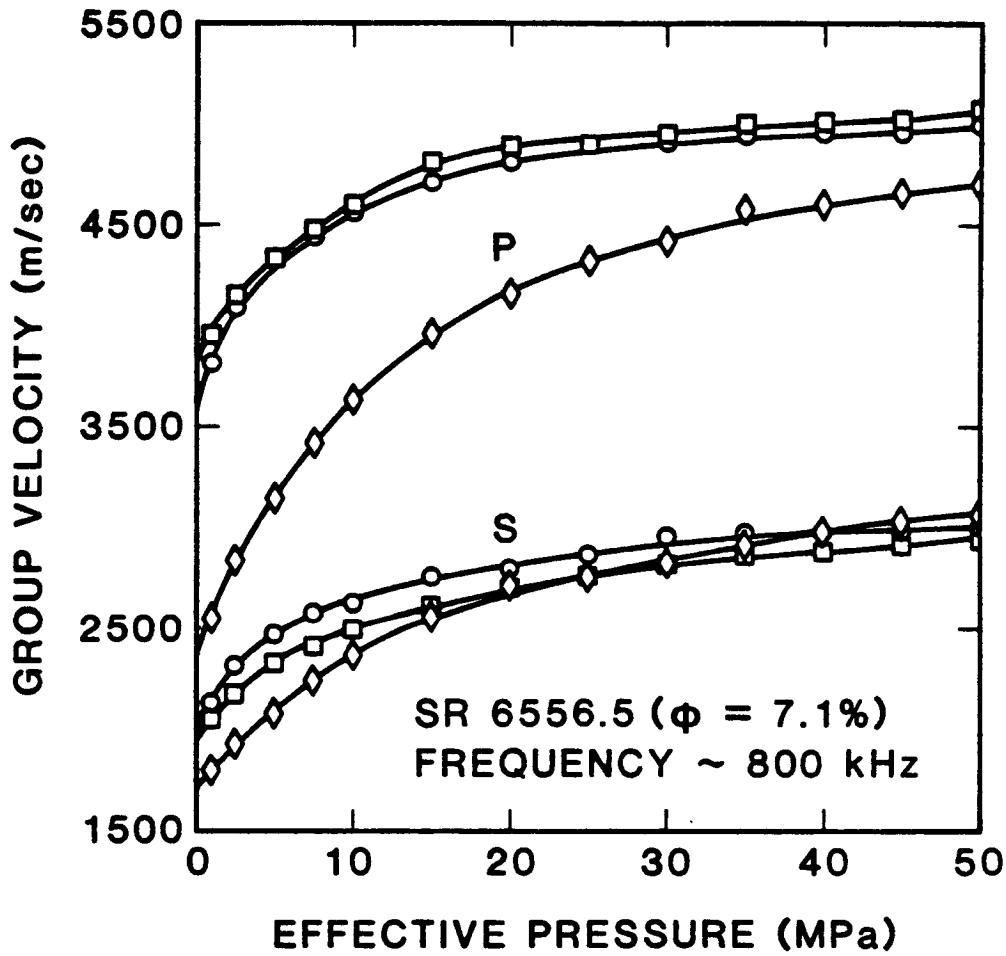
5500
4500
3500
2500
1500
GROUP VELOCITY (m/sec)
P
S
SR 6556.5 (Φ = 7.1%)
FREQUENCY ~ 800 kHz
0
10
20
30
40
50
EFFECTIVE PRESSURE (MPa)

Figure 25c.

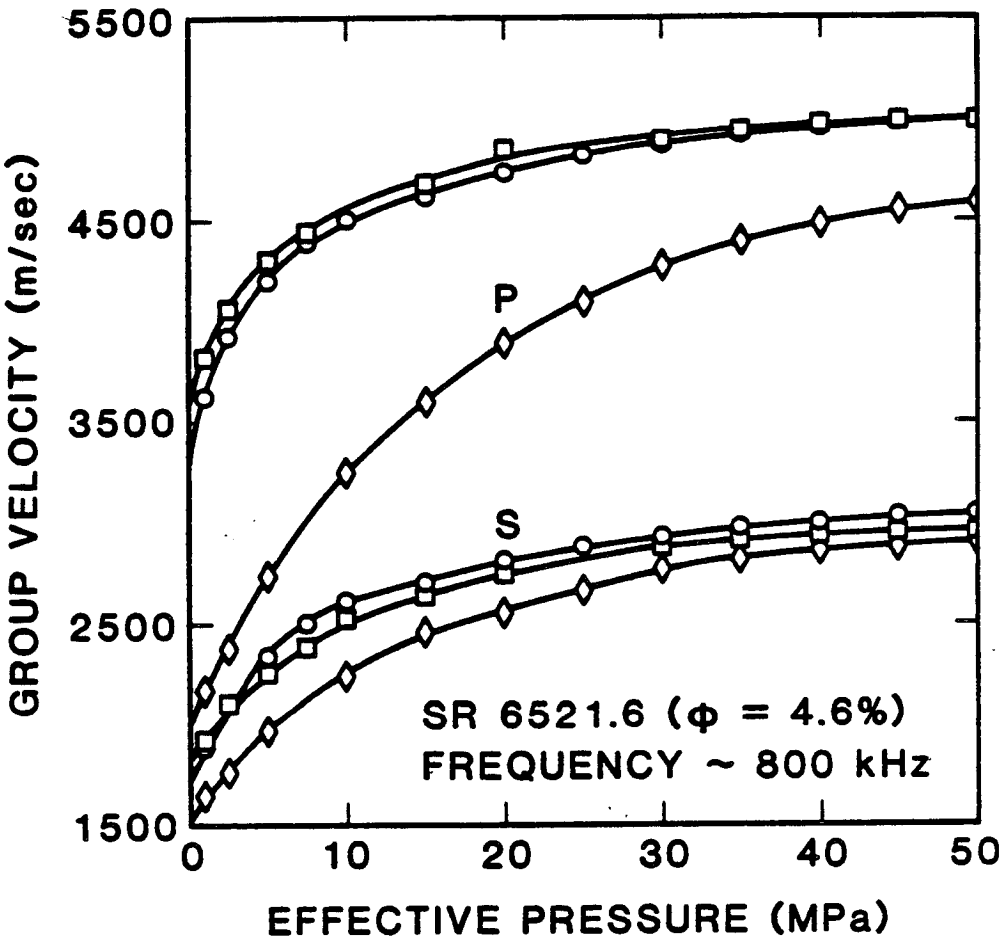
5500
4500
3500
2500
1500
GROUP VELOCITY (m/sec)
P
S
SR 6521.6 (Φ = 4.6%)
FREQUENCY ~ 800 kHz
0
10
20
30
40
50
EFFECTIVE PRESSURE (MPa)

Figure 25d.

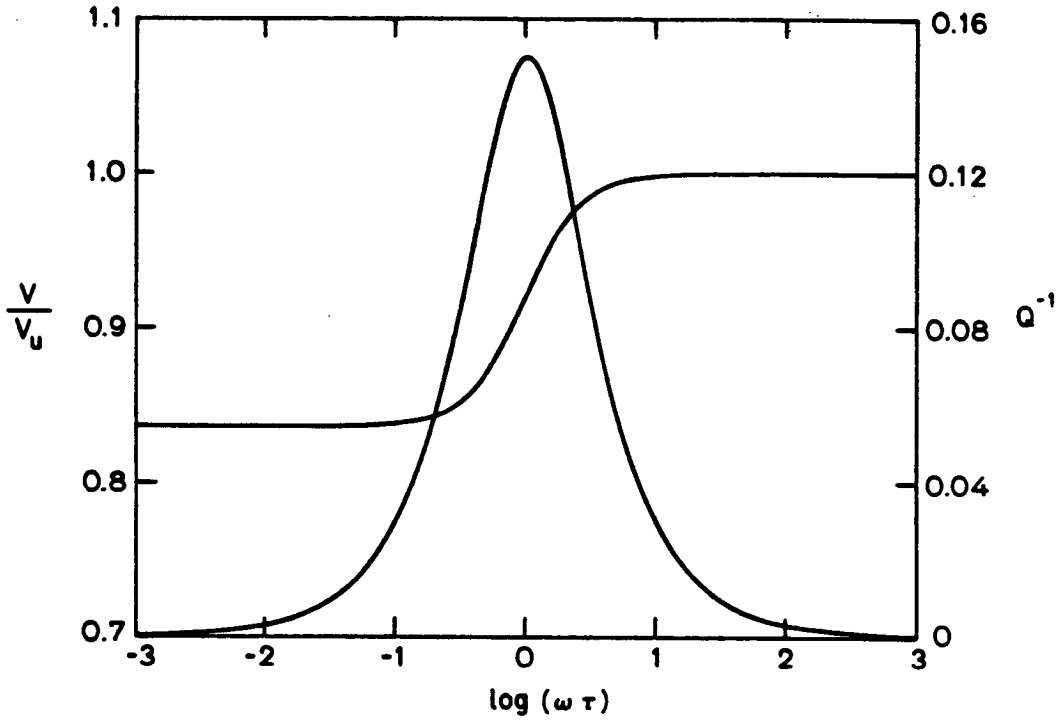

Fig. 26. Velocity dispersion and specific attenuation as a function of normalized frequency in a standard linear solid. Velocity dispersion is normalized to the unrelaxed velocity.

and

$$V_s = V_{su}\left(1 - \frac{\Delta N/N_u}{1 + \omega^2\tau^2}\right)^{1/2} \qquad (10b)$$

where τ is the characteristic relaxation time, and the modulus dispersions, M/M_u and N/N_u are related to Q_p^{-1} and Q_s^{-1}, respectivly, by

$$\frac{\Delta M}{M} = \left(\frac{1 + \omega^2\tau^2}{\omega\tau}\right) Q_p^{-1} \qquad (11a)$$

and

$$\frac{\Delta N}{N} = \left(\frac{1 + \omega^2\tau^2}{\omega\tau}\right) Q_s^{-1} \qquad (11b)$$

The dispersion and attenuation are maximum at the center frequency, or the inverse of the characteristic relaxation time. It is important to note that the two extremes in phase velocity are achieved where Q^{-1} is still appreciable. In other words, the range of significant velocity dispersion is narrower than the range of significant Q^{-1} frequency dependence. The low frequency extreme is the relaxed velocity. The high frequency extreme is the unrelaxed velocity.

In sandstones, we interpret the dominant relaxation mechanism to be local water flow in pores to and from compliant contact gaps during each cycle of compression and rarifaction. As mentioned above in section 4, the long wave period at sufficiently low frequency allows water flow to diffuse the wave induced local pressure gradients in the fluid. This case is governed by the Biot-Gassmann relations. At sufficiently high or infinite frequency, the infinitesimally short period does not permit flow to develop; the water behaves as a

compressible solid, essentially adding a component stiffness to a composite elastic solid.

In Fort Union sandstone, neither the 4-6 kHz V_p and V_s nor the 200 kHz $\overline{V}_p$ and $\overline{V}_s$ are relaxed velocities. Both measurements are in the transitional range (fig. 26). By comparing figure 22 with with figure 13, one finds that the difference between the acoustic V_p and V_s and the ultrasonic $\overline{V}_p$ and $\overline{V}_s$ is roughly i) 10% in P and 25% in S at full saturation, ii) 28% in P between S_w = 0.95 and 0.7, and iii) 20% in both P and S below $S_w = 0.7$. These observations are consistent with the attenuation data shown in figure 20. As $1000/Q_s$ is significantly larger than $1000/Q_p$, we expect the phase velocity dispersion in S to be larger than in P at full saturation (fig. 27). The peak in $1000/Q_p$ at $S_w = 0.8$ is related to a high P dispersion in that range of water saturation (fig. 27b). And below $S_w = 0.7$, $1000/Q_p \simeq 1000/Q_s$, and the P and S dispersions should be roughly the same (fig. 27c).

We caution that the observed velocity differences are not a direct measure of the phase velocity dispersion from ~5 kHz to ~200 kHz not only because the phase and group velocities may differ, but also because the sample configurations in the two measurement systems differ considerably. In the resonant bar technique, the sample is supported at the midpoint, and the ends are free. In the ultrasonic technique, the sample is lightly compressed along its axis. In this particular case however, we expect the error due to these factors to be no more than 5-10%.

Recall from equations (2a and 2b) that the difference between the group and phase velocities goes as $\frac{\partial V}{\partial \omega}$ <u>at the frequency of the</u>

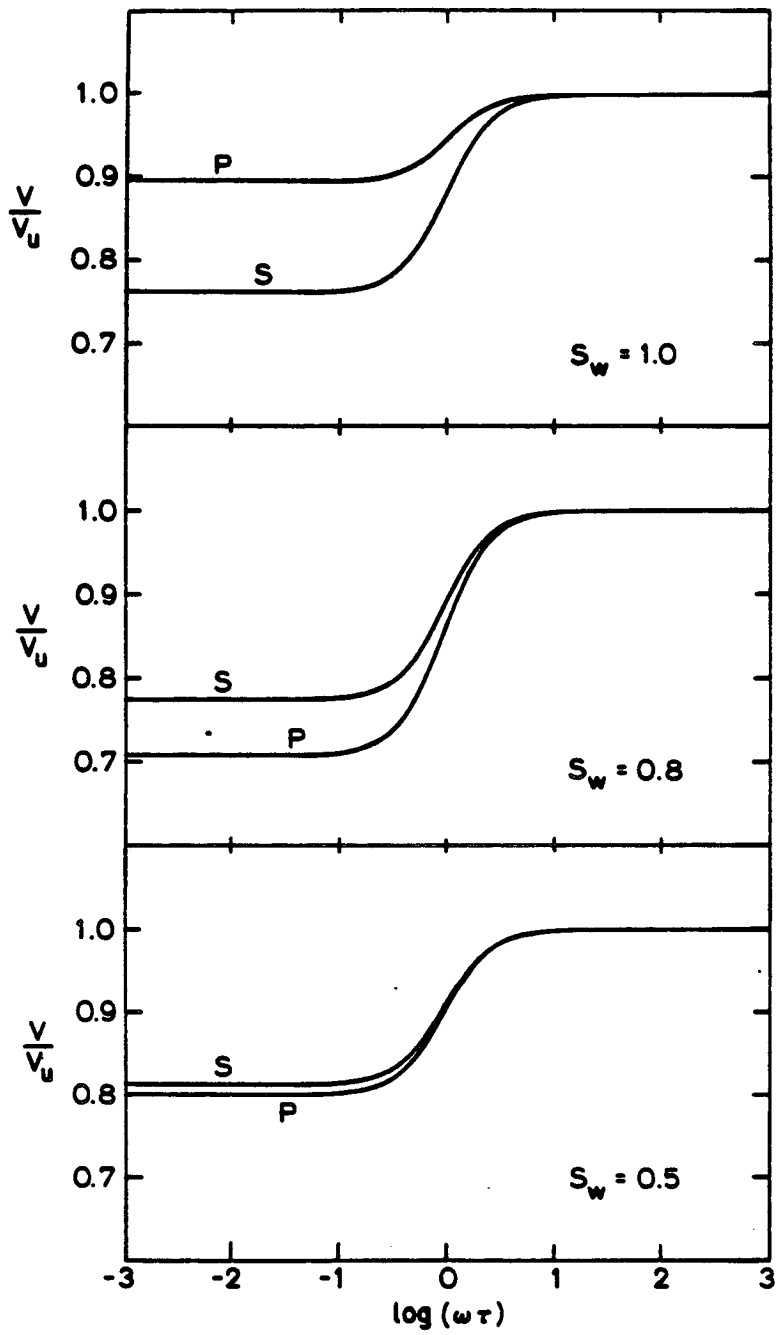

Fig. 27. Schematic of P and S velocity dispersions in Fort Union sandstone at three different states of water saturation. Calculations were made by assuming $\tau = 2 \times 10^{-4}$ and inputing the relevant measured Q^{-1} values from fig. 20 into equations (10) and (11).

measurement. All evidence suggests that the relaxation peak in the tight sandstones is centered between 100 Hz and 10 kHz. We therefore expect $\frac{\partial V}{\partial \omega}$ in the high ultrasonic frequencies to be quite small. The signal velocity measurement, particularly the 800 kHz pressure data, ought to be quite close to the actual phase velocity.

Our measurements of ultransonic $\overline{V}_p$ and $\overline{V}_s$ vs. S_w and P_e as a function of saturation agree well with Gregory's (1976) 1 MHz data for three Travis Peak sandstones (ϕ = 4.45, 4.58, and 8.02). Like ours, Gregory's data are neither well described by the Biot-Gassmann relations nor do they conform to our acoustic measurements. In fact, both our ultrasonic results and Gregory's show a closer resemblence to his 1 MHz velocity vs. S_w measurements in Chugwater (ϕ = 11.0), Green River (ϕ = 11.7), and Tensleep (ϕ = 15.2) sandstones, and even to those in Bandera (ϕ = 17.9) and Berea (ϕ = 19.11) sandstones. The effect of water saturation is relatively weak in all of these measurements. This weakness and the similarity between the hgih and low ϕ sandstones indicates that ultrasonic measurements are unrelaxed in consolidated sandstones in general.

In order to compare the water saturation effect on ultrasonic $\overline{V}_p$ and $\overline{V}_s$ with that of acoustic V_p and V_s in a high ϕ sandstone, we have measured $\overline{V}_p$ and $\overline{V}_s$ as a function of continuously varying S_w at ~200 kHz and as a function of P_e at 800 kHz in a Massilon sandstone (ϕ = 23%). Results are shown in figures 11, 12, and 28 through 30. An axial pressure ~0.5 MPa was required in order to achieve an adequate coupling for the measurements in figure 28. The velocities are higher than they would be at P_e = 0. Thus, direct qualitative comparison with figure 18 in Murphy (1982c)

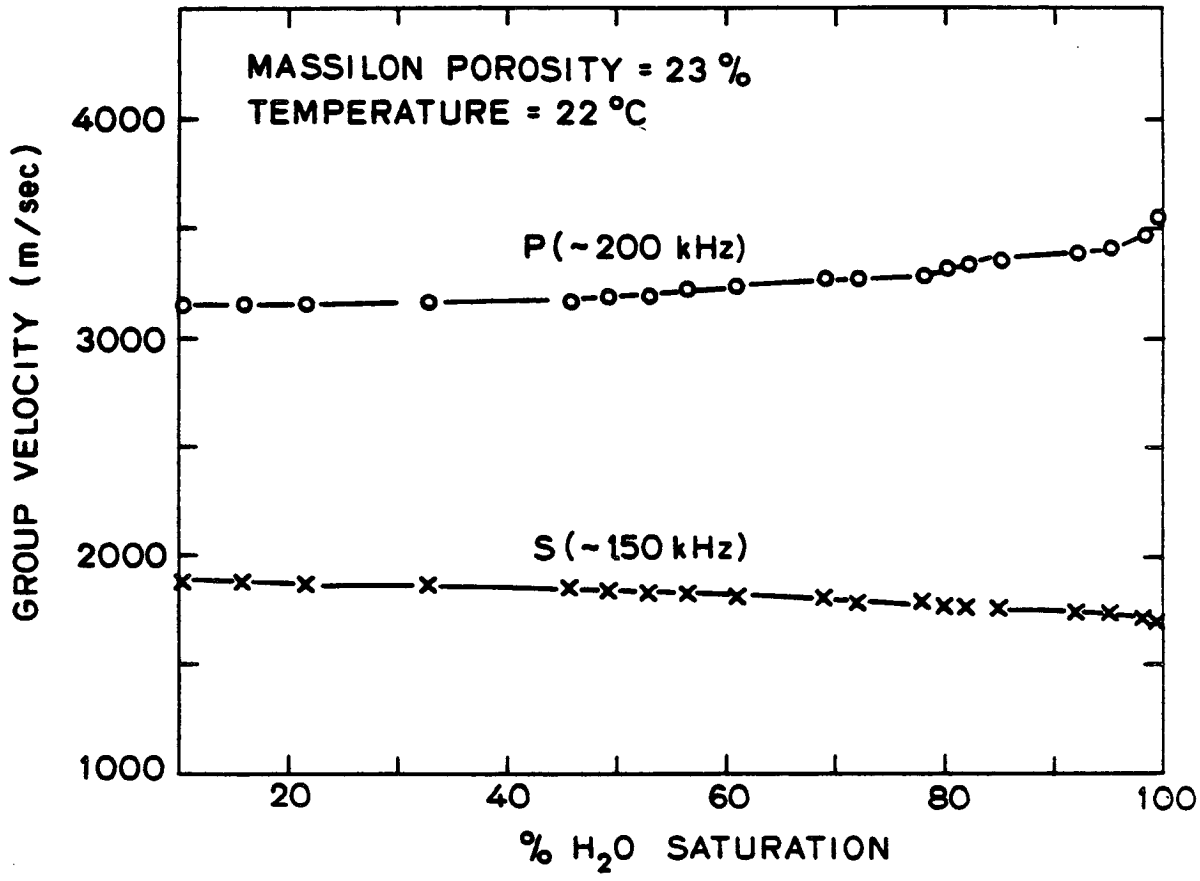

Fig. 28. Ultrasonic $\overline{V}_p$ and $\overline{V}_s$ vs. % water saturation (S_w = 0.1 - 1.0) in Massilon sandstone.

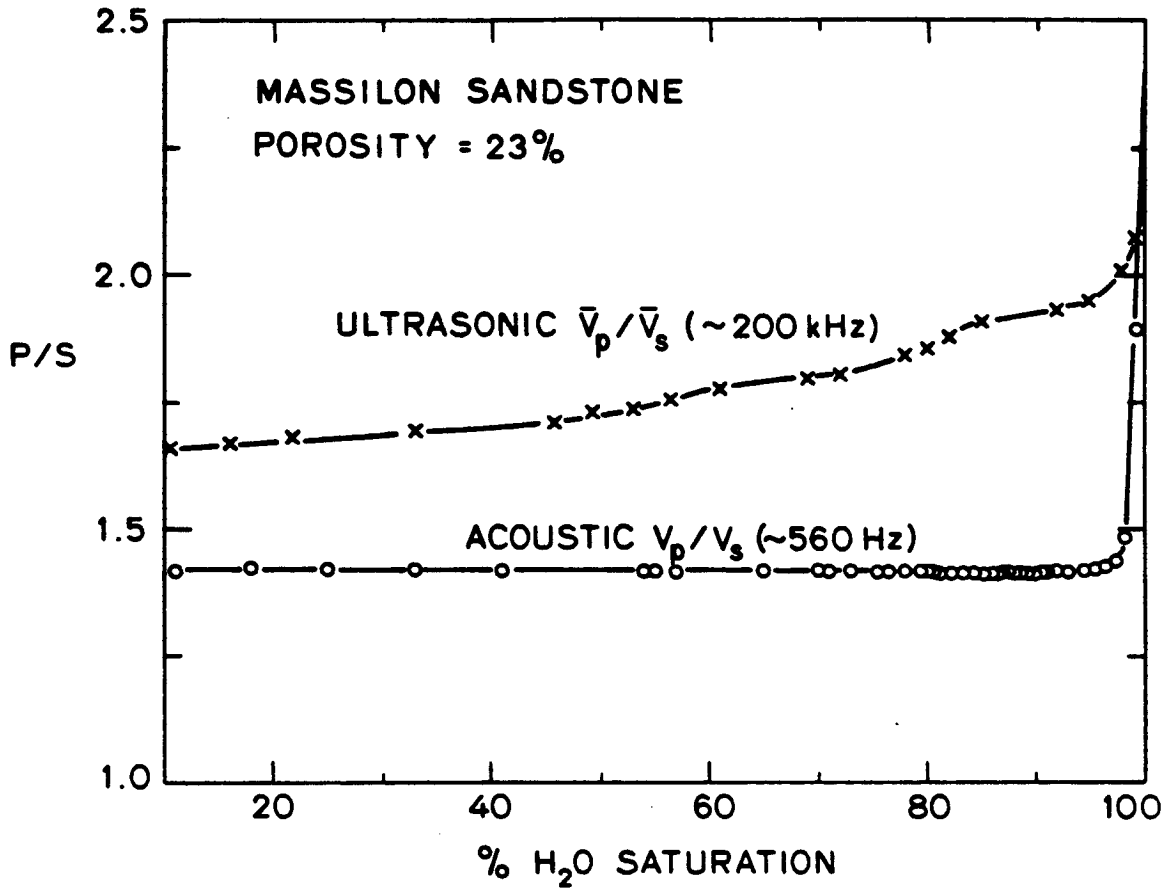

Fig. 29. Comparison of ultrasonic $\bar{V}_p/\bar{V}_s$ and acoustic V_p/V_s vs. % water saturation in Massilon sandstone.

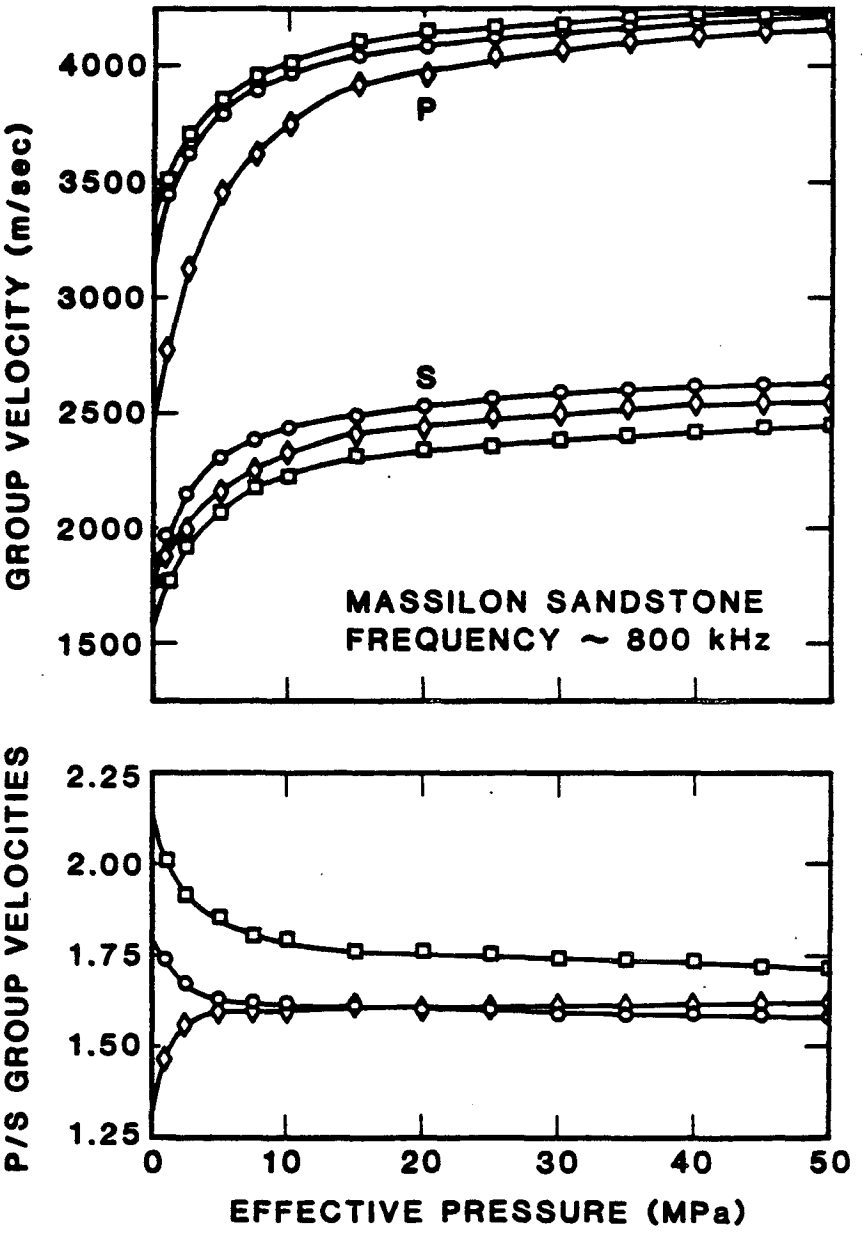

Fig. 30. Ultrasonic $\overline{V}_p$, $\overline{V}_s$, and $\overline{V}_p/\overline{V}_s$ vs. effective pressure in Massilon sandstone when dry (◇), 70% partially water saturated (○), and fully water saturated (□).

which shows V_p and V_s vs. S_w at 550 Hz is risky. The comparison is better made by the P/S ratios as shown in figure 29. Figure 30 may be compared to figure 5 in Winkler and Nur (1982), and the Massilon data in figures 11 and 12 to figure 15 in Winkler and Nur (1982). These comparisons should also be made with extreme caution. However, we may say without qualification that the 500 Hz data are well described by the Biot-Gassmann relations (i.e. completely relaxed); while the ~500 kHz data appear again to be unrelaxed. In short, these observations suggest considerable dispersion between ~500 Hz and ~500 kHz in fully and partially saturated Massilon sandstone.

7. CONCLUSIONS

To conclude, we find the following in tight sandstones:

i) Fine (<10μm), low aspect ratio pores form both the pore neighborhood and pore network connectivities, and dominate local and global compliances.

ii) At borehole frequencies, V_p and V_p/V_s are sensitive to partial gas saturation. More precisely, V_p and V_p/V_s drop 20% as S_g goes grom 0 to 0.1.

iii) At 3-6 kHz, Q_p and Q_s are very sensitive to partial gas saturation. $1000/Q_s$ is 189 at full saturation and declines linearly and steeply with decreasing S_w. $1000/Q_p$ is less than 100 at full saturation, abruptly jumps to a peak, ~200, at $S_w = 0.8$, and then declines linearly with S_w, emulating $1000/Q_s$.

iv) Borehole measurement of V_p, V_s, Q_p and Q_s may delineate the range of partial gas saturation. Further laboratory measurements are required under pressure.

v) Ultrasonic pulse transmission measurements yield unrelaxed group velocities in consolidated sandstones. In predicting velocities at borehole and seismic frequencies, such measurements, if uncorrected for dispersion, will lead not only to significant quantitative errors, say roughly on the order of 10-15%, but exhibit unrelaxed qualitative relationships which may be strongly misleading.

vi) These results in low ϕ sandstones, when compared to results in high ϕ sandstones (Murphy, 1982a), tend to refute the significance of Biot's (1956) inertial coupling mechanism in the acoustic frequency range and support frame relaxation involving local water flow.

ACKNOWLEDGEMENTS

This paper constitutes the fourth chapter of W. Murphy's Ph.D. Dissertation at Stanford University. Joel Walls stimulated our interest in tight sandstones. Russell Gordon helped in preparing samples and in various other ways. Ken Winkler reluctantly reviewed the long manuscript. Stephanie Williams and Terri Ramey drafted most of the figures. We are grateful to Canadian Hunter Exploration Ltd., Schlumberger-Doll Research, and DOE Bartlesville for providing the Spirit River, Cotton Valley, and Fort Union samples, respectively. W. Murphy was supported as a graduate student by the Office of Naval Research under contract N00014-77-C-0390 with the Marine Geology and Geophysics Program. Aspects of the research were funded by the Department of Energy under contract DE-AS19-81BC10498 with the Bartlesville Energy Technology Center.

WORKS CITED

Biot, M.A., 1956, Theory of propagation of elastic waves in a fluid-saturated porous solid, I. Low Frequency range, J. Acoust. Soc. Am. 28, 168-178. Theory of propagation of elastic waves in a fluid-saturated porous solid, II. High frequency range, J. Acoust. Soc. Am. 28, 171-191.

Brennan, B.J., and Smylie, D.E., 1981, Linear viscoelasticity and dispersion in seismic wave propagation, Rev. Geophys. Space Phys. 19, 233-246.

Brown, R.J.S., and Korringa, J., 1975, On the dependence of the elastic properties of a porous rock on the compressibility of the pore fluid, Geophys. 40, 608-616.

Defay, R., and Prigogine, I., 1966, Surface tension and absorption, Longmans Green, London.

Domenico, S.N., 1974, Effects of water saturation of sand reservoirs encased in shales, Geophys. 29, 759-769.

Domenico, S.N., 1976, Effect of brine-gas-mixture on velocity in an unconsolidated sand reservoir, Geophys. 41, 882-894.

Domenico, S.N., 1977, Elastic properties of unconsolidated sand reservoirs, Geophys. 42, 1339-1368.

Elliott, S.E., and Wiley, B.F., 1975, Compressional velocities of partially saturated unconsolidated sand, Geophys. 40, 949-954.

Fatt, I., 1953, The effect of overburden pressure on relative permeability, J. Pet. Tech. 5, technical note 194, 15-15.

Frisillo, A.L., and Stewart, T.J., 1980, Effect of partial gas/brine saturation on ultrasonic absorption in sandstone, J. Geophys. Res. 85, 5209-5211.

Gardner, G.H.F., Wyllie, M.R.L., and Droschak, D.M., 1964, Effects of pressure and fluid saturation on the attenuation of elastic waves in sands, J. Pet. Tech. 16, 189-198.

Gassmann, F., 1951, Ueber die elastizitat poroser medieu, Vierteljahrsschr. Naturforsch. Ges. Zuerich, Heft I.

Geertsma, J., and Smit, D.C., 1961, Some aspects of wave propagation in fluid saturated porous solids, Geophys. 26, 169-181.

Gregory, A.R., 1976, Fluid saturation effects on dynamic elastic properties of sedimentary rocks, Geophys. 41, 895-921.

Kjartansson, E. and Nur, A., 1982, Attenuation due to thermal relaxation in porous rocks, Geophys, in press.

Korringa, J., and Brown, R.J.S., 1979, Discussion on "Elastic properties of unconsolidated porous sand reservoirs" (S.N. Domenico, author), Geophys. 44, 830-831.

Mavko, G.M., and Nur, A., 1979, The effect of nonelliptical cracks on the compressibility of rocks, J. Geophys. Res. 83, 4459-4468.

Morse, P.M., and Ingard, K.V., 1968, Theoretical Acoustics, McGraw Hill, New York, 927 p.

Murphy, W.F., 1982a, Effects of partial water saturation on attenuation in Massilon sandstone and Vycor porous glass, J. Acoust. Soc. Am. 71, Chapter III in this volume, in press.

Murphy, W.F., 1982b, Grain contacts, disordered microstructure, and dynamic frame moduli in granular sediments, J. Geophys. Res., Chapter II in this volume, subm. July.

Murphy, W.F., 1982c, Micromechanics of acoustic dissipation in fully and partially water saturated granular sedimentary materials, J. Geophys. Res., Chapter V in this volume, subm. August.

Murphy, W.F., and Walls, J.D., 1981, Diagenesis of marine sands to tight gas sands: effects on acoustic and hydraulic properties, Bull. Am. Assoc. Petr. Geol. 65, 963.

Nur, A., and Simmons, G., 1969, The effect of saturation on velocity in low porosity rocks, Earth Planet. Sci. Lett. 7, 183-193.

Ostrander, A., 1981, Direct hydrocarbon detection, Visiting Lecture at Dept. Geophys., Stanford Univ.

Palmer, I.D., and Traviolia, M.L., 1980, Attenuation by squirt flow in undersaturated sands, Geophys. 45, 1780-1792.

Peselnick, L. and Outerbridge, W.F., 1961, Internal friction in shear and shear modulus of Solenhofen limestone over a frequency range of 10^7 cycles per second, J. Geophys. Res. 66, 581-588.

Spencer, J.W., 1981, Stress relaxations at low frequencies in fluid saturated rocks: attenuation and modulus dispersion, J. Geophys. Res. 86, 1803-1812.

Stoll, R.D., 1979, Experimental studies of attenuation in sediments, J. Acoust. Soc. Am. 66, 1152-1160.

Strick, E., 1981, Application of the general anelastic model in water saturated rock, Geophys., subm. June.

Tatham, R.H., 1982, V_p/V_s and lithology, Geophys. 47, 336-344.

Walls, J., 1981, Tight gas sands: permeability, pore structure, and clay, Proc. 1981 SPE/DOE Low Permeability Symposium, May 27-29, Denver, Colorado, 399-407.

Winkler, K.W., and Nur, A., 1982, Seismic attenuation: effects of pore fluids and frictional sliding, Geophys. 47, 1-15.

Zener, C., 1948, Elasticity and Anelasticity in Metals, Univ. Chicago Press, Chicago, Ill., 170 p.

ADDITIONAL REFERENCES

DeVilbiss, J.W., 1981, Wave dispersion and absorption in partially saturated rocks, Ph.D. Dissertation, Stanford Univ., 128 p.

King, M.S., 1966, Wave velocities in rocks as a function of changes in overburden pressure and pore fluid saturants, Geophys. 31, 50-73.

Jones, T., 1978, Some compressional and shear velocities in Berea, Massilon and St. Peter sandstones, Stanford Rock Physics Project 5, 165-183.

Clark, V.A., Tittmann, B.R., and Spencer, T.W., 1980, Effect of volatiles on attenuation (Q^{-1}) and velocity in sedimentary rocks, J. Geophys. Res. 85, 5190-5199.

Tosaya, C. and Nur, A., 1981, Effects of diagenesis and clays on compressional velocities in rocks, Geophys. Res. Lett. 9, 5-8.

Wyllie, M.R.L., Gregory, A.R., and Gardner, G.H.F., 1958, Elastic wave velocities in heterogeneous and porous media, Gephys. 21, 41-70.

Appendix

Comparison to the Acoustic Properties of Granites

Sierra White is a 0.8% porosity granite. It is composed of a sparse population of low aspect ratio cracks embedded in a composite of elastic graing (figure 1). As far as the class of granular sedimentary materials goes, granite may be envisioned as the microstructural antithesis of unconsolidated glass beads or as the ultimate microstructural extension of tight sands. In either case, we have made a series of measurements on Sierra White granite similar to those in Murphy and Nur (1982). Figures 2 and 3 give phase velocities and 1000/Q, respectively, versus water saturation at frequencies from 1 to 2 kHz. Figure 4 demonstrates a small but significant dispersion in extensional phase velocity across frequencies from 2 to 7 kHz. Figure 5 shows the variation in $1000/Q_e$ with frequency from 2 to 13 kHz. In figure 6, group velocities measured at ~200 kHz are plotted against water saturation. An finally, figure 7 presents group velocities measured at ~800 kHz versus effective pressure under various states of water saturation.

Works Cited

Murphy, W.F. and A. Nur, On velocities and attenuation as a measure of partial water saturation in tight sandstones at borehole and ultrasonic frequencies, Geophysics (subm. July, 1982). Chapter IV in this volume.

Additional References

DeVilbiss, J.W., Wave Dispersion and Absorption in Partially Saturated Rocks, Ph.D. Dissertation, Stanford University, 1980, 128p.

Jones, T., 1978 (unpublished measurements).

Nur, A. and G. Simmons, The effect of saturation on velocity in low porosity rocks, Earth Plan. Sci. Lett. 7, 183-193, 1969.

Spencer, J.W., Stress relaxations at low frequencies in fluid saturated rocks, J. Geophys. Res. 86, 1803-1812, 1981.

Stierman, D.J. and R.L. Kovach, An in situ velocity study, the Stone Canyon well, J. Geophys. Res. 84, 671-678, 1979.

Winkler, K.W., 1979 (unpublished measurements).

Fig. 1. SEM photomicrograph of Sierra White granite. The scale in microns is given by the bar at the base of the photomicrograph.

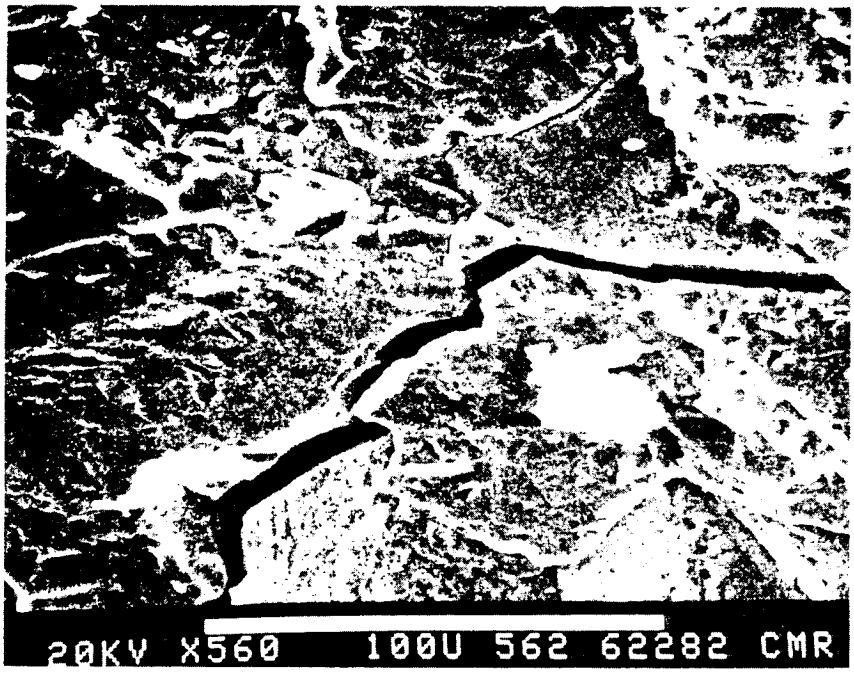
20KV X560 100U 562 62282 CMR

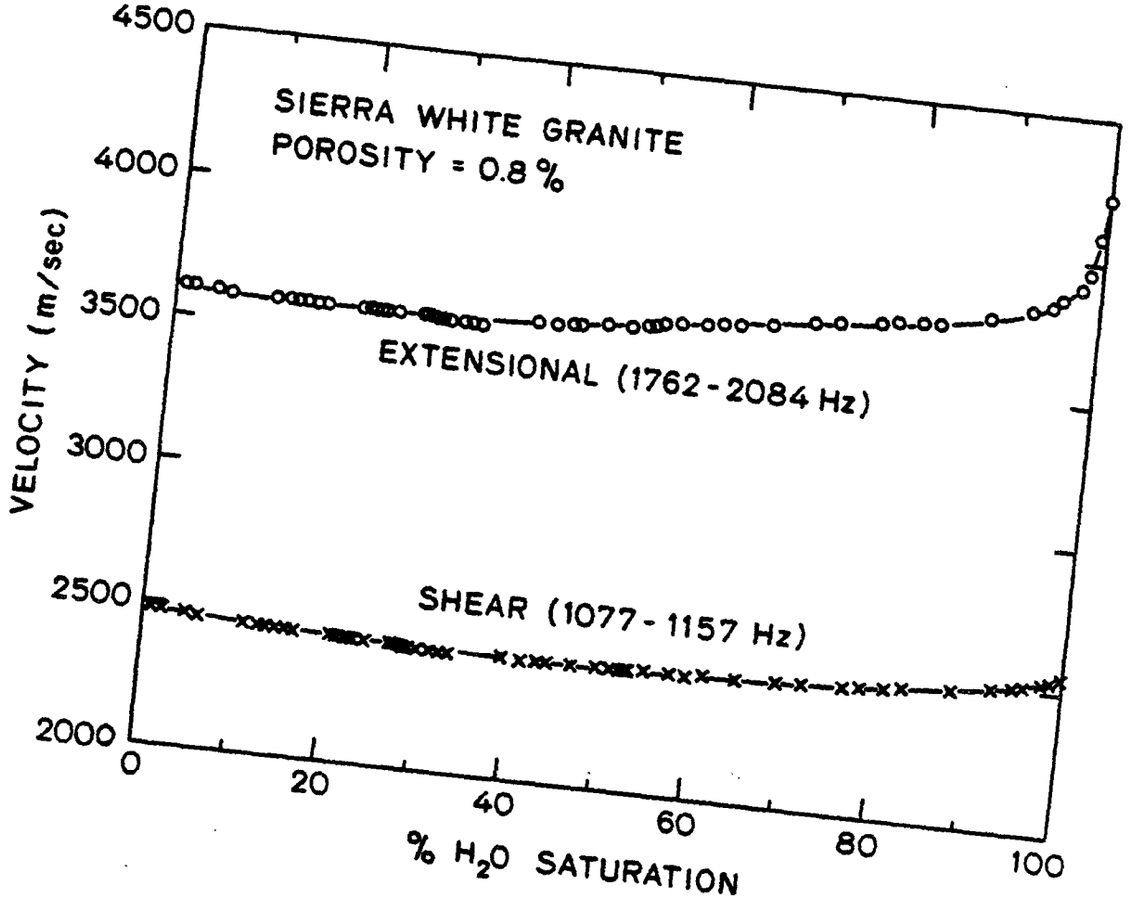

Fig. 2. V_e and V_s *vs.* % water saturation in Sierra White granite at ~2 kHz.

Fig. 3. $1000/Q_e$ and $1000/Q_s$ vs. water saturation in Sierra White granite at 2 kHz:

a) 22.5°C ,

b) 18-20°C.

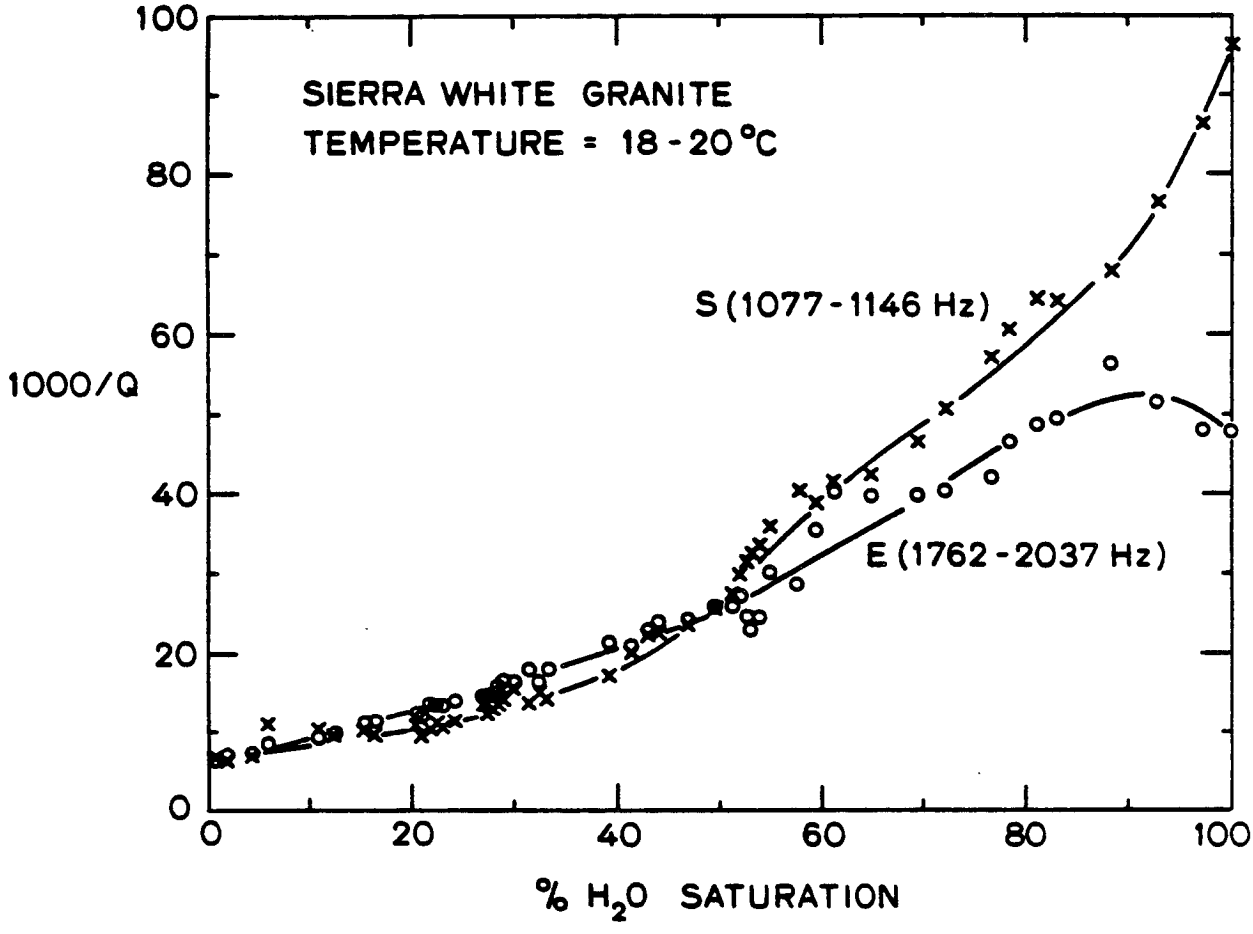
SIERRA WHITE GRANITE
TEMPERATURE = 18 - 20 °C
S (1077 - 1146 Hz)
E (1762 - 2037 Hz)
1000/Q
% H_2O SATURATION
0
20
40
60
80
100

Figure 3a.

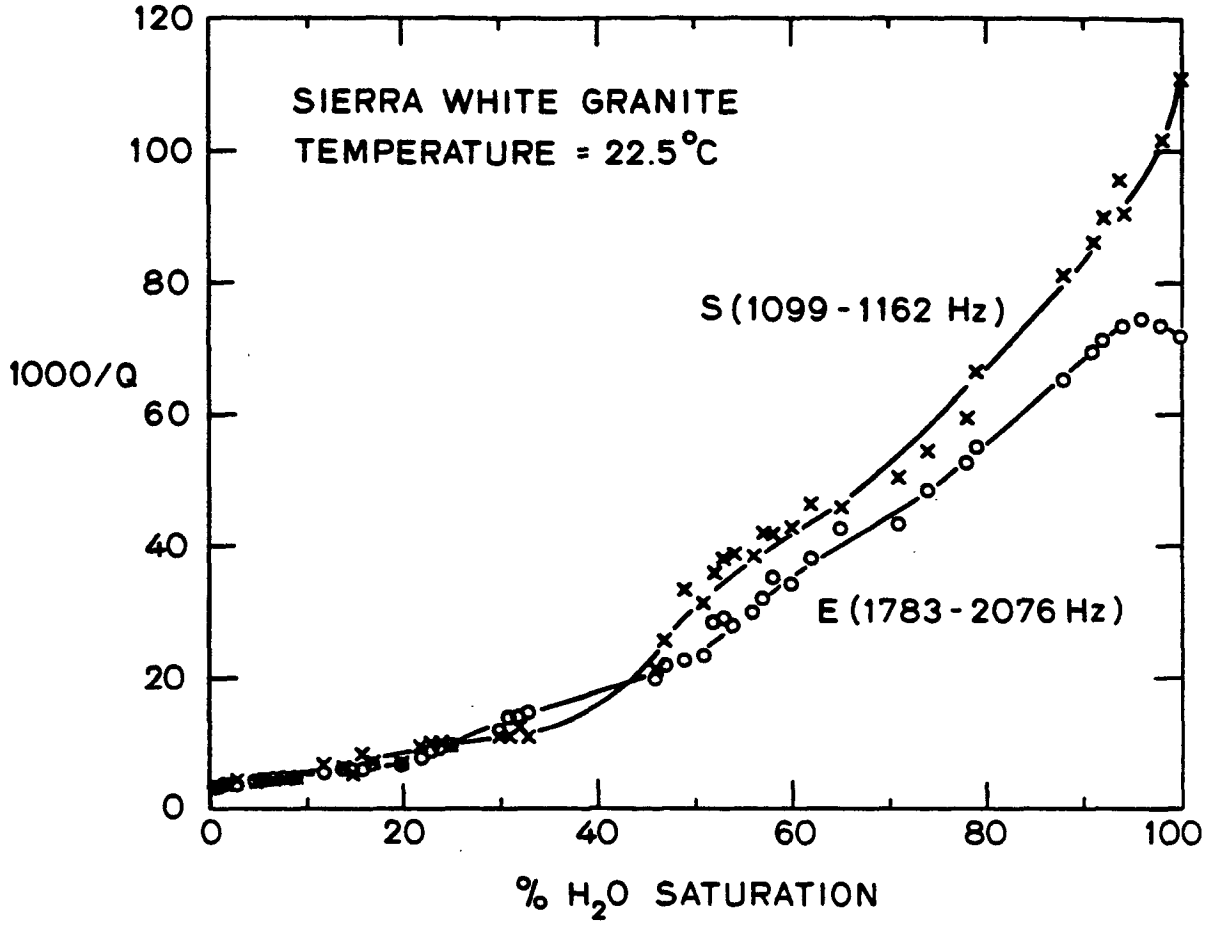
SIERRA WHITE GRANITE
TEMPERATURE = 22.5°C
S (1099 - 1162 Hz)
E (1783 - 2076 Hz)
1000/Q
% H2O SATURATION
0
20
40
60
80
100
120

Figure 3b.

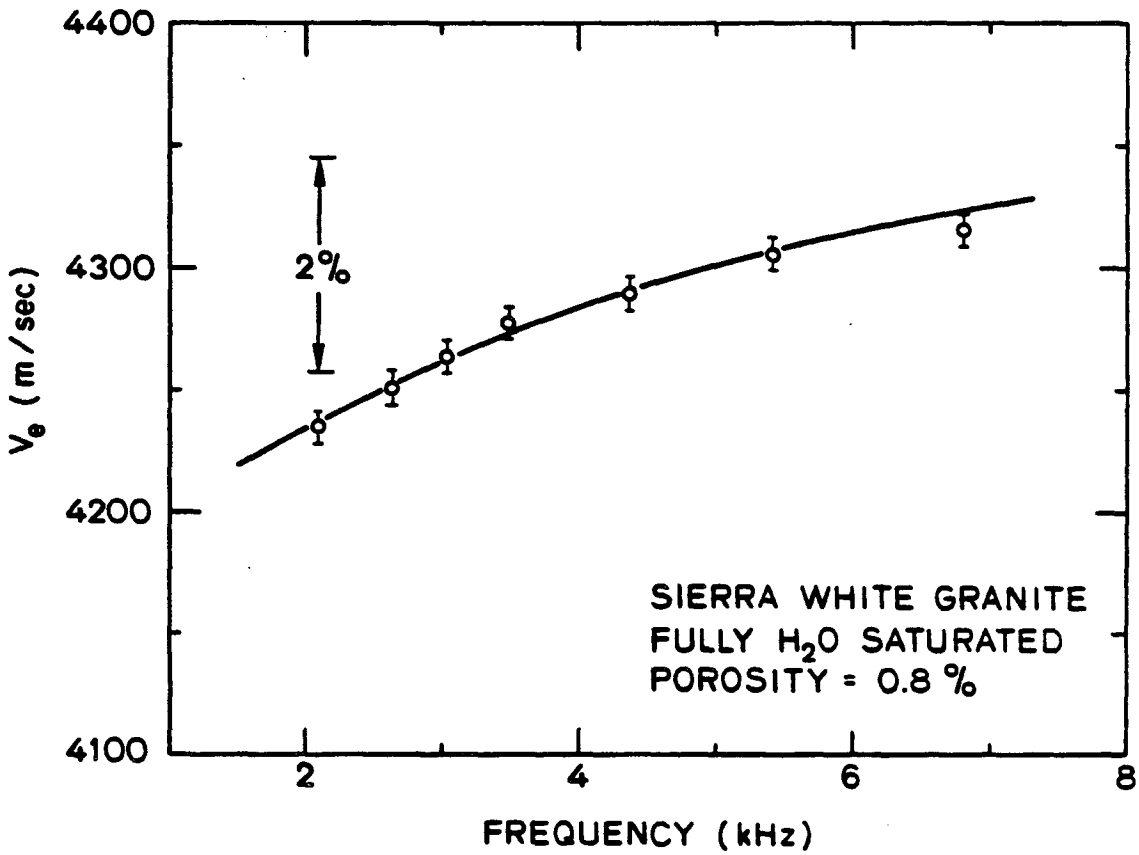

Fig. 4. V_e vs. frequency in fully water saturated Sierra White granite.

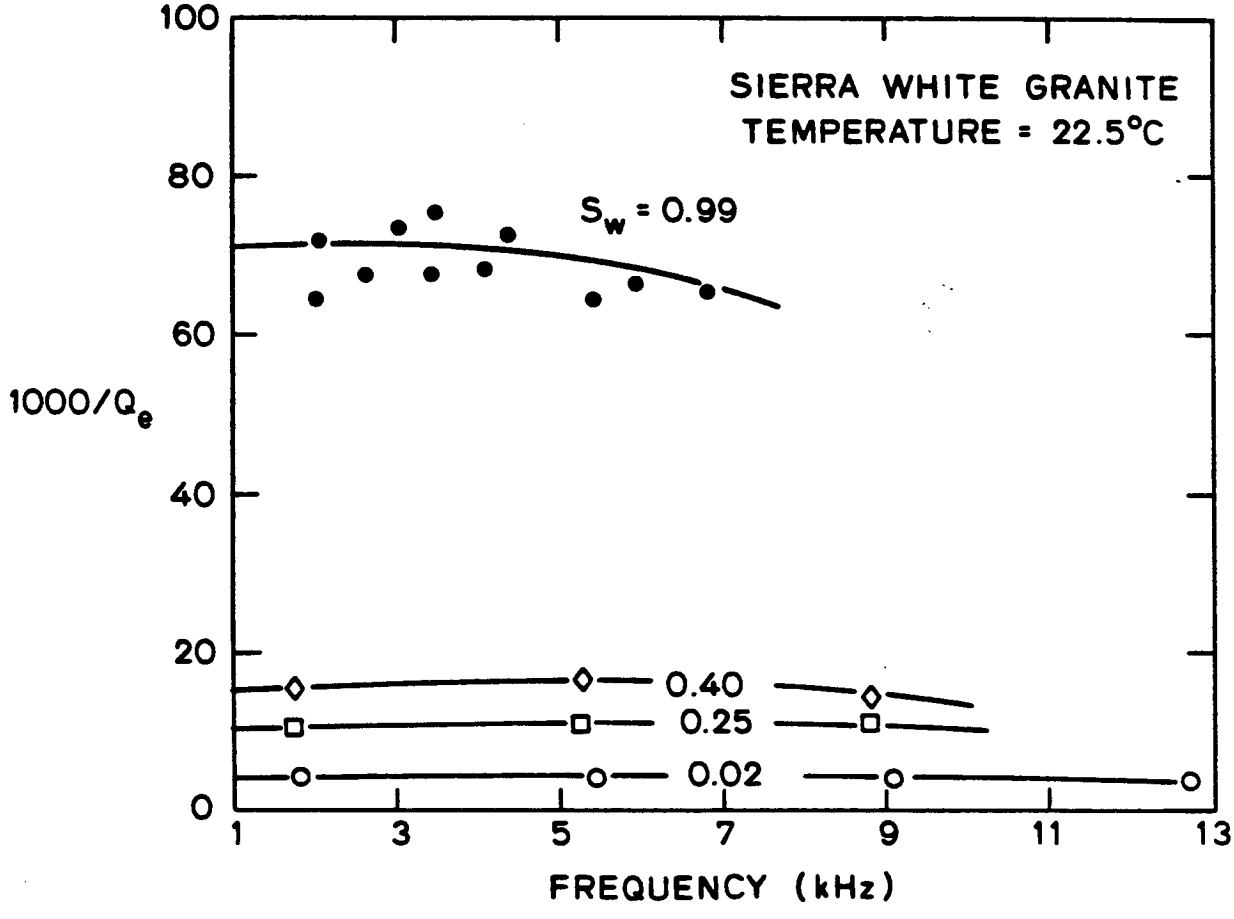

Fig. 5. $1000/Q_e$ vs. frequency in a 99% water saturated Sierra White granite.

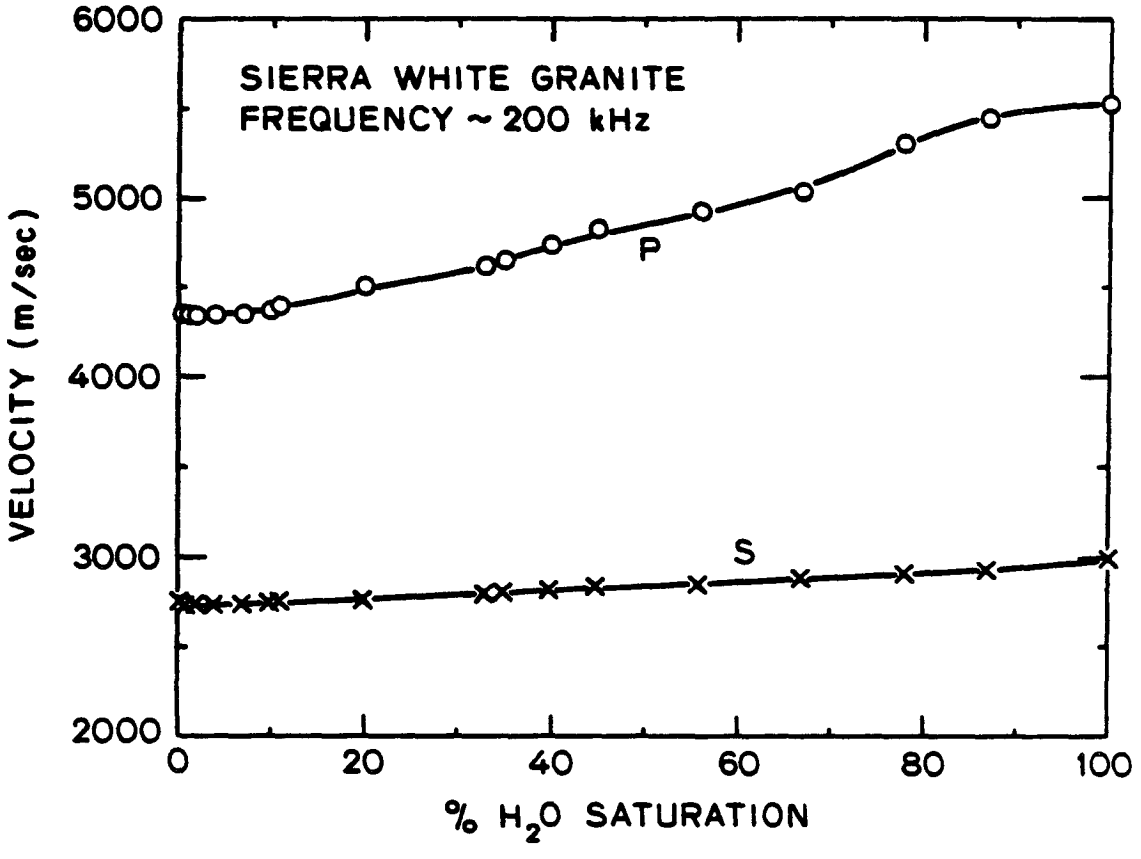

Fig. 6. Ultrasonic $\overline{V}_p$ and $\overline{V}_s$ vs. % water saturation (S_w = 1.0 - 0) in Sierra White granite at a uniaxial pressure of 0.1 MPa.

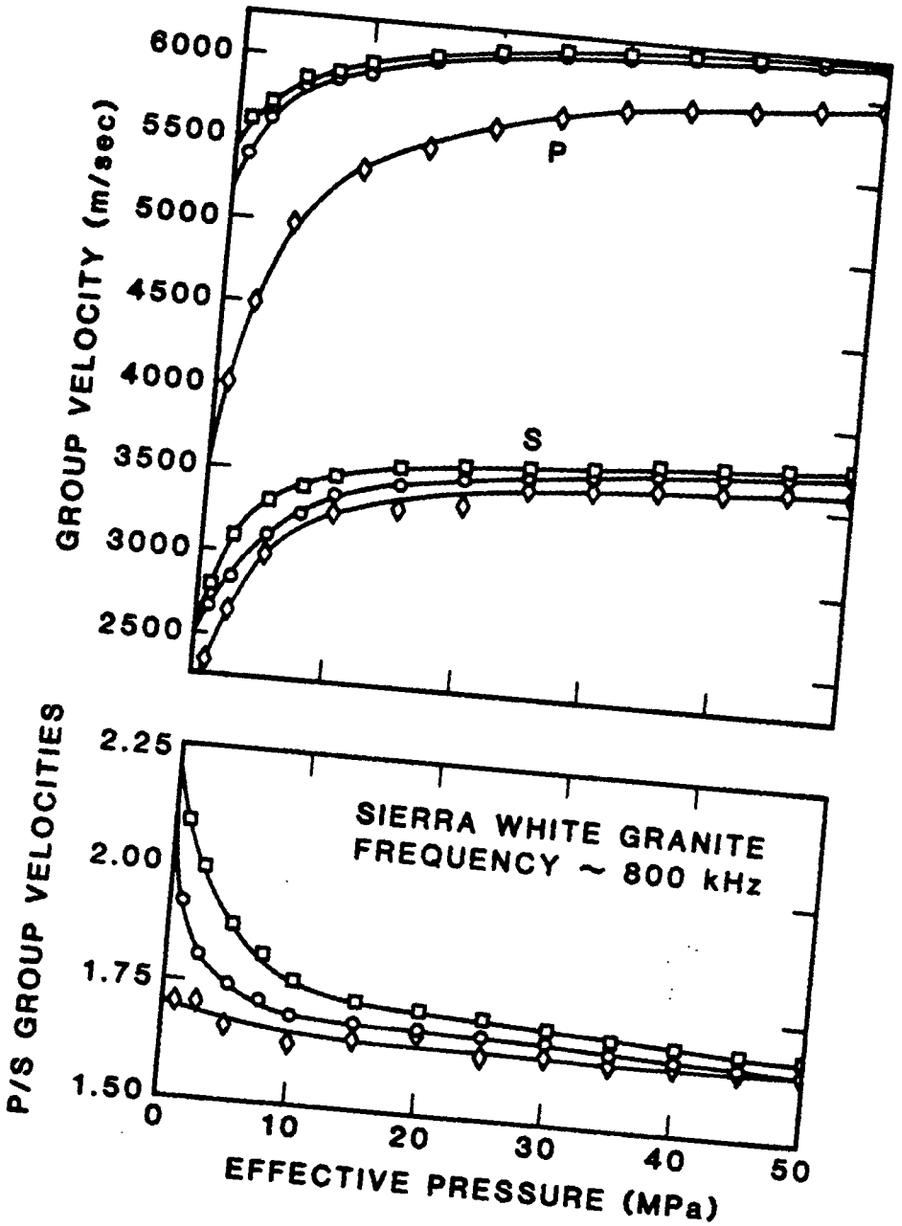

Fig. 7. Ultrasonic P and S group velocities and P/S vs. effective pressure at three states of water saturation: dry (◇), 70% partially saturated (○) , and fully saturated (□).

Chapter V

Micromechanics of Acoustic Dissipation in Fully and Partially Water Saturated, Granular Sedimentary Materials*

Contents

1. INTRODUCTION

The response to small stress waves is the principle measure used in geophysics to study material bodies in the earth's crust. The class of granular sedimentary materials, which includes sands and sandstones, holds considerable interest in geology and engineering (fig. 1). Several particular problems in the acoustic properties of

*Parts to be submitted to the Journal of Geophysical Research and Journal of the Acoustical Society of America in July or August, 1982.

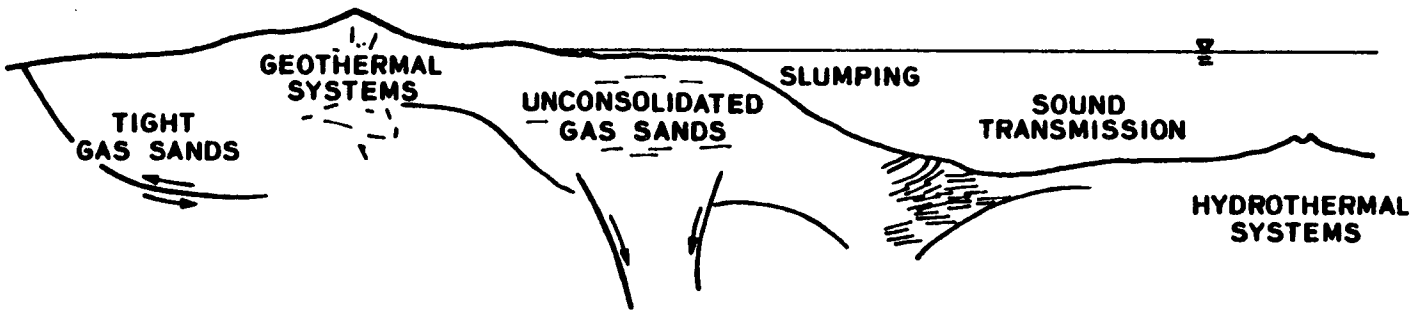

1. MARINE ACOUSTICS
2. SEISMIC EXPLORATION
3. GEOTECHNICAL PREDICTION
4. RESERVOIR ENGINEERING

Fig. 1. Practical applications of geoacoustics.

these materials have been solved recently (Winkler et al., 1979; Spencer, 1981; Murphy, 1982a,b; Murphy and Nur, 1982a). This paper attempts to explain how the granular microstructure and pore water saturation control wave attenuation and velocity dispersion. We are primarily interested in frequency range from 10 to 10^6 Hz.

Our experiments (Murphy, 1982a; Murphy and Nur, 1982a) have shown that in the acoustic frequency range (fig. 2), compressional and shear wave velocities and specific attenuation are strongly dependent on water saturation and frequency. Maurice Biot (1956) has proposed a theory for acoustic wave propagation which has been experimentally corroborated in *simple* porous media such as sintered glass beads (Plona, 1980; Plona and Johnson, 1980). Yet Biot's theory is inconsistent with our observations on sands and sandstones in the acoustic and low ultrasonic frequency ranges. Biot's theory fails because it neglects the *granular* nature of the sedimentary materials.

I wish to propose a model which relates the micromechanics at the grain contacts to linear viscoelastic frame moduli. The frame moduli describe the continuum stiffness and relaxation of the granular frame, and are strongly dependent on frequency and water saturation. When we embed the micromechanical model in general equations for wave propagation in porous media (Biot, 1962; Burridge and Keller, 1981), specific predictions are derived. The predictions test very well against our recent experimental results. Moreover, the theory provides a coherent explanation of the seemingly disparate work of Gregory (1976), Winkler et al. (1979), Pandit and King (1979), Stoll (1979), Plona (1980), Clark et al. (1980), Spencer (1981), Winkler and Nur (1982), and Winkler and Plona (1982).

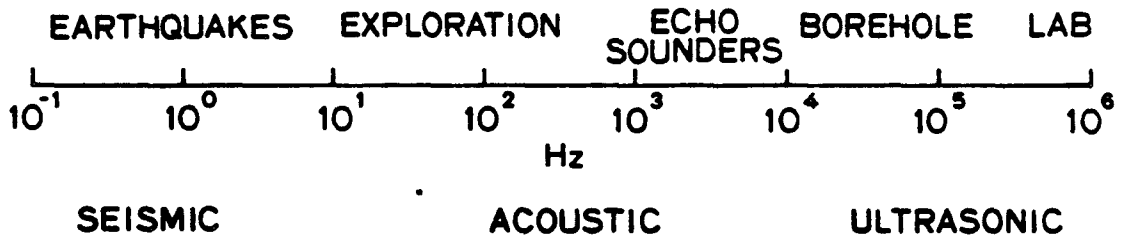

Fig. 2. Spectrum of geoacoustic interest.

The model is by no means fully developed. However, I think that we have laid much of the foundation and correctly identified the specific microprocesses involved.

2. REVIEW OF PREVIOUSLY PROPOSED MECHANISMS IN LIGHT OF RECENT EXPERIMENTAL OBSERVATIONS

Sharp relaxations centered roughly between 1 and 10 kHz (fig. 3) are observed in sandstones (Massillon, Navajo, Schuler-Cotton Valley, and Spirit River), granites (Sierra White and Oklahoma), and Vycor porous glass. Q^{-1} is found to depend strongly on water saturation. Moduli are relaxed below 100 Hz and unrelaxed above 100 kHz (fig. 3). None of the following mechanisms can coherently explain these observations.

Scattering

When the wavelength approaches the size of the grains or pores, scattering will occur (Devaney et al., 1982). The center frequency, f_ψ, of scattering by the pores is given by

$$f_\psi = \frac{3}{R}\left(\frac{M}{\rho_c}\right)^{1/2} \qquad (1)$$

where R is the radius of the grains, ρ_c is the radius of the grains, ρ_c is the composite density, and M is the wave modulus. For our Massillon, Fort Union, Cotton Valley, and Spirit River samples, f_ψ is above 5 MHz (fig. 3). A small negative dispersion, indicative of scattering, has been measured in brine saturated Massillon and Boise sandstones at frequencies above 500 kHz (Winkler and Plona, 1982). These particular Massillon and Boise samples had grain diameters of ~300 and ~200 μm, respectively. Scattering is not important in sandstones below 100 kHz.

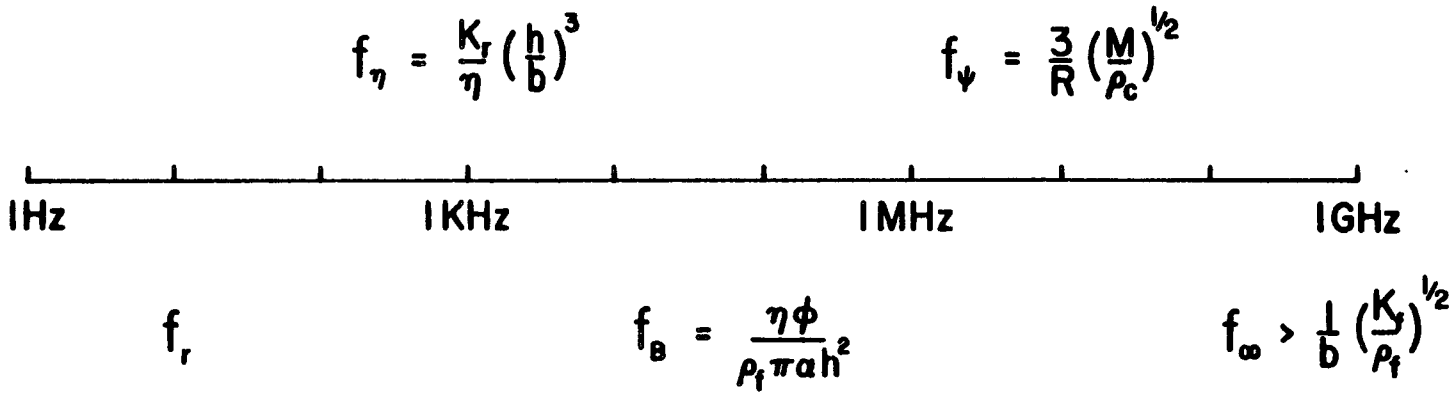

Fig. 3. Specification of critical frequencies for various mechanisms. (See text for explanation.)

Frictional Grain Sliding

Frictional grain sliding is restricted to situations in which strains are greater than 10^{-6}; they are not important in far-field seismic exploration, echo sounding, or borehole sonic logs (Winkler et al., 1979; Mavko, 1979; Murphy, 1982).

Thermoelasticity

Thermal relaxation has been proposed as an attenuation mechanism by Kjartansson and Nur (1982). The center frequency, f_T, of such a relaxation is given by

$$f_T = \frac{h^2}{D} \quad , \tag{2}$$

where h is the half width of the pore and D is the thermal diffusivity of the composite. f_T is roughly 10 kHz for Massillon sandstone. This is indeed very close to the observed 3-5 kHz center frequency (Murphy, 1982a). However, thermal relaxation is diffusion controlled and thus predicted to be quite broad (see fig. 5.4 in Kjartansson, 1979). The observed relaxations in Massillon sandstone (Murphy, 1982a) and Navajo sandstone (Spencer, 1981) are very narrow, nearly single Debye or Zener peaks. The predicted dependence on water saturation is also inconsistent with our observations. Furthermore, Q^{-1} at 1 kHz has been observed to decrease with increasing temperature (Jones, personal communication). This result directly contradicts Kjartansson's model. Thermal relaxation is irrelevant in sands and sandstones at low temperatures and pressures.

Ionic Relaxation Absorption

An important mechanism for low frequency sound absorption in the oceans (Yeager et al., 1973; Fischer and Simmons, 1975; Simmons, 1975; Schulkin and March, 1978) is the two step reaction

$$B(OH)_3 + (OH)^- \rightleftarrows B(OH)_e(OH)^- \rightleftarrows B(OH)_4^- \quad . \tag{3}$$

Boric acid reacts with hydroxyl ions to form borate ions. This reaction is of interest because we have measured a strong dependence of Q^{-1} on water saturation and frequency in Vycor porous glass (Murphy, 1982a). Vycor consists of 4% boric acid which is concentrated near the pore surface. The center frequency of the ionic relaxation is roughly between 1 to 10 kHz. However, the process is diffusion controlled, and the predicted magnitude of the losses is too small.

Dislocations

Mason (1969, 1971a,b, 1978) has proposed that dislocations move in the grain surfaces as a response to acoustic loading. Dislocations are not activated in quartz at low temperatures and pressures (Griggs, 1969).

Vibrational Relaxation in the Water-Air Mixture

Zuckerwar and Griffin (1981) have measured the absorption of sound in N_2 as a function of relative humidity. The losses are too small to account for those in granular sedimentary materials.

Biot's Solid-Fluid Coupling

Biot's solid-fluid coupling mechanism, which will be discussed in detail in section 4 and 6, implies a sharp peak in Q^{-1} centered at a frequency, f_B , given by

$$f_B = \frac{\eta}{\rho_f h^2} \tag{4}$$

where η is the viscosity of the fluid and ρ_f is the density of the fluid. For Massillon and Navajo sandstones, f_B, is above 100 kHz (fig. 3). The predicted losses in the 1 to 10 kHz range are very small compared to observed losses. f_B is very sensitive to the pore width parameter, h. But, as h goes from ~10 μm in Massillon sandstone to less than 1 μm in Fort Union sandstone or Sierra White granite, the observed peaks shift hardly, if at all. Nor does this model account for the effects of partial water saturation.

Biot's mechanism may be important in the ultrasonic frequency range in certain materials (Plona, 1980; Winkler and Plona, 1982).

"Squirt" (Mavko and Nur, 1979)

Imagine an ordinary laboratory squirt bottle containing some water. Upon squeezing the outside of the bottle, the water discharges as a high Reynold's number jet into an infinite reservoir. This is a process which does not occur during acoustic propagation in sands and sandstones. As we shall later show, Reynolds' numbers are significantly less than 1 in the acoustic frequency range. Moreover, Mavko and Nur (1979) mistakenly formulate the center of the squirt relaxation to be the transition from incompressible to compressible flow in the pore fluid. This choice of fre ncies is in fact an infinite frequency, f_∞. Above f_∞ no flow can occur because the period is too short. The pore fluid behaves as an elastic solid. f_∞ is given by

$$f_\infty > \frac{1}{b} \left(\frac{K_f}{\rho_f} \right)^{1/2} \tag{5}$$

where b is the length of the fluid drop in the contact gap and K_f is the bulk modulus of the fluid. f_∞ approaches 1 GHz in sands and sandstones (fig. 3).

Surface Mechanisms

It has been established beyond doubt that small amounts of water interact with the dry surface of quartz grains, thus reducing the frame moduli and increasing attenuation (Clark et al., 1980; Spencer, 1981; Murphy, 1982a,b; Murphy and Nur, 1982a). However, the physics of the process is still an open question. For example, Spencer (1981) suggests that a surface mechanism controls the sharply peaked relaxation he observes at high water saturations. However, Pandit and King (1979) have shown that Q^{-1} remains independent of frequency as relative humidity increases from 0 to 82%. At a relative humidity of 98%, the data indicates the onset of frequency dependence. 82% relative humidity is equivalent to 5 monolayers of water (Tittmann et al., 1980). The onset of frequency dependence is thus evidently with bulk liquid water and not surface films.

3. THE CONCEPT OF THE MODEL

Sands and sandstones are porous, granular materials. Microstructures vary greatly within the scope of these materials (fig. 4). The resulting differences among their acoustic properties are discussed in Murphy and Nur (1982a). All sands and sandstones however, are distinguished by a common character. They consist of elastic quartz grains in contact, immersed in a viscous pore fluid (fig. 5). The pore fluid in which we are most interested is a binary mixture of water and air. The grains are of course described by bulk and shear moduli, and pore fluid by viscosities and compressibilities.

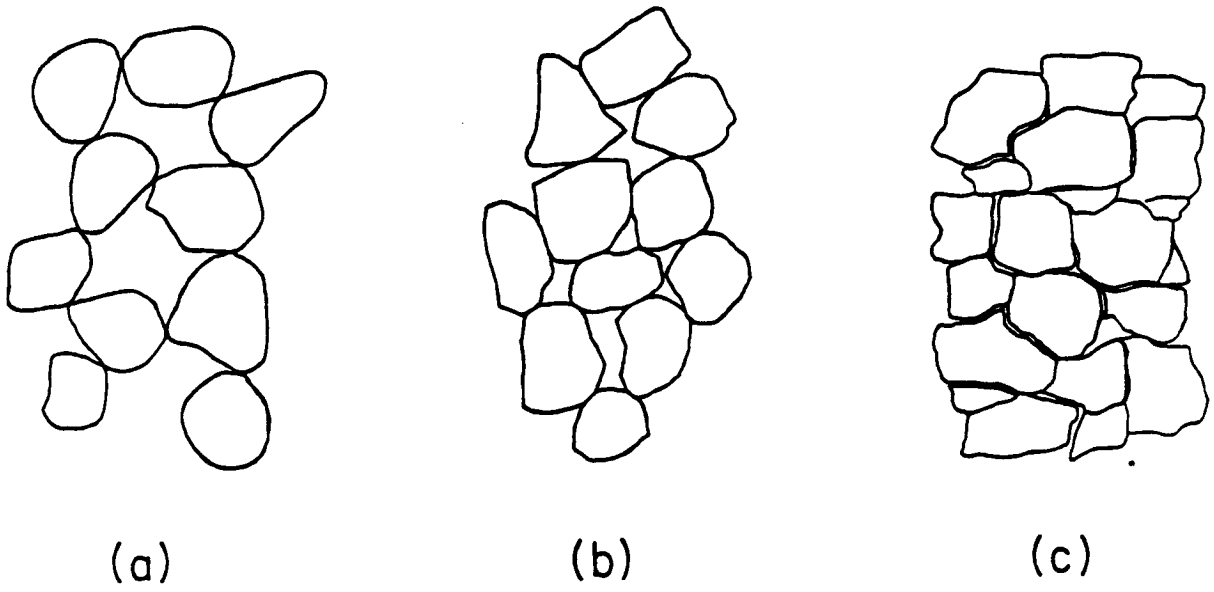

Fig. 4. Sketch of the three extreme types of granular sedimentary materials: (a) unconsolidated sands, (b) high porosity sandstones, and (c) low porosity sandstones.

Fig. 5. Photomicrograph of a Massilon sandstone under partially polarized transmitted light. Porosity is shown by the light blue epoxy. Grain size is roughly 150 μm.

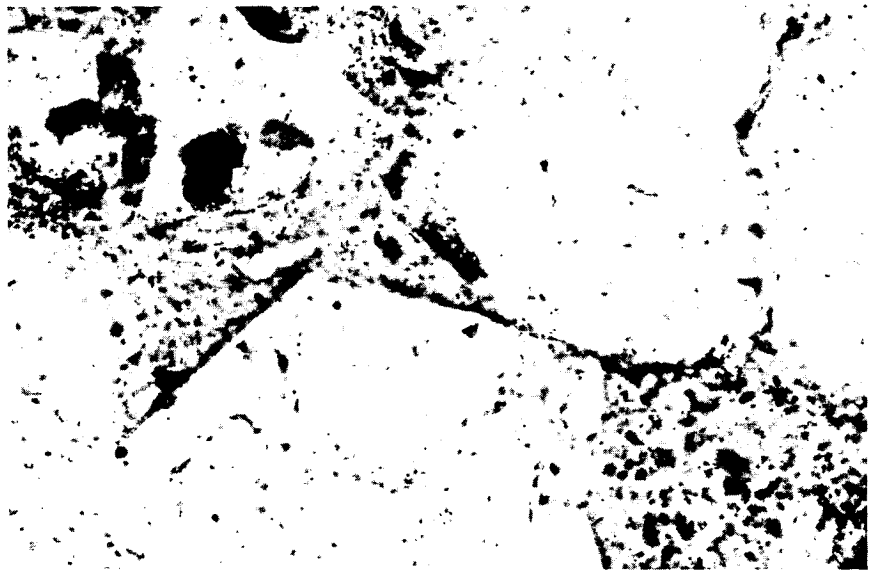

The acoustic behavior however is dominated by the interactions at the contacts. The grain to grain interactions are discussed in Murphy (1982b). The grain/fluid/grain interactions are the cause of attenuation and dispersion. As the grain contacts close and open under oscillatory loading, the water must be squeezed out and sucked back in the thin gaps between grains. These "squeeze films" are coupled to the fluid in the local pore neighborhood. The water also reacts electrochemically with the surface of quartz grains. When exposed to water, the quartz surfaces hydroxylate, and water adsorbs on the hydroxylated or silanol surfaces. An electrical double layer is formed. The double layer may be ~10 nm thick. A layer of silica gel may also be formed.

4. SURFACE ELECTROCHEMISTRY

The three principle effects of mosture or vapor pressure on dry sands and sandstones are the modulus defect, the volume expansion of the granular frame, and the increased constant Q energy losses. Each is a consequence of the electrochemical interactions at the quartz-water interface.

The Structure of the Electrical Double Layer

Consider a freshly broken, clean quartz surface. Such a surface has "dangling bonds". That is to say that silica and oxygen ions lack neighbors on at least one side. These sites are unstable. The surface ions may polarize and relax into a modified structure of lower potential energy. This surface, called the disturbed layer, consists mainly of Si-O-Si bridging or siloxane groups (Parks, 1982). This configuration, for instance, might be the state of a freshly

cleaved quartz surface under a vacuum of 10^{-10} torr at high temperature.

Both dangling bond sites and siloxane groups are chemically reactive. The surface possesses a strong negative charge easily sufficient to drive the ionization of water. Quartz (Gallei and Parks, 1972), amorphous silicas, and glasses hydroxylate upon exposure to water vapor. The hydroxylated surface is dominated by SiOh or silanol groups of various types. The surface retains a reduced yet substantial negative charge. The pore surface of all sands and sandstones are expected to be hydroxylated, probably even those in Tittmann's (1980) experiments (which are subjected to a 10^{-10} torr vacuum and moderate temperatures).

Given a finite vapor pressure or relative humidity, a layer of water adsorbs chemically on the hydroxylated quartz surface. This layer, called the inner Helmholtz layer (fig. 6a) is hydrogen bonded to silanol sites with the bonding strength of 8 to 12 kJ/mole (Parks, 1982). The layer is roughly 1 nm thick. It is structured and possesses low entropy, mobility, and polarizability relative to bulk water.

Increasing vapor pressure deposits a second layer of water, known as the outer Helmholtz layer (fig. 6a). It consists of a surplus of positively charged ions (counterions) and a small deficit of negatively charged ions. The counterions are held by electrostatic attraction. This layer is also about 1 nm in thickness. It is less structured than the inner Helmholtz layer. But it is more structured than the water residing outboard of the Stern double layer (fig. 6a).

Beyond the Stern double layer, we move into the diffuse double layer (fig. 6a). Here, the electrostatic attraction falls off expon-

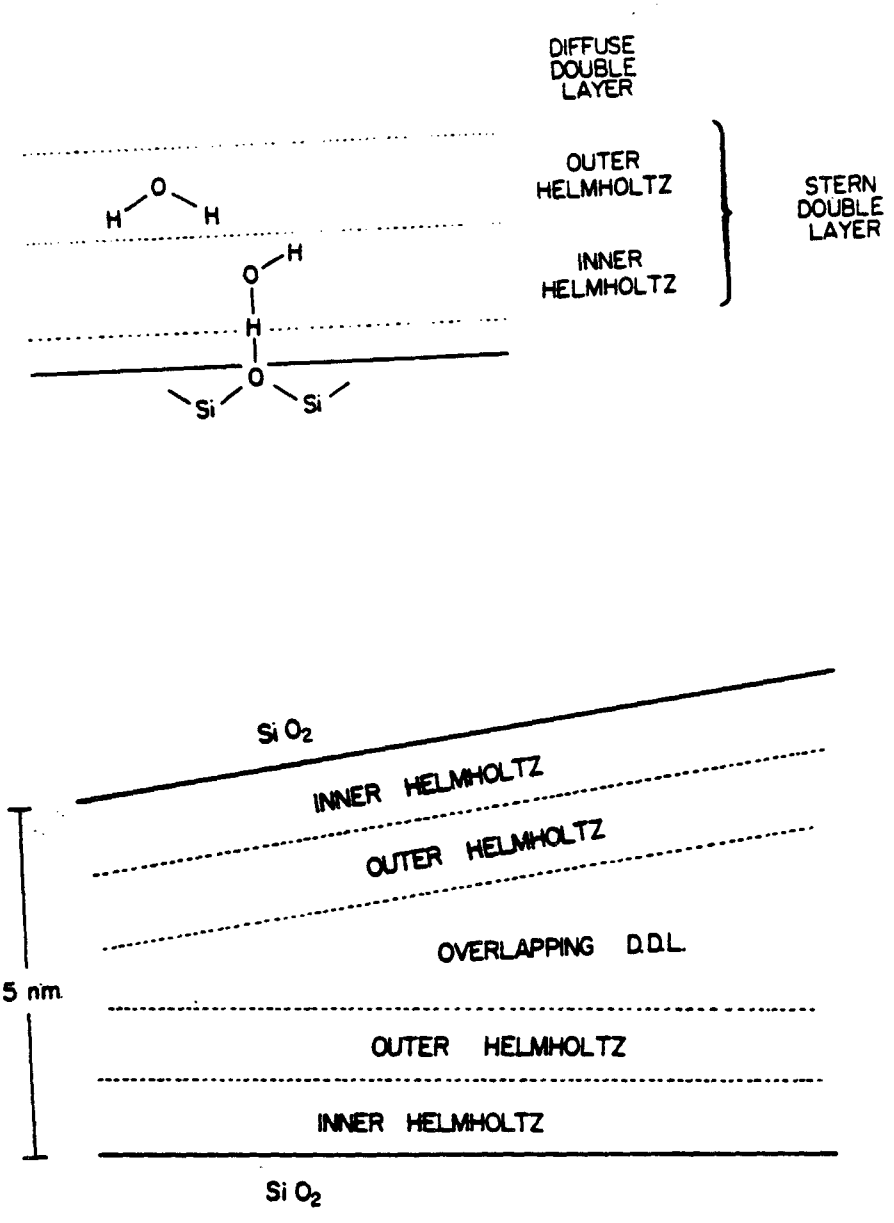

Fig. 6. Sketches of the electrical double layer:
(a) The structure of the double layer, and
(b) the interaction between the double layers on two adjacent grains.

entially, and the properties in this layer asymptotically approach those of bulk water. The combined thickness of Stern and diffuse double layer is roughly 5 to 10 nm.

Surface Energy and Contact Compliance

Surface free energy, γ , is the work required to produce new surface area. Since deformation by acoustic waves involves changes in surface area, γ is an important factor in contact compliance.

The density and strength of the bonds broken in the fracture principally determine the γ of the freshly cleaved quartz surface (Adamson, 1976). Parks (1982) estimates a γ of as much as 2000 mJm^{-2}. Chemical and electrical interaction of any sort whatsoever will reduce γ relative to the clean surface. Hydroxylation, adsorption, and double layer formation progressively and dramatically reduce γ. This reduction is shown schematically in figure 7.

The reduction in γ causes a proportional decline in the contact and frame moduli (c.f. Amberg and McIntosh, 1952; Spencer, 1981). There are three possible molecular mechanisms. First, the van der Waals attraction between grain surfaces is lowered. The contact area decreases, and the granular frame expands as explained in Murphy (1982b). Second, any hydrogen bonds bridging surface hydroxyls between grains are broken. And third, the intrinsic grain moduli, K_s and μ_s , may be lowered.

Clark et al. (1980), Tittmann et al. (1980), and Spencer (1981) have measured the modulus defect as a function of the composition of the fluid. The results may be understood readily with the aid of the following equations.

The reduction of surface energy by specific or chemical adsorption

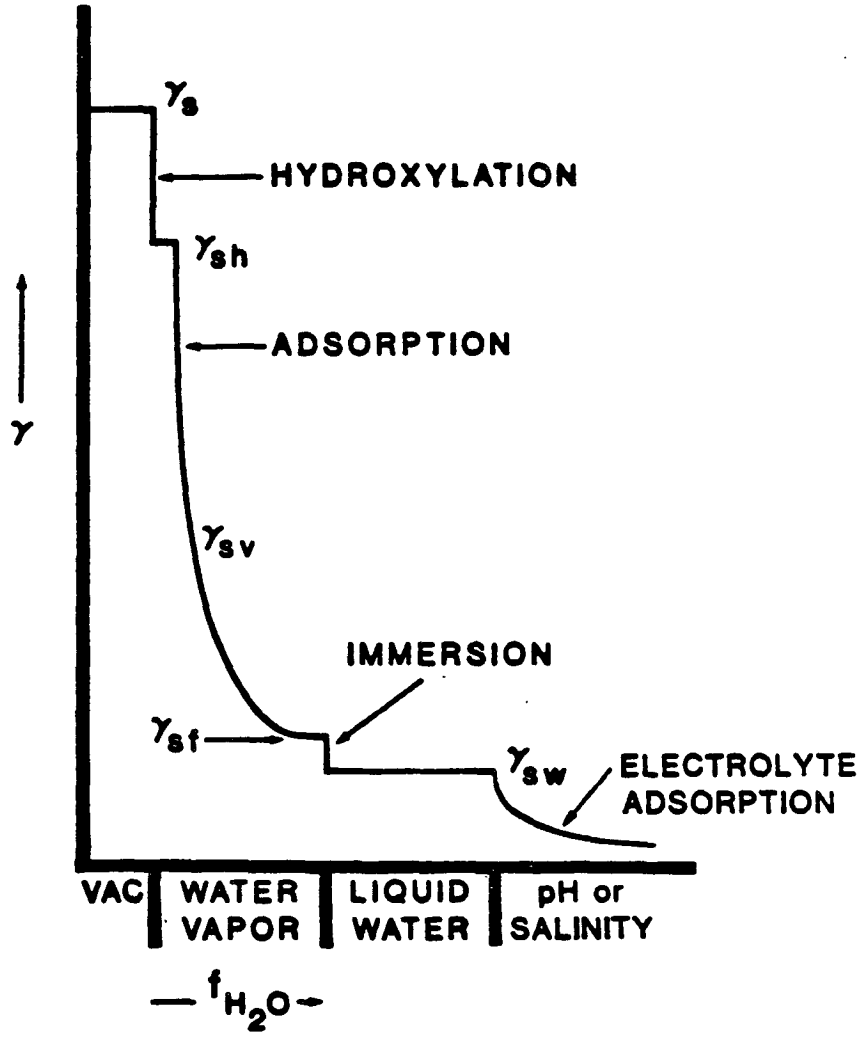

Fig. 7. The surface free energy of quartz as a function of moisture content (after Parks, 1982).

is described by the Gibbs adsorption equation (Hiemez, 1977)

$$d\gamma = -\sum_i \Gamma_i \, d\tilde{\mu}_i \tag{7}$$

where Γ_i is the Gibbs excess adsorption density of species i and $\tilde{\mu}_i$ is the chemical potential of species i. The reduction of surface energy by combined chemical and electrical effects is given by

$$d\gamma = -[\sum_i \Gamma_i \, d\tilde{\tilde{\mu}}_i + \sum_i \Gamma_i \, d\tilde{\tilde{\mu}}_i] \tag{8}$$

where $\tilde{\tilde{\mu}}_i$ is the electrochemical potential of species i which is related to $\tilde{\mu}_i$ as follows

$$\tilde{\tilde{\mu}}_i = \tilde{\mu}_i + z_i e \, \psi \tag{9}$$

where ψ is the potential of the charged species in i, z_i is the valence number of the i^{th} charged species, and e is unit positive charge.

Six fluids were tested. Listed in decreasing order of effect observed on the moduli, they are water, ethanol, methane, n-decane, benzene, and hexane. This is also the order of decreasing change in chemical and electrochemical potential.

This model predicts that the addition of an electrolyte to the water would further reduce the frame moduli.

Constant Q Energy Losses

As the contacts oscillate under acoustic loading, the surface near the contacts is deformed. Hydrogen bonds are broken as the film is squeezed away and drawn back to bonding sites. New sites may arise and disappear or the double layers may overlap and separate (fig. 6b). The relaxations are diffusion-controlled. The relaxation times are

broadly distributed because of the variation in mobility across the double layer. The attenuation due to electrochemical surface mechanism is thus constant Q (fig. 8), at least in the frequency range between 10 and 10^6 Hz. The actual relaxation times ought to be predicted from statistical mechanics.

Explanation for the increased loss with increasing moisture or vapor pressure is straightforward. Consider that

$$Q^{-1} \propto \tilde{S} \sum_j n_j \phi_b \tag{10}$$

where $\tilde{S}$ is the total surface area deformed, j is the number of layers in the double layer at the given vapor pressure, n_j is the number of fluid molecules per layer per unit surface area, and ϕ_b is the energy lost in breaking a hydrogen bond. ϕ_b is a constant. n_j increases (by definition) with increased deposition on the surface. $\tilde{S}$ also increases with vapor pressure because the contacts become more compliant.

Several investigators (Born, 1941; Spencer, 1981; Murphy, 1982a) have found that Q^{-1} is frequency independent in dry sandstones. Pandit and King (1979) have shown that Q^{-1} remains independent of frequency up to relative humidities between 80 and 90%. At this vapor pressure, bulk liquid water begins to condense in the smaller contact gaps or capillaries. Frequency dependent Q is associated with the presence of bulk liquid water.

5. MICROHYDRODYNAMICS

When bulk liquid water is present in the contact gaps (fig. 9), oscillatory displacement of the grain surfaces will drive local fluid flow. This process determines the large losses that are dependent on

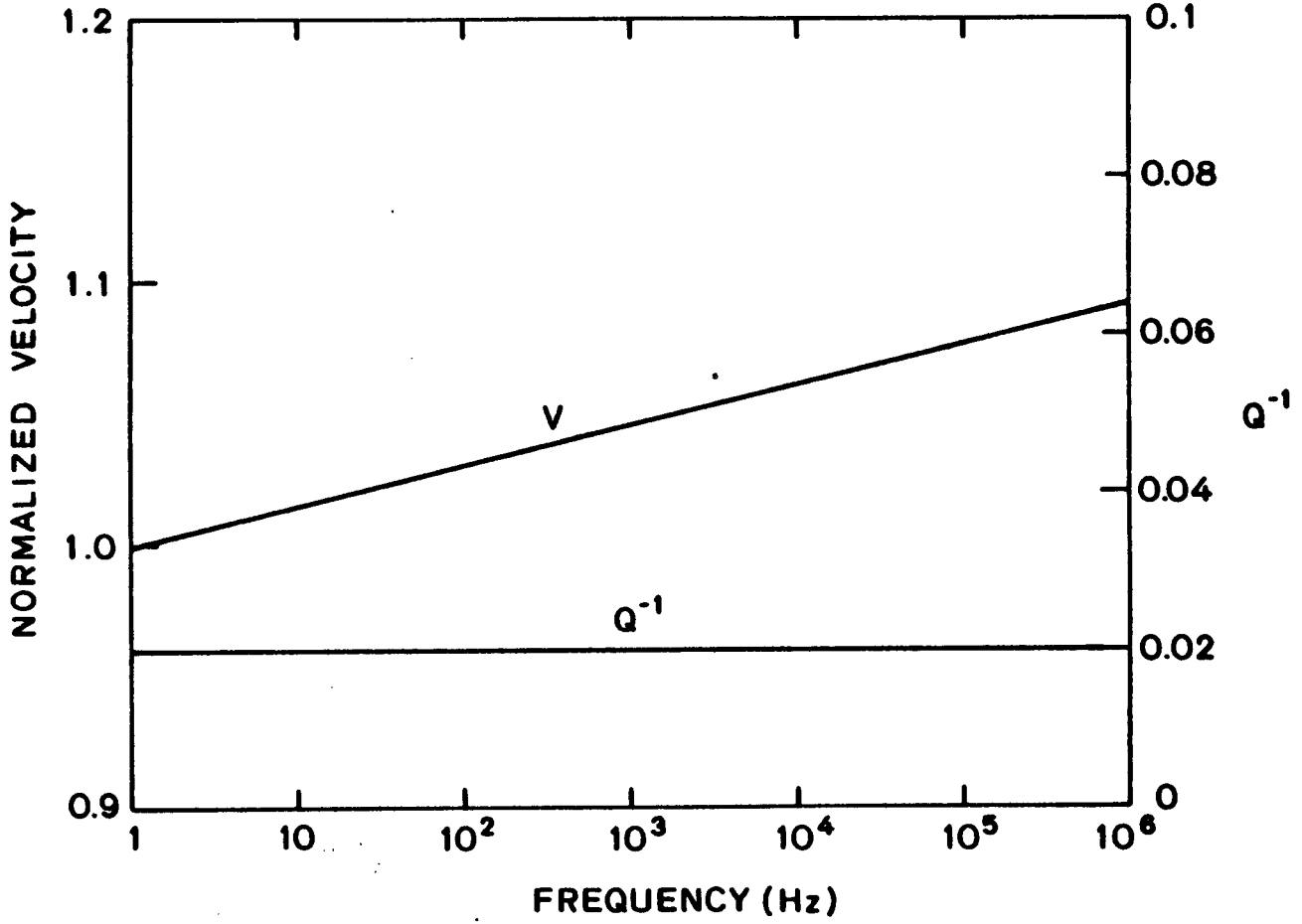

Fig. 8. Phase velocity and Q^{-1} versus frequency at $P/P_0(H_2O) \approx 0.60$ in a dry granular sedimentary material.

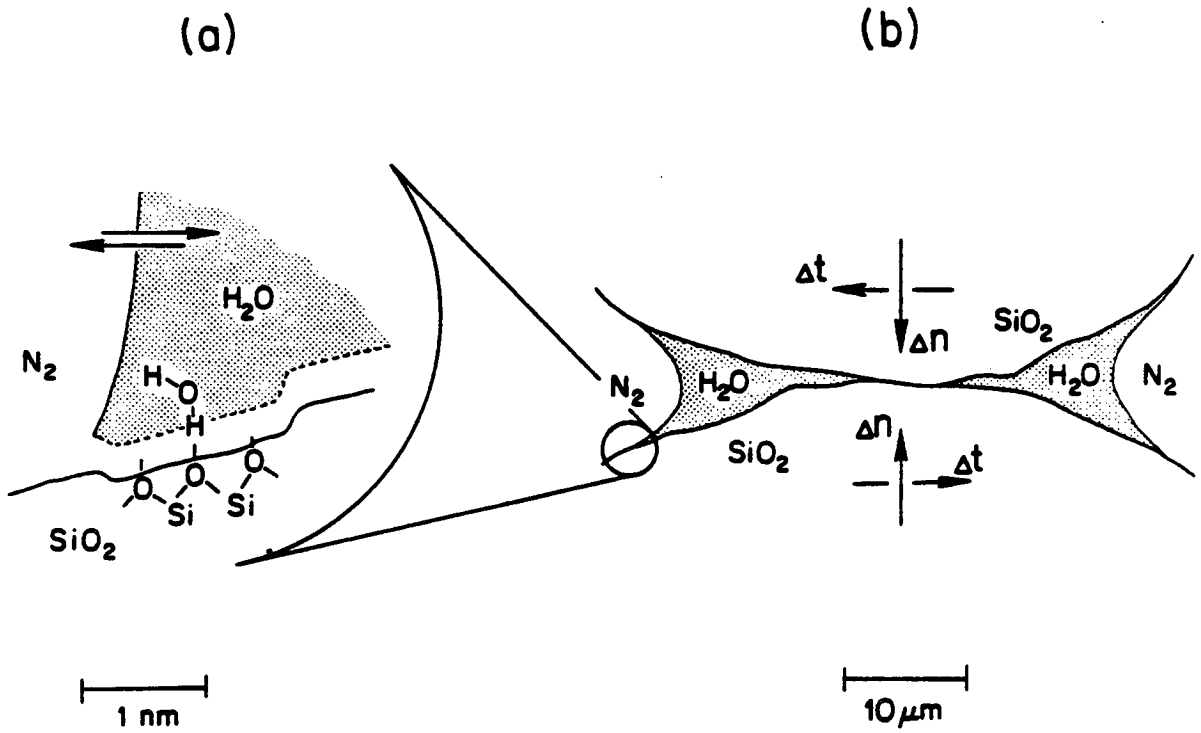

Fig. 9. Two grains in contact in a partially saturated granular sedimentary material.

both water saturation and frequency. Of course, the electrochemical surface mechanism continues to operate. It provides a frequency independent background loss. But in the range from 100 Hz to 100 kHz, local fluid flow dominates. There are three parts to the fluid flow problem: i) boundary layer development, ii) squeeze film elasto-hydrodynamics, and iii) propagation and flow in a compact pore neighborhood.

Boundary Layer Development

In a porous medium under acoustic loading, the pore fluid moves relative to the solid frame (Biot, 1956). Consider a half cycle of an oscillatory displacement of a cylindrical pore in the plane of its axis (fig. 10a). The fluid in contact with the wall adheres to it. A velocity profile develops as viscous tangential stresses diffuse vorticity across the pore width with a diffusivity

$$\nu = \frac{\eta}{\rho_f} \tag{11}$$

where ν is the kinematic viscosity. Energy is dissipated by the viscous tangential stresses. The depth to which the boundary layer has penetrated before reversal is the skin depth

$$\delta = \left(\frac{\nu}{\omega}\right)^{1/2} . \tag{12}$$

Dissipation is confined to the boundary layer.

When δ reaches h, the flow profile becomes parabolic (i.e. a Poiseuille flow). It is said to be fully developed. At 1 MHz, the flow would be fully developed in pores 3 μm in width. At 10 kHz, flow in 300 μm pores would be fully developed.

Viscous dissipation is defined in general as

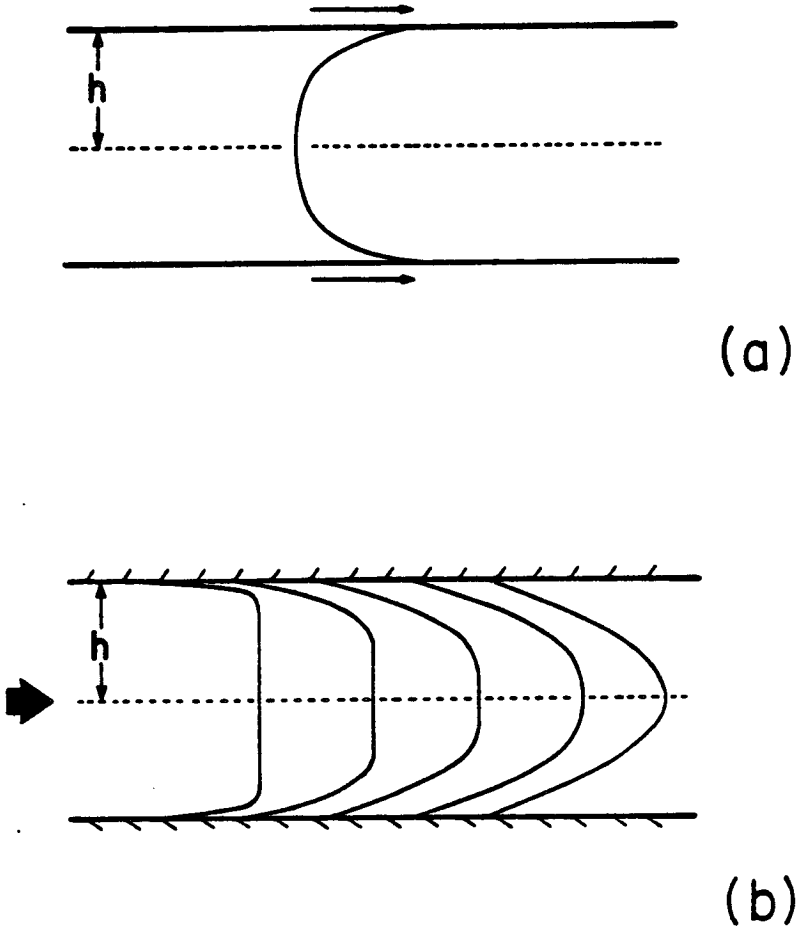

Fig. 10. Boundary layer development: (a) wall is beginning to move, and the fluid is still; and (b) the wall is fixed, and the fluid is beginning to flow.

$$\phi_v = \text{the rate of energy loss per unit volume per unit time} \tag{13a}$$

$$= \frac{1}{2}\,\tilde{\tau}\cdot\varepsilon \tag{13b}$$

$$= \frac{\eta}{2}\,(\nabla v) + (\nabla v)^T \;:\; (\nabla v) + (\nabla v)^T \tag{13c}$$

where ∇ is the del operator and v is the fluid velocity. In this specific solid-fluid coupling model, the dissipation per cycle is a tradeoff between the velocity gradient and the boundary layer thickness. The peak loss occurs at that frequency in which $\delta = h$. This is the micromechanics of Biot's (1956) attenuation mechanism. It is not important at acoustic frequencies in granular sedimentary materials.

However, the basic physics of boundary layer development carries over into another flow model. Consider the flow through a fixed cylindrical pore driven by an oscillatory pressure gradient (fig. 10b). This process is clearly relevant to flow in and out of a contact gap. The rate of energy dissipation per unit area of solid boundary is approximately

$$\frac{1}{2}\; s\; (\rho\omega)^{-1} \left| \frac{\partial p}{\partial x} \right|^2 \left(\frac{\nu}{2\omega} \right)^{1/2} \tag{14}$$

per unit length of tube, where s is the circumference. The energy loss per cycle is proportional to the boundary layer thickness.

Squeeze Film Elastohydrodynamics

The compression of a contact gap (fig. 11) will drive water out of that gap. If the length b is much greater than the width $2h$ and the flow profile is fully developed, the motion of the squeeze film is governed by the Reynold's equation

$$\nabla^2 p = \frac{3\eta}{2h^3}\,\frac{\partial h}{\partial t} \quad . \tag{15}$$

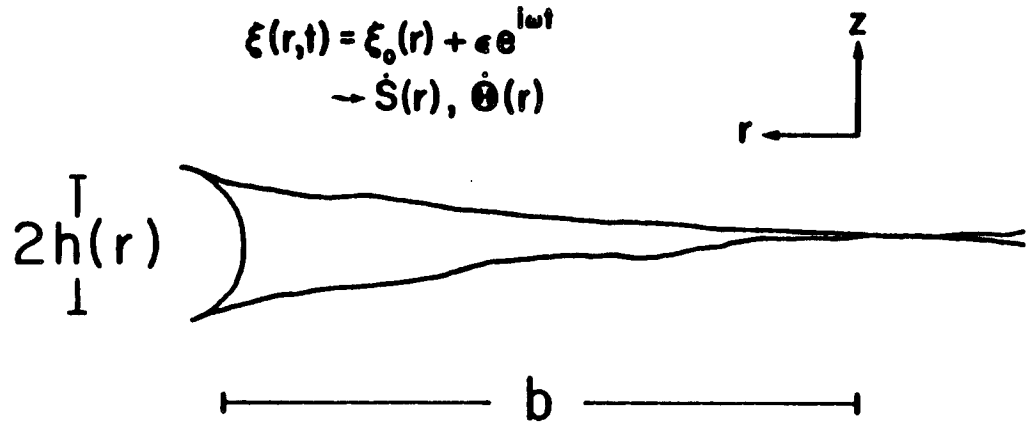

Fig. 11. The gap between two grains in contact.

The rate of closure of the gap $\partial h/\partial t$ is the driving or squeeze term. It is related to the elasticity of the contact gap by

$$\frac{\partial h}{\partial t} = -\frac{b}{M_{gap}} \left(i\omega\sigma - \frac{\partial p}{\partial t} \right) f(\xi) \tag{16}$$

where $i\omega\sigma$ is the acoustic loading, M_{gap} is the modulus of the gap, and $f(\xi)$ is a function of the gap shape.

Phenomenalogically, this micromechanism defines a Zener relaxation or standard linear solid (fig. 12). The elastic grains constitute a spring which is in series with a parallel spring (the grain contact) and dashpot (the squeeze film). The characteristic relaxation time, τ, is simply

$$\tau \approx \frac{\eta}{M_{gap}} \left(\frac{b}{h} \right)^m \tag{17}$$

where the exponent m is dependent on the shape of the gap. As the grain surfaces approach parallelism, n approaches 3. The observed relaxations in sandstones are in the range 10^{-3} to 10^{-4} s. Thus, for $\eta \approx 10^{-3}$ Nsm^{-2} and $M_{gap} \approx 1$ GPa, the aspect ratios involved would be in the range 10^{-2} to $10^{-2.5}$. In other words, the gap length is required to be 100 times the half length. This is a very flat gap, but not unreasonable when we consider that the displacements of the gap wall are of the order of nannometers.

For water drops isolated in small constrictions, surface tension may be included in equation 14 by subtracting $2\gamma_w/h$ from the pressure. γ_w is the surface tension of water.

Propagation and Flow in a Compact Pore Neighborhood

The water saturation effects (fig. 13) have yet to be explained. Thus far, we have considered the sites for pore pressure buildup,

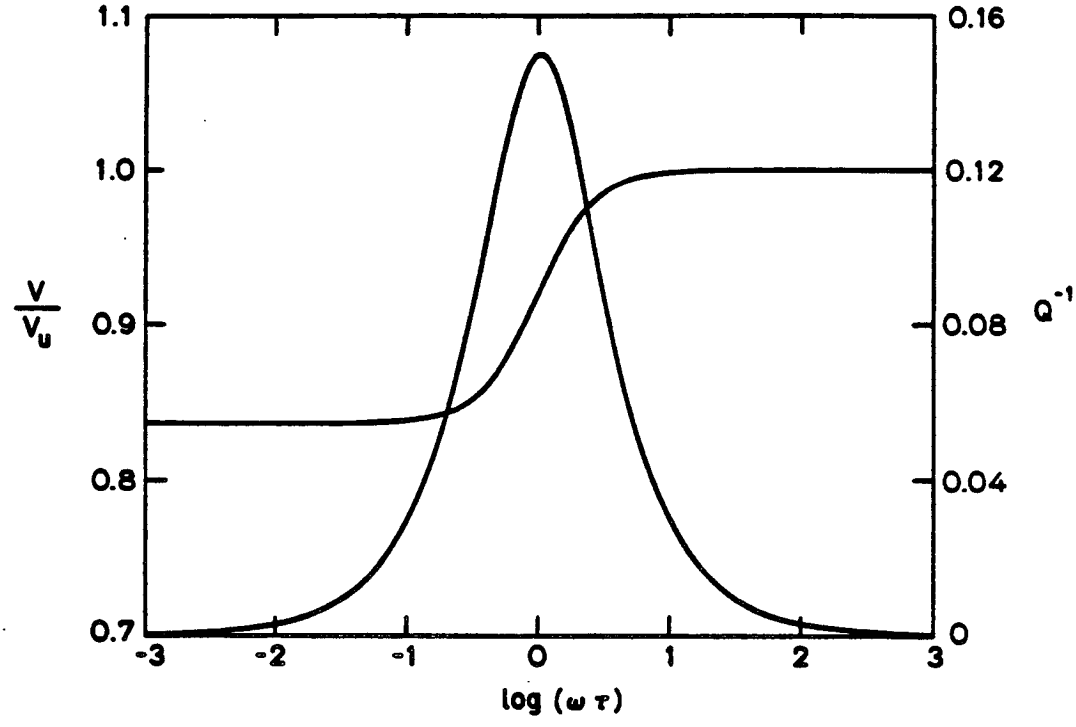

Fig. 12. Phase velocity and Q^{-1} versus frequency in a Zener standard linear solid.

Fig. 13. (a) Q^{-1} versus % water saturation (S_w = 0.1 - 1.0) in Massillon sandstone.

(b) The ratios of compressional (P) and shear (S) wave velocities and attenuation versus % water saturation (S_w = 0.1 - 1.0) in Massillon sandstone.

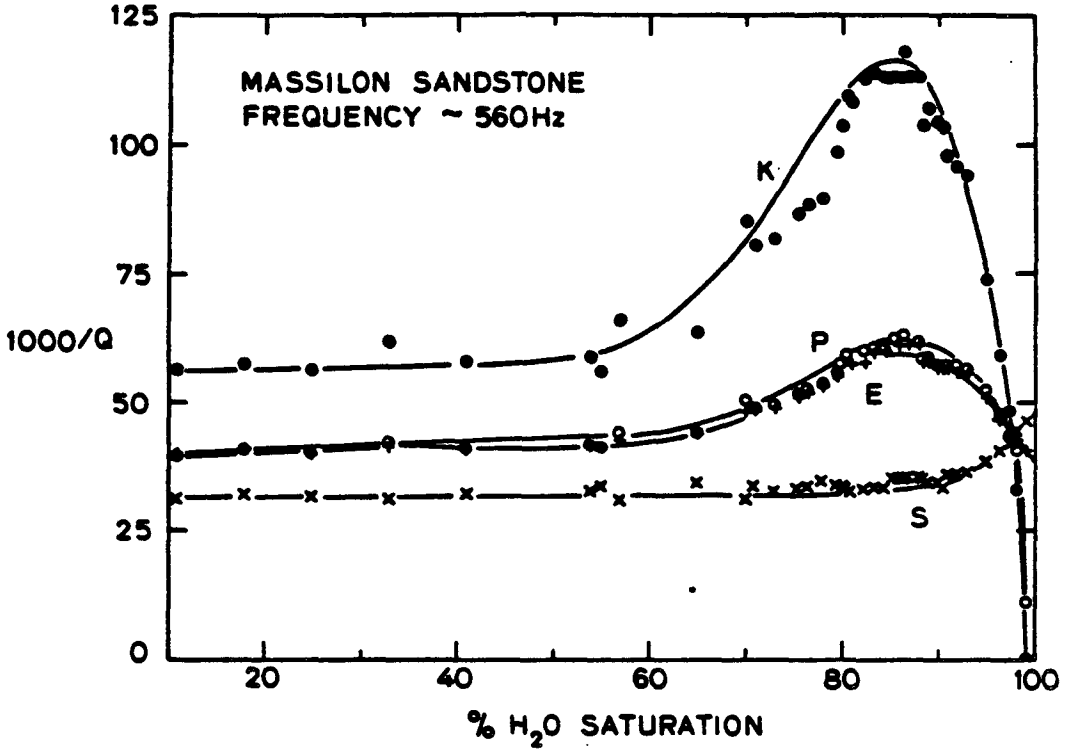
MASSILON SANDSTONE
FREQUENCY ~ 560Hz
K
P
E
S
1000/Q
125
100
75
50
25
0
20
40
60
80
100
% H2O SATURATION

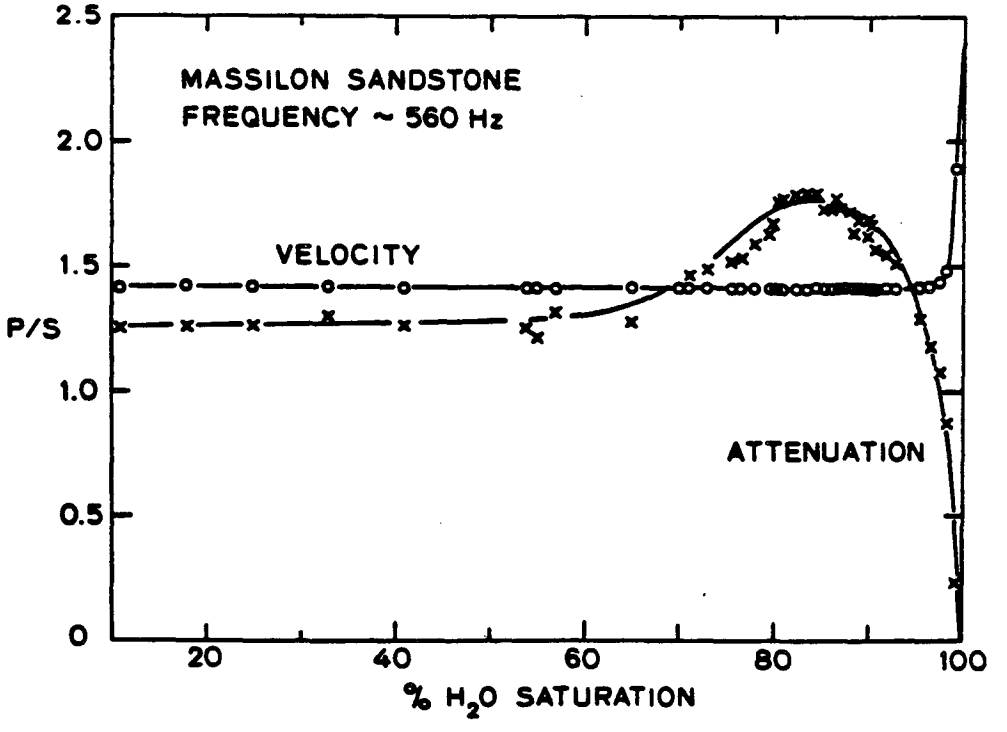
MASSILON SANDSTONE
FREQUENCY ~ 560 Hz
VELOCITY
ATTENUATION
P/S
2.5
2.0
1.5
1.0
0.5
0
20
40
60
80
100
% H2O SATURATION

the contact gaps, in terms of discharge into an infinite reservoir at null pore pressure. We have not yet considered the flow in the contiguous pore. In order to understand the effects of water saturation on Q^{-1}, we need to consider flow throughout the local pore neighborhood.

The property which defines the volume flow out the contact gap, or constriction, into the adjacent pore, or cavity, is the admittance. The admittance, β, is defined as the ratio of the volume flow to pressure excess. An effective admittance, β_e, can be defined such that it takes into account the configuration of the pores and gaps in the entire neighborhood (Lighthill, 1975; 1978). Such a device allows us to map complex pore configurations such as those in real sands and sandstones into simple models such as those in figure 14.

If the pore neighborhood is small compared to the wavelength, it is said to be compact. The equations of fluid motion for frequency ω can be expressed as

$$\frac{\partial J}{\partial t} = -\beta_e \left[\rho_f (B_f + D)\right]^{-1/2} \frac{\partial p}{\partial x} \left[1 - \left(\frac{\nu}{i\omega}\right)^{1/2} \frac{s}{S_o}\right] \qquad (18)$$

where J is the volume flow, D is the distendibility of the constriction walls, and S_o is the crossectional area. These motions must satisfy the linearized equations of continuity.

$$\frac{\partial p}{\partial t} = -\beta_e^{-1} \left[\rho_f (B_f + D)\right]^{-1/2} \frac{\partial J}{\partial x} \; . \qquad (19)$$

The pressure buildup $\partial p/\partial t$ is related to the elasticity of the contact through equation 15. Dissipation is calculated from equation 13.

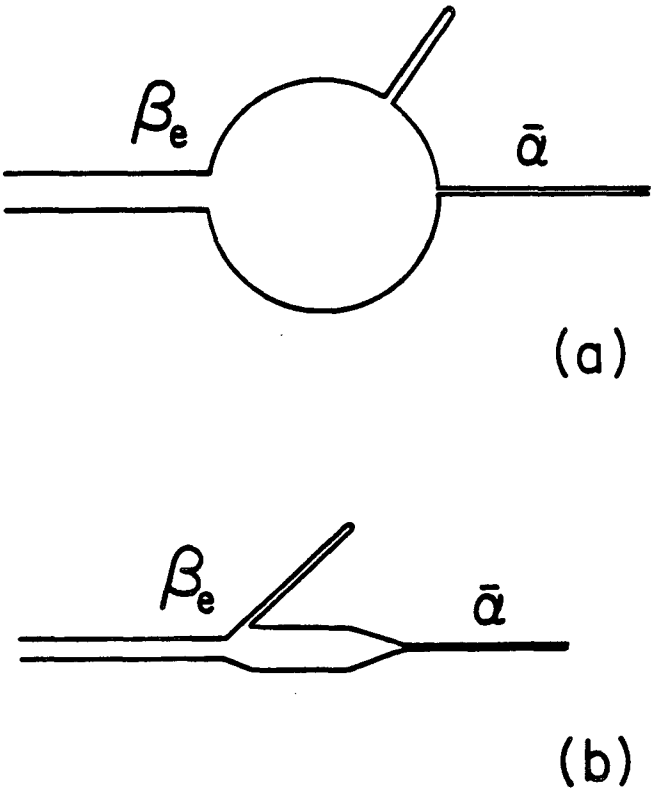

Fig. 14. Models of the local pore neighborhood in (a) high porosity sandstone and (b) low porosity sandstone. The contact gap is the constriction on the left. The cavity in the center is the contiguous pore. The closed end constriction represents connected contact gaps and closed pores. The constriction on the right constitutes the connectivity to the pore network. β_e is the admittance of the contact gap. $\bar{\alpha}$ is Biot's structural factor.

This system of equations provides the foundation to formulate the model rigorously. That task is beyond the scope of this paper.

Consider the pore configuration in figure 14a to be fully water saturated. It is subjected to pure bulk compression as sketched in figure 15. As the entire pore neighborhood is compressed isotropically and the compressibility of the fluid B_f is low, the pore pressure gradient $\partial p/\partial x$ is weak. Volume flow J and the dissipation per cycle Q_k^{-1} is small. The contact gap closure dh/dt cannot occur because the pore pressure buildup $\partial p/\partial t$ cannot relax. The real part of the frame modulus is very high.

On the other hand, pure shear is polarized (fig. 15). Contact gaps having differing azimuths with respect to the polarization may undergo compression or extension. The pore fluid is simultaneously subjected to compression and suction. Pressure gradients $\partial p/dx$ are high. Volume flow J is high and Q_s^{-1} is high. The pore pressure buildup $\partial p/\partial t$ can relax, and gap closure dh/dt proceeds.

When the pore neighborhoods (fig. 14) are partially saturated the situation is quite different. The high compressibility of the fluid in the cavity allows strong pore pressure gradients to occur, particularly under bulk compression. Volume flow and Q_k^{-1} are high.

We can heuristically summarize the model with the following proportionality

$$Q^{-1} \propto \underbrace{\phi S_w}_{(a)} \underbrace{\left(\frac{\delta}{h}\right)}_{(b)} \underbrace{\sum_i n_i \left|\left(\frac{\partial p}{\partial x}\right)_i\right|^2}_{(c)} \tag{20}$$

where the factor (a) merely expresses the volume of viscous fluid per

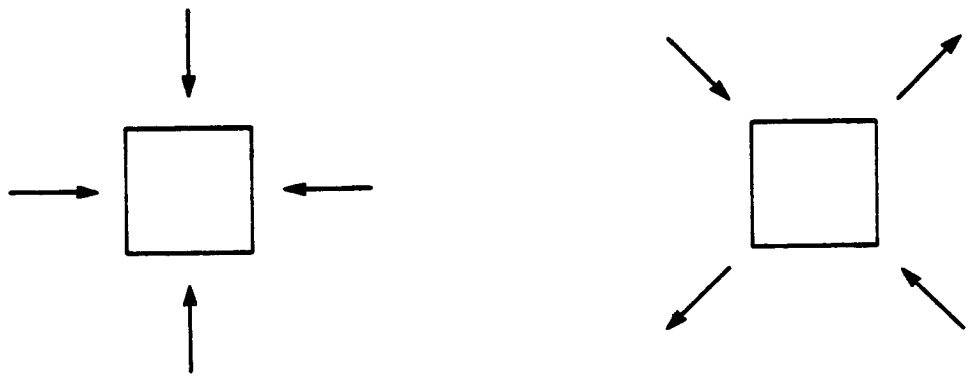

Fig. 15. Stress configurations for bulk compression and pure shear.

volume of the composite material, factor (b) represents the boundary layer thickness, and factor (c) is the sum of the number of pore pressure sites times the square of the pore pressure gradient at that site. Factor (c) is controlled by a combination of the aspect ratio of the gaps, the stress configuration, and the compressibility of the fluid in the cavity.

6. GENERAL EQUATIONS FOR ACOUSTIC PROPAGATION IN POROUS MEDIA

Biot (1956) and Morse and Ingard (1968) have studied the macroscopic elastodynamics of a porous, two component system. These theories track the motions and forces in the solid and fluid in two separate equations. The solid frame is perfectly elastic. Granularity is not considered.

Biot (1962) and Burridge and Keller (1981) have proposed a generalized set of equations which can accommodate linear viscoelastic frame moduli. To the best of my knowledge, these equations have not as yet been exploited in the literature. A schematic breakdown of the generalized equations is presented in figure 16. Detailed discussion is beyond the scope of this paper. We wish, however to sketch the theory in order to discuss several predictions.

The equations of motion are for the porous, granular composite

$$\rho_c \ddot{u} + \rho_f \ddot{w} = \text{div } T \tag{21}$$

and for the macroscopic motion of the pore fluid

$$\rho_f \ddot{u} = -\frac{\partial p}{\partial x} + \bar{Y}\,\dot{w} \tag{22}$$

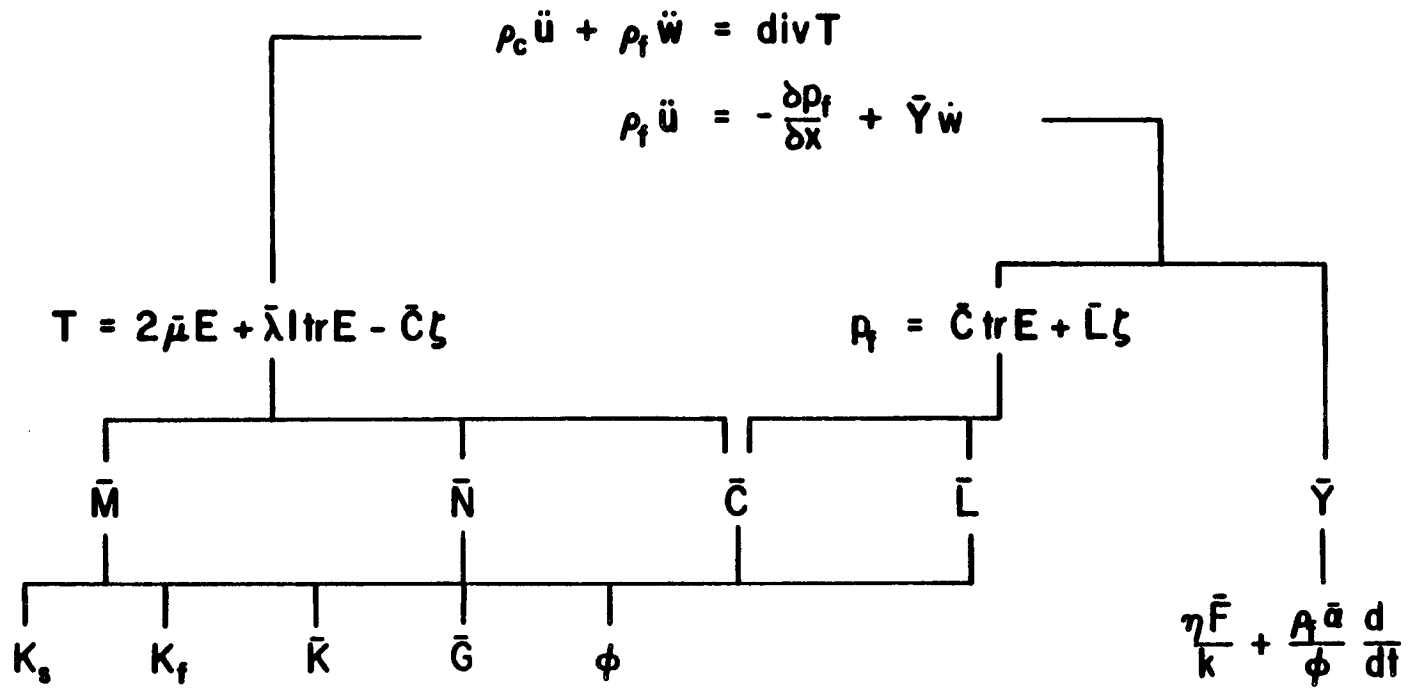

Fig. 16. Outline of the general equations for acoustic propagation in general porous media. (See text for explanation.)

where $\rho_c = (1-\phi)\,\rho_s + \phi\rho_f$

$\rho_f = (1-S_w)\,\rho_g + \phi S_w \rho_w$

ρ_g = density of the gas

ρ_w = density of the water

S_w = water saturation

ϕ = porosity

u = displacement of the solid

$w = u-U$ = relative displacement of the fluid and the solid

U = displacement of the fluid.

$\bar{Y}$ is the viscodynamic solid-fluid coupling operator.

$$\bar{Y} = \frac{\rho_f \bar{\alpha}}{\phi} \frac{d}{dt} + \frac{\eta \bar{F}}{k} \quad . \tag{23}$$

The first term on the right hand side of equation 21 describes the inertial coupling, while the second term describes the dissipation. p_f is the macroscopic pore pressure

$$p_f = \bar{C}\ \mathrm{tr}\ E + \bar{L}\ \zeta \tag{24}$$

where $\mathrm{tr}\ E$ is the trace of the stress tensor and ζ is the fluid volume increment per unit pressure, $-\phi\,\mathrm{div}\ w$. Equations 21 through 23 govern Biot's solid-fluid coupling, and hereafter shall be neglected.

T is the stress tensor of the composite material

$$T = 2\bar{\mu}E + \bar{\lambda} 1\ \mathrm{tr}\ E - \bar{C}\ \zeta \tag{25}$$

where $\bar{\lambda}$ and $\bar{\mu}$ are the complex Lame's constants.

The complex moduli $\bar{M}$, $\bar{N}$, $\bar{C}$, and $\bar{L}$ can be given in terms of the intrinsic material properties ϕ, K_s, K_f, $\bar{K}$, and $\bar{G}$ as

$$\bar{M} = \bar{\lambda} + 2\bar{\mu} + \bar{R} + 2\bar{Q} = \frac{(K_s - \bar{K})^2}{K_s(1-\phi-\frac{\bar{K}}{K_s}+\phi\frac{K_s}{K_f})} + \bar{K} + \frac{4}{3}\bar{\mu}\,, \qquad (26)$$

$$\bar{N} = \bar{\mu} = \bar{G}\,,$$

$$\bar{C} = \frac{\bar{R}+\bar{Q}}{\phi} = \frac{(K_s - \bar{K})}{(1-\phi-\frac{\bar{K}}{K_s}+\phi\frac{K_s}{K_f})} \qquad (27)$$

and

$$\bar{L} = \frac{\bar{R}}{\phi} = \frac{K_s}{(1-\phi-\frac{\bar{K}}{K_s}+\phi\frac{K_s}{K_f})}\,. \qquad (28)$$

K_s is the bulk modulus of the solid grains. The bulk modulus of the fluid is

$$\frac{1}{K_f} = (1 - S_w)\,B_g + S_w B_w\,, \qquad (29)$$

where B_g is the compressibility of the gas and B_w is the compressibility of the water.

$\bar{K}$ and $\bar{G}$ are the linear viscoelastic frame moduli, which are determined by the granular micromechanics. The variation of the real part of $\bar{K}$ and $\bar{G}$ as a function of frequency and water saturation is shown in figure 17.

The compressional and shear wave velocities are given by

$$V_p = \left(\frac{\bar{M}}{\rho_c}\right)^{1/2} \qquad (31)$$

and

$$V_s = \left(\frac{\bar{N}}{\rho_c}\right)^{1/2}\,,$$

respectively. Specific attenuation is

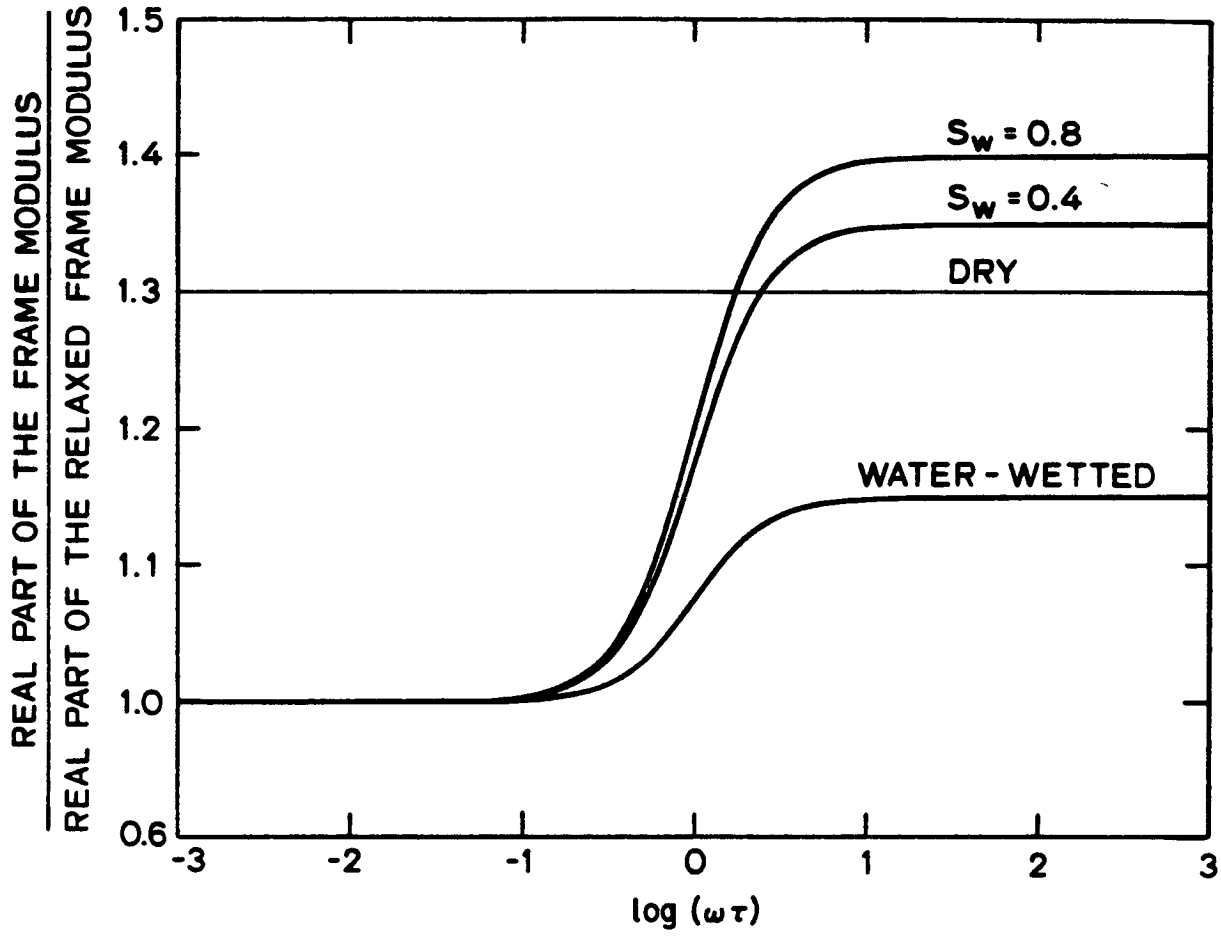

Fig. 17. Theoretical modulus dispersion in sandstones as a function of water saturation. Constant Q loss is suppressed. Water-wetted curve assumes certain degree of capillary condensation.

$$Q_p^{-1} = \frac{\text{Im } \bar{M}}{\text{Re } \bar{M}} \tag{32}$$

and

$$Q_s^{-1} = \frac{\text{Im } \bar{N}}{\text{Re } \bar{N}} \quad . \tag{33}$$

7. DISCUSSION

Although the model is not yet complete, I am reasonably confident that most of the major concepts are moving into place.

The velocity equations reduce to the Biot-Gassmann relations at frequencies a decade below the center frequency. This is accomplished as the frequency dependent frame moduli $\bar{K}$ and $\bar{G}$ approach relaxed values K_r and G_r in equations 24, 25, 29, and 30. The center frequency for Massillon sandstone is ~5 kHz. Figure 18 compares the predictions for V_p and V_s vs. S_w with measured values at 550 Hz.

Clark et al. (1980), Tittmann et al. (1980), and Spencer (1981) have added various pore fluids to dry sandstones. The fluids were of varying composition but of similar viscosity. They found that the fluids reduced the real part of the moduli and increased the Q^{-1} in the following order. From

water
ethanol
methanol
n-decane
benzene
hexane (35)

Clark et al. (1980) and Tittmann et al. (1980) suggest that the process has something to do with the dipole moment. While Spencer (1981)

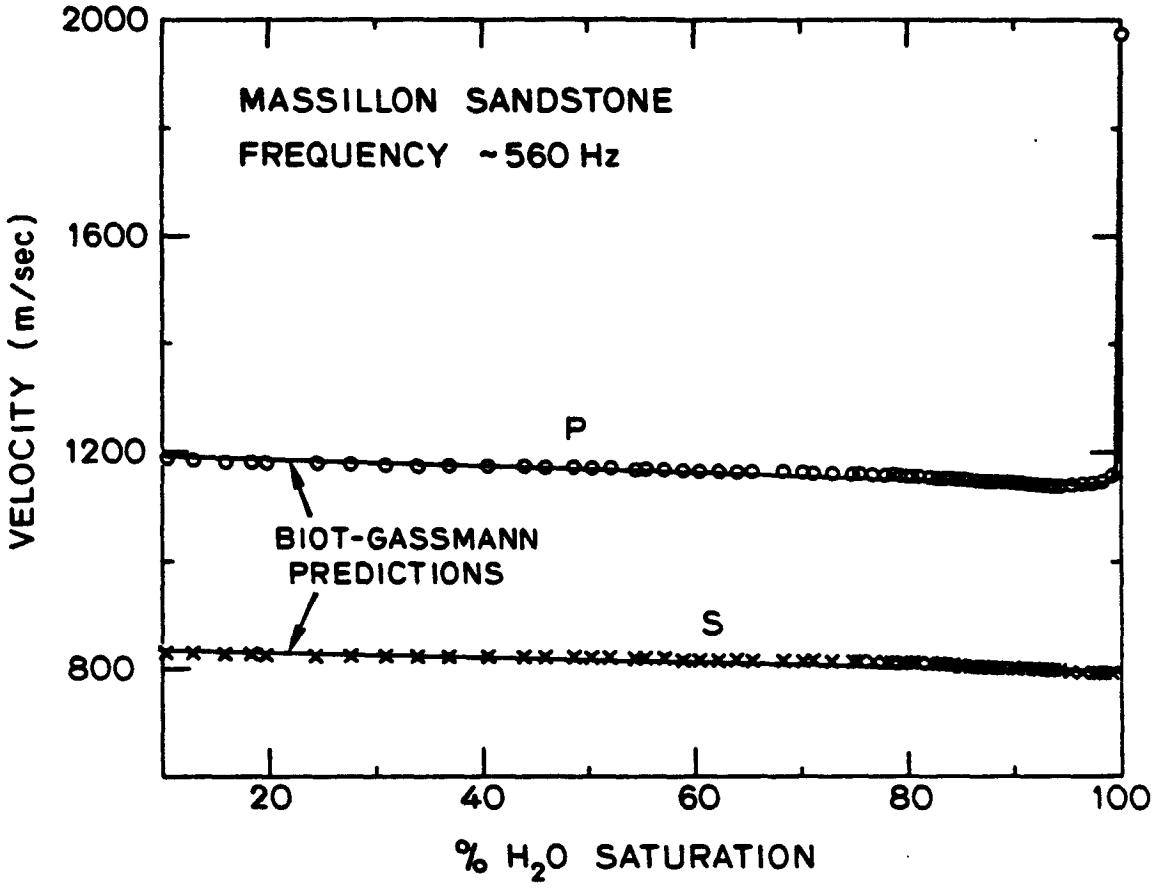

Fig. 18. V_p and V_s vs. % H_2O saturation (S_w = 1.0 - 0.1) in Massillon sandstone. Biot-Gassmann predictions plotted against measured values.

discusses physisorption. Once again, the specific chemical properties of importance are the chemical potential $\tilde{\mu}$ and the electrochemical. potential $\tilde{\tilde{\mu}}$. The order in (35) is the order of descending $\int_i d\tilde{\mu}$ and $\int_i d\tilde{\tilde{\mu}}_i$.

Spencer (1981) further claims that because the observed frequency peaks. are depressed in the same order, these peaks must result from the surface effect. Well it is an interesting point, but the conclusion is wrong. From equations 14 and 15, we see that the more compliant the contact, the greater the pore pressure gradient driving the volume flow. Dissipation goes as the square of the pore pressure gradient. The magnitude of the electrochemical effect on contact compliance follows the same descending order as in (35). It stands to reason the height of the peaks due to viscous loss would be depressed correspondingly.

A similar argument can be used to explain the difference between the losses in Massillon sandstone and Vycor porous glass as reported in Murphy (1982a). Although Vycor has a surface area of ~200 m^2/gm^3 and Massillon has a surface area roughly 10 m^2/gm^3, the losses in Vycor are consistently 1/6 that in Massillon at all saturations. The difference lies in the compliance of the grain contacts. Vycor has a structure which under a SEM appears similar to sintered glass beads (fig. 19b). Massillon on the other hand has many small aspect ratio near-contact gaps (19a). The basic difference between the contacts is sketched in figure 20. The near contact gaps in the Massillon sandstone provide the sites necessary for pore pressure generation.

Finally, the effect of temperature may be included in the model by considering the temperature dependence of the viscosity. The

Fig. 19. SEM photomicrograph of (a) Massillon sandstone and (b) Vycor porous glass. The white bar at the base of the photograph is the length scale.

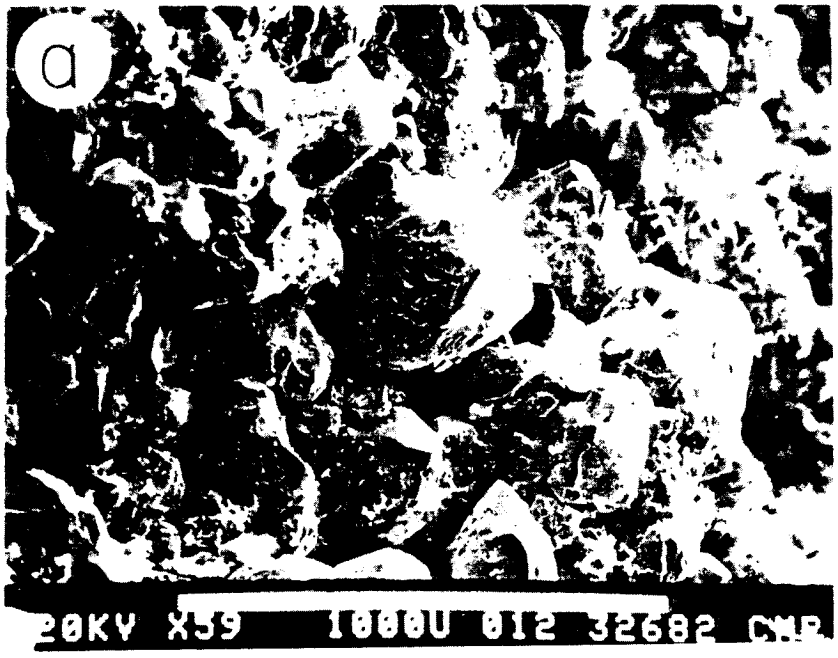
a
20KV X59 1000U 012 32682 CMR

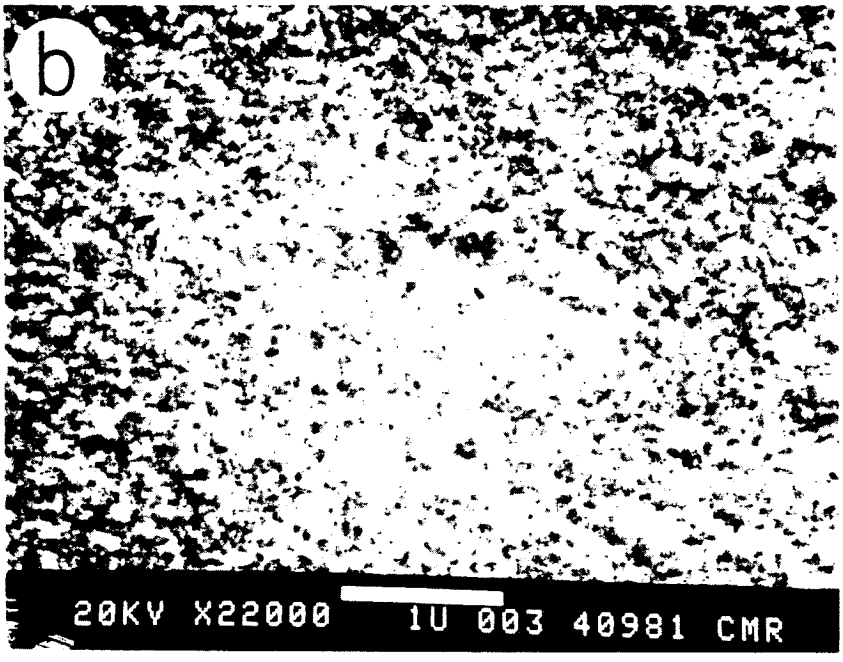
b
20KV X22000 1U 003 40981 CMR

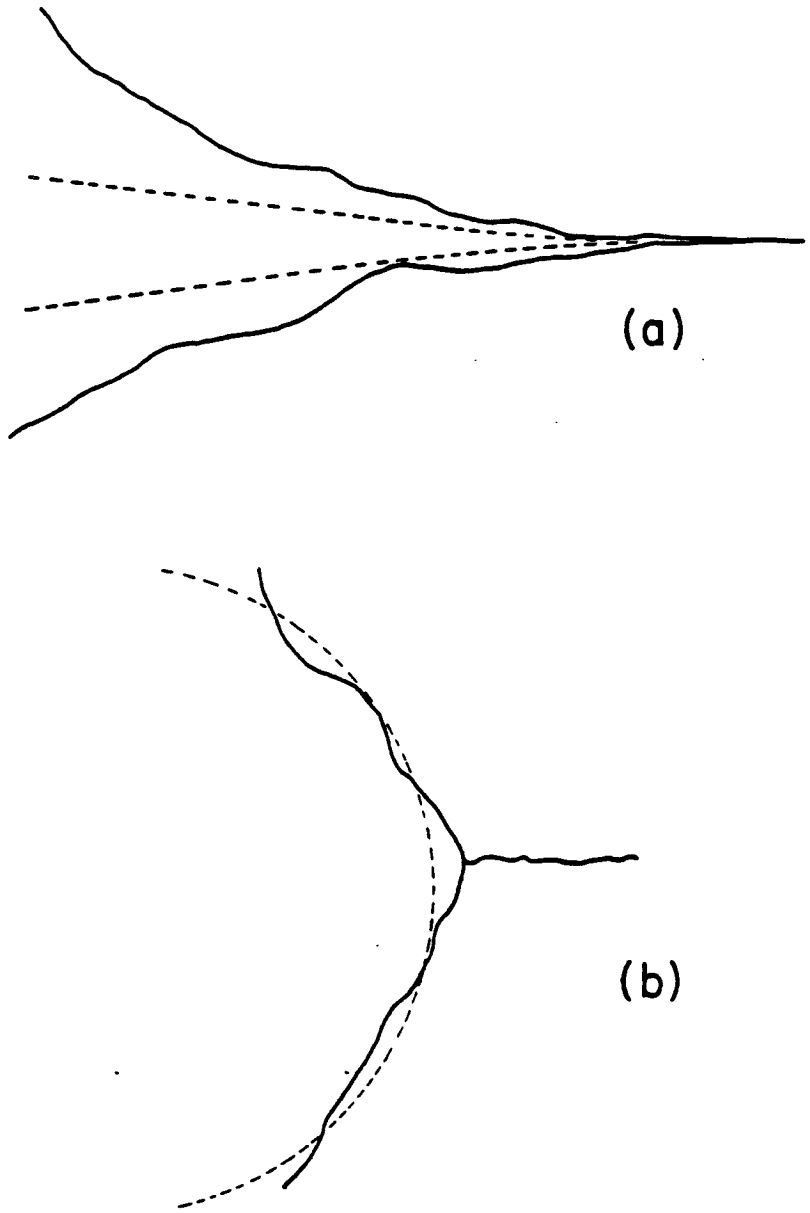

Fig. 20. Sketch of the contact gaps in (a) a granular sedimentary material (eg. Massillon sandstone) and (b) Vycor porous glass.

Arrehenius equation predicts that

$$\eta = \eta_o e^{-\frac{\tilde{E}}{R\theta}} \quad . \tag{36}$$

where θ is the temperature, R is the gas constant, η_o is the viscosity as $\theta \to 0$, and $\tilde{E}$ is the activation energy of the fluid. The preliminary experimental results of T. Jones (personal communication) are encouraging along this line of reasoning.

WORKS CITED

Adamson, A.W., 1976, Physical Chemistry of Surfaces, Wiley, N.Y., 697 p.

Amberg, C.H. and McIntosh, R., 1952, A study of adsorption hysteresis by means of length changes of a rod of porous glass, Canad. J. Chem. 30, 1012-1032.

Biot, M.A., 1956, Theory of propagation of elastic waves in a fluid-saturated porous solid,
I. Low frequency range, J. Acoust. Soc. Am. 28, 168-178.
II. High frequency range, J. Acoust. Soc. Am. 28, 179-191.

Biot, M.A., 1962, Generalized theory of acoustic propagation in porous dissipative media, J. Acoust. Soc. Am. 54, 1254-1264.

Clark, V.A., Tittmann, B.R. and Spencer, T.W., 1980, Effect of volatiles on attenuation (Q^{-1}) and velocity in sedimentary rocks, J. Geophys. Res. 35, 5190-5198.

Devaney, A.J., Levine, H., and Plona, T.J., 1982, Attenuation due to scattering ultrasonic compressional waves in granular media, in Elastic Wave Scattering and Propagation (V.K. Varadom and V.V. Varadom, eds.), Ann Arbor Sci., Ann Arbor, 131-148.

Fischer, F.H., and Simmons, V.P., 1975, Discovery of boric acid as the cause of low frequency sound absorption in the ocean, IEEE Ocean '75, 21-24.

Gregory, A.R., 1976, Fluid saturation effects in dynamic elastic properties of sedimentary rocks, Geophys. 41, 895-921.

Griggs, D., 1967, Hydrolytic weakening of quartz and other silicates, Geophys. J. R. Soc. 14, 19-31.

Hiemenz, P.C., 1977, Principles of Colloid and Surface Chemistry, Dekker, NY, 516 p.

Kjartansson, E., and Nur, A., 1982, Attenuation due to thermal relaxation in porous rocks, Geophys. (in press).

Lighthill, M.J., 1978, Waves in Fluids, Cambridge Univ. Press, 504 p.

Lighthill, M.J., 1975, Mathematical Biofluiddynamics, SIAM, Phila., 281 p.

Mavko, G.M., 1979, Frictional attenuation: an inherent amplitude dependence, J. Geophys. Res. 84, 4769-4775.

Mavko, G.M., and Nur, A., 1979, Wave attenuation in partially saturated rocks, Geophys. 44, 161-178.

Mason, W.P., 1969, Internal friction mechanism that produces an attenuation in the earth's crust proportional to frequency, J. Geophys. Res. 74, 4963-4966.

Mason, W.P., 1971a, Internal friction at low frequencies due to dislocations: Applications to metals and rock mechanics, in Physical Acoustics: Princples and Methods (W.P. Mason and R.N. Thurston, eds.) 8, 347-371.

Mason, W.P., 1971b, Internal friction in moon and earth rocks, Nature 234, 461-463.

Morse, P.M., and Ingard, K.V., 1968, Theoretical Acoustics, McGraw-Hill, NY, 927 p.

Murphy, W.F., 1982a, Effects of partial water saturation on attenuation in Massillon sandstone and Vycor porous glass, J. Acoust. Soc. Am. 71, 6 (in press). Also Chapt. III in this volume.

Murphy, W.F., 1982b, Micromechanics of acoustic dissipation in fully and partially water saturated granular sedimentary materials, J. Geophys. Res., subm. July. Also Chapter V in this volume.

Murphy, W.F. and Nur, A., 1982a, On velocities and attenuation as a measure of partial gas saturation in tight sandstones at borehole and ultrasonic frequencies, Geophys., subm. July. Also Chapter IV in this volume.

O'Connell, R.J., and B. Budanisky, 1977, Viscoelastic properties of fluid-saturated cracked solid, J. Geophys. Res. 82, 5119-5736.

Parks, G.A., 1982, The surface and interfacial free energies of quartz, J. Geophys. Res., to be submitted.

Pandit, B.I., and King, M.S., 1979, The variation of elastic wave velocities and quality factor Q of a sandstone with moisture content, Canad. J. Earth Sci. 16, 2187-2195.

Schulkin, M., and Marsh, W.H., 1978, Low-frequency sound absorption in the ocean, J. Acoust. Soc. Am. 63, 43-48.

Simmons, V.P., 1975, Investigation of the 1 kHz sound absorption in sea water, Ph.D. Dissertation (Univ. Calif. San Diego).

Spencer, J.W., 1981, Stress relaxations at low frequencies in fluid-saturated rocks: Attenuation and modulus dispersion, J. Geophys. Res. 86, 1803-1812.

Stoll, R.D., 1979, Experimental studies of attenuation in sediments, J. Acoust. Soc. Am. 66, 1152-1160.

Tittmann, B.R., Clark, V.A., Richardson, J.M. and Spencer, T.W., 1980, Possible mechanisms for seismic attenuation in rocks containing small amounts of volatiles, J. Geophys. Res. 85, 5199-5208.

Winkler, K.W., Nur, A. and Gladwin, M., 1979, Frictional sliding and seismic attenuation in rocks, Nature 227, 528-531.

Winkler, K.W. and Nur, A., 1982, Seismic attenuation: Effects of pore fluids and frictional sliding, Geophys. 47, 1-15.

Winkler, K.W., and T. J. Plona, 1982, Technique for measuring ultrasonic velocity and attenuation spectra in rocks under pressure, J. Geophys. Res., submitted.

Yeaker, E., Fischer, F.H., Miceli, J. and Bressel, R., 1973, Origin of the low frequency sound absorption in sea water, J. Acoust. Soc. Am. 53, 1705-1707.

Zuckerwar, A.J., and Griffin, W.A., 1981, Effect of water vapor on sound absorption in nitrogen at low frequency/pressure ratios, J. Acoust. Soc. Am. 69, 150-154.

ADDITIONAL REFERENCES

Batchelor, G.K., 1976, Developments in microhydrodynamics, in Theoretical and Applied Mechanics (W.T. Koiter, ed.), North Holland, Amsterdam, 33-55.

Brennan, B.J., and Smylie, D.E., 1981, Linear viscoelasticiy and dispersion in seismic wave propagation, Rev. Geophys. Space Phys. 19, 233-246.

Coleman, B.D., and Noll, W., 1961, Foundations of linear viscoelasticity, Rev. Mod. Phys. 33, 239-249.

de Jong, B.H.W.S., and Brown, G.E., 1980, Polymerization of silicate and aluminate tetrahedra in glasses, melts and aqueous solutions, II. The metwork modifying effects of MG^{2+}, K^{+}, Na^{+}, Li^{+}, OH^{-}, F^{-}, Cl^{-}, H_2O, CO_2 and H_3O^{+} on silicate polymers, Geochim. Cosmochim. Acta 44, 1627-1642.

Dutta, N.C., and Ode, H., 1979, Attenuation and dispersion of compressional waves in fluid-filled porous rocks with partial gas saturation (White model), Part I. Biot theory, Geophys. 44, 1777-1788. Part II. Results, Geophys. 44, 1789-1805.

Dutta, N.C. and Sherif, A.J., 1979, On White's model of attenuation in rocks with partial gas saturation, Geophys. 44, 1806-1812.

Ferry, J.D., 1970, Viscoelastic roperties of olymers, Wiley, NY, 671 p.

Gurtin, M.E., and E. Sternberg, 1962, On the linear theory of viscoelasticity, Arch. Rat. Mech. Anal. 11, 291-356.

Moore, D.F., 1965, A review of squeeze films, Wear 8, 245-263.

Moore,D.F., 1975, Principles and Applications of Tribology, Pergamon, Oxford, 388 p.

Moore,D.F., 1972, The Friction and Lubrication of Elastomers, Pergamon, Oxford, 288 p.

McDonald, D.A., 1974, Blood Flow in Arteries, Arnold, London, 496 p.

Pedley, T.J., 1980, The Fluid Mechanics of Large Blood Vessels, Cambridge Univ. Press, 446 p.

Pinkus, B., and Sternlicht, O., 1961, Theory of Hydrodynamic Lubrication, McGraw-Hill, NY 465 p.

Strick, E., 1981, Application of the general anelastic model to water saturated rock, Geophys., submitted.

Wormsley, J.R., 1955, Oscillatory motion of a viscous liquid in a thin-walled elastic tube, I. The linear approximation for long waves, Phil. Mag. 46, 199-221.

Wormsley, J.R., 1957, Oscillatory flow in arteries: the constrained elastic tube as a model of arterial flow and pulse transmission, Phys. Med. Biol. 2, 178-187.

Yates, D.J.C., 1954, The expansion of porous glass on the adsorption of non-polar gases, Proc. Roy. Soc. London, 224, 526-544.